Mud and mangroves in Suriname

Multi-decadal analysis of a mud-dominated coast using earth observation

Job de Vries

281 UTRECHT STUDIES IN EARTH SCIENCES

Mud and mangroves in Suriname

Multi-decadal analysis of a mud-dominated coast using earth observation

Modder en mangroves in Suriname

Multi-decennia analyses van een modder gedomineerde kust met gebruik van aardobservatie

(met een samenvatting in het Nederlands)

PROEFSCHRIFT

ter verkrijging van de graad van doctor aan de Universiteit Utrecht
op gezag van de rector magnificus, prof. dr. H.R.B.M. Kummeling,
ingevolge het besluit van het college voor promoties
in het openbaar te verdedigen op woensdag 24 mei des middags te 4.15 uur

door

Job de Vries

geboren op 28 januari 1990 te Amsterdam

Promotoren:
Prof. dr. S.M. de Jong
Prof. dr. B.G. Ruessink
Dr. P.A. Verweij

Copromotor:
Dr. B. van Maanen

Beoordelingscomissie:
Prof. dr. M.A. Allison
Prof. dr. E.J. Anthony
Dr. L.L. Govers
Pof. dr. P. Verburg
Prof. dr. D. van der Wal

Mud and mangroves in Suriname

Promotoren:
Prof. dr. S.M. de Jong
Prof. dr. B.G. Ruessink
Dr. P.A. Verweij

Copromotor:
Dr. B. van Maanen

Examination committee:
Prof. dr. M.A. Allison
Prof. dr. E.J. Anthony
Dr. L.L. Govers
Prof. dr. P. Verburg
Prof. dr. D. van der Wal

ISBN 978-90-6266-651-5

Published by Faculty of Geosciences, Universiteit Utrecht, The Netherlands in: Utrecht studies in Earth Sciences (USES 281), ISSN 2211-4335

Cover: Landsat (USGS) composites, created by Job de Vries
Cartography and figures: Job de Vries
Design and lay-out: Job de Vries
Correspondence to: Job de Vries (**jobdevries90@gmail.com**)
Printed by: Ipskamp Drukkers B.V., Enschede, The Netherlands
Chapter labels: warming stripes, © Ed Hawkins

Chapters 2 to 5 and Appendices are either unpublished, submitted articles or final author's versions of previously published articles, © by Job de Vries and co-authors. More information and citation suggestions are provided at the beginning of these chapters.

Utrecht Studies in Earth Sciences 281

Mud and mangroves in Suriname

Multi-decadal analysis of a mud-dominated coast using earth observation

Job de Vries

Utrecht 2023

Faculty of Geosciences, Utrecht University

Not all who wander are lost

J.R.R. Tolkien

Contents

Summary

Mudbanks are pertinent features that can be found along the 1,500-km long coastline of the Guianas. These mostly subtidal banks consist primarily of sediments that originate from the Amazon River in Brazil. After formation near Amapá, they migrate along the coasts of French Guiana, Suriname and Guyana to the Orinoco Delta in Venezuela. Each mudbank consists of a mud layer that can be between 1 and 5 meters thick, stretching between 10 and 20 km alongshore and up to 60 km seaward. These large amounts of fine sediment damp incoming waves that predominantly come from north eastern directions and simultaneously provide a source of sediment for coastal expansion. Due to the erosion on the east side and transport of sediment under the influence of waves and currents towards the leeward side, mudbanks migrate westward with a speed of 1 to 5 km per year.

The specific conditions of mobile and migrating mudbanks result in 10 - 15 year long phases of progradation and erosion that can be associated with their presence and absence, respectively. As a consequence of these alternating phases, coastal management must account for non-linear and abrupt changes in the coastal zone, including coastline and mangrove cover variations. This cyclic instability is especially challenging for implementing coastal protection strategies, nature conservation initiatives, blue carbon policies and agricultural development.

The coastal plain of Suriname, ~450 km downdrift of the Amazon, is of special interest because it has an estimated 100,000 ha of pristine mangrove forests. In their natural state these areas are composed of mangrove belts in various stages of succession, intertidal areas with distinct levels of consolidated mud or sandy substrates. These mosaics of terrestrial landcover are separated by diffuse and temporally changing boundaries. Significant variability in landcover changes can be observed on timescales that range from days to multiple decades and longer.

The multi-decadal variability in local changes along the coastal zone, induced by alongshore migrating mudbanks remains poorly understood and unquantified. Especially at scales ranging from sub-kilometre to multiple kilometres have remained unquantified for the entire coastal zone. This is because the coastal zone is often inaccessible and mudbank footprints are difficult to demarcate from their surroundings. The lack of consistent estimates of mudbank footprints makes it difficult to differentiate between natural changes related to mudbank migration and human- or climate-induced changes in the coastal zone. To be able to better estimate coastlines and mangrove changes and to simultaneously constrain predictions of future changes, it is thus important to demarcate mudbank footprints, study indicators of stress in mangrove forests and detect unusual coastline position changes at relevant spatial scales.

In this thesis a remote-sensing workflow was developed to utilize the spatial and temporal resolution of the complete Landsat satellite data archive since 1986. Simultaneously, the semi-automatic processing steps discriminate between subtidal mudbanks, intertidal areas and coastal land surfaces (Chapter 2). The implemented linear spectral unmixing approach made it possible to untangle distinctive reflectance signals into representative landcover fractions of water, mud and vegetation. Especially the estimates of mud abundance in the water column allowed the detection of diffuse boundaries associated with mobile migrating mudbanks. By applying this workflow it

became possible to show the paramount effect of migrating mudbanks on the multi-decadal coastline dynamics in Suriname. We show that on average 36 m/yr of accretion occurs during mudbank presence and 18 m/yr of erosion during mudbanks absence, although spatial and temporal variability was high (Chapter 3).

The use of all available Landsat images increased the temporal resolution beyond perennial changes, while simultaneously considering the entire 1,500-km coast of the Guianas for the first time. Simultaneously, this approach allowed to highlight the large alongshore variability in observed coastlines changes. This becomes especially apparent when the effect of mudbank migration on the coasts of Suriname is compared with French Guiana and Guyana (Chapter 4). The computed frequency of mudbank occurrence, which is linked to the position and shape of mudbanks, proves to be a key factor controlling the number of years a coastal section is protected and accretion is facilitated. Differences between countries highlight the importance of considering non-linear changes of coastline positions and mangrove dynamics (Chapter 5) for future interventions, including building with nature initiatives, ecosystem restauration and coastal protection efforts.

The optimal use of the opensource Landsat archive to detect the changes in mangrove forests that result from mudbank dynamics was explored (Chapter 5). This gave insight into the characteristics and spatiotemporal distribution of mangrove gain and losses along the coast of the Guianas. Patches of mangrove change were found to be spatially clustered and linked to mudbank migration. However, more and significantly larger changes occurred in the coastal hinterland, not directly influenced by mudbank migration. These observations suggests that all causes of mangrove changes should be explored, not only the losses when mudbanks are absent and mangrove colonization when present.

This thesis proposes that the established conceptual model of mudbank migration along the Guiana coastline, prescribing a cyclic instability of progradation and erosion related to bank and interbank phases, captures general trends but requires additional attention when addressing local coastal dynamics (which are crucial for coastal management). Especially the lack of progradation during mudbank phases, the heterogenous coastline response and the variability in mangrove cover changes are, until now, often neglected. The here developed methodology provides a way forward to specify where changes are happening and might take place in the future in the coastal zone of Suriname and the wider Guianas.

Samenvatting

Modderbanken zijn kenmerkend voor de 1,500 kilometer lange kustlijn van de Guianas. Deze voornamelijk subgetijde banken migreren van de monding van de Amazone Rivier in Brazilië, langs de kusten van Frans-Guyana, Suriname en Guyana tot aan de Orinoco Delta in Venezuela. Bij elke individuele modderbank wordt een laag modder van een tot vijf meter dikte in suspensie gehouden, die zich 10-20 kilometer langs de kust uit kan strekken en tot 60 kilometer zeewaarts. Deze grote hoeveelheden fijn sediment zorgen voor bescherming van de kust door extra golfdemping en vormen tegelijkertijd een bron van sediment voor natuurlijke kustaangroei.

Door continue afslag van sediment aan de oostzijde en transport naar de luwere westzijde onder invloed van lokale golven en zeestroming, verplaatsen modderbanken zich westwaarts met één tot vijf kilometer per jaar. De migrerende modderbanken zorgen voor fases van kustaangroei en erosie die 10-15 jaar kunnen duren, afhankelijk hun respectievelijke aan- of afwezigheid. Door deze afwisselende fases moet het kustbeheer in de Guianas rekening houden met niet-lineaire erosie en uitbreiding van de kust, bijvoorbeeld in mangrovebossen. Zo'n cyclische instabiliteit is vooral een uitdaging voor de implementatie van lange termijn strategieën op het gebied van kustbescherming, natuurbehoud, natuurlijke opslag van CO_2 en de ontwikkeling van landbouw en aquacultuur.

De kustvlakte van Suriname, 450 kilometer van de Amazone Rivier, is bovendien interessant omdat er ongeveer 100,000 hectare natuurlijk mangrovebos groeit. In hun natuurlijke staat bestaat de kusvlakte uit stroken mangrovebossen in verschillende stadia van ontwikkeling, intergetijdengebieden met variabele consolidatie van modder of juist zandige afzettingen. Deze lappendeken van landbedekkingen worden gescheiden door diffuse en snel veranderende grenzen. Daarnaast is er significante variatie in landbedekking over de tijd, met veranderingen die plaatsvinden in enkele dagen tot veranderingen over meerdere decennia.

Informatie over de veranderingen op jaarlijkse tijd- en lokale ruimteschaal krijgt tot op heden beperkte aandacht omdat consistente kwantificatie hiervan moeilijk is. Dit wordt mede veroorzaakt door de beperkte toegankelijkheid van de kustzone en de uitdaging om modderbanken af te bakenen is op satellietobservaties. Hierdoor is het lastig om natuurlijke veranderingen te onderscheiden van de veranderingen die worden veroorzaakt door modderbank migratie, menselijk ingrijpen of de invloed van klimaatverandering. Om een betere inschatting te maken van veranderingen die plaatsvinden in mangrovebossen en langs de kustlijn is het dus belangrijk modderbanken af te kunnen bakenen in observaties. Tegelijkertijd biedt dit soort observaties de mogelijkheid toekomstige voorspellingen te verbeteren, indicatoren van achteruitgang in mangrovebossen te bestuderen en onnatuurlijke veranderingen in de kustlijn op kleine en grote schaal te detecteren.

In deze thesis is een dataverwerkingsproces ontwikkeld om de ruimtelijke en temporele resolutie van Landsat aardobservaties, beschikbaar sinds 1986, beter te benutten voor de detectie van veranderingen in de kustgebieden. Daarbij zijn semiautomatische verwerkingsstappen geïmplementeerd om het onderscheid te maken tussen subgetijde delen van modderbanken, het intergetijdengebied en terrestrische landschapselementen (Hoofdstuk 2). Daarvoor is lineaire spectrale unmixing toegepast om kenmerkende reflectiesignalen te onderscheiden en representatieve

landbedekking van water, modder en vegetatie te berekenen. De hieruit voortkomende geschatte aanwezigheid van sediment in de bovenste waterkolom faciliteert de detectie van diffuse modderbank grenzen. Met deze methode werd het mogelijk het overweldigende effect van migrerende modderbanken op de lange termijn veranderingen van de Surinaamse kustlijn te kwantificeren. Gemiddeld vond er in Suriname 36 meter per jaar aan uitbouw van de kustlijn plaats als er een modderbank aanwezig was en 18 meter per jaar erosie als die er niet was, met grote ruimtelijke en temporele variatie (Hoofdstuk 3).

Door gebruik te maken van alle beschikbare Landsat observaties werd de temporele resolutie van veranderingen voor het eerst hoger dan enkel meerjarige of zelfs per decennium. Tegelijkertijd werd voor het eerst de gehele 1,500 kilometer lange kust van de Guianas in beschouwing genomen. Deze benadering zorgde ervoor dat het mogelijk werd de grote variatie in veranderingen langs de kust te analyseren. Dit wordt ook geïllustreerd door het effect van modderbank migratie voor de kust van Suriname te vergelijken met die voor de kust van Frans-Guyana en Guyana (Hoofdstuk 4). Het verschil in frequentie van voorkomen van modderbanken, wat gelinkt is aan de positie en vorm ervan, blijkt namelijk een dominante factor te zijn die bepaalt hoeveel jaar een kustlijn beschermd wordt of zelfs uitbouwt. Zulke verschillen tussen landen illustreren het belang van het meenemen van niet-lineaire veranderingen in kustlijn posities en mangrove dynamiek (Hoofdstuk 5) bij toekomstige interventies, zoals kustbescherming, building with nature en ecosysteemrestauratie.

Het optimale gebruik van de beschikbare Landsat observaties werd verkend om veranderingen in mangrovebossen, die sterk beïnvloed worden modderbank migratie, te detecteren (Hoofdstuk 5). De resultaten boden nieuwe inzichten over de eigenschappen van veranderingen in mangrovebossen langs de kust van de Guianas en de bijbehorende ruimtelijke en temporele verspreiding van groei en verlies. Veranderingen in mangrovebossen bleken geclusterd te zijn en gelinkt te kunnen worden aan modderbankmigratie. Echter vonden er ook significante veranderingen plaats in het achterland, wat niet direct beïnvloed kan zijn door modderbank migratie. Deze observaties suggereren dat andere oorzaken van veranderingen in mangrovebossen ook verder onderzocht moeten worden.

Deze thesis toont aan dat het gevestigde conceptuele model van modderbank migratie, dat een cyclische instabiliteit van kustuitbouw en erosie door modderbank migratie beschrijft, de algemene trends langs de kust van de Guianas goed beschrijft. De lokale veranderingen, die cruciaal zijn voor adequaat management van de kustlijn, verdienen echter meer aandacht. Vooral het uitblijven van kustuitbouw terwijl er een modderbank aanwezig is, en de heterogene reactie van, én variatie aan veranderingen in, mangrovebossen worden tot nu toe vaak genegeerd, terwijl deze factoren van grote invloed blijken te zijn. De methodes die in deze thesis zijn ontwikkeld kunnen gebruikt worden om verder te verduidelijken waar veranderingen plaatsvinden en verwacht worden langs de kusten van Suriname en de Guianas.

Chapter 1 | Introduction

1.1 Societal context

1.1.1 Competition for space

Coastal zones have been among the most accommodating environments for human settlement for centuries and remain so today for 10-20% of the global population (Cohen et al., 1997; Cohen and Small, 1998; Kummu et al., 2016; Neumann et al., 2015). Almost without exception, densely populated coastal areas face a growing pressure to balance their social, economic, natural and protective functions (Brown et al., 2014; Lotze et al., 2006). As a result, the natural functioning of habitats in these regions often conflicts spatially with a growing population. This increases the demand for managing coastal protection, economic activities and compensating the impact of human-induced climate change by sequestrating carbon (Pendleton et al., 2012). In addition, anthropogenic activities have already altered the coastal environment by, among other activities, means of land reclamation (Sengupta et al., 2018), deforestation (Ahmed and Glaser, 2016), agricultural development (Giri et al., 2011), dredging (Bolam and Rees, 2003), groundwater extraction (Ferguson and Gleeson, 2012) and the introduction of (toxic) waste water (Dachs and Méjanelle, 2010; Jones et al., 2022, 2021; Meijer et al., 2021). There is also strong evidence that many densely populated coastal regions are subsiding due to climatic and human-induced disturbances. Despite the positive feedback loops that facilitate sediment accumulation and raised these environments above the mean sea level in the first place (Ericson et al., 2006; Nicholls et al., 2021; Oppenheimer et al., 2019; Syvitski et al., 2009).

Gradients in abiotic factors, such as salinity and inundation frequency, provide habitats for a rich variety of flora and fauna in coastal ecosystems (Duke et al., 1998; Nicholls et al., 2007). This results in dynamic and ecologically rich environments, including salt marshes and mangrove coasts. Communities that utilize associated advantageous ecosystem services, such as biodiversity, food production on fertile soils and a reliable water supply, can therefore be provided with a beneficial livelihood (Kummu et al., 2016). Globally over 100 million inhabitants (Douglas and Peltier, 2002) also rely on the capability of coastal zones to protect against incoming waves, sea level rise and storm surges under a changing climate (Nicholls et al., 2007; Oppenheimer et al., 2019; Temmerman et al., 2013).

Since the start of industrial revolution in the 19th century, average global temperatures have increased by 1.1 °C (WMO, 2019), contributing to accelerated sea level rise of 3-4 mm/yr since 1993 (Cazenave et al., 2018). Together with subsidence rates, going up and beyond 20 mm/yr for some coastlines (Nicholls et al., 2021), relative sea level rise has caused severe, yet variable coastlines retreat across the globe (Luijendijk et al., 2018). Expected climate warming of 0.1 to 0.4 °C per decade will most likely result in additional sea level rise up to two mm per year, further increasing coastal hazards during the coming century and beyond (Oppenheimer et al., 2019). For larger deltas, such as those in South America, effective sea level rise has been estimated to be at least 3.5 mm/yr (Ericson et al., 2006) with a relative small contribution from subsidence.

Coastal management should aim to balance the diverse demands and ensure the livelihoods of coastal communities by avoiding rather than only mitigating increased flood risk, salinization of agricultural lands, land loss, coastal squeeze and ecosystem degradation (Nicholls, 2011). Especially land cover conversions near pristine coastal zones are potentially unsustainable and may cause severe habitat degradation, ultimately leading to additional losses of land and property. This is particularly undesirable for low- and middle-income countries, as they are already more vulnerable to climate change (Barbier, 2015). When local communities have little ability to adapt to changing conditions, there is an increasing likelihood of severe hazards with irreversible impacts. In such cases, mitigation measures are required, including artificial sediment supply, green and grey coastal protection and nature-based solutions. To ensure successful implementation, in-depth knowledge on the current state of the coastal environment, including local variability in coastal processes, biodiversity, hydrology, the response under anticipated climate changes and the resulting changes in spatial claims is required. This is crucial as such interventions do not only require large investments, they also have the potential to aggravate erosion risk and adversely affect the recovery capacity of a coastal zone following degradation. Therefore, there is an urgent need for reliable data on exposure to coastal hazards, as well as timely and specific information for those who need it.

1.1.2 Muddy coasts

Open coasts are generally dominated by rocky or sandy shores but can under specific conditions also be composed of muddy and vegetated shores (Anthony et al., 2013b). These coasts are often associated with the alongshore distribution of sediments that originate from large rivers and sediment-rich catchments such as the Yangtze, Mekong, Mississippi and Amazon River. The redistribution of sediment and thus the fate of coastal zones, is shaped under the influence of hydrodynamic forcing mechanisms, such as wind-generated waves, tides, currents and complex interactions between them (Vuik et al., 2019).

In tropical regions, muddy coastal zones are predominantly characterized by mangrove belts in different stages of succession (Fabre et al., 1999; Gilman et al., 2008; McKee, 1995). Mangroves can thrive in salt water environments due to their root systems, providing enhanced stability under regular flooding and continued oxygen uptake via pneumatophores (Alongi, 2008; Krauss et al., 2008). Simultaneously, the roots bind and stabilize sediment (Ellison, 2008), reduce water flow (Bryan et al., 2017) and wave energy (Horstman et al., 2014), further enhancing sedimentation (Furukawa et al., 1997). This raises the local bed level (Furukawa and Wolanski, 1996) and protects coasts against rising water caused by waves (Melet et al., 2018), storms (Woodroffe and Grime, 1999) and sea level rise (Krauss et al., 2014; McKee et al., 2012; Saintilan et al., 2020).

Globally, mangrove coastlines are threatened by agricultural activities, aquaculture, subsidence, reduced accommodation space for landward migration and a changing climate. This includes sea-level rise and an increasing frequency and intensity of storms (Osland et al., 2017; Passeri et al., 2015). As a result, an estimated one-third of the world's mangrove forest was lost between the start of the industrial revolution and the 2000s (Alongi, 2008, 2002), although significant regional variations exists (Friess et al., 2019; Gebhardt et al., 2012). The decline in these valuable ecosystems will likely continue under the influence of global climate change and increasing anthropogenic pressures (McKee et al., 2012). Mangroves are, however, deemed invaluable when aiming at mitigation of climate changes and related impacts such as sea level rise (Duke et al., 2007; Krauss et al., 2014). The regulatory ecosystem services provided by mangroves, such as carbon sequestration and protection from sea-level rise, have therefore gained increased attention (Macreadie et al., 2019).

1.1.3 Coastal behaviour

As coastal systems are at the interface of land and water, they are subject to ever changing conditions, both internal and external to the system (Bitencourt et al., 2020; Brown et al., 2014; Cowell et al., 2003; Kombiadou et al., 2019). External control factors include, for example, sea level rise, tidal forcing and wave climate at regional to global scales (Green and Coco, 2014; Viles and Goudie, 2003). Internal controls are more often intrinsic to local environments and play a critical role in coastline evolution by determining sediment distribution, production, interaction between local wave climate and shoreline changes or the accommodation space for coastal progradation (Cahoon et al., 2006). Interactions between multiple controls will result in a spectrum of unique coastal systems with different shapes, land cover and future trajectories (Barbier et al., 2008; Koch et al., 2009). This is, for example, reflected by coastlines, as their position, shape and natural characteristics can vary spatially and change over time (Ashton et al., 2001; Geleynse et al., 2012). Additionally, coastal morphology may also behave non-linear, due to alternating periods of dominant controlling factors or due to feedback mechanisms unrelated to timescales in external forcing (Ruessink and Terwindt, 2000). Cycles can range from seasons to years and multiple decades (Hu et al., 2018). External control mechanisms, like climate variability and wave forcing, work at different spatial and temporal scales, adding complexity when trying to explain observed heterogeneity and variability in coastal land cover (Stive et al., 2002).

The feedbacks between these control factors generate a shoreface that tends towards an equilibrium state for a given time-averaged wave climate and associated sediment transport (Anthony and Aagaard, 2020). Stationary coastal zones may thus sound intuitive for timescales

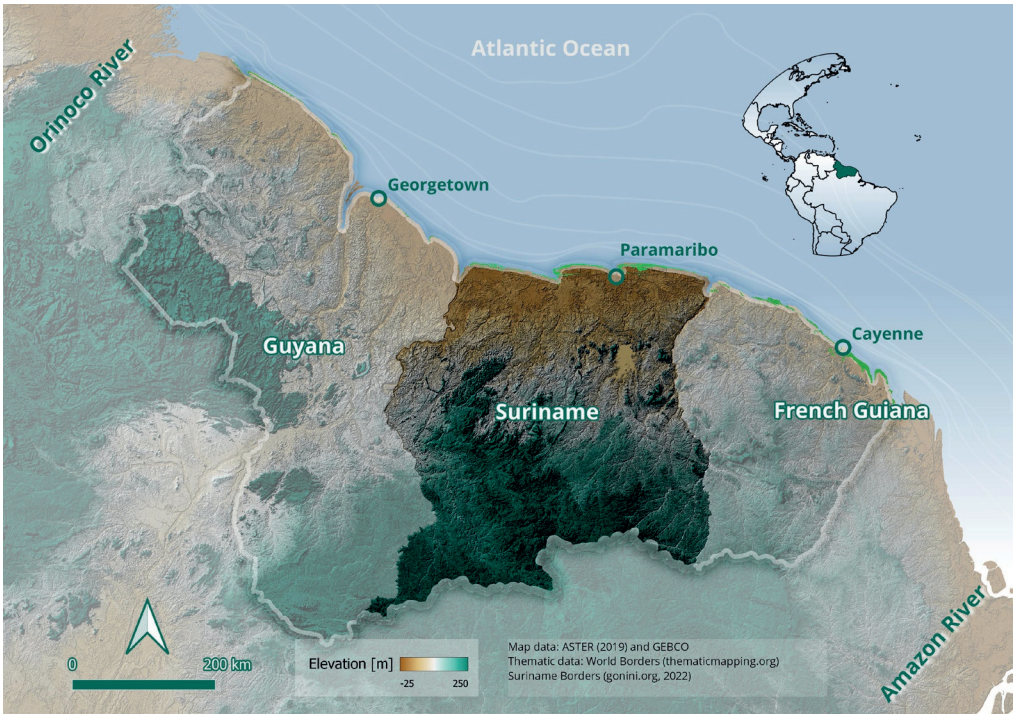

Figure 1.1: Suriname and its location in the context of the wider Guianas' coastal zone, which stretches from the mouth of the Amazon River to the Delta of the Orinoco River.

ranging from seconds to hours or even days. However, also dynamic equilibria over years or decades, implying a balance between alternating progradation and erosion phases, are common (Kirwan and Megonigal, 2013; Moffett et al., 2015; Proisy et al., 2021). Yet, changes in weather, climate or oceanic forcing have the potential to affect the interplay between control factors and coastal zone changes. This inherently dynamic character of coastal zones, including land cover changes, variable coastline response, mangrove colonization over tidal flats or loss of mangroves, thus provide a way to simultaneously monitor the state of our climate and indicate the resilience of coastal zones against such changes.

1.2 Suriname and the wider Guianas coastal zone

1.2.1 Anthropogenic influence in a dynamic mangrove system

This thesis focuses on the mud-dominated Suriname coast and the wider Guianas' coastal zone (Figure 1.1), stretching over 1,500-km from the mouth of the Amazon River in Brazil, along the shores of French Guiana, Suriname, Guyana to the Orinoco Delta in Venezuela (Allison et al., 1995b; Anthony et al., 2010; Augustinus, 1980, 1978; Eisma and Marel, 1971; Gersie et al., 2018; Rine and Ginsburg, 1985; Toorman et al., 2018; Wong, 1992). A significant body of research has been performed in this area, accelerating from the 1940s in Suriname (Allison et al., 1995a; Augustinus, 1980; Eisma and Marel, 1971; Teunissen, 1976; Wells and Coleman, 1981a) and from 1980 onwards increasingly more in Guyana (Lakhan and Pepper, 1997) and especially French Guiana (Anthony et al., 2010, 2002). These field studies, supplemented with multi-decadal satellite observations, aerial photographs (Augustinus et al., 1989) and modelling efforts (van Ledden et al., 2009; Winterwerp et al., 2007), revealed that reshaping of the coastal zone has been recurring under influence of migrating subtidal mudbanks since the Holocene in distinct sedimentation phases (Augustinus et al., 1989; Wong, 1992; Wong et al., 2009).

The pristine mangrove coastlines of the Guianas, particularly Suriname and French-Guiana, remain a welcome exception to declining global trends in mangrove cover over the last decades. Despite local to regional erosion hotspots (Brunier et al., 2019), these mangrove coast are showing net progradation over the last centuries (Plaziat and Augustinus, 2004). The coastal zone of Suriname, 450 km downdrift of the Amazon Delta, is a relative flat area that stretches from the landward extent of mangrove cover to the seaward limit of the intertidal area. In their natural state these areas compose of mangrove belts in different stages of succession and of intertidal areas with different levels of consolidated mud or sandy substrates (Anthony et al., 2010; Toorman et al., 2018). These mosaics of terrestrial and oceanic environments are separated by diffuse and changing boundaries (Figure 1.2).

The mangrove fringe of Suriname varies in width and is mainly occupied by *Avicennia germinans,* sometimes backed by *Rhizophora spp.* and to a lesser extent *Laguncularia racemosa* (Fromard et al., 1998; Marchand et al., 2004). Behind this belt a marsh forest may develop, containing several tree species, including older *Avicennia germinans* (Teunissen, 1976). The entire coastal plain is covered by an estimated 100.000 ha of mangroves, but this may fluctuate significantly at decadal timescales (Guzman et al., 2017). For the remainder, swamps, savannahs and tropical forest are most frequently observed habitat types (Lindeman, 1953; Teunissen, 1976). Several anthropogenic activities may impact the functioning of these natural systems in the Guianas, including sand mining, dredging, shrimp farming, logging of mangroves, construction of infrastructure, such as coastal protection measures and dredging to allow continued access to the harbours (Anthony and Gratiot, 2012; Nijbroek, 2014). Due to the low population density, there

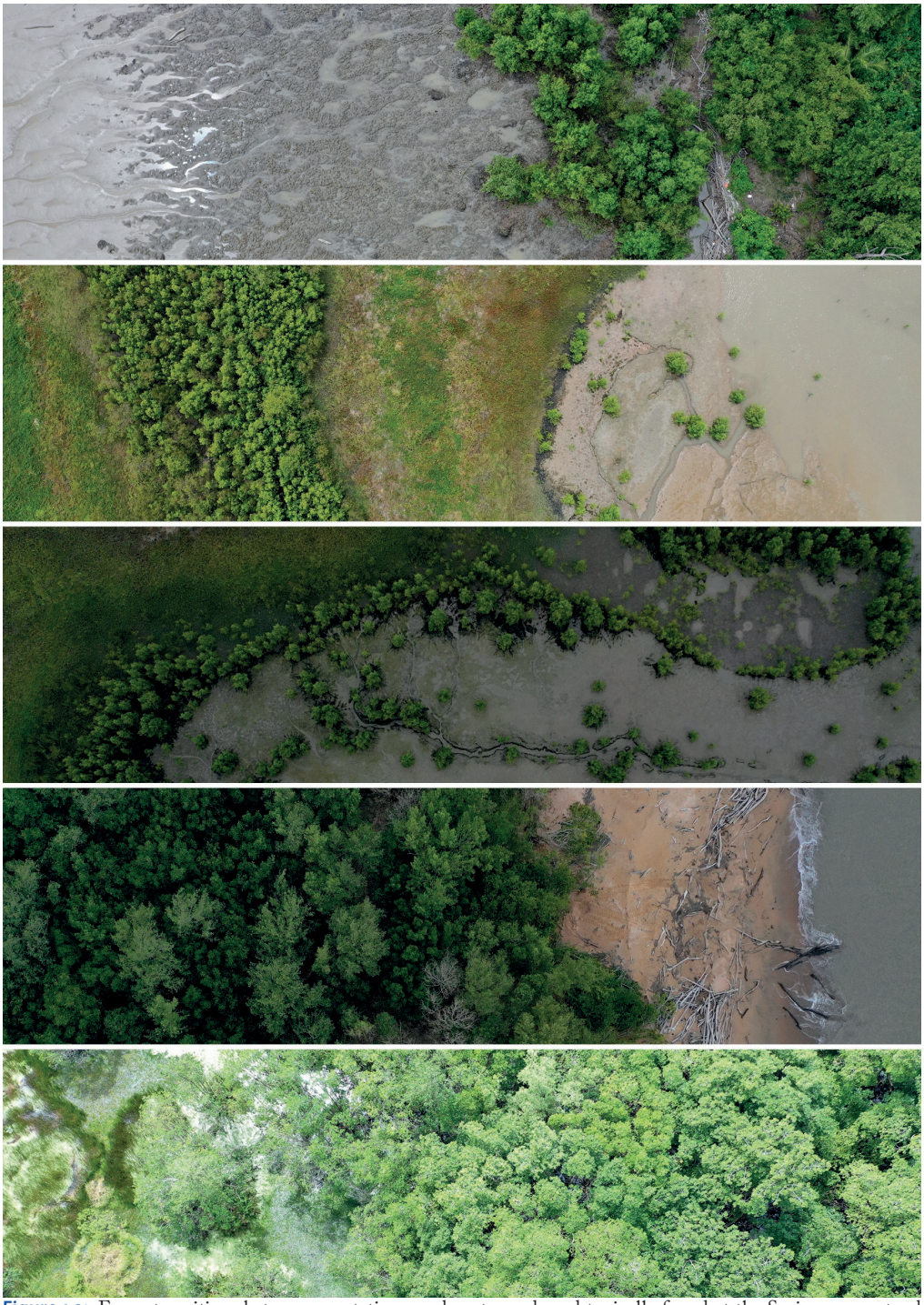

Figure 1.2: Fuzzy transitions between vegetation, mud, water and sand typically found at the Suriname coastand the wider Guianas. Photographs were collected at 50-75 m flying height with a DJI Mavic Pro 2 UAV platform.

is limited groundwater extraction and consequently, subsidence rates are relatively small. This has resulted in an estimated sea-level-rise of less than two mm/yr between 1950 and 2000 in the region (Church et al., 2004; Losada et al., 2013; Milne et al., 2005; Saintilan et al., 2020).

Natural climate variability along Guianas' coastal zone is due to a complex interaction of atmospheric oscillations, ocean forcing mechanisms, temperature changes and high precipitation (Kushnir et al., 2006; Ortega et al., 2021). The relatively southern location of the Inter-Tropical Convergence Zone (ITCZ) between February and April causes the onset of a short dry season with north eastern trade winds (Allison et al., 2000). Between April and July the ITCZ moves north, heralding the onset of a longer wet season with lower wind speeds from the north east and occasionally the south east (Augustinus, 2004; Wells and Coleman, 1981a). Between August and December, the ITCZ is located north of the coastline, marking the start of the major dry season characterized by south-east trade winds. After this period, the ITCZ moves south of the coastline again, initiating a shorter wet season where the north eastern trade winds start to pick up again (Xie and Carton, 2004). Coupled climate phenomena such as the El Nino-Southern Oscillation (ENSO) are thought to enhance annual variability in precipitation in the Guiana shield countries (Servain et al., 2014).

The offshore wave climate is assumed to be relevant for changes in the coastal zone, as incoming waves control sediment dynamics and thus the natural variability in the coastal zone (van Ledden et al., 2009). Due to the movement of the ITCZ, a distinct seasonality in wave climate can be observed along Guianas' coastline (Augustinus, 2004; Gratiot et al., 2007). Between December and April, when the ITCZ is located further south, north east trade winds have a relative longer fetch, therefore enhancing swell waves coming from the Atlantic Ocean (Best et al., 2022; Walcker et al., 2015). As a result, wave heights up to two m can be observed offshore, with periods between 6 and 10 s (Wells and Coleman, 1981b). Closer to the shore, locally generated wind-waves are smaller and typically have shorter periods, but contribute significantly to resuspension of sediments during falling tides (Gratiot et al., 2007; Green and Coco, 2014). Variations in average wave height, period and incidence angle, with timescales ranging from annual to multiple decades, have previously been linked to the North Atlantic Oscillation phases (NAO) and variability in the ENSO (Cai et al., 2020; Gratiot et al., 2008; Viles and Goudie, 2003; Walcker et al., 2015).

Despite the high annual precipitation, the larger rivers along Guianas' coast, such as the Maroni, Suriname and Corantijn rivers, have relative low discharges that range from 46 m^3/s to 2,104 m^3/s for the Maroni River (Gardel et al., 2022). Additionally, they contain low suspended sediment loads (1 – 150 g/m^{-3}), especially compared to the total sediment load that originates from the Amazon River and is transported alongshore (Anthony et al., 2013a; Wright and Nittrouer, 1995). The nearshore coastal waters do have a high turbidity that is associated with suspension (1 – 300 g/m^{-3}) of these Amazonian sediments (Froidefond et al., 2004; Gensac et al., 2016; Vantrepotte et al., 2011). The local rivers do, however, influence the coastal dynamics by supplying local sand to erosion-resistant cheniers (Augustinus et al., 1989).

1.2.2 Mudbanks and their migration

Some 15-20% of the total sediment outflow from the Amazon migrates as subtidal mudbanks (Figure 1.3) attached to Guianas' shoreline (Allison et al., 2000; Anthony et al., 2013a; Eisma et al., 1991; Nittrouer et al., 2021; Plaziat and Augustinus, 2004). The silty sediment is advected in turbid suspension by tidal and local currents (Lefebvre et al., 2004) along the coastline from east to west. Each mudbank can be up to 10-60 km long, 20-30 km wide and five m thick (Chevalier et al., 2004; Winterwerp et al., 2007) and can store up to six billion m^3 of fine sediment (Gratiot et

al., 2007). The subtidal part is the largest part of the mudbank and can range from high suspensive (1-10 g m^{-3}) to unconsolidated mud through fluid mud (70 to <650 g m^{-3}) (Péron et al., 2013). A threshold of 13 g m^{-3} has been used previously to delineate the subtidal parts of mud banks (Froidefond et al., 2004; Vantrepotte et al., 2013).

At any given time at least 15 of these mudbanks, roughly 15-25 km apart, move with a variable speed, varying from 0.5 to 5 km/yr (Froidefond et al., 1988; Gardel and Gratiot, 2005) along the coastline of the Guianas (Figure 1.1), while constantly changing in shape and orientation (Augustinus et al. 1989). Mudbanks promote coastal progradation, directly linked to the fluid mud they partially consist of, their wave-damping potential and enhanced sediment supply. These specific conditions of mobile and migrating mudbanks thus result in phases of erosion and progradation of the coastline that last up to 30 years, with enhanced erosion during inter-bank and progradation during bank-phases (Allison and Lee, 2004; Anthony and Dolique, 2004).

The continuous coalesce of mud in distinct mudbanks is caused by hydrodynamic forcing mechanisms (Anthony et al., 2013b), including waves (Gardel and Gratiot, 2006) and currents (Allison et al., 1995a). Due to the refraction of waves, convergent and divergent areas of wave energy are created on the trailing and leading edges of the mudbank, respectively (Figure 1.3). This gives rise to differences in wave energy with higher waves at the trailing edge and lower waves on the leading edge (Chevalier et al., 2008). As a consequence, mud is eroded from the trailing edge and transported as fluid mud patches towards the leading edge of a bank. When waves propagate with an oblique incidence angle, they will result in a cross-shore and alongshore sediment energy flux (Allison et al., 1995b). As a result, continuous mud-wave interactions transport the fluid

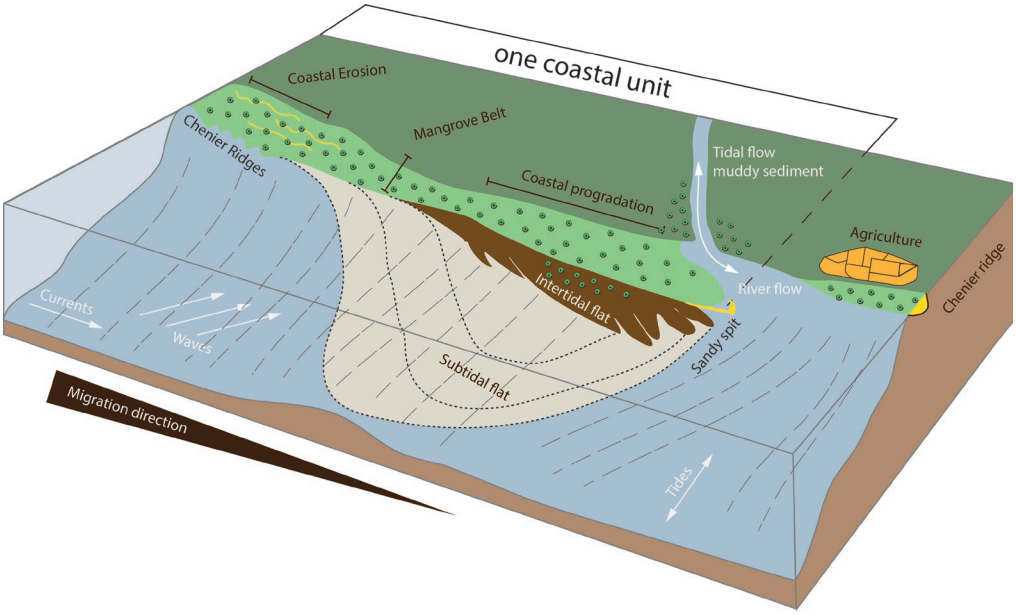

Figure 1.3: Conceptual overview of a mudbank and the factors that control dynamics of the coastal zone, including wave climate, alongshore current, tidal propagation, river discharge, sediment transport as well as mangrove growth and zonation. It remains unclear how all these natural control factors, together with agricultural development, urbanization, dredging and sand mining, determine the fate of the Guiana coastal zone in terms of coastal safety and natural ecosystem functioning. Adapted from Plaziat and Augustinus (2004).

mud layer in the direction of those fluxes, ultimately leading to increase in bank elevation in the terrestrial parts of mudbanks (Allison and Lee, 2004) or the formation of elongated mud bars (Gardel et al., 2011). When these bars dry, surface mud cracks can form, facilitating the growth of pioneering mangroves like *Avicennia germinans* (Anthony et al., 2008; Gardel et al., 2009; Proisy et al., 2009). After on average 20 years of being fronted by a mudbank, dense vegetation on the by then consolidated muds starts to erode again (Augustinus, 1980; Augustinus et al., 1989). The mud released will be transported towards the leading edge, restarting the process.

The preceding outline reveals that the general dynamics of coastline changes along Guianas' coastline can be captured in a conceptual model of mudbank migration (Figure 1.3); however, spatiotemporal variable and non-linear changes in coastline positions, mudbank footprints and mangrove development make it difficult to differentiate between the natural variability, anthropogenic changes and the effect of climate change (Allison and Lee, 2004; Orseau et al., 2020). Especially variability in mudbank footprints and the consequential migration behaviour, as response to uncertain feedbacks in hydrodynamic and wave forcing, remain poorly understood and unquantified for the entire Guiana coastline. Therefore, it remains unclear how all these natural control factors, together with agricultural development, urbanization, dredging and sand mining, determine the fate of the Guiana coastal zone in terms of coastal safety and natural ecosystem functioning.

1.3 Monitoring coastal zones

Information of local variability in mangrove development, coastline changes and mudbank migration is crucial for the inhabitants of the Guiana shield countries. Because the vast majority of their inhabitants live in the coastal zone, indicators to track signals of stress in mangroves (Heumann, 2011), coastline position trajectories (Vos et al., 2020), mudbank footprints (Zorrilla et al., 2018), land cover changes (Kuenzer et al., 2019) and the success of nature-based restoration efforts are of increasing importance (Gijsman et al., 2021). These signals, especially when indicating rapid shifts or prolonged adverse trends, can signify potential risks and subsequently contribute to mitigation and prevention of irreversible changes. Because the coastal zone in the Guianas is often inaccessible, the spatial scales are large and consistent long-term field observations that capture the full range of ecosystems dynamics are lacking, remote sensing will be used in this thesis.

1.3.1 Satellite remote sensing

Air- and spaceborne observations offer numerous possibilities to efficiently monitor coastal changes at local to global scales (Figure 1.4). There is a wealth of remote sensing data available nowadays, equipped with optical, multispectral, hyperspectral, radar and LiDAR sensors. Each remote sensing platform, with a unique sensor, is designed to observe the earth surface with a predefined coverage, spatial resolution and spectral sensitivity. In the last decade, the use of high-resolution sensors (0.01-10 m), preferred to approximate field observations, increased (Mancini et al., 2013; Ruwaimana et al., 2018). While unmanned aerial vehicles (UAVs) allow maximum control over spatial, temporal and spectral resolution, acquisition of large temporal and especially spatial coverage is very labour intensive, if not impossible for regional studies (Smith et al., 2015). More recently almost daily observations with high spatial resolution have become available due to the launch of fleets of smaller satellites (e.g., Planet with three m spatial resolution). Yet, due to their spectral limits, including radiometric accuracy and spectral resolution platforms with medium-

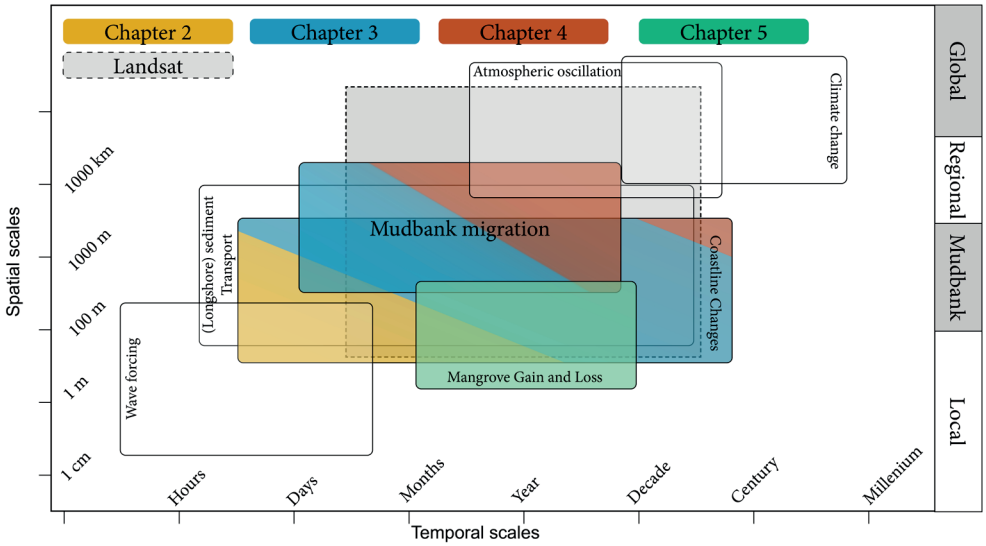

Figure 1.4: Natural dynamics that commonly occur in the Guiana coastal zone. Variability considered in the thesis are related to mudbank migration, coastline changes and mangrove gain and losses. Spatial scales (y-axis) considered in the thesis range from centimeter accurate coastline position estimates to local-scale coastline changes and ultimately global-scale external control factors that influence mudbank migration and regional differences in mangrove- and coastline dynamics. Temporal scales (x-axis) range from sub-daily variations in water level that complicate the detection of coastlines and mudbank footprints, to multi-decadal trends in coastline changes that are almost never linear. For reference the range of scales covered by Landsat observations are indicated. Adapted from Orseau et al. (2020).

resolution (e.g., 10-30 m) sensors, such as Landsat and Sentinel (Figure 1.4), are still commonly considered.

In image analysis, spectral information is assumed to be related to the land cover that the signal reflects from. As such, reflectance signals often describe subtle differences within pixels that result from radiation interacting with all active substances (Odermatt et al., 2012; Shi and Wang, 2014). This results in spectral confusion and within-class variability, especially in coastal systems and mangrove-dominated regions, such as the Guianas. Here boundaries are fuzzy, land cover classes are similar and thus the spectral similarity between (groups of) pixels is large (Matthews, 2011; Ryu et al., 2002). Accordingly, image analysis techniques that can deal with this confusion offer an approach to characterize gradients, define groups of matching pixels and separates classes of interest. Some examples that have been applied to coastal studies include spectral unmixing, (supervised) classification, machine learning algorithms and geographic object-based image analysis (Kuenzer et al., 2011; Matthews, 2011).

1.3.2 Landsat: Potential for monitoring

For the Guianas, researchers have previously used single satellite images (Froidefond et al., 2004) or focussed on limited areas (Baghdadi et al., 2004; Fromard et al., 2004; Gardel and Gratiot, 2006) due to high costs of acquiring and processing multiple to hundreds of images. The, release of remote sensing observations, including the Landsat data archive, to the public and the availability

of cloud computing platforms, such as Google Earth Engine (GEE), now allows parallel processing petabyte sized datasets (Gorelick et al., 2017). This sprouted a new paradigm within remote sensing, referred to as pixel based image compositing (White et al., 2014). To overcome missing data from cloud cover, aerosol contamination and inconsistent view angles, observations (e.g. pixels) within an 'composite period' are reduced to a single 'best' observation (Flood, 2013; Roberts et al., 2017). Change detection and classification studies increasingly used aggregated pixel composites representing epochs, years or seasonal observations (Hermosilla et al., 2015; Sagar et al., 2018). The image selection is often temporal, like closeness to a reference date, data quality like cloud proximity or an aggregation (e.g. mean, min, max or median) of spectral bands (Flood, 2013).

These aggregated snapshots hold meaningful spectral information to quantify temporal and spatial dynamics on larger scales and spanning longer periods (White et al., 2014). Examples include change detection over forests (Senf and Seidl, 2021), water bodies (Donchyts et al., 2016), intertidal areas (Murray et al., 2019) and coastlines (Vos et al., 2019). They potentially misrepresent local-scale landform characteristics and temporal evolution when conditions during acquisition vary over shorter time scales (e.g., stages of a tidal cycle). Also when features are migrating (Figure 1.4) and adjacent images do not consistently represent the dynamics of the system, aggregated images are likely to be inadequate (Koohafkan and Gibson, 2018). This limits the use of the created composite images for change detection of morphological features along the Guiana coastline, where sediment concentrations are extremely variable, coastline changes can be rapid, fluctuating water levels determine the visibility or data quality and availability (Zhang et al., 2022).

To overcome the limits associated with satellite monitoring in the coastal zone of the Guianas (Figure 1.4), observations with sufficient temporal coverage and resolution are required. As such, individual images from the Landsat archive may provide insights into the variability in mudbank footprints, their migration rates, consequential coastline change trends and mangrove ecosystem response. Landsat observations have been acquired since the 1970s, and over the last 25 years at least every 16 days at a spatial resolution of 30 m (Zhang et al., 2022). This makes the Landsat data archive a consistent, and still growing source of long-term observations, appropriate for multi-decadal monitoring now and in the future (Mondal et al., 2018). Finally, image analysis techniques that can address the inherent spectral confusion between similar land covers and diffuse boundaries, offer an approach to characterize the dynamics. This makes it possible to monitor landscape evolution for the entire Guiana coastal zone by characterizing seemingly blended responses to complex interacting processes (Koohafkan and Gibson, 2018).

1.4 Objective and thesis outline

The migration of mudbanks, dynamic climate controls, changes in heterogeneous land cover in the coastal zone and feedback between forcing mechanisms result in complex local to regional variable coastline and mangrove cover changes. To better quantify changes and constrain predictions coastal zone changes for future scenarios, it is important to elucidate on the spatial variability related to mudbank migration. The added benefit of improved predictions to coastal communities is supported in the United Nations Sustainable Development Goals (SDG; United Nations, 2015). These goals describe the ambitious aims the international community set out to achieve by 2030 and beyond. They include the reduction of CO^2 emissions and restrain temperature increases, while simultaneously minimizing the impact of unavoidable climate changes. Relevant sustainable development goals are explicitly defined in SDG 4: quality education, SDG 13: climate action, SDG 14: life below water and SDG 15: life on land. Numerous efforts have been initiated to

incorporate coastal protection, restoration and a beneficial livelihood for coastal communities in generic coastal management plans and engineering projects (Gijsman et al., 2021; Sutton-Grier et al., 2015; van Zelst et al., 2021). This dissertation is also part of a project that is a direct spinoff from the agreements adopted during COP 21 in Paris on 12 December 2015. Funded by NWO-Wotro the MangroMud project aims to enhance adequate management in coastal ecosystem of Suriname by improving scientific understanding of the coastal ecosystem in Suriname.
The main objective of this thesis is

To increase the understanding of multi-decadal variability in local changes along the Suriname coastal zone induced by the migration of subtidal mudbanks along the entire Guianas' coastline and regional-scale differences in control factors.

To achieve this, 4 research questions have been formulated:

1. How can mudbanks and their fuzzy boundaries be detected in medium-resolution Landsat images given the heterogeneous and dynamic character of the Suriname coastal landscape?
2. What is the spatiotemporal variability in the position of the Suriname coastline imposed by alongshore migrating mudbanks, as mapped from Landsat images available between 1985 and 2020?
3. What is the spatiotemporal variability in coastlines changes along entire Guiana coast and to what extent are these differences due to variability in mudbank footprints or to external control factors?
4. What is the spatiotemporal variability in mangrove loss and gain along the Guiana coast and to what extent can this variability be explained by alongshore mudbank migration?

In **Chapter 2**, an unsupervised decision tree (UDT) is developed to discriminate between different landforms at the Suriname coast, while utilizing the spatial and temporal resolution of the complete Landsat dataset. In **Chapter 3**, the developed UDT is extended to quantify effect of multi-decadal mudbank migration on the dynamics of the Suriname coast. In **Chapter 4** the local difference in coastline changes for the entire Guianas are untangled and linked to the variability in mudbank footprints and compared to various control factors. In **Chapter 5**, a novel temporal segmentation method is applied to detect, quantify and characterize mangrove cover changes at patch level along the Guiana coastal zone with respect to migrating mudbanks. Finally, **Chapter 6** contains the synthesis with an outline of the major findings and a discussion on coastal sustainability in the Guianas.

Chapter 2 | Unmixing water and mud

Abstract

Mapping of subtidal banks in mud-dominated coastal systems is crucial as they influence not only shoreline and ecosystem dynamics but also economic activities and livelihoods of local communities. Due to associated spatiotemporal variations in suspended particulate matter concentrations, subtidal mudbanks are often confined by diffuse and rapidly changing boundaries. To avoid inaccurate representations of these mudbanks in remote sensing images, it is necessary to unmix distinctive reflectance signals into representative land cover fractions. Yet, extracting mud fractions, in order to characterize such diffuse boundaries, is challenging because of the spectral similarity between subtidal and intertidal features. Here we show that an unsupervised decision tree, used to derive spatially explicit and spectrally coherent image endmembers, facilitates robust linear spectral unmixing on an image-to-image basis, enabling the separation of these coastal features. We found that resulting abundance maps represent cross-shore gradients of vegetation, water and mud fractions present at the coast of Suriname. Furthermore, we confirmed that it is possible to separate land, water and an initial estimate of intertidal zones on individual images. Thus, spectral signatures of end-member candidates, determined from relevant index histograms within these initial estimates, are consistent. These results demonstrate that spectral information from well-defined spatial neighbourhoods facilitates the detection of diffuse boundaries of mudbanks with a spectral unmixing approach.

Based on:

de Vries, J., van Maanen, B., Ruessink, G., Verweij, P. A., & de Jong, S. M. (2021). **Unmixing water and mud: Characterizing diffuse boundaries of subtidal mud banks from individual satellite observations**. *International Journal of Applied Earth Observation and Geoinformation, 95,* 102252. https://doi.org/10.1016/j.jag.2020.102252

2.1 Introduction

Accurately mapping boundaries of geomorphological landforms in mud-dominated coasts is crucial for integrated coastal management, and for understanding landscape evolution in these dynamic areas (Koohafkan and Gibson, 2018). These landforms are often associated with the distribution of large sediment concentrations, originating from high-discharge rivers such as the Amazon, Mississippi and Yangtze rivers (Murray et al., 2019). The coalesce of mud is typically favoured when coastlines are confined, wave energy is low and tidal range is large (Anthony et al., 2013), resulting in characteristic landforms and coastline fringing wetland vegetation such as mangroves and salt marshes. In some settings the presence of fluid mud can also trigger the formation of subtidal mudbanks along open coasts (Anthony et al., 2010).

These banks are associated with extreme spatiotemporal variations in suspended particulate matter (SPM) concentrations in the water column (Gratiot and Anthony, 2016). This can be related to their non-linear response to for example, wave climate, tidal stage, currents, proximity to the coastline and liquefaction processes (Vantrepotte et al., 2011). As a result, the boundaries between mudbanks and adjacent heterogeneous coastal features are inherently diffuse and change rapidly. Sediment exchange and increased wave damping potential associated with mudbanks, provide a window of opportunity for mangrove species to colonize large intertidal surfaces (Balke et al., 2011). These mangroves provide regulating services, such as protection against sea level rise and carbon sequestration (Anthony et al., 2013). Hence it is vital to monitor mud-bank dynamics, to support adaptive coastal management and conservation strategies that account for material exchange between these banks and the coastline.

Due to the inaccessibility of mudbanks and the spatial and temporal scales involved in their dynamics, monitoring via remote sensing emerged as a cost effective alternative to field surveys (Augustinus, 1980; Vantrepotte et al., 2011) and aerial photographs (Augustinus et al., 1989). Various methods, including SPM inversion algorithms (Froidefond et al., 2004; Zorrilla et al., 2018), as well as supervised and unsupervised classifications (Anthony et al., 2008), have been developed to estimate mud-bank characteristics. Some of these methods have been applied over increasingly large areas and improved the temporal resolution, especially since the introduction of data-cubes such as Google Earth Engine (GEE) (Gorelick et al., 2017).

At the same time, challenges emerged in the identification of these mudbanks from time-series of satellite observations due to missing data and uneven sampling across tidal stages. This is related to the sun-synchronous orbits of satellite constellations, such as those from Landsat, that never capture the extremes of low- and high-tide with favourable cloud cover (Murray et al., 2019). Previous attempts successfully focussed on extracting spatially coherent information of intertidal features by selecting (Murray et al., 2012) and aggregating observations for specific tidal stages (Sagar et al., 2017). Yet, for subtidal features, resuspension of mud and migration processes at seasonal timescales are responsible for the spatiotemporal variability of their footprints (Zorrilla et al., 2018). This suggests that pixel based image compositing, where one tries to overcome missing data by reducing multiple observations to a single 'best' observation, potentially misrepresents diffuse boundaries and temporal evolution of these features (Koohafkan and Gibson, 2018).

This is related to the fact that reflectance signals describe subtle differences in composition, resulting from radiation interacting with multiple active substances in a pixel (Odermatt et al., 2012). Consequently, the spectral similarity in muddy coastal systems, together with differences in grain sizes, turbidity and soil moisture content, complicates differentiation between subtidal- and intertidal features (Ryu et al., 2002). Accordingly, image analysis techniques that involve semi-

Figure 2.1: Median composite image of available Landsat images between 2008 and 2010 for the region of interest with in the bottom left panel, in white the intertidal area as estimated by Murray et al. (2019). The red line indicates the transect location used in this study, black pixels indicate masked clouds.

automatic unmixing of land cover fractions from distinctive reflectance signals, offer an approach for the analysis of gradients in mud-dominated coastal system that are associated with diffuse mud bank boundaries (Alcântara et al., 2009). Where per-pixel classifiers assign each pixel to a class based on its similarities, unmixing methods model abundance as a linear- or non-linear combination of each provided spectral signature. This means that the presence of more materials within one pixel is estimated, based on the provided end-member signatures (Shanmugam et al., 2006). Especially linear spectral unmixing (LSU) is a convenient unmixing tool to handle mixed pixels, as it does neither require extensive training data nor a computationally demanding analysis (Somers et al., 2011).

The aim of this study was to develop a data-driven approach to analyse diffuse boundaries of mudbanks from individual Landsat images using LSU and cloud computing in GEE. The method is evaluated on its ability to consistently select end-member candidates for the purpose of unmixing land cover fractions of water, mud and vegetation, using a section of the Suriname coast as case study.

2.2 Materials and methods

2.2.1 Study area

The study area is located near Paramaribo, the capital of Suriname (Figure 2.1). This area was selected because it is part of the Guyana coastline, a prime example of a mud-dominated coast

(Augustinus, 1980). About 15-20% of the sediment migrates (0.5-5 km a year) alongshore as mudbanks attached to the coastline, which are continuously reworked by waves and currents (Anthony et al., 2010). Due to the dynamics of these mudbanks, the topography and bathymetry of the Suriname coastline experiences quasi-cyclic variations in erosion and progradation, related to inter-bank and bank phases that last up to 30 years (Allison and Lee, 2004). Trade winds and precipitation vary on a seasonal scale, with more south-easterly trade winds (3-9 m/s) during the major dry season (August-November) and more easterly to north-easterly winds during the major wet season (April – August). This change in wind direction results in higher swell waves in the wet period. The tide is semidiurnal with a range up to 2.5 m during spring tide. As a result of these environmental conditions, the migrating mudbanks continuously change in shape and orientation (Augustinus, 2004; Augustinus et al., 1989), adding to the diffuse character of their boundaries (Vantrepotte et al., 2011).

2.2.2 Selecting end-member candidates

The coastal system of Suriname is characterized by spatially heterogeneous mixtures of vegetation, mud and water. In order to define a collection of spectral signatures that represents these distinct substances, endmembers are identified. Because endmembers from spectral libraries and field surveys do not handle variability between image acquisition very well, a more suitable approach was chosen by deriving these spectra directly from end-member pixels in each image (Somers et al., 2011). For this we used Top of atmosphere (TOA) reflectance data available in GEE (Gorelick et al., 2017). This includes data from geometrically corrected Landsat-4 and -5 Thematic Mapper and Multispectral Scanner system, Landsat-7 Enhanced Thematic Mapper and Landsat-8 Operational Land Images sensors. Any pre-processing steps are described in this section, followed the step-by-step decisions (steps 1-4 in Figure 2.2) made for each pixel, to determine whether it was a candidate endmember for either of the representative land cover types. Such an Unsupervised Decision Tree (UDT) was used to consistently separate land, water and an initial estimate of the intertidal area. By adding this spatial context and these spectral criteria, we selected image endmembers that represent characteristics found in the image at the time of acquisition (Shi and Wang, 2014). The abundance maps that result from the subsequent LSU can therefore indicate the mixed pixels, in our case related to diffuse boundaries.

2.2.2.1. Pre-processing

For each image the flags from the pixel assessment band were used to mask out clouds and shadows, as detected by the automatic cloud mask algorithm (Zhu and Woodcock, 2014). The here used blue, green, red, near infrared (NIR) and shortwave infrared (SWIR) bands have 30 m resolution. The thermal infrared (TIR) band with a resolution of 120 m was resampled to 30 m to match the other bands. From these bands the Normalized Difference Vegetation Index (NDVI) and Normalized Difference Water Index (NDWI) were calculated. The NDWI uses the green wavelengths to maximize the reflectance of water features and simultaneously takes advantage of their low reflectance in the NIR range (McFeeters, 1996):

$$\mathrm{NDWI} = \frac{\mathrm{GREEN} - \mathrm{NIR}}{\mathrm{GREEN} + \mathrm{NIR}} \qquad (2.1)$$

As a result of higher NIR reflectance, both vegetation and mud usually have low or negative values.

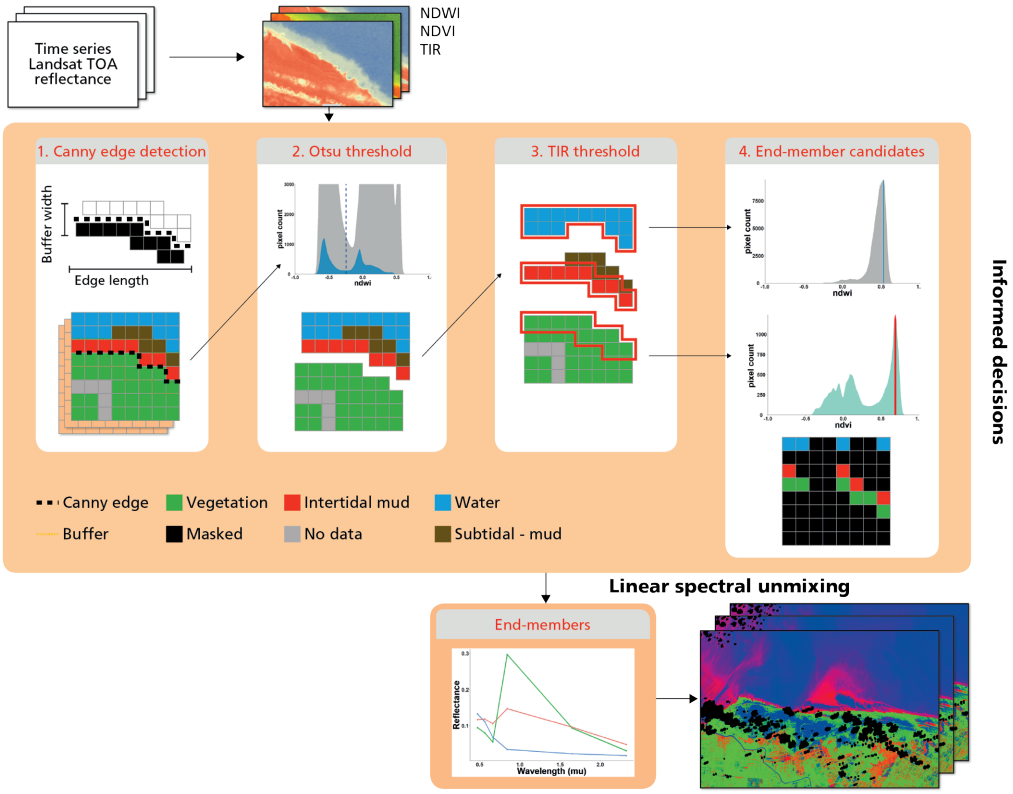

Figure 2.2: Workflow applied to individual image: (1) canny edge detection with the relevant parameters, (2) the Otsu thresholding on the NDWI histogram resulting from canny edge detection, (3) TIR thresholding on the TIR histogram to separate intertidal zone from turbid water, (4) defining the spectral ranges used to select end-member candidates. The resulting end-member graphs are used to apply linear spectral unmixing, resulting in maps representing fractions of water, vegetation and mud.

2.2.2.2. Land or water

After the pre-processing, land and water pixels were separated based on grey level histograms of the NDWI. Therefore a Canny Edge detection algorithm (step 1) was used on these NDWI values to distinguish locally between homogeneous land and water pixels (Liu and Jezek, 2004). This algorithm detects edges by looking for maximum gradients, or sharpest changes of values, in the NDWI image. A Gaussian pre-filter (GPF) filtered noise by smoothing the original image and a minimum gradient (MG) excluded edges with weaker gradients. Subsequently, edges were filtered with a minimal length of connected pixels to avoid selecting discontinuities between other land covers (e.g. urban – agriculture or cloud – shadows). A buffer was applied around these edges, resulting in a set of spatial neighbourhoods. The pixels from these neighbourhoods form a bimodal histogram (Donchyts et al., 2016), emphasizing the difference in spectral properties in the Green and NIR reflection bands for water (NDWI values approaching 1) and land (NDWI values approaching -1) pixels. The adaptive Otsu thresholding algorithm (step 2) was then employed on the smoothed bimodal histogram, to separate the two dominant lobes with distinct mean values,

corresponding to land and water values (Lu et al., 2011). This threshold was used to simultaneously mask terrestrial vegetation and bare ground.

Finally, the mask was updated with land cover classes urban, agriculture and forests from the yearly MODIS land cover classification (Friedl and Sulla-Menashe, 2015). Derived from Terra and Aqua reflectance data, this layer (international Geosphere-Biosphere program classification) was used to ensure urban, agriculture and forest classes were included in the land mask. The relevant pixels were eroded by 120 m to avoid interference in the coastal waters and intertidal surfaces resulting from differences in pixel size.

2.2.2.3. Initial estimate intertidal zone

The spectral similarity between intertidal flats and turbid waters prevents the use of generic thresholds or aggregation of images when trying to separate them (Ryu et al., 2002). Thermal Infrared (TIR) bands are sufficiently sensitive to separate these two classes, but they lack the spatial resolution to extract the waterline (Sørensen et al., 2006). Therefore, an initial estimate of the intertidal zone was made using a thermal threshold (step 3) derived from the modal pixel value in the detected Canny Edge neighbourhood zone (from step 1). This temperature threshold was applied on all water pixels that remained after applying the land mask (step 2). In this way all exposed water pixels with a different radiant temperature were isolated, serving as the initial estimate of the intertidal zone.

2.2.3 Linear spectral unmixing

Unique image histograms, made up of from the canny edge neighbourhood zones and water mask, were used select end-member candidates (step 4). Thus, spatial information to extract the endmembers was added (Shi and Wang, 2014). For vegetation, NDVI values of all land pixels inside the detected canny edge neighbourhood zones were selected (see section 2.2.2.1). This resulted in a histogram with a clearly distinguishable peak that corresponded to dense vegetation. Afterwards, pixels were selected based on a 5% buffer on both sides of this NDVI peak. For the water end-member candidates a similar approach was adopted, deriving the peak NDWI value from the water pixels (see section 2.2.2.2) with a buffer of 1% around it. The driest mud pixels were selected from the initial estimate of intertidal zone (see section 2.2.2.3), excluding vegetation by adopting a NDVI threshold < 0.3. From these sets of pixels, the mean values per band were derived to define the spectral signatures per end-member group.

Fractions of the reflectance signal were untangled by applying the spectral signatures for each endmember to a fully constrained standard linear mixture model (Alcântara et al., 2009):

$$R_i = \sum_{i=1}^{n} P_{ij} f_i + e_i \qquad (2.2)$$

where n is the number of bands, p_{ij} the surface reflectance of land cover type j in band i, f being the fraction of the pixel covered by type j and e_i the error. This model assumes that the total reflectance is the sum of the components that make up the pixel, without interaction between them (Somers et al., 2011). This results in a set of fractions that linearly represent the proportion of each active component to the signal per pixel. Our LSU model was constrained, so that the fractional cover f_j is always between zero and one, and such that the sum cannot be larger than one for each pixel (R_i).

2.2.4 Decision tree performance

Because of limited availability of field observations that can relate end-members and LSU fractions to sediment concentrations and the subtidal footprint of mudbanks in Suriname, validation is restricted here to a robustness check of the described decision tree. Especially in muddy coastal environments the combination of canny edge detection and Otsu thresholding methods can be sensitive to the input parameters (GPF and MG), the buffer width and minimum edge length (section 2.2.2.2.) (Bishop-Taylor et al., 2019). This sensitivity expresses itself in spatial variability of the spatial neighbourhood zones from which to sample end-member candidates, resulting from variability in the Otsu threshold, vegetation peak, water peak and temperature threshold. The temporal consistency of end-member signatures was therefore quantified by comparing changes in Otsu thresholds, vegetation peak, water peak and temperature threshold for parameter combinations for a subset of 88 images, acquired between 2008 and 2010 over Paramaribo, Suriname (Figure 2.1). Values of 0.3, 0.5, 0.7, 0.9 and 1 were used for the GPF; for the MG values of 0.7, 0.9, 1.1 and 1.3; minimum length values of 10, 25, 50 and 75 pixels; for the buffer values of 5, 10 and 15 pixels were tested.

2.3 Results

2.3.1 Image histograms

To show the benefits of using an UDT and the application of the resulting fractions for the purpose of analysing cross-shore gradients of mud, water and vegetation fractions, two relatively cloud-free Landsat-5 images were selected from the subset (see section 2.2.4.). The image acquired on 12 September 2009 was captured near high-tide while the second image, acquired on 15 November 2009 was captured near low-tide. A GPF of 0.7, MG of 0.9, buffer width of 10 pixels and minimum length of 25 pixels were used to derive the canny edge neighbourhood zones. Based on their different NDWI histograms, made up of pixels in these zones, image specific thresholds of -0.186 and -0.246 were derived to separate land and water pixels (Figure 2.3, panel A). In the high-tide and low-tide images the NDWI peaks, between 0.422 – 0.438 and 0.524 – 0.534, correspond with water end-member candidates (Figure 2.3, panel B). For vegetation end-member candidates the peak values, derived from histograms with pixels from the canny edge neighbourhood zones, were between 0.684 - 0.696 and 0.678 - 0.700 (Figure 2.3, panel C). Mud pixels were separated from water pixels that remained after applying the land mask, based on a radiant temperature threshold of 296 and 294.2 Kelvin for low- and high-tide (Figure 2.3, panel D). These observations of unique threshold values illustrate the rationale behind the decision to apply an UDT procedure that automatically separates land, water and an initial estimate of the intertidal zone. Threshold values for the low- and high-tide image, derived with alternative input parameters are shown in Table A1 (Appendix A).

2.3.2 Fractions

In Figures 2.4 and 2.5 fractions of vegetation, water and mud, from the selected high- and low-tide image, respectively, are compared along a 30 km cross-shore transect (see Figure 2.1). These profiles reveal that the outlined approach was able to generate abundance maps of the end-member classes that match expected cross-shore patterns. Namely, the mud fractions show a discontinuous decrease for the visually estimated subtidal part, from 0.95 to 0.50 during low tide (Figure 2.4). The water fractions show a contrary pattern, implying variable SPM concentrations. At around 6,000 – 6,041

m the ratio of mud and water fraction changes more quickly; more specifically this rearmost rapid decline of mud abundance reveals a diffuse, and thus seaward mud-bank boundary.

During high tide (Figure 2.5) absolute mud-fractions were significantly lower over the visually estimated subtidal mud bank, ranging from 0.30 to 0.10. This difference can potentially be attributed to the amount of SPM, variable tidal elevation, wave climate (Zorrilla et al., 2018) or difference in spectral signatures. For this reason, it is more difficult to use an absolute fraction value as indication of diffuse mud-bank boundaries. Still, like the low-tide transect, the rearmost decline in mud abundance around 5,982 to 6,000 m suggests the same seaward mud-bank boundary.
The edge of the land mask remained fixed at its position around 817 m, between 12 September 2009 and 15 October 2009. This location coincided with a decreasing vegetation fraction, from 1 to ± 0.25 for both images, indicating that the detected boundary between land and water follows the mangrove fringe. The lower vegetation fractions seaward of this fringe may correspond to a change in vegetation type, the presence of microphytobenthos or even sparse mangroves standing in turbid waters.

The intertidal extent visible during low tide, that is, the cross-shore distance between the land mask edge and sea-mudflat boundary, coincides with scattered mud fractions between 817 m and

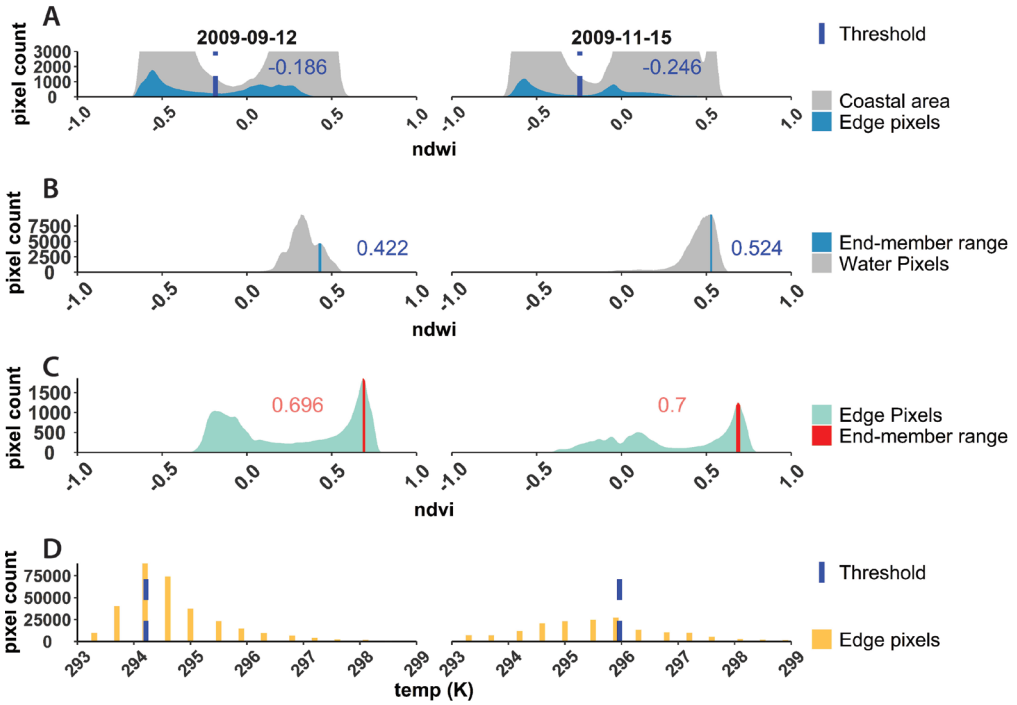

Figure 2.3: The histograms for the high-tide (left column) and low-tide (right column) image that are used to derive end-member candidates. Panel A shows the histogram (blue) used for separating land and water with the corresponding Otsu threshold for the selected images. In grey the histogram is shown corresponding to all pixels in the coastal zone. Panel B and C indicate the ranges of index values used for selecting the water and vegetation end-member (NDWI for water, NDVI for vegetation). The temperature threshold (in Kelvin), shown in panel D, indicates the value used to separate intertidal mud from water pixels and is based on the histogram derived from land pixels in the detected canny edge neighborhood zones.

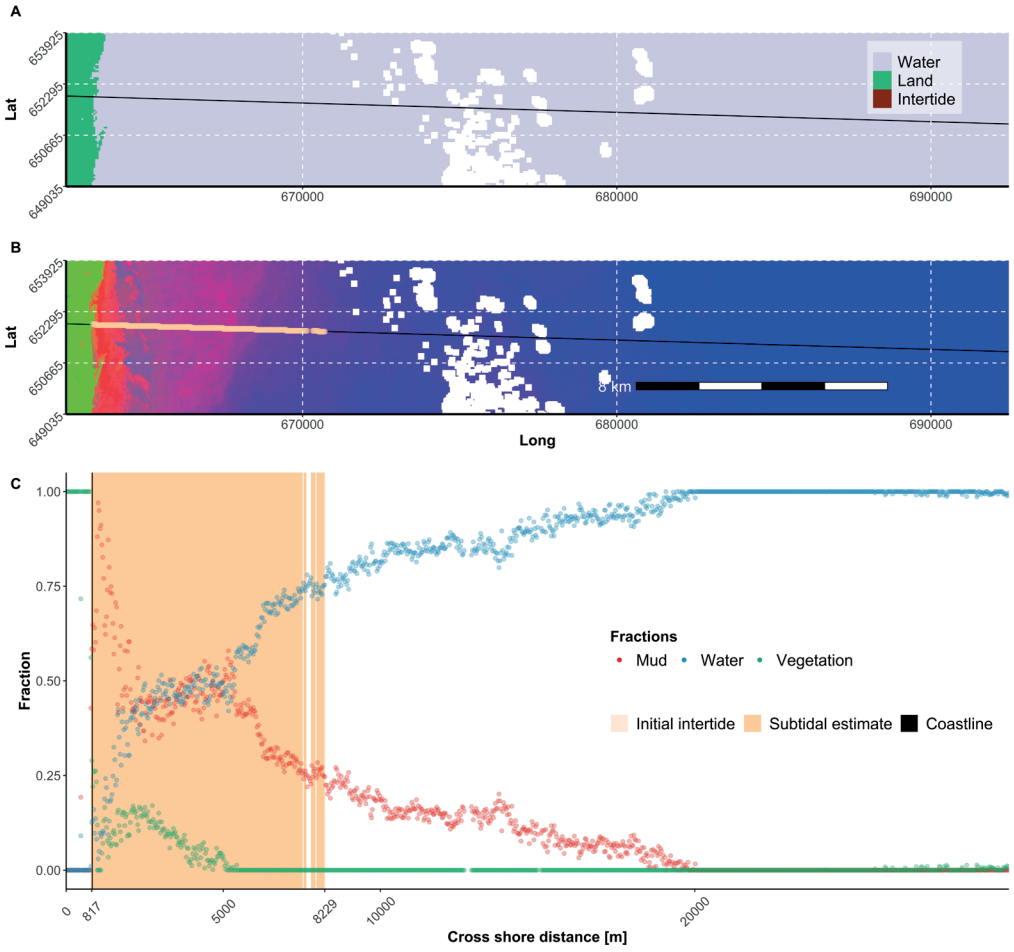

Figure 2.4: Cross-shore patterns in pixel fractions for the defined end-member classes for the low-tide image (15-11-2009). The land mask, derived by applying a threshold value of -0.246, is shown in panel A. Panel B shows the LSU fraction outputs in RGB (R = mud, G = vegetation and B = water). Panel C shows the cross-shore development of fractions and the land mask boundary at 817 m. The subtidal extent of the mud-bank is visually estimated to align it with the rearmost rapid decline of mud abundance. Patches in panel A and B indicate masked clouds.

roughly 2,000 m (Figure 2.4). For the high-tide image (Figure 2.5), the intertidal zone was also visible from the initial estimate based on the TIR threshold. These results highlight that the image's TIR threshold did not match the local thermal difference between water and land locally, due to weather conditions and shallow water depths in the low-tide image.

2.3.3 Robustness of the approach

To test the robustness of the UDT approach, all available Landsat images (88) between 2008 and 2010 were selected. A total of 68 images resulted in explicit end-member candidates that could be used to extract spectral signatures for LSU. The excluded images did not contain enough detected

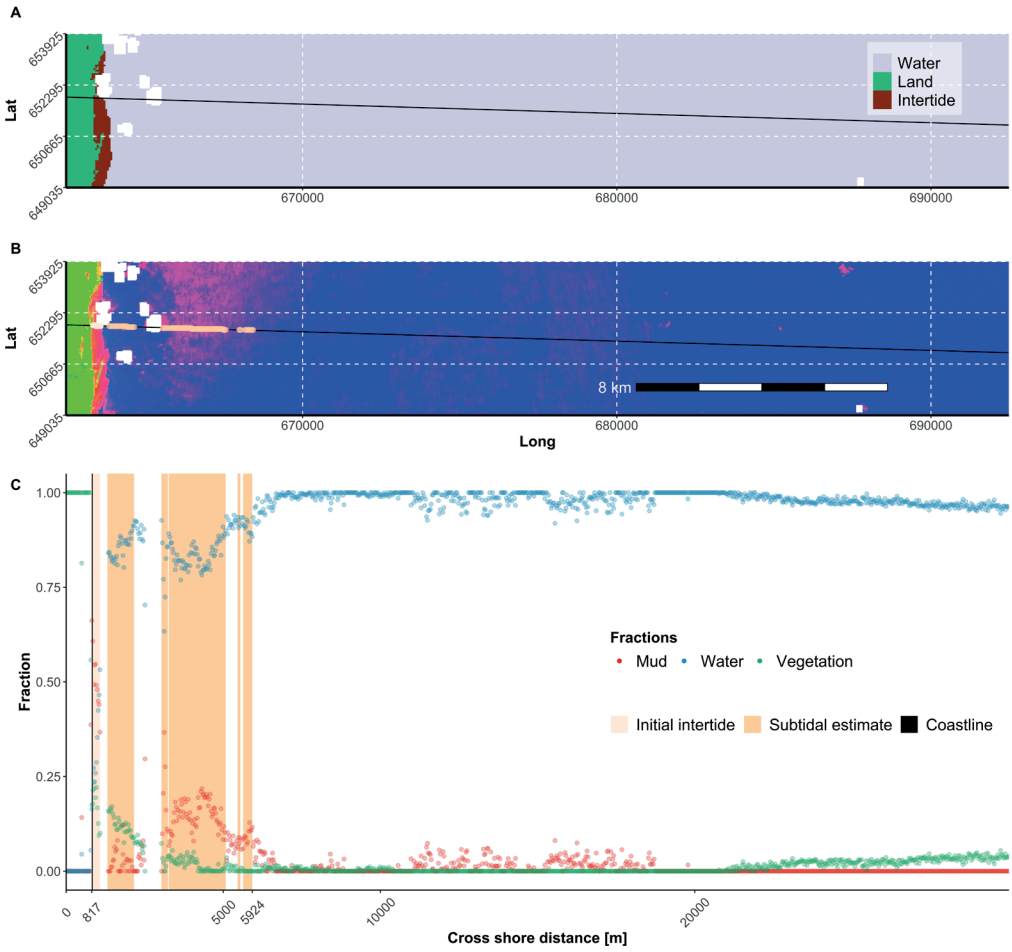

Figure 2.5: For the same location as in Figure 2.4, now during high tide (12-9-2009). The in initial estimate of the intertidal extent and land mask, derived by applying a threshold value of -0.186 are shown in panel A. Panel B shows the LSU fraction outputs in RGB (R = mud, G = vegetation and B = water). Panel C shows the cross-shore development of fractions and the land mask boundary at 817 m. The subtidal extent of the mud-bank is visually estimated to align it with the rearmost rapid decline of mud abundance. Patches in panel A and B indicate masked clouds.

canny edge neighbourhood zones to sample endmembers from, while matching the UDT informed decisions. Figure 2.6 shows the reflectance variation of all endmembers of vegetation, water and mud. Although images originated from different sensors, they show similar values and recognizable signatures within the same order of magnitude.

The NDWI threshold to separate land and water proved to be an important parameter in the UDT workflow. With each parameter combination in the canny edge computation the median value, range and distribution of threshold values changed slightly (Figure 2.7), especially when comparing them to the stable NDVI peaks and TIR thresholds for the same parameter combinations (Figure A1 and A2, appendix A). For all parameter combinations the NDWI

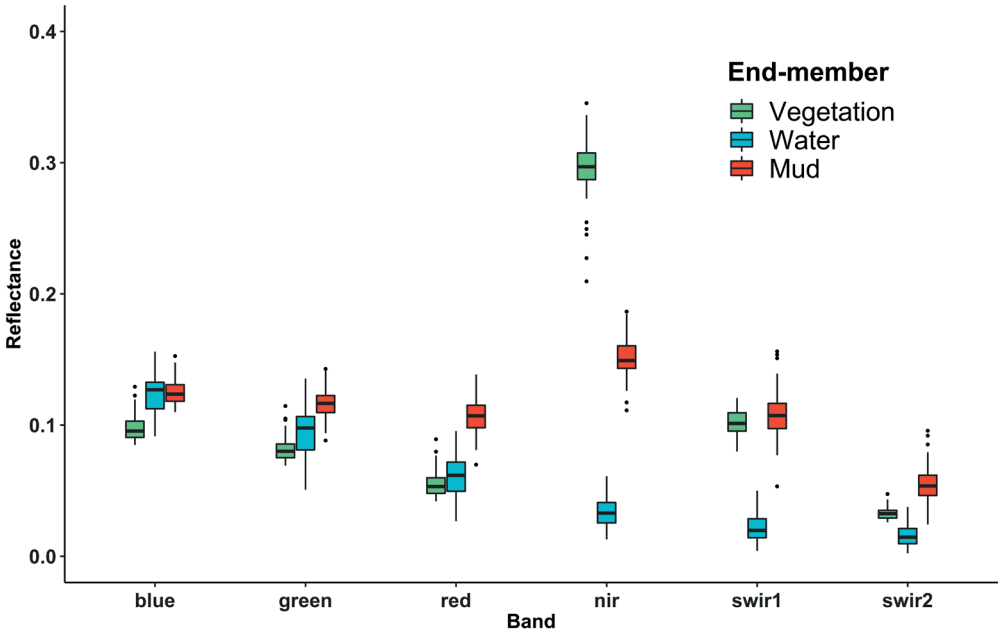

Figure 2.6: Variation in spectral signatures for the baseline scenario with a buffer of 10 pixels, a minimal length of 25 pixels, a gaussian pre filter sigma 0.7 and a minimal gradient of 0.9. End-member signatures are taken from selected images between 2008 and 2010.

threshold ranged from -0.326 to -0.050, with outliers up to 0.034 (Figure 2.8). Especially with MG values of 1.1 or 1.3, a higher GPF reduced the Otsu threshold, while the opposite can be seen for an MG of 0.7 (Figure 2.7). This implies that the combination of MG and GPF influenced the edge detection, and thus the NDWI histogram used to separate land and water pixels. The NDWI threshold reduced also with an increasing buffer size (Figure 2.8), because of the larger amount of land and mixed pixels included in larger buffers. The opposite can be seen when increasing the minimum length of detected canny edges (Figure A3, Appendix A). This effect disappears for MG > 1.1, suggesting that the effect of filtering on a minimal edge length is comparable with applying a higher MG threshold. Hence, the higher the MG, the more likely these larger magnitude changes in NDWI are detected; with the potential of not detecting any boundaries at all with a MG > 1.1 and GPF > 0.5. These results show that it is possible to consistently select boundaries from NDWI images that correspond with transitions from land to water. This robustness is supported by table A1 (see appendix A) where four parameter combinations were applied on the selected low- and high-tide images. The variation in NDWI threshold resulted in differences in land-water boundaries, and thus selection of end-member candidates. Yet, both the signal to noise ratio of the end members and mean LSU error (see equation 2) remained consistent.

2.4 Discussion

2.4.1 Gradients and diffuse boundaries

By using spatial selection criteria for the definition of robust image endmembers, we developed an UDT for analysing diffuse boundaries of subtidal mudbanks. The pixel fractions resulting from the

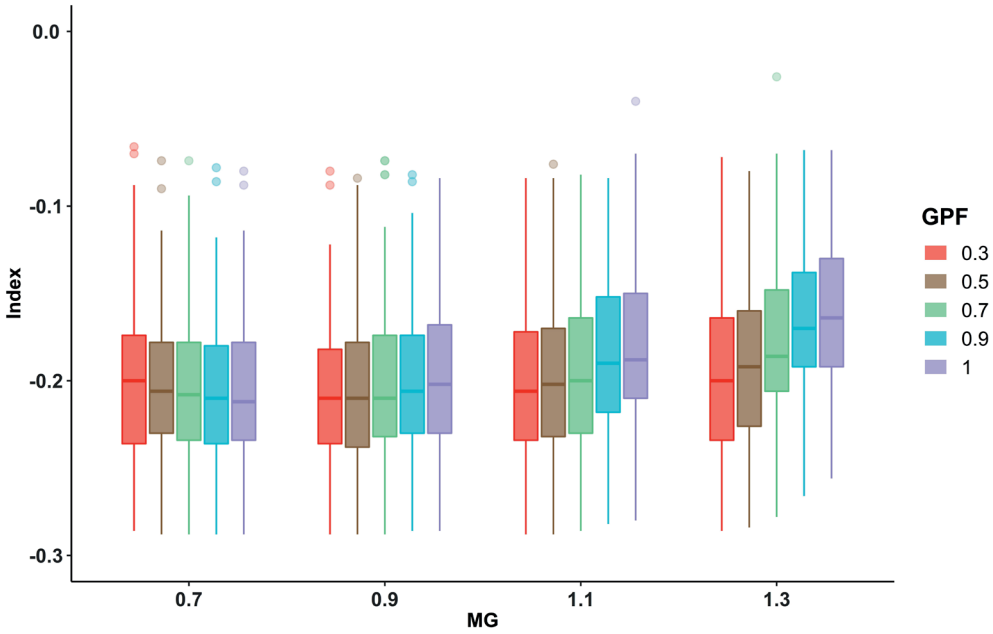

Figure 2.7: Variation in the NDWI threshold, used to separate land and water, for different input parameters sets variation of the minimal gradient (0.7, 0.9, 1.1 and 1.3) and gaussian pre filter sigma (0.3, 0.5, 0.7, 0.9 and 1). Minimum length of the edges and buffer size around them are fixed at the defaults of 25 and 10 pixels, respectively

LSU represent mud, vegetation and water gradients, as shown in the selected transect for a low-tide and high-tide image (Figure 2.4 and 2.5). Thus, we account for mixed pixels and avoid aggregating multitemporal image observations with different tidal heights.

The mud fractions show a discontinuous decrease in the offshore direction for both selected images (Figure 2.4 and 2.5). Yet, more abrupt changes at 6,041 and 5,982 m in both mud and water fractions indicate changes in the presence of mud in the upper water column. These are considered fuzzy transitions between higher and lower mud concentrations, corresponding with diffuse boundaries of mudbanks. This indicates that, despite differences in tidal elevation and the time between acquiring the images, this seaward mud bank boundary remains relatively stable at approximately 6,000 m offshore. The remaining difference can be attributed to mud bank migration and the temporal variability of SPM concentration, resulting from waves, tides and currents (Zorrilla et al., 2018). Absolute values of mud fractions in the estimated subtidal area also varied between the two images, with lower mud fractions for the high-tide image than for the low-tide image. This reflects the difference in sediment concentrations, preventing the use of an absolute mud fraction threshold to indicate diffuse boundaries.

2.4.2 Intermediate results

Besides the pixel fractions, the intermediate results, so far mainly used in the UDT procedure, show promising signs of added value. For example, Figure 2.5 indicates that the intertidal zone can be estimated with the TIR band, when image quality is sufficient. In our case this allowed us to isolate pure mud pixels as endmember for the entire image. The undetected intertidal area in Figure 2.4 is an example where the image TIR threshold locally didn't result in an estimate of the intertidal area.

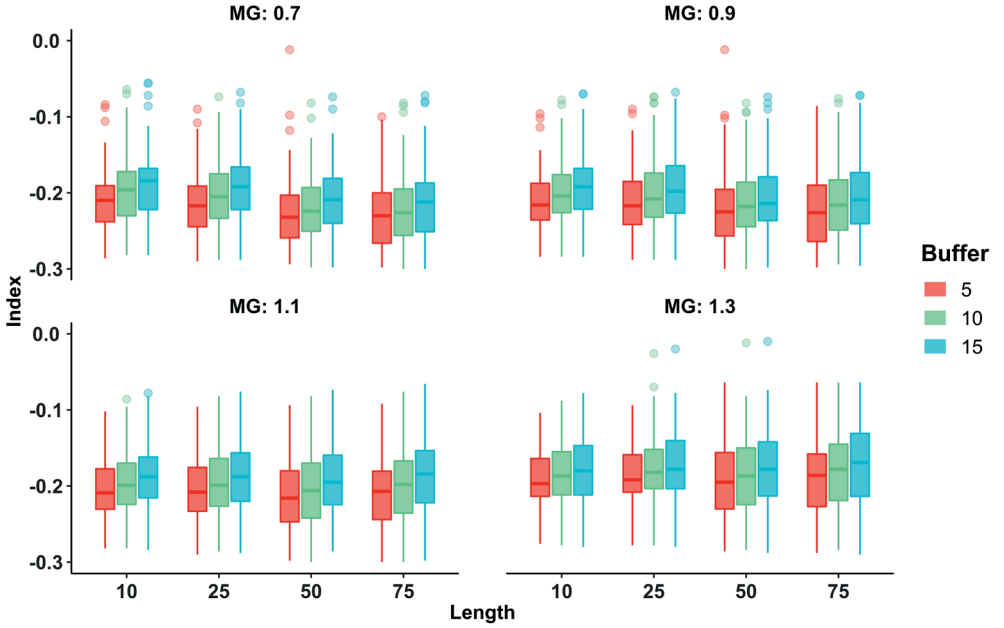

Figure 2.8: Variation in the NDWI threshold (n = 68) used to separate land and water for different input parameter set: variation of the buffer size (5, 10 and 15 pixels), different minimum edge length values (10, 25, 50 and 75 pixels) and MG values (0.7, 0.9, 1.1 and 1.3) and the GPF is set at its default of 0.7.

However, when the threshold is determined locally from well-defined spatial neighbourhoods, the intertidal zone can be demarcated more precisely. This is in line with findings from earlier studies that relate exposure time and intertidal topography to de difference in thermal irradiance between land and water (Ryu et al., 2002; Sørensen et al., 2006).

The boundaries of the terrestrial land masks, for example between 12-09-2009 (Figure 2.5) and 15-11-2009 (Figure 2.4), were consistently estimated at 817 m. As a result it becomes possible to analyse transitions from intertidal- to terrestrial land cover classes without using a static global or regional land mask product (Laengner et al., 2019). Especially in Suriname, where analysis of coastal morphology is hampered by limited data availability and changes are rapid and omnifarious, this type of spatial information can be beneficial to coastal managers. It allows for example to detect changes in vegetation composition for terrestrial and intertidal zones and incorporate that in coastal conservation- and protection measures.

2.4.3 Robustness and sensitivity

The sensitivity analysis on the NDWI threshold provided a better understanding of the capabilities of combining canny edge detection algorithm and Otsu thresholding for separating land and water pixels. The range of unique NDWI thresholds supports earlier observations (Bishop-Taylor et al., 2019) that especially in mud-dominated systems, a dynamic threshold is required to separate sea from land.

We found that the canny edge algorithm complemented with buffer and length filters results in a consistent, spatially explicit and robust neighbourhood zone when the MG and GPF are set appropriately. By applying a sufficiently large length filter, only true land-water boundaries are included (Figure A3). For a larger buffer, when more pixels are included, the threshold values shift towards the land lobe of the histogram. This implies that more pixels are included in the terrestrial land mask, resulting in the boundary shifting seaward. Nonetheless, the resulting neighbourhood zone consistently creates histograms that can be used to estimate representative image endmembers from ranges in both NDWI and NDVI values. This is supported by the relatively small temporal variation in spectral endmembers, sampled from these neighbourhoods, which we observed for all images between 2008 and 2010 in the area (Figure 2.6). This facilitates the comparison of the linear spectral unmixing outputs for different images.

2.4.4 Limitations & improvements

A disadvantage of the outlined approach is that resulting fractions are only approximations of SPM or vegetation cover, as non-linear responses in reflectance spectra are not accounted for (Somers et al., 2011). Moreover, the spectral signatures of the image endmembers were not selected based on their pixel purity but rather on spatial and spectral selection criteria. However, monitoring requires an objective and standardized end-member extraction technique that allows for spatiotemporal analysis of LSU outputs (Figure 2.4 and Figure 2.5). The here discussed UDT approach consistently selects these endmembers and thus results in comparable LSU outputs between different dates and environmental conditions during acquisition.

Also, automatically estimating the position of the seaward boundary of mudbanks from the LSU outputs remains a future improvement. As we showed in the fraction profiles (Figure 2.4 and Figure 2.5), the cross-shore transects reveal multiple rapid declines of mud fractions, indicating diffuse boundaries. Especially automatically selecting the rearmost rapid decline requires additional advancements in processing the LSU outputs and sufficient field observations for validation. This diffuse boundary position estimate is required to facilitate multitemporal position analysis of mud-bank footprints. The thresholds and index ranges used to define end-member candidates can then be used to assess the suitability of the image in a timeseries analysis, compared to for example only using estimates of cloud cover.

2.5 Conclusions

We developed a data-driven method that facilitates the detection of diffuse boundaries of subtidal banks along mud-dominated coastlines, as exemplified for a section of the Suriname coast. The developed unsupervised decision tree includes 1) advances in separating land and water with Otsu thresholding, 2) a novel approach to automatically estimate the intertidal zone and 3) an assessment of cross-shore gradients in mud, water and vegetation fractions from individual Landsat observations. We reaffirm that efficiently separating land and water is possible in mud-dominated coastal systems by defining a spatial neighbourhood with an edge detection algorithm applied to the NDWI index. However, selecting the appropriate input parameters is a non-trivial exercise. The resulting terrestrial boundary allows the separation of the remaining exposed intertidal zone from water, based on a temperature threshold. Consistently sampling potential end-member candidates from these initial estimates of water, intertidal and land surface can be done from their index histograms. The resulting spatially explicit and spectrally coherent image endmembers facilitate multitemporal LSU outputs with fraction maps of water, vegetation and mud. From these,

spatiotemporal differences in their sub-pixel proportions can indicate much needed information about changing gradients and the presence of coastal features.

Supplementary Materials

https://code.earthengine.google.com/?accept_repo=users/jobdevries90/MangroMud

Chapter 3 | Multi-decadal coastline dynamics in Suriname controlled by migrating subtidal mudbanks

Abstract

For the development of climate-resilient coastal management strategies, which focus on challenges in the decades to come, it is critical to incorporate spatial and temporal variability of coastline changes. This is particularly true for the mud-dominated coastline of Suriname, part of the Guianas, where migrating subtidal mudbanks cause a cyclic instability of erosion and accretion of the coast that can be directly related to interbank- and bank phases. The coastline hosts extensive mangrove forests, providing valuable ecosystem services to local communities. Recent studies on mudbank dynamics in Suriname predominantly focused on large-scale trends without accounting for local variability, or on local changes considering the dynamics of a single mudbank over relatively shorter time scale. Here we use a remote sensing approach, with sufficient spatial and temporal resolution and full spatial and temporal coverage, to quantify the influence of mudbank migration on spatiotemporal coastline dynamics along the entire coast of Suriname.

We show that the migration of six to eight subtidal mudbanks in front of the Suriname coast has a strong imprint on local coastline dynamics with an average 32 m/yr accretion during mudbank presence, and 4 m/yr retreat of the coastline during mudbank absence between 1986 and 2020. Coastal erosion can, however, still occur when mudbanks are present and coastal aggregation may happen in the absence of mudbanks, exemplifying local variability and thus suggesting the importance of other drivers of coastline changes.

Based on:

de Vries, J., van Maanen, B., Ruessink, G., Verweij, P. A., & de Jong, S. M. (2022). **Multi-decadal coastline dynamics in Suriname controlled by migrating subtidal mudbanks**. *Earth Surface Processes and Landforms, 47 (10)*, https://doi.org/10.1002/esp.5390.

3.1 Introduction

Coastal wetlands provide a livelihood for local communities and simultaneously provide services that include coastal protection, enhanced carbon storage and habitats provision for both wild- and ocean life (Kirwan and Megonigal, 2013). Yet, these economically and ecologically important ecosystems, including mangroves, saltmarshes and tidal flats, are under constant pressure from climate change, natural disturbances and increasing anthropogenic activities (Friess et al., 2012). Variable responses of coastal ecosystems to forcing mechanisms pose challenges for the development of climate resilient management strategies that need to account for changes in coastal zones that might occur in the coming decades (Dolan et al., 1991).

Mangrove forest are (sub) tropical ecosystems typically located in sheltered coastal environments such as estuaries and tidal embayment's, where climatic drivers, tidal currents and sediment dynamics control their distribution, abundance diversity and dynamics (Osland et al., 2017; Woodroffe et al., 2016; Xie et al., 2020). At the same time, mangroves can also occur along open coasts, changing forcing mechanisms that determine the long-term fate of these ecosystems compared to sheltered mangrove forests. In such open settings, mangrove forests can expand seaward when waves are low and sediment availability is sufficiently high, or retreat when the opposite is true (Pardo-Pascual et al., 2012). On top of that, variability in coastline positions can occur gradually or episodically, with alternating phases of stability, retreat and progradation (Stive et al., 2002). This is because the driving processes operate at varying spatial- and temporal scales, like the redistribution of sediment, anthropogenic interference, sea level rise or hydro-meteorological forcing mechanisms (Ellison, 2015; Luijendijk et al., 2018).

The coastal zone of the Guianas, stretching from the mouth of the Amazon River to the Orinoco Delta in Venezuela, shows exactly this spatiotemporal variability in coastline dynamics (Anthony et al., 2013a; Toorman et al., 2018). Earlier work already linked this to the migration of subtidal mudbanks, consisting of fine grained sediments that originate from the Amazon River and are transported along the coast (Augustinus et al., 1989; Eisma and Marel, 1971). A mudbank is for the most part a muddy subtidal feature, obliquely attached to the coast through its subaerial intertidal extension (Wells and Coleman, 1981b).

Migrating mudbank are only found in a few places around the globe including India (Samiksha et al., 2017) and the USA (Taylor and Purkis, 2012). In the Guianas these mudbanks are longer and wider and migrate more quickly; they can therefore be identified by their irregular and triangular shape that can extend up to 20 km offshore and on average 30 km alongshore (Chevalier et al., 2008). Conceptually, where a mudbank migrates alongshore under the influence of waves and currents, coastal accretion can be initiated. This is due to enhanced wave damping and increased sediment deposition near the coastline that is associated with these mudbanks (Winterwerp et al., 2007). Consequently, mud flats form and pioneer mangrove species colonize these flats, further enhancing mud deposition and attenuation of waves (Balke et al., 2011; Baltzer et al., 2004; de Jong et al., 2021). Finally, when the mudbank after 10-15 years has migrated further, the coastline and mangrove ecosystems are again susceptible to enhanced erosion as a result of increased wave activity (Anthony et al., 2010; Toorman et al., 2018).

The conceptual model of mudbank migration has been extensively studied, including field observations of mangrove development and coastline evolution (Augustinus, 2004; Wells and Coleman, 1981a). Also, studies using a variety of publicly available remote sensing observations, including radar, medium-resolution multispectral satellite observations and aerial photographs show that coastlines of the Guianas are changing due to migrating mudbanks (Baghdadi et al.,

2004; Vantrepotte et al., 2013; Walcker et al., 2015). In fact, it was pointed out that a variety of mechanisms may affect mudbank dimensions, migration speeds and thus coastline changes. Especially waves, but also other controlling factors such as variable trade wind regimes (Augustinus, 2004), the 18.6 year nodal tidal cycle (Gratiot et al., 2008), coastline angle and coastal currents (Lefebvre et al., 2004) are deemed important. This implies a degree of complexity at local scales, going beyond relatively simple alternating phases of erosion and accretion that, despite the attention, are not well understood.

As coastline changes are reflecting the complex interplay between controlling factors (Boak and Turner, 2005), it is necessary to interpret changes from datasets that have high temporal and spatial resolution, cover large stretches of coastline and go back at least one complete cycle of mudbank migration including a bank- and interbank phase (Li and Gong, 2016). This avoids masking of trends, due to for example changing water-levels (Klemas, 2013) and allows capturing subtle local effects within a broader regional context (Almonacid-caballer et al., 2016). Yet, it also remains challenging to differentiate between subtidal mudbanks, that can extend to intertidal parts of the coastal area, and other coastal land cover classes. Especially when preferred 3D observations, from for example LiDAR, GNSS or Terrestrial Laser scanners, are lacking or have insufficient spatial- and temporal coverage, we rely on two-dimensional interfaces that are visible in images (Moore et al., 2006). Especially the Landsat archive can be considered as a consistent source of long-term observations with an unprecedented combination of global coverage and a high temporal- (16 days return period) and spatial (30 m) resolution (Mondal et al., 2018; Xu, 2018).

The aim of this study is to quantify the effect of mudbanks being present or absent on long-term spatiotemporal dynamics of local coastline changes in Suriname from medium-resolution Landsat imagery. We used an Unsupervised Decision Tree (UDT) that has the ability to extract coastline positions and estimate spatiotemporal differences in mud gradients (de Vries et al., 2021; Chapter 2) on the available Landsat images between 1986 and 2020. This series of decisions incorporates a Linear Spectral Unmixing (LSU) model, necessary to estimate sub-pixel coverage of the three dominant types of land cover in muddy coastal ecosystems: water, vegetation and bare consolidated mud. The sub-pixel approach is required because medium-resolution pixels often contain mixed spectral signals, especially in inter- and subtidal regions due to the presence of diffuse boundaries between different land-use classes (Odermatt et al., 2012). This especially hampers the identification of mudbanks in the upper water column, that are rapidly changing as a result of wave climate, tidal flow and river outflow (Zorrilla et al., 2018). While it is the detection of mudbank presence that is required to separate their effect on coastline changes from other forcing mechanisms.

3.2 Study area

The sparsely populated coastal region of Suriname can be divided into three regions that are intersected by the Suriname River near Paramaribo and the Coppename River (Figure 3.1). This area receives an average of 2-3 m of annual rainfall, of which most falls in the wet seasons between December-February and April-July. Despite high precipitation, the rivers in Suriname have relative low discharges (~150 km^3/yr) and suspended loads (1-130 mg/L), especially compared to the total along-shore sediment transport and the mud supply originating from the Amazon River (Willems et al., 2015). Nearshore brown waters, between zero and twenty km offshore, have a high turbidity that can be associated with the suspension of muddy sediments or presence of mudbanks (Figure 3.1).

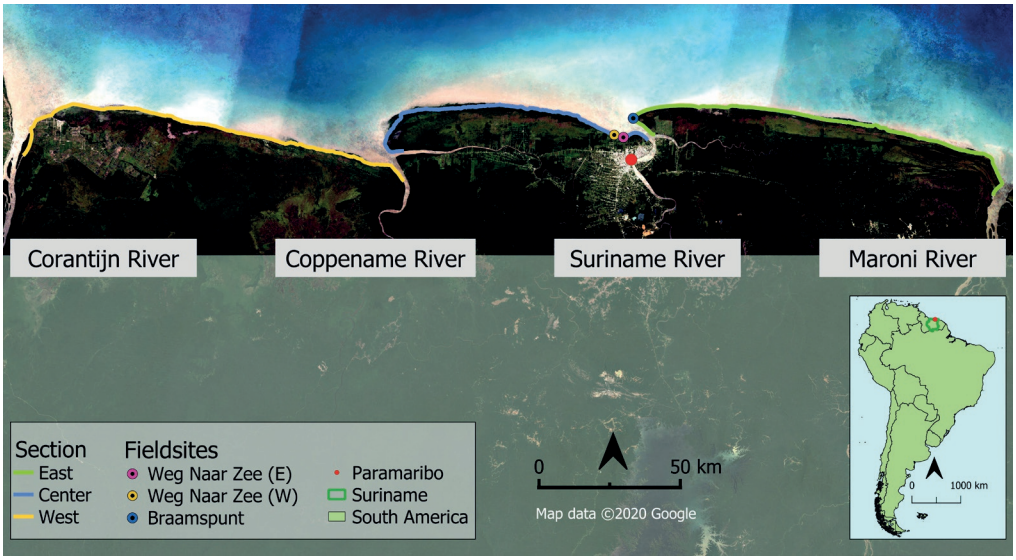

Figure 3.1: The coastal area of Suriname with the different coastline sections. The eastern section is situated between the Maroni and Suriname River, the western section between the Corantijn River and the Coppename River and finally the centre section of the coastline is located in between the Coppename River and Suriname River. The field sites near Weg naar Zee (2x) and Braamspunt that are used for the validation, are also shown. The image is an RGB median composite of all Landsat observations available between 2017 and 2019, clearly showing the high concentrations of sediment that are associated with the presence of subtidal mudbanks.

The dominant wind direction at the coast is from northeast to the southwest during all months of the year. The majority is coming from northeast to eastern directions, with average speeds ranging from 3 to 9 m/s. Relative stronger winds between December and April coincide with most energetic offshore waves, up to two meters significant wave height and periods of 6-10 s (Anthony et al., 2010). This wave-dominated coastal regime shows variations in wave height at timescales ranging from annual to multi-decadal timescale, caused by North Atlantic Oscillation phases and other large-scale atmosphere-ocean interactions (Walcker et al., 2015).

Tides along the coast of Suriname are semi-diurnal with a micro to mesotidal scale, ranging from 1.5 to 3 m (Rine and Ginsburg, 1985). The resulting tidal currents are orientated perpendicular to the coastline which is especially relevant for sediment transport in the mouth of rivers (Augustinus, 2004). All along the coast the Guiana current runs parallel to the coast with a velocity varying between 0.2 to 0.6 m/s in the nearshore zone (Pujos and Froidefond, 1995) and 0.5 to 0.9 m/s outside the coastal boundary (Wells and Coleman, 1981b). The nearshore currents, directly related to residual currents due to wave breaking and tidal flow, contributes to the alongshore migration of mudbanks (Allison et al., 1995; Gratiot et al., 2007). Although coastal dynamics in Suriname are mainly driven by natural processes and interactions between waves, currents, sediment transport and mangrove growth, anthropogenic activities interfere with these natural processes and can locally modify coastal behaviour (Nijbroek, 2014). This includes the building of dikes, removal of mangroves, conversion to agriculture, and the development of aquaculture.

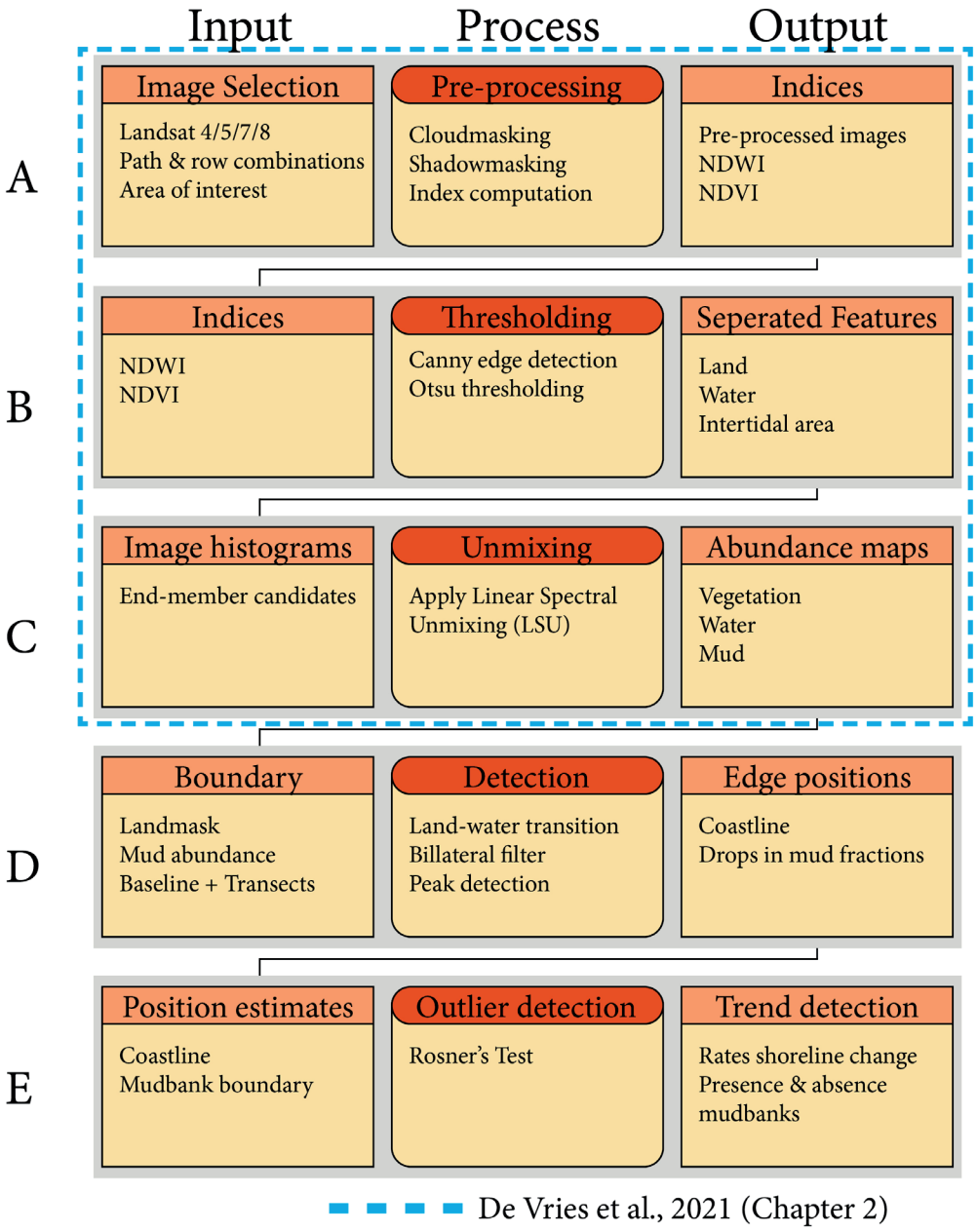

Figure 3.2: The applied workflow used to extract coastline positions and simultaneously determine the presence or absence of mudbanks in Landsat observations. The steps from the used Unsupervised Decision Tree (UDT) are indicated with the blue dashed line (step A-C). The resulting binary land mask and mud abundance map were then used to estimate the presence of mudbanks simultaneously with the coastline position (step D-E).

3.3 Methods and data

We studied the spatial and temporal dynamics of the Suriname coastline between 1986 and 2020, in relation to alongshore migrating mudbanks. We therefore first applied an Unsupervised Decision Tree (UDT; de Vries et al., 2021; Chapter 2) inside the Google Earth Engine environment (GEE; Gorelick et al., 2017). Afterwards, intermediate outputs from the UDT, consisting of binary land masks and mud abundance maps (Figure 3.2, step A-C), were analysed for the presence or absence of mudbank boundaries in relation to estimates of coastline positions (Figure 3.2, step D-E). All steps, including a short summary of the UDT, are described below.

3.3.1 Pre processing and UDT

In this work we applied the UDT and subsequent workflow on all Top of Atmosphere (TOA) images collected over the coastal area of Suriname between 1986 and 2020 by Landsat 4, 5, 7 and 8. These tier-1 products are corrected for atmospheric, illumination and viewing geometry effects, with estimated spatial accuracy sufficient for timeseries analysis (Vos et al., 2019).

Due to high cloud-cover throughout the year in the study area, the pixel assessment bands were first used to mask out clouds and shadows in all images. To minimize false detection of coastline changes, biased estimates of spectral indices and inaccurate representation in mud abundance maps due to undetected shadows, an additional masking step was implemented (step A, Figure 3.2). By using the pixels that were initially indicated as clouds and the image metadata describing the solar azimuth, different shadow paths were estimated on a range of pre-defined cloud heights. Within these paths, pixels that reflected low in Near Infrared (NIR) and two Shortwave Infrared (SWIR1 and SWIR2) bands were considered shadow pixels (Housman et al., 2018).

For the non-cloud pixels Normalized Difference Water Index (NDWI) and the Normalized Difference Vegetation Index (NDVI) were calculated according to:

$$\mathrm{NDWI} = \frac{\mathrm{GREEN} - \mathrm{NIR}}{\mathrm{GREEN} + \mathrm{NIR}} \tag{3.1}$$

$$\mathrm{NDVI} = \frac{\mathrm{NIR} - \mathrm{RED}}{\mathrm{NIR} + \mathrm{RED}} \tag{3.2}$$

The NDWI uses the reflection in both green and NIR wavelengths to maximize the difference for water features compared to non-water features (McFeeters, 1996). As a result, vegetation and mud usually have low or negative values, whereas water has positive NDWI values. Similarly, the NDVI uses the difference in NIR and red reflectance to indicate vegetated pixels with positive values (Tucker, 1979).

The NDWI index was first utilized to detect the interface between land and water (Donchyts et al., 2016). A Canny edge detection algorithm was used to detect local edges based on gradients in the NDWI image (Liu and Jezek, 2004). After filtering these edges on a minimum length, and buffering the remaining edges, a set of spatial neighbourhoods remained (Figure 3.2, Step B). The bimodal histograms resulting from pixels in these neighbourhoods, reflect the difference in spectral properties between land and water that is contained in the NDWI index (Donchyts et al., 2016). An Otsu thresholding algorithm was applied to separate these two dominant lobes in the resulting

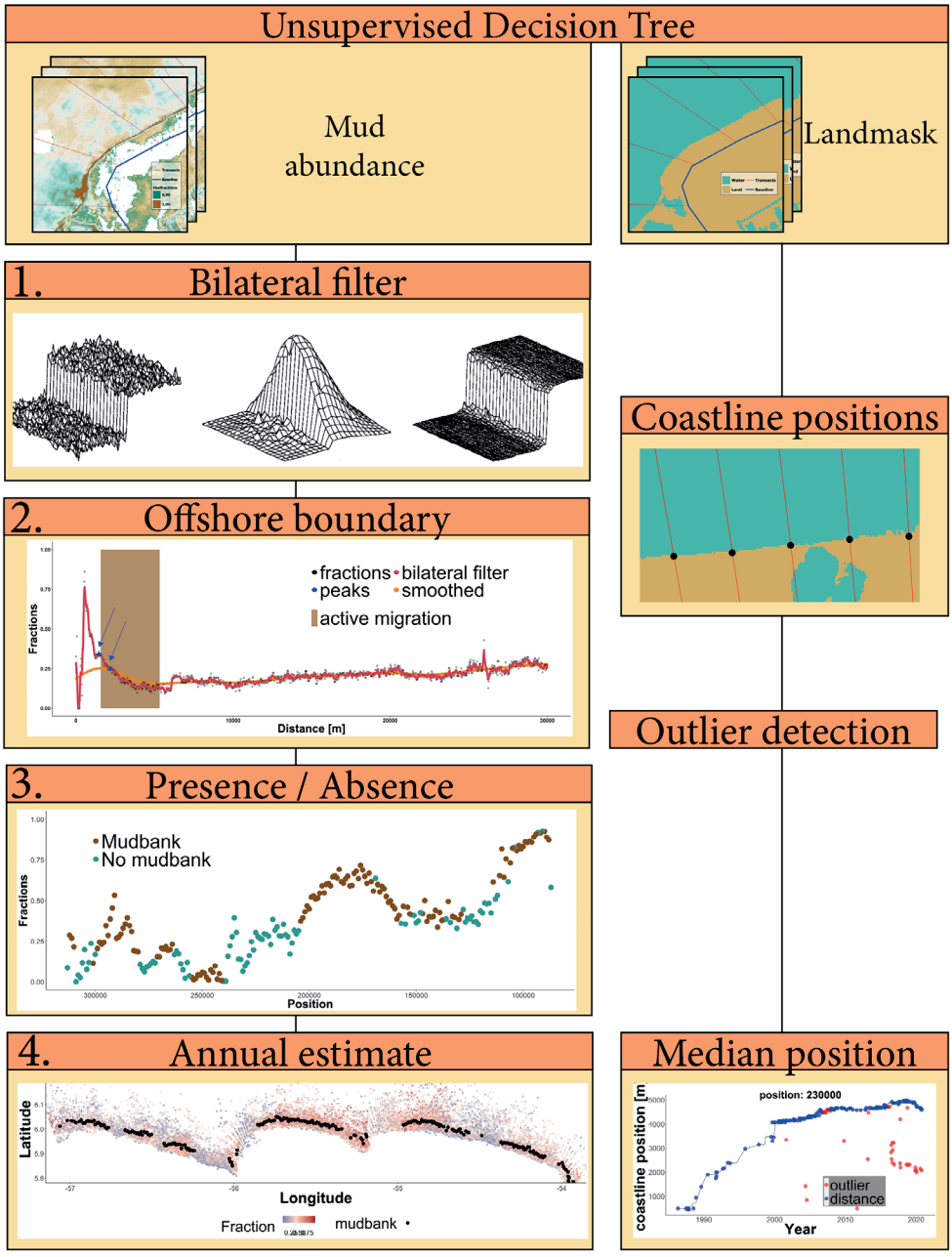

Figure 3.3: The applied steps, following the Unsupervised Decision Tree (UDT), to simultaneously determine the exact position of the coastline and absence or presence of mudbanks. On the right-hand side, the extraction of coastline position and consequential outlier detection to define median annual coastline positions is displayed as was applied on the binary land masks that resulted from the UDT. Steps 1-4 on the left-hand side show the sequence of steps that were taken to determine the presence of mudbanks for each year from the mud abundance maps that resulted from the UDT.

histogram (Lu et al., 2011), to simultaneously separate terrestrial vegetation and bare ground from water pixels, resulting in a land- and water mask (Figure 3.2, step B).

The NDWI and NDVI were used to detect image endmembers required for linear unmixing the fraction cover of mud in each image pixel. Therefore, image histograms, extracted from the canny edge neighbourhood zones and the water masks, were defined to select image end-member candidates (de Vries et al., 2021; Chapter 2). By selecting the most abundant NDVI value in the coastal zone, the driest mud pixels in the intertidal zone and the most abundant NDWI value from water pixels, mean spectral signatures were derived for each end-member group. By applying a fully constrained standard linear mixture model, the reflectance signatures were used to derive fractions of land cover type for each pixel in separate bands (Figure 3.2, step C). These fractions represent the proportion of each active component to the signal per pixel, with a cover always between zero (absent) and one (full cover) and the sum of all land cover fractions not exceeding one (Alcântara et al., 2009).

To simultaneously characterize the coastline change rate and mudbank extents along the coastline, transects were defined. As opposed to an area-based method, this transect-based method facilitates analysing rates of coastline change with respect to the presence or absence of mudbanks (Xu, 2018). A series of ~380 transects with a spacing of 1,000 m was defined perpendicular to a baseline spanning the coastal zone of Suriname. The baseline is a manually digitized line that is always landward of historic coastlines included in the time series of satellite images.

3.3.2 Mudbank detection

The presence or absence of mudbanks was determined by detecting abrupt changes in sediment fractions in abundance maps of mud, which result from the UDT method (Figure 3.2, steps D and E). The rationale behind using abrupt changes is that resuspension at the leeward side and deposition at the front side of mudbanks, associated with the migration of mudbanks, results in highly variable mud abundance (Zorrilla et al., 2018). Abrupt changes in the mud abundance were considered as fuzzy transitions that correspond to diffuse mudbank boundaries. To limit the effect of noise and simultaneously preserve and enhance the changes in sediment fractions in these active migration areas, we opted for a bilateral filtering approach (Figure 3.3, step 1).

The bilateral filter is a non-iterative technique that uses the weighted average of intensity in nearby pixels, thus taking the local difference in intensity into account while eliminating noise but simultaneously preserving edges (Tomasi and Manduchi, 1998). The filter has two kernels: one spatial filter to smooth the image, based on a gaussian function in the neighbourhood, and a second to highlight the similarity in intensity of the pixel value, compared to other pixels inside the kernel (Asokan and Anitha, 2020):

$$I_X(x=p) = \frac{1}{w_p} \sum_{q \varepsilon S} g_s \left(|| \, p-q \, || \right) \bullet f_r (I_p - I_q) \bullet I_q \qquad (3.3)$$

where p represents the selected pixel and q the coordinates in the neighbourhood S, G_s the spatial gaussian function needed to reduce the influence of distant pixels and f_r the range that reduces the pixels in the neighbourhood when their intensity values differ from pixel p with value I_q. The normalization factor, W_p can be computed as:

$$W_p = \sum_{q \varepsilon S} g_s \left(|| \, p-q \, || \right) \bullet f_r (I_p - I_q) \tag{3.4}$$

The weight assigned to neighbouring pixels (e.g., with coordinates *k,l*) to denoise a certain pixel (*i,j*) can be calculated according to:

$$w(i,j,k,l) = \exp\left(-\frac{(i-k)^2+(j-l)^2}{2\sigma_d^2} - \frac{||I(i,j)-I(k,l)||^2}{2\sigma_r^2} \right) \tag{3.5}$$

with σd and σr the smoothing parameters that control the intensity and spatial behaviour of the filter.

The resulting filtered fractions of mud were analysed along each of the intersecting cross-shore transects (Section 3.3.1). In general, these two-dimensional representations show a discontinuous decrease in sediment abundance over the subtidal parts of a mudbank, with abrupt changes being associated with diffuse mud-bank boundary (de Vries et al., 2021; Chapter 2). Therefore, the smoothed bilateral filter output and a smoothed approximation of the original mud fraction were extracted for each pixel that intersected with the transect (Figure 3.3, step 2). The smoothed approximation was used to define the range of decreasing mud fractions that coincides with this active migration area of subtidal mudbanks, containing the mudbank boundary (Zorrilla et al., 2018). We thereby excluded significant changes in mud fractions that were not related to mudbank boundaries, but for example with high mud fractions often found in wetlands. Transects with insufficient valid intersecting pixels (<70%), due to clouds and shadows, were also excluded from the analyses.

Within the estimated active migration area, abrupt changes in the mud fractions were extracted from the filtered mud abundance that result from bilateral output (Equation 3.5). These discontinuities were defined as local maxima that have been extracted from the zero crossings of the first order derivatives of the filtered mud fractions. Local maxima were then selected based on different criteria associated with their fraction value and position along the transect. In this way we ensured that the positions were: (1) farther offshore than the land boundary, (2) not associated with cloud- and shadow remnants, (3) represented an abrupt change in mud fraction and (4) had a sufficiently high fraction value to be associated with mudbanks. Then for each transect maxima were selected that can be associated with the largest absolute decrease, largest-, relative decrease and quickest decrease (slope), and exported from GEE for further analysis (Figure 3.3, step 2). These decreases in sediment fraction were considered potential mudbank boundaries as they indicated abrupt changes in mud abundance.

An annual frequency of mudbank presence was computed to compare coastline changes (Section 3.3.3 for a detailed description) with the presence of mudbanks during a given year. This indication was defined for all transects in individual images: first, we determined along each transect the average increase or decrease in mud abundance. Secondly, we labelled transects with an offshore increasing mud abundance as no mudbank and excluded the concerning observations from further analysis (Figure 3.3, step 2). Thirdly, we defined an alongshore orientated search window and used it to identify local clusters of previously defined abrupt changes, with relative low mud fractions and thus not considered to be a mudbank (Figure 3.3, step 3). Finally, a mudbank was

Table 3.1: Characteristics of the different surveys, including the XY error representing the average horizontal offset computed from a set of independent ground control points (n). The Landsat images column indicates the number of Landsat images that are validated with the corresponding orthophoto

Date	Location	substrate	Images (flights)	Flying height [m]	Area [km^2]	xy error [m]	Landsat images [n]
2019-06-20	Weg naar Zee (W)	Mud	1102 (6)	50	0.51	~0.02 (n=21)	8
2019-07-13	Weg naar Zee (E)	Mud	1192(6)	30	0.21	~0.02 (n=13)	5
2019-07-24	Braamspunt	Sand	1188(9)	75	1.16	~0.1 (=10)	6
2020-02-19	Weg naar Zee (W)	Mud	1385(9)	75	0.63	0.04 (n=9)	3
2020-03-03	Braamspunt	Sand	885(8)	100	0.73	0.06 (n=37)	4
2020-03-04	Braamspunt	Sand	478(6)	100	0.63	0.02 (n=22)	4

considered present when at least 60% of the observations for a given year contained an indication of a mudbank (Figure 3.3, step 4).

3.3.3 Coastline change detection

For each image the binary land mask, that resulted from the UDT (Figure 3.2, step B), was used in this research to extract the last transition from land (1) to water (0) on each individual transect (Figure 3.3). We then implemented a modified end point rate method to estimate rates of coastline change from the median coastline distance for a given year, compared to the median distance in the year before (Dolan et al., 1991). By doing so, we avoided omitting important trends in dynamic areas on longer timescales and were still able to separate annual from decadal trends. Even though taking a median value already reduced the effect of random error introduced by our methodology (Boak and Turner, 2005), we applied an outlier test to also exclude systematic erroneous observations (Figure 3.3).

Systematic errors were mainly related to inaccurate thresholding (Figure 3.2, step B) and data gaps that result from for example clouds, shadow and Landsat 7 ETM Scan Line Corrector (SLC) -off striping. Due to hampered visibility of the actual coastline, when no observation was available, potential false-positive detection of land-water transitions occasionally occurred. These erroneous coastline observations in the time series, measured in meters from the origin of the transect, were removed with the use of Rosner's hypothesis test within time windows of three years (Rosner, 1983). The time window was extended by maximum two years when the observation density was lower than ten observations. This allowed us to detect several unusual large or small coastline distances for each individual transect. The testing is performed in R's *EnvStats* package (version 2.3.1) that has the function *rosnerTest* implemented (Millard, 2014).

3.3.4 Coastline validation

Due to the complexity of coastal morphology in muddy coastal areas and the errors associated with the interpretation of coastline proxies from remote sensing images, we opted to compare our coastline estimates with different coastline interpretations (Li and Gong, 2016; Moore et al., 2006). These coastline proxies were manually digitized, based on visual cues in high-resolution

orthophotos that we retrieved from different Unmanned Aerial Vehicle (UAV) campaigns. When present, mature vegetation was considered as a robust indicator of the coastline (Gratiot et al., 2008). Yet, when vegetation was sparse the contrast between dry and wet pixels, also referred to as the high water line (HWL), was considered a more suitable indicator (Boak and Turner, 2005). Alternatively, the mean high-water line (MHW), a more static estimate, was based on visible features, including cliffs, scarps washed up brushwood and human constructions. It is important to mention these different proxies of coastlines may overlap.

Three orthophotos were created for three highly dynamics sites (Figure 3.1): two at Weg Naar Zee and a sandy chenier at Braamspunt (Anthony et al., 2019). Therefore, we used a DJI Mavic Pro 2 UAV, with a L1D-20C camera model which acquires 20 megapixels photographs that can be used to construct high-resolution orthophotos (Westoby et al., 2012). We collected these photographs at different flying heights with a forward- and side overlap of 80% and 60%, respectively (Table 3.1). During low-tide, 6-9 separate flights were planned and executed in *Litchi* software, aimed at collecting alternating nadir and off-nadir pictures to minimize doming (Carbonneau and Dietrich, 2017). Markers and natural terrain features, measured with *Emlid Reach+ RKT GPS*, were used as ground control points to process the photographs in *Agisoft Metashape (*version 1.5) to point clouds and ultimately orthophotos with a downscaled resolution of 50 cm. Accuracy of these orthophotos ranged between 0.02 and 0.1 m (Table 3.1), substantially smaller than the uncertainty associated with the acquisition of Landsat images.

Satellite images taken within 100 days of the orthophoto acquisition date were considered for validating the coastline position. This selection resulted in 12 satellite images for which coastline positions were estimated, following the procedure described in previous sections (Section 3.3.3 and Figure 3.3). As opposed to using transects with 1,000 m spacing like we did for the entire coast of Suriname (Section 3.3.1) we used transects with a spacing of 50 m for the validation. Euclidean distances between the resulting position estimates and the different manually delineated coastline proxies (vegetation interface, MWL and MHW) were calculated as indicator for the overall accuracy of position estimates.

3.4 Results

3.4.1 Mudbank dynamics

The alongshore variation in mud fractions can be associated with the presence or absence of six to eight mudbanks of varying length in front of the Suriname coast between 1986 and 2020 (Figure 3.4). Especially in the western part of Suriname, between 0 and 120 km, three or four clearly distinguishable alongshore migrating mudbanks can be seen. Also, in the middle section it is possible to distinguish segments associated with the front of one migrating mudbank between 2000 and 2010. Finally, in the eastern section, two segments that are associated with mudbanks are visible. All these segments show a clear shift from east to west, associated with their migration direction and speed. The smaller east to west shift for each segment between different years in the western sector, compared to the middle and eastern parts of Suriname, suggests slower migration rates of mudbanks towards the Corantijn River (Figure 3.1).

In general, high mud fractions, ranging from ~0.4 to ~0.8, indicate the presence of mudbanks because continuous transport of mud towards the front of mudbanks causes a higher turbidity. Mud at the coast, especially near the back of mudbanks and in the interbank zones, is consolidated and therefore not easily resuspended, causing lower mud abundances in the water column (Vantrepotte

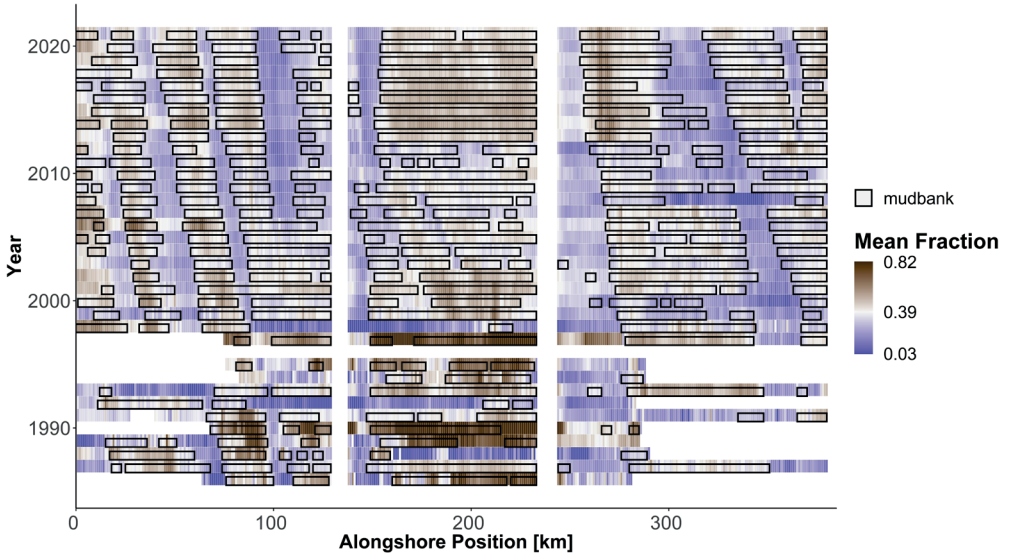

Figure 3.4: Mean values of the peaks of mud fractions and position estimates of mudbanks, distributed along the coastline of Suriname for all years between 1986 and 2020. The peaks of sediment fractions were calculated as described in section 3.3.2 and Figure 3, step 2. The presence of mudbanks was estimated for each transect-based on the steps explained in section 3.3.2 and Figure 3.3, step 3. Masked out values are related to transects that are in the mouth of the Suriname- and Coppename River (Figure 3.1) or missing satellite data.

et al., 2013). This can for example be illustrated by the band of lower mud fractions (~0.05 and ~0.3) in the eastern sector between 300 and 350 km (Figure 3.4).

3.4.2 Validation of coastline position

Coastline positions, derived from Landsat images, are compared to different coastline interfaces digitized in the UAV images acquired over Weg Naar Zee at 2019-06-20 (Figure 3.5, Panel A). Coastline positions retrieved from the Landsat images that were acquired 72 days (2019-08-31) and 80 days (2019-09-08) after the UAV acquisition date (2019-06-20) show significantly larger mean distances compared to the digitized coastlines (Figure 3.5, Panel B).

We developed similar comparisons between the automatically derived coastline positions in all the selected Landsat images and the defined coastline proxies in the different high-resolution UAV images (Figures B1-B4, Appendix B). Overall, position estimates agree with the observations, indicating on average less than 50 m distance (<1.67 Landsat pixel) to the different reference lines (Figure B5, Appendix B). The median euclidian distance from each coastline position to the nearest line is less than 30 m. The coastline position estimates agree with the lines corresponding to the MHW and HWL (Appendix B, Figure B6). Exceptions are the MHW acquired in the Weg Naar Zee UAV image of 2020-02-19 and the vegetation interface acquired at Braamspunt in 2019-07-2 (Figures B2 and B3, Appendix B). Comparisons between Landsat derived coastline positions and the coastline proxies retrieved from the UAV images acquired over Braamspunt show 8-12 significant outliers, with distances of up to 600 m. These offsets can be attributed to the spit that has formed with a width sometimes smaller than the size of one Landsat pixel (Figure B4, Appendix B)

3.4.3 Coastline dynamics

The annual rate of coastline changes between 1986 and 2020, in relation to the presence of mudbanks in front of the Suriname coastline, is shown in Figure 3.6 (Panel A). Of all coastline position changes, 90% ranges from -125 m/yr of erosion to 150 m/yr of accretion. Overall, there are no clear trends with dominant accretion or erosion rates between 1986 and 2020 for the entire coastline (Figure 3.6, Panel B). Yet, years of erosion and accretion are alternating, with on average erosion in the last six years. Especially in the western region (Figure 3.6, Panel C) alternating zones with on average accretion or erosion are visible, although no single transect shows continuously erosion or accretion for the studied period 1986-2020.

Figure 3.7 supports the general observation that in the period 1986-2020 Suriname has an accreting coastline with an averaged total of 310 m between 1986 and 2020, yet there is strong alongshore variability. More specifically, the western section is characterized by erosion with a mean coastline position change of 88 m, but also with occasional accretion compared to 1986. The eastern

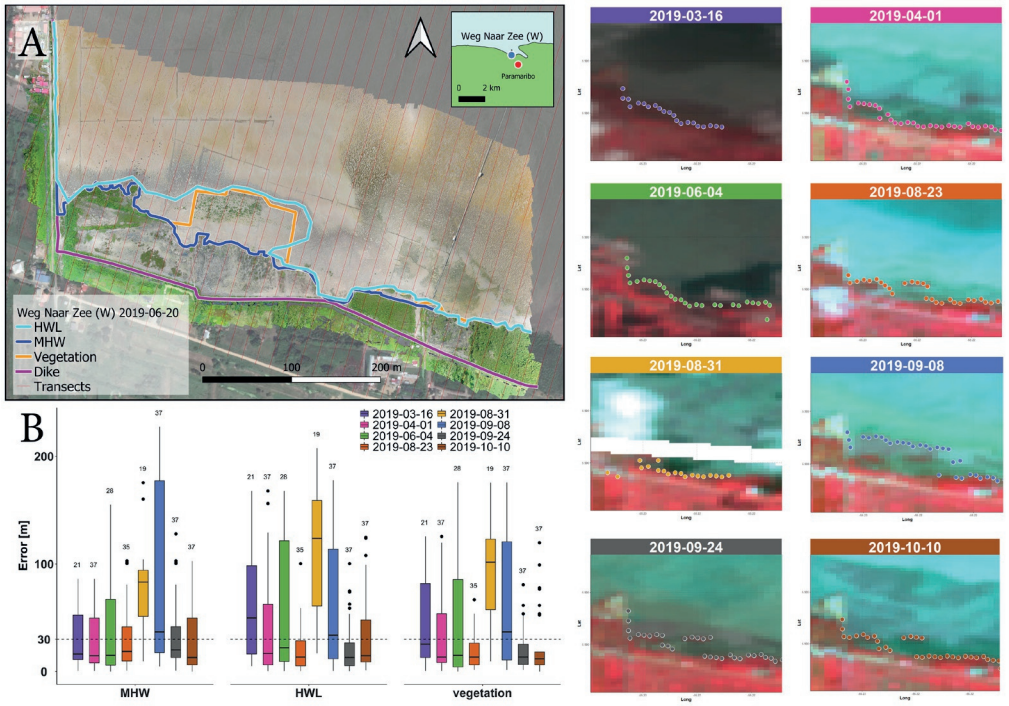

Figure 3.5: Validation results of the Landsat images acquired within 100 days of acquiring the high-resolution UAV image near Weg naar Zee West (2019-06-20). Panel A shows the digitized shorelines in the UAV image that are used for validation. The panels on the right show the different Landsat images that are used, together with their automatically derived shoreline positions. The coloured boxplots in Panel B summarize the difference for each of these Landsat derived shoreline positions compared to the different digitized shoreline positions visible in panel A (MHW, HWL and vegetation interface). The Landsat 7 image acquired at 2019-08-31 shows missing data related to SLC-off striping.

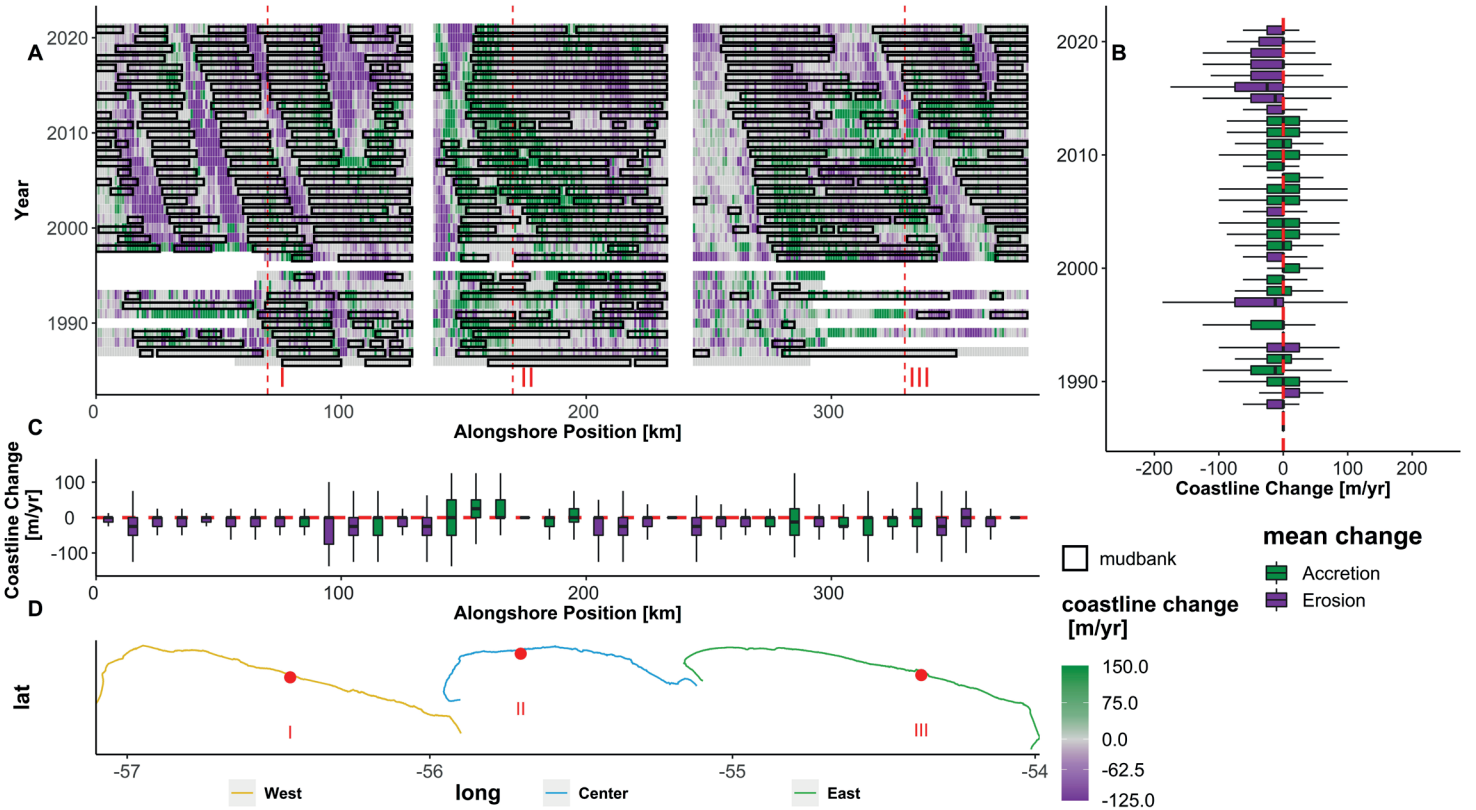

Figure 3.6: The presence and absence of mudbanks in relation to observed coastline changes in Suriname between 1986 and 2020 (Panel A). Panel B shows ranges of annual coastline changes, where green indicates mean accretion and purple mean erosion for the given years. In panel C the alongshore distribution of coastline changes is given for every ten transects. Panel D shows the coastline of Suriname with the coastal sections indicated by east, centre and west. The position of the selected example transects are indicated with I, II and III. Note that the x-axis of panel D (in units of longitude degrees) is not the same as the x-axis of panel A and C (in units of alongshore distance).

section has an average accretion in coastline position of 212 m compared to 1986. Finally, the middle section shows overall accretion for each transect with an average coastline change of 1,004 m compared to 1986. For the studied period, a significant part of the total accretion in Suriname occurs in the central region, with the majority of it between 2002 and 2011. From the year 2000 onwards accretion reduces, first from km 200 and then shifting in the western direction (Figure 3.6, Panel A).

Both accretion and erosion occurred at local scale, i.e., difference in order of magnitudes change within 10-30 km alongshore distances (Figure 3.6, Panel A). This suggests that spatial zones can be defined, where either accretion or erosion of the coastline was dominant in a specific period (Figure 3.6, Panel C). For each year inversion points along the coastline can be seen where this accretion changes to erosion or vice versa (Figure 3.6, Panel A). Not only do these inversion points mark the accreting zones under influence of mudbanks, their position changes between years are a good indication of migrating mudbanks (Froidefond et al., 1988).

Examples of variability in these inversions at local scale are visualized in Figure 3.8, where the coastline position in the eastern region (transect III, Panel C) changes from roughly 100 m in 2002 to almost 1,350 m two years later and eventually ~1,100 m in 2009. A mudbank was already present from 1997 and completely passed in 2009. From 2009 the coastline eroded slightly to 1,200 m, with stabilization from 2015 onwards. Also, between 160- and 230 km alongshore a phase of coastal accretion can be observed with occasionally accretion rates surpassing 150 m/yr (Figure 3.6, Panel A). As opposed to transect III the accretion of the coastline for this location (transect II, Figure 3.8, Panel B), starts within one year of the arrival of a mudbank. Also, between 275- and 400 km

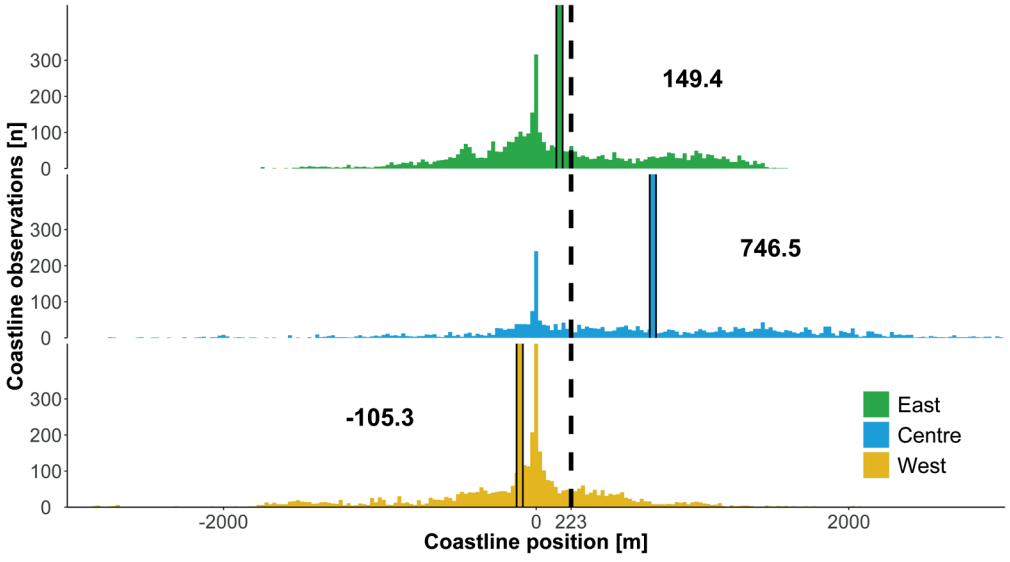

Figure 3.7: Changes occurring in coastline position between 1986 and 2020 in the eastern, centre and western sections of the Suriname coastal area as shown in figure 3.1 and figure 3.6. The y-axis values correspond to the number of observations in each bin of normalized coastline position estimates. The solid and dashed lines indicate the mean values for each section and entire coastline, respectively. For each transect all coastline positions are compared to the first observed valid coastline observation.

alongshore, westerly deflecting strips of accretion are clearly distinguishable (Figure 3.6, Panel A). Under the influence of a mudbank the coastline remains stable between 1999 and 2004, with rapid accretion of +/- 300 m until 2011 (Transect I, Figure 3.8, Panel A). Then erosion rates rapidly go up to, or sometimes even surpass, 125 m/yr between 2012 and 2015 followed by stabilization of the coastline and the appearance of a new mudbank in 2018. These differences in the magnitude and timing of coastline responses to appearing mudbanks exemplifies the spatiotemporal variability present in the system.

Overall, accretion zones coincide with the presence of mudbanks, and erosion zones can be linked with the absence of mudbanks (Figure 3.6A and Figure 3.4). As supported by Figure 3.9, mudbanks tend to be associated with accretion rates of 32 m/yr. Vice versa, the absence of mudbanks is in general associated with mean erosion rates of four m/yr. The difference between the two skewed groups (Shapiro-Wilk test, p-value, < 0.0001) of coastline changes, affected by the presence or absence of mudbanks (Figure 3.9), are significantly different (Wilcoxon Rank Test, p-value <0.0001). Relative smaller erosion rates are also observed when a mudbank is present or moderate accretion rates when a mudbank is absent.

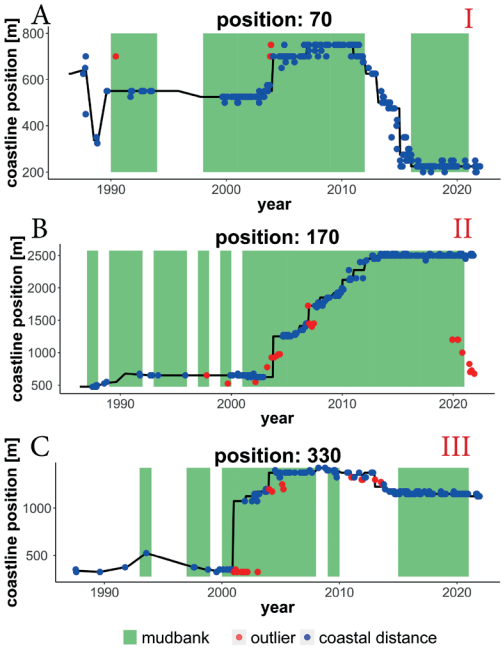

Figure 3.8: Development of the coastline position between 1986 and 2020 of the three transects indicated in figure 3.6. Coastline position is expressed as distance of the last land-water transition compared to the origin of the transect. The median values are connected by the black line. Note the different Y-axis ranges for each subplot.

3.5 Discussion

3.5.1 Mudbanks

Our semi-automatic methodology allowed us to visualize the alongshore variation in mud abundance between 1986 and 2020, link it to the presence or absence of mudbanks and identify likely mechanisms that dominate nearshore variations (Figure 3.4). The satellite derived estimates of mud abundance in shallow waters indicated the presence of six to eight migrating mudbanks along the coast of Suriname. These mudbanks show strong spatial- and temporal variations mud abundance. Previous research already coupled the local variation of mud abundance in the upper water column to active resuspension and migration of an individual mudbank (Vantrepotte et al., 2013; Zorrilla et al., 2018).

Variations in mud fractions clearly exist when looking at multiple mudbanks simultaneously at different moments in time. This illustrates the link between the changes in the footprint of mudbanks that are visible in remote sensing images and variability in hydrodynamic forcing mechanisms such as waves, tides, currents and river flow (Orseau et al., 2020). This is because so called wave-bank interactions constantly affect the migration rate, shape and mud budget of these

banks (Anthony et al., 2013a; Gardel and Gratiot, 2005). Suggesting that spatiotemporal variable mud fractions can be associated with the presence or absence of a mudbank. Also, within the footprint of these mudbanks variable mud fractions are observed (Figure 3.4), probably associated to wave-mud interactions that control resuspension at the leeward and deposition at the front side (Zorrilla et al., 2018). This not only limits the use of generic thresholding on sediment fraction or concentrations to separate mudbanks from their surroundings, but it also indicates these interactions enhance variability between separate mudbanks and consequential coastline dynamics.

3.5.2 Implication for foreshore changes

For the first time we were able to identify hotspots of contrasting behaviour, overall trajectories of coastline change and relate to those presence or absence of mudbanks (Figures 3.4 and 3.6). In general, the Suriname coast accretes with an average of 32 m/yr when a mudbank is present (Figure 3.9), comparable to the previously reported range of 13-100 m/yr in French Guiana (Plaziat and Augustinus, 2004). Occasionally rates up to 400-800 m/yr were detected, which is significantly higher than the previously reported upper limit of 200 m per year (Allison et al., 2000; Augustinus, 2004; Proisy et al., 2021). We show that the coast erodes by four m per year on average under mudbank absence, reaffirming that coastal erosion prevails when a mudbank has migrated further alongshore and no longer protects the coast against incoming waves (Allison et al., 1995; Anthony et al., 2010; Gardel and Gratiot, 2006).

Coastline positions in the different sections along the coast of Suriname showed variable responses to the presence or absence of mudbanks, between 1986 and 2020 (Figure 3.7). One explanation for the regional difference comes from cheniers, sand ridges that are created by sand supplied from local rivers, such as the Suriname and Corantijn River, together with winnowing

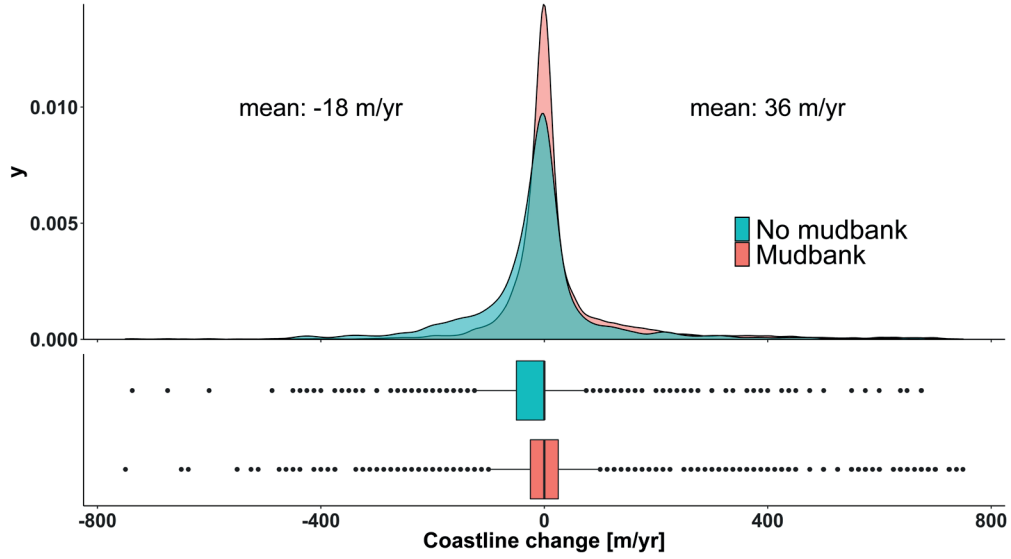

Figure 3.9: Annual rates of coastline change between 1986 and 2020 for transects that are either fronted by a mudbank or not. The distribution of change is indicated by the density plots and the median, interquartile ranges and outliers are indicated by the boxplots in the bottom panel. For visualization purposes the x-axis range is limited to -800 m/yr to +800 m/yr.

of sand from deposits by constant wave reworking. Especially in the western sector the cheniers, if present at all, are smaller and thus provide less protection against erosion than in the east (Augustinus et al., 1989), potentially explaining the difference in erosion.

Exceptional accretion rates in the central section of Suriname suggest however that this is at best only part of the explanation (Figures 3.7 and 3.8, Panel B). Due to changes in the orientation of coastlines and presence of sufficiently large coastal features, such as mudcapes and small islands that provide shelter against incoming waves and might even promote accretion. Together with the slowing down of the mudbank approaching the mouth of the Coppename river from 2008 onwards (Figure 3.6, Panel A), caused by the hydraulic groyne effect (Anthony et al., 2013a), this might explain the enhanced sedimentation and coastline east of the river mouth (~ km 140). Consequently, sediment deposition downdrift becomes limited, thus promoting enhanced erosion west of the river mouth (~km 100), starting from 2013 onwards (Figure 3.6, Panel A). This examples clearly highlights the difference in coastline response to a passing mudbank, but also the different magnitude of changes induced by a single mudbank on different stretches of coastline with the passing of time.

Our results further highlight the episodic, rather than uniform, nature of the coastline position changes on local scale, with rapid coastline accretion and retreat as response to changes in forcing mechanisms, including mudbank migration (Augustinus, 1989). Yet, variability in timing can occur, as coastal accretion can immediately follow the arrival of a mudbank (Figure 3.8, Panel B), lag several years (Figure 3.8, panels A and C) or not happen at all. This again emphasizes the importance of other factors such as the variation in topography of the intertidal area (Anthony et al., 2008; Proisy et al., 2009). As a result, differences in submersion time, flooding frequency and drying-wetting cycles cause mud cracks and development of mud bars. Altering conditions for successful seed trapping and thus mangrove growth (Gensac et al., 2011).

Previous research has shown that shoreline trends lasting multiple decades occur, as opposed to the alternating phases of accretion and erosion that the conceptual model of migrating mudbanks describes (Fromard et al., 2004; Plaziat and Augustinus, 2004). Our results (Figure 3.6, Panel A) can now indicate where erosion, despite the presence of mudbanks (e.g., around km 350 after 2012), and accretion can occur, even when mudbanks are absent (e.g., km 150). The former are examples of potential new shoreline trends of prolonged and persistence erosion, due to for example polders or mangrove removal (Brunier et al., 2016). Also, observations of mudbanks not promoting coastal accretion (e.g., km 35 and 180) despite enhanced wave damping, suggest additional factors are playing a role in successful mangrove colonization and establishment. Previous research indicated that this can be related to reduced material exchanges between mudbanks and shorelines, especially at leading and inner edges of mudbanks (Anthony et al., 2013b). This streaming of mudbanks, a process where mudbanks are disconnected from the shoreline, results in reduced material exchange, smaller intertidal mudflats and thus less accommodation space for mangrove colonization and coastal accretion (Gensac et al., 2011; Proisy et al., 2009). It is estimated that these long-term process may involve local changes in wave-bank interactions as well as coastal mud budget adjustments alongshore (Anthony et al., 2013b).

In general we can see that the extent to which the shore welded part of a mudbank is preserved from erosion in interbank phases determines the degree of coastal progradation in the following mudbank phase (Allison and Lee, 2004; Anthony et al., 2010). Complex patterns of erosion and accretion, however, confirm again that the coastline positions and their trajectories are not only influenced by mudbank dynamics. The average erosion or accretion rates should therefore be considered more as a mid-term (e.g., one full mudbank cycle) tendency on local to regional

scale, rather than a definitive indicator of what may happen on a longer timescale. Yet, additional research on the extent of intertidal areas and factors that control successful mangrove colonization, in relation to forcing mechanisms such as wind-wave regimes (Augustinus, 2004) and currents, is required to quantify the potential impact of each individual aspect.

3.5.3 Coastline accuracy

The different coastline definitions, namely HWL, MHW and the vegetation interface, as mapped in the high-resolution UAV imagery (Figures 3.5 and B1 - B4, Appendix B) are in good agreement with the coastline position estimates. These estimates from 12 Landsat images, acquired within 100 days of the UAV acquisitions, are on average within 50 m of the reference lines (Figure B5, Appendix B). Disparity in error between the Landsat observations and the different coastline proxies exemplify the uncertainty associated with the selected point-based method for estimating coastline position from land-water transitions along a transect. This method is a computation efficient way of analysing spatiotemporal variation in coastlines, yet the accuracy depended on the orientation and location of the transects, as spatial context of the coastline estimate is one-dimensional. As a result, information from adjacent pixels is not incorporated in the estimation of coastlines, resulting in the potential detection of incorrect land-water transitions. Variation in the average error for the different UAV images also represents the difficulty in consistently mapping land-water boundaries over complex, heterogeneous landscapes. This can be seen for example in the larger error estimates of Braamspunt, a sandy chenier with relative complex land cover and coastline shape, compared to the two sites at Weg Naar Zee (Figure B6, Appendix B).

When the true coastline position cannot be determined due to missing data, offsets in accuracy can be large. This is for example indicated by the outliers found in the Braamspunt UAV images (Figures B3 and B4, Appendix B). As the most seaward land-water transition is obstructed from sight by clouds, the detected transition behind it is classified as coastline. This can also occur in coastal areas where coastlines are often backed by wetlands, resulting in an incorrect land-water boundary classified as coastline. For this reason, we implemented an outlier detection workflow, ensuring that significantly deviating observations are excluded from further analysis. This ensures that our coastline estimates for the entire coast of Suriname are on average within 50 m of the land-water boundary found across the heterogeneous coastal landscape. Especially median annual coastline positions should therefore be used to analyse mid- to long-term coastline changes on a regional scale in a complex heterogeneous mud-dominated landscape, where annual changes are frequently exceeding 30 m.

The difference in error estimates between the sites (Figure B5, Appendix B) also indicates that coastline indicators are not uniformly applicable along the Suriname coastline. Coastal stretches show differences in agreement between the observation and coastline proxies, suggesting that our method is not overly sensitive to several types of transitions between land and water that can naturally be found along the Suriname coastline. This indicates that the applied method can be used in heterogeneous and complex landscapes for the consistent estimate of coastline positions.

False positive detection of coastline position estimates, when the true coastline position is not visible, manifested due to the applied transect method. Especially when morphology of the coastline is more complex or is not aligned with the defined baseline, land-water transitions are falsely detected as coastline positions. For coastline detection we therefore included both temporal and spatial context to improve the accuracy of position estimates, by comparing the position with other position estimates on the transect within a time window. Rosner's outlier detection was chosen for its possibility of simultaneously detecting multiple outliers.

3.5.4 Limitations and improvements

The standardized and objective end-member extraction technique applied here resulted in comparable estimates of mud abundance, useful to derive indications of subtidal mudbank presence and absence. Yet, due to image artefacts, cloud- and shadow contamination this estimated presence or absence required filtering and outlier detection. The steps to do so required finetuning and parameterization to make the methodology applicable for the Suriname coastline. These steps ensure that: 1) spectral unmixing results are applied consistently, 2) clouds and shadow contamination is minimized, 3) bilateral filtering on the abundance maps is applied, 4) discontinuities along transects are consistently selected and 5) annual changes in coastline positions, in relation to the presence or absence of mudbanks, are determined with a reasonable accuracy.

Despite the implemented filtering steps mudbanks were occasionally falsely detected (Figure 3.4). This is because automatically estimating the exact mudbank boundary locations is hampered by high sediment concentrations, related to high river discharges near river mouths and the observed natural variability in mud abundance (Section 3.5.1). To optimize the parameterization of the workflow it is therefore necessary to validate the mudbank positions with field observations. Consequently, it is necessary to determine the extent of mudbanks and simultaneously relate that to the extent of mudbanks that can be detected from remote sensing images (Zorrilla et al., 2018).

With respect to the estimated coastline positions, uncertainty in estimates is related to the observation frequency, obstruction of visibility by clouds and the accuracy of the applied UDT, used here to separate land and water by means of Otsu thresholding. Only for the latter source of error it is possible to improve the accuracy by for exampling including the definition of sub-pixel coastlines (Pardo-Pascual et al., 2018) and use of a water frequency index to perfect the estimate of the annual coastline position (Xu, 2018).

Although our coastline change analysis for Suriname quantified rates and directions of change with unprecedented spatial coverage and temporal resolution, further analysis can shed light on coastal system behaviour. This can be achieved by analysing mudbanks beyond the presence and absence estimates as presented in this manuscript. Demarcating mudbank footprints from observations with high temporal resolution can then shed light on migration rates, sediment storage and changes therein. When linked with information regarding other external forcing mechanisms like land-use, wind data, coastline shape and morphology that govern the coastal dynamics in all the Guiana coast countries, it becomes possible to truly support decision makers in their task to untangle subtleties in coastline behaviour for coastal wetlands. Variable responses of coastal ecosystems to ever changing forcing mechanisms can then be incorporated in climate resilient management strategies.

3.6 Conclusion

By analysing all available Landsat images in our workflow autonomous, its temporal and spatial resolution are fully utilized to estimate, for the first time, coastline changes for the entire coast of Suriname between 1986 and 2020. These changes are then linked to presence and absence of migrating subtidal mudbanks. We show that regional-scaled forcing mechanisms caused by these mudbanks, have a strong imprint on the local coastline trajectories, with on average 32 m/yr accretion during mudbank presence and four m/yr erosion during mudbank absence. Yet, significant spatial and temporal variation in these trajectories exists on local scale. This suggests that linear

and large-scale approaches to analyse annual to decadal coastline dynamics in Suriname, and other Guyana countries, should be handled with caution.

We reaffirm that currently at least six mudbanks are migrating along the coast of Suriname and that when mudbanks are present, coastal accretion or stabilization of erosion occurs. Due to the use of all available Landsat images, we are now also capable of showing where the effects of mudbanks are minimal or even opposite of what the conceptual mudbank model prescribes. This suggests that it is evident that not every mudbank phase results in the same amount of coastal accretion at each location is passes, or to the contrary, every inter-bank phase result in the same amount of coastal erosion.

These timescale dependencies might reflect combined effects of natural and anthropogenic factors that control both the mudbank and hydrodynamic forcing on the coast of Suriname, illustrating the difficulty of attributing all observed coastline changes to forcing imposed by mudbank migration alone. Although it is likely that mudbanks will continue to migrate alongshore in the decades to come, the variability in coastal morphology, sediment concentration and especially the structural intervention (both anthropogenic and natural) will exert a complex influence on erosion and accretion of coastline positions. This implies that predictions of change for management purposes, should be conducted with extreme care as they might create a false sense of security on short to medium timescales.

Our results further suggest that the potential for erosion during an interbank phase can be significantly larger than accretion rates in the mudbank phase before, especially when local settings including hydrodynamics, land-use and other forms of anthropogenic interference are altered. This suggests that local coastal behaviour, not captured by linear rates of change, should be included in theoretical frameworks that are used to support decision makers and coastal managers. For that purpose, quantitative information on coastlines position changes from satellite observations spanning multiple decades are needed to supplement scattered, incomplete and poor-quality field observations and further refine modelling efforts that aim at predicting future changes in Suriname.

Chapter 4 | The effect of mudbank morphometrics and coastal morphology on multi-decadal coastline changes in the Guianas

Abstract

The relative contributions of controlling factors on coastline changes are typically difficult to untangle and quantify. Consistently defining, mapping and following coastline development, however, is indispensable to address the capability of coastal environments to cope with the adverse effects of natural and anthropogenic changes. For the Guiana shield countries in South America, coastline changes can shed light on the relative contributions of controlling factors internal to the natural system, with respect to the influence of migrating subtidal mudbanks. A quantitative analysis focusing on mudbank morphometrics and coastal planform characteristics over large temporal and spatial scales including the entire Guianas' coastline is currently missing. In our research, show the paramount effect of spatiotemporal variable mudbank morphometrics, including length, width and migration rate, on coastline changes between 1985 and 2021 from Landsat observations. Overall progradation during mudbank phases was considerably larger, with an average between 2 and 44 m/yr, compared to interbank phases. When mudbanks are not damping waves, average coastline retreat is between 13 and 18 m/yr. Migration rate and morphometrics of mudbank footprints, measured here as a frequency of mudbank occurrence, partially explain coastal progradation or retrogradation ($R^2 = 0.18$, $p < 0.05$). Differences between Guyana ($R^2 = 0.21$, $p < 0.05$), Suriname ($R^2 = 0.14$, $p < 0.05$) and French Guiana ($R^2 = 0.36$, $p < 0.05$) exemplify that not every mudbank has the same effect on each stretch of coastline it passes. These local to regional differences suggest that the internal and external factors that influence the position and shape of mudbanks also influence the frequency of occurrence and therefore the number of years a coast is protected and facilitated to accrete. It is critical to consider these factors for future interventions or building-with-nature initiatives that aim at ecosystem restauration and coastal protection. Our observations of mudbank footprints and coastline changes make it possible to pinpoint coastlines that are not accreting under the influence of mudbanks, potentially related to irreversible system changes.

Based on:

de Vries, J., van Maanen, B., Ruessink, G., Verweij, P. A., & de Jong, S. M. (2023). **The effect of mudbank morphometrics and coastal morphology on multi-decadal coastline changes in the Guianas.** In preparation for publication

4.1 Introduction

An improved understanding of the behaviour of coastal systems is needed due to the advancing human development in these areas. Understanding the factors that influence coastline dynamics is a key step to addressing how coastal environments cope with the adverse effects of disturbances, such as storms and sea level rise, while maintaining essential functionality (Masselink and Lazarus, 2019; Phillips, 2018). For coastal zones with complex formation processes, such as wetlands and mangrove forests, it is increasingly important to define, map and follow developments (Moffett et al., 2015). In addition, coastal systems, especially mud-dominated coasts are projected to experience unprecedented economic loss and environmental change in the decades to come (Oppenheimer et al., 2019). Yet, despite increased attention in recent years, uncertainties related to complex feedback mechanisms between cohesive sediments, waves, vegetation and coastal landforms remain (Kirby, 2000; Xie et al., 2022). This calls for additional efforts to monitor coastline evolution to enhance our understanding of controlling factors in mud-dominated coastal zones, especially in less-developed parts of the world.

Coastlines are elements of littoral systems that define the interface between land and water (Boak and Turner, 2005) and can comprise several coastal landforms including salt marshes, coastal barriers, sandy beaches and mangrove forests. Their position is controlled by factors than can be external to the system, including short-term water level fluctuations due to the constant rise and fall of water levels (e.g. waves), different modes of climate variability (e.g. El Niño or the Southern Oscillation) and long-term sea-level rise (Castelle et al., 2022; Vos et al., 2021). The influence of these external factors can be mediated by internal control factors (i.e., sediment supply and coastline profiles) that can exert far larger changes. The relative strength of all these external and internal factors that control the evolution of coastlines and associated landforms is typically difficult to untangle and quantify (Warrick et al., 2022). This is especially true when the availability of observations is limited, making it difficult to specify where, when and how much these individual factors contribute to changing coastlines (Lauzon et al., 2019).

One way to assess the influence of controlling factors on the dominant formation processes, current state and potential future trajectories in littoral systems is by looking at the shape and locations of a coastline (Geleynse et al., 2012; Lazarus and Murray, 2007; Murray and Ashton, 2013; Shaw et al., 2008). This is also referred to as its morphology (Ashton et al., 2001). For example, variability in coastline morphology and changing sediment fluxes are induced by variations in local wave conditions, such as wave height and incoming angle with respect to the coastline orientation (Ashton and Murray, 2006; Murray and Ashton, 2013). Coastline morphology changes can provide invaluable insights into its sensitivity to environmental gradients and controlling factors such as sediment dynamics, hydrodynamic forcing and feedbacks between them (Albeke et al., 2010; Ashton and Murray, 2006; Lauzon et al., 2019).

Depending on the type of coastal landforms that are present, identifying coastlines can be challenging, especially in mangrove environments, where the mangrove forest fringe is often used as a proxy for the coastline (Kuenzer et al., 2011). To measure the location of coastlines, we ideally rely on cross-shore orientated height observations, in combination with lateral position estimates. Consistent and quantitative three-dimensional observations, with sufficient spatiotemporal resolution, are often lacking, especially in data poor regions. The hydrodynamic control, such as tides and waves, on the cross-shore shape has been shown to extend to the lateral distribution of coastline positions, and thus the planform morphology of coastlines (Kirby, 2000). Thanks to the increased availability of remote sensing observations, consistent means to analyse planform

morphology of coastlines, in relation to the factors that influence them, have become feasible (Geleynse et al., 2012). This provides invaluable observations of coastline changes with sufficient temporal and spatial coverage for coastal managers to follow coastal development.

The relative contribution of different controlling factors on the long-term fate of coastlines can vary significantly on local to regional spatial scales and timescales that can range from days to multiple decades (Castelle et al., 2022; Warrick et al., 2022). This is especially true for the Guianas, a mud-dominated coastal zone between the mouth of the Amazon River in Brazil and the Orinoco Delta in Venezuela. This coastal zone is a relative flat area that, in its natural state, stretches from the landward extent of mangrove cover to the seaward limit of the intertidal area. Especially the contributions of climate variability (Gratiot et al., 2008) to long-term coastline changes have been studied extensively. Processes include the changing trade winds (Augustinus, 2004) and effect of the North Atlantic Oscillations (NAO) on swell waves (Walcker et al., 2015) and anthropogenic activities (Anthony et al., 2013a; Toorman et al., 2018) with respect to the influence of migrating subtidal mudbanks (Allison et al., 1995). It is widely accepted that the conceptual model of mudbank migration, with retrogradation during interbank and progradation during bank phases, leaves a strong imprint on annual to multi-decadal trends in mangrove cover and coastline behaviour. Yet, local to regional variability in coastline changes (Brunier et al., 2019), patterns in mangrove growth (de Jong et al., 2021), complex intertidal morphology (Gardel et al., 2009) and persistent alteration of heads and bays during interbank phases (Augustinus et al., 1989) hint at scale dependencies that reflect a more complex combination of natural and anthropogenic influences. Previous research has suggested that a potential explanation for this variability lies in the morphology of a coastline (Augustinus, 1980; Gratiot et al., 2007), the orientation of coastline stretches with respect to incoming waves (Augustinus, 2004) or highlighted the importance of currents (Lefebvre et al., 2004).A systematic characterization of mudbank morphometrics, including their migration rate and subtidal extent, and the link to changes in coastline morphology and positions at relevant spatial and temporal resolution has been lacking thus far. This is partly related to the difficulty in quantifying the footprints of migrating subtidal mudbanks along the entire Guianas' coastline, despite increasing availability in remote sensing observations. The challenge is to distinguish between the dominant effect of wave damping and enhanced sediment supply during mudbank phases and the opposite situation, when there is no mudbank in front of the coast (Froidefond et al., 2004). Attempts to untangle the relative contributions of mudbank migration on coastline changes are complex as they involve timescales ranging from seasons to multiple decades and spatial scales that go from local, to landscape and regional settings (Augustinus, 2004).

The aim of our work is to assess the morphometrics of mudbanks, including the subtidal extent, in remote sensing images, and their effect on coastline changes in the Guianas between 1985 and 2021. We do this by quantifying spatial and temporal differences in coastline position, shore-normal orientation and curvature. Simultaneously, we link this to the extent in which subtidal mudbanks affect different coastline stretches. These results should indicate to what extent coastline responses, caused by the constant migration of subtidal mudbanks, are also influenced by other factors.

4.2 Study area

The Guianas' coastline is situated along the subtropical north-east coast of South America, between the Amazon and Orinoco Deltas (Figure 4.1). French-Guiana, Suriname and Guyana, together with parts of Brazil and Venezuela, make up this 1,500 km long mud-dominated coastal system

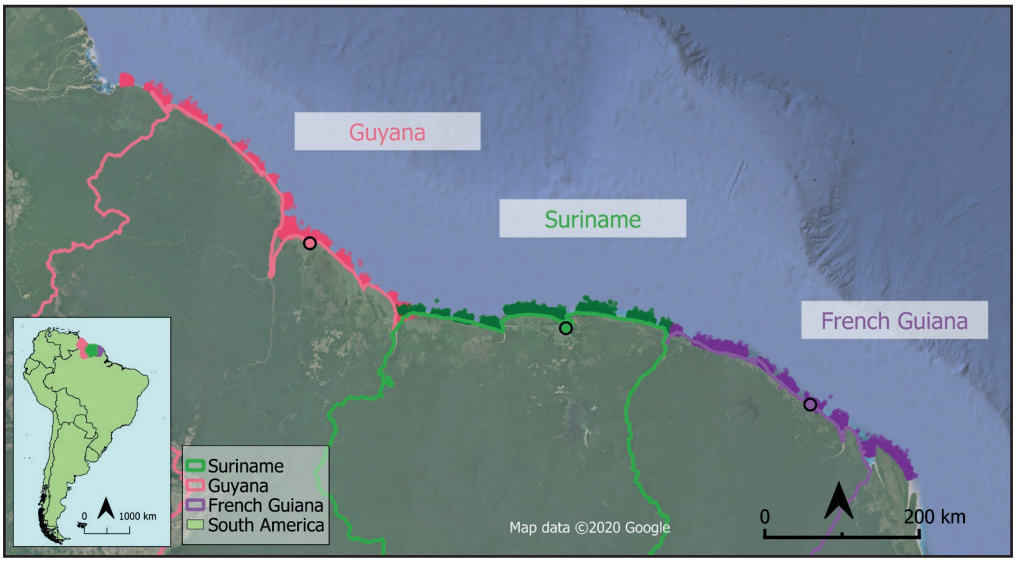

Figure 4.1: Guiana coastline, situated between the mouth of the Amazon River in Brazil and the Orinoco River in Venezuela comprising of Guyana, Suriname and French Guiana. The coastline is characterized by 20-25 migrating subtidal mudbanks (indicating by the colored dots for 2019) which leave a strong imprint on the coastline dynamics of the region. The origin of the color points is described in section 4.3.1.

(Anthony et al., 2010). Fine sediment, originating from the Amazon River, is transported along this coast in north-western direction in the form of migrating subtidal mudbanks (Allison et al., 2000; Augustinus, 1980). These mudbanks form on the northern coast of Amapa in Brazil (Allison 1995), east of French Guiana (Figure 4.1) and can be 20-30 km wide, 10-60 km long and 10-30 km apart. A single mudbank can contain up to 15% (Wells and Coleman, 1981) of the annual sediment load of the Amazon River and migrate with a speed of 0.5-5 km/yr from east to west (Froidefond et al., 1988; Gardel and Gratiot, 2005). Where a mudbank moves in front of the coast, enhanced wave damping (van Ledden et al., 2009; Winterwerp et al., 2007) and sediment deposition (Gratiot and Anthony, 2016) give opportunistic mangroves the chance to rapidly colonize the newly accreted mudflats (Gardel et al., 2011). This can result in coastline accretion up to 150 m /yr, or more (Allison and Lee, 2004). When a mudbank has passed the coast, the consolidated coastal mud and mangroves start to erode due to increased wave energy (i.e. no mud-induced wave dissipation) (Wells and Coleman, 1981).

The movement of the Inter-tropical Convergence Zone (ITCZ) induces a distinct seasonality in precipitation and wind along Guianas' coastline (Allison et al., 2000). The relatively southern location of the ITCZ between February and April marks the start of a shorter dry season with north-east trade winds, measuring on average 3-9 m/s (Augustinus, 2004; Wells and Coleman, 1981). Between April and July, the ITCZ moves north, heralding the onset of a longer wet season with lower wind speeds from the northeast and occasionally the southeast. From August to December, the ITCZ is located north of the coast, marking the start of the major dry season. This is characterized by dominant trade winds directed offshore to the south-east. After this period, the ITCZ moves south of the coastline again, initiating a shorter wet season with the north-eastern trade winds picking up again (Xie and Carton, 2004).

Between December and April, when the ITCZ is located further south, trade winds coming from north-eastern directions have a relatively longer fetch, therefore enhancing swell waves coming from the Atlantic Ocean (Gratiot et al., 2007). As a result, wave heights of up to two m can be observed offshore with periods between 6 and 10 s (Wells and Coleman, 1981). The regime in this wave-season leaves the open coast of the Guianas exposed to incoming waves and thus susceptible to erosion. This is only mitigated when almost complete wave dissipation is ensured by the presence of migrating subtidal mudbanks (Best et al., 2022).

Overall, the region receives an average of two to three m of rainfall per year, with the majority falling in the wet seasons. Coupled climate phenomena such as the El Niño-Southern Oscillation (ENSO) are thought to cause annual variability in precipitation in the Guiana shield countries (Labat et al., 2012). Despite the high precipitation, rivers along Guianas' coast have relative low discharges that range from 46 m^3/s for the Cayenne River to 2,104 m^3/s for the Maroni River (Gardel et al., 2022). Additionally they contain low suspended sediment loads, especially compared to the discharge (209,000 m^3/s) and total sediment load (1.2 x 109 ton per year) that originates from the Amazon River and is transported alongshore (Wright and Nittrouer, 1995). The local rivers do, however, influence the coastline dynamics by supplying sand to cheniers that provide additional resistance against erosion (Augustinus, 1989). Simultaneously, the outflow of these local rivers can produce a hydraulic groyne effect, slowing down mudbank migration 'upstream' of the coast (Anthony et al., 2013b), especially adding to the complexity of coastal morphology near river mouths (Gardel et al., 2022).

4.3 Methods and data

First, we created an unprecedented dataset with coastline position estimates and morphological data of coastline profiles (1,318 transects) from all available Landsat observations between 1986 and 2021. We then applied an unsupervised decision tree (UDT) to simultaneously define estimates of mudbank footprints and coastline position changes from individual remote sensing observations. Part of the workflow (Figure 4.2) has been published previously (de Vries et al., 2021, Chapter 2; de Vries et al. 2022, Chapter 3) and is briefly explained in the text where applicable. Where appropriate, results are presented on a country-by-country basis to facilitate comparison and interpretation of the different coastal management strategies (Nijbroek, 2012, 2014).

4.3.1 Satellite image processing

In the satellite image processing work, we applied the UDT (de Vries et al., 2021; Chapter 2) and subsequent workflow (de Vries et al., 2022; Chapter 3) on all Top of Atmosphere (TOA) reflectance Landsat images, collected over the coastal area of the Guianas between 1986 and 2021 by Landsat 4, 5, 7 and 8 (Figure 4.2). Not all acquired images are available in the Tier-1 collections, particularly before 2000. This is a classification that guarantees sufficient geometric accuracy and spectral precision of the images that is needed for change detection analysis (Wulder et al., 2016; Qiu et al., 2019). As a result, 2,088 images available in Tier-1, of the 8,000 images acquired over the Guianas' coastline, have been processed in the Google Earth Engine (GEE) environment (Gorelick et al., 2017).

Due to the spectral similarity between mudbanks and intertidal areas, it is necessary to unmix distinctive reflectance signals in remote sensing images into representative land cover fractions. (Alcântara et al., 2009). This means that the presence of multiple materials, such as water and mud, within one pixel are estimated from multiple spectral signatures. In this case, the UDT (Figure 4.2

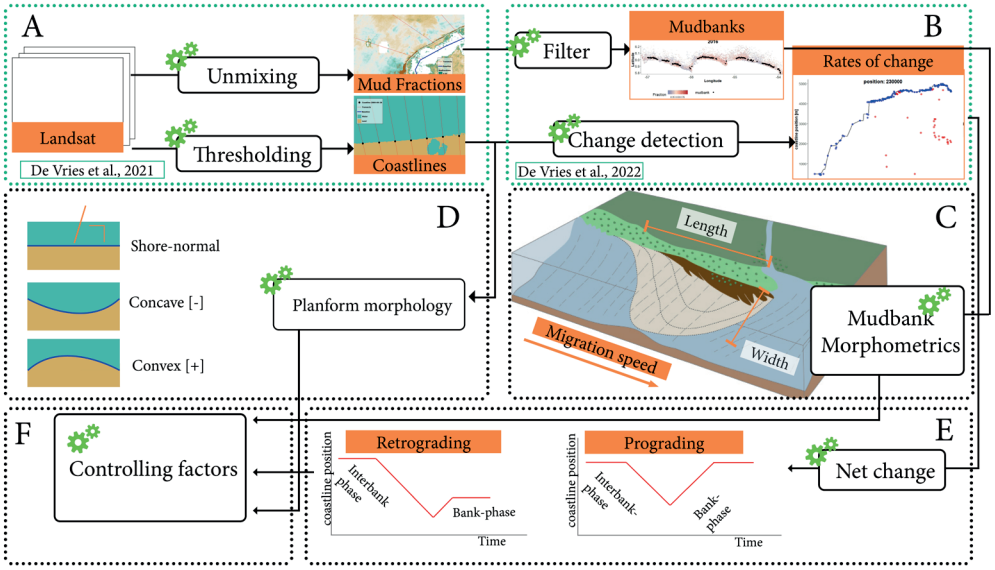

Figure 4.2: Methodology overview describing the unmixing and thresholding approach that is used to define annual median coastline position estimates. Additionally, the resulting mud abundance estimates are used to estimate mudbank morphometrics and, together with the coastline planform morphology, quantify the effect of the different controlling factors on long-term coastline change rates. Dashed, green boxes indicate the processing steps that have been published previously by de Vries et al., 2021 (Chapter 2) and de Vries et al., 2022 (Chapter 3).

A) implements a series of decisions to detect pixels that can be used as image end-members of pure mud, vegetation and water. From this spatially explicit selection, we can extract their corresponding mean spectral signatures for a fully constrained standard linear mixture model (de Vries et al., 2021; Chapter 2). The resulting fractions of land cover represent the proportion of each active component to the signal per pixel (Figure 4.2, A). The cover is always between zero (absent) and one (full cover) and the sum of all land cover fractions does not exceed one (Alcântara et al., 2009). From these abundance estimates of vegetation, water and mud, only the mud estimate is used from here on to estimate the presence or absence of subtidal mudbanks. We applied additional processing steps to the unmixed images to make them applicable for the Guianas' coastline. Further details of these filtering steps are described by de Vries et al. (2022; Chapter 3).

4.3.2 Mudbank detection

Although the offshore limits of subtidal mudbanks are diffuse and therefore difficult to quantify, we estimated it at yearly intervals by quantifying wave damping limits in each individual image. We assumed that changes in mud fractions are associated with variable sediment concentrations, often found in active migration areas of subtidal mudbanks (Zorrilla et al., 2018). These abrupt changes are considered as diffuse mudbank boundaries and can be visualized as discontinuous decreases in mud fractions along a transect orientated offshore (de Vries et al., 2021; Chapter 2). By automatically detecting these discontinuities and selecting them based on different criteria, we ensure that they can indicate probable mudbank boundaries (Figure 4.2, B). Discontinuities are defined as the local maxima that are extracted from the zero crossings of the first order derivatives of the filtered mud fractions. These are then filtered to ensure that positions and fraction values are

farther offshore than the land boundary, are not associated with cloud and shadow remnants and have sufficiently high fraction values to be associated with mudbanks (de Vries et al., 2022; Chapter 3).

The presence and absence of mudbanks on an annual basis was estimated by repeating the filtering steps for all 1,318 transects (Figure 4.2, A), equally spaced 1,000 m apart along Guianas' coastline and each available Landsat image (de Vries et al., 2022; Chapter 3). This indication was determined by identifying alongshore orientated clusters (minimal four transects) where abrupt changes in mud fractions are present in at least 30% of the observations for a given year (Figure 4.2, C). Transects in river mouths are excluded from this analysis. Morphometrics, including alongshore length, and maximum cross-shore width, are estimated from the estimates of mudbank presence (Figure 4.2, C). Simultaneously, the migration speed of mudbanks is estimated by comparing the fronting (i.e., leading edge) position for each mudbank with the previous year. For some years, we compared the average position change (e.g., centre) when this resulted in an unrealistic migration speed higher than 10 km, partially explained by inaccurate estimation of the footprint or shortening of the alongshore length. Afterwards, the frequency of mudbank occurrence was estimated based on the number of years a mudbank was present in the time series of observations. This results in a normalized estimate with values ranging from zero (never) to one (all years) for each transect.

4.3.3 Coastline position and planform morphology

We conducted a coastline change detection analysis on position estimates from individual satellite images, as detailed by de Vries et al. (2022; Chapter 3). By simultaneously separating terrestrial vegetation, including mature mangrove, and bare ground from water pixels (Figure 4.2, A) we created a binary land-water map using an Otsu thresholding approach (Donchyts et al., 2016). This is a computation-efficient method to define coastline positions without being overly sensitive to different types of transitions between land and water, including mangrove fringes, sandy cheniers and consolidated sediment, that can be naturally found in the coastal zone (de Vries et al., 2022; Chapter 3). Despite this one-dimensional approach for detecting land-water transitions along a transect, the estimates are consistently within 50 m of the true land-water boundary and on average within one Landsat pixel (de Vries et al., 2022; Chapter 3). After extracting the last transition from land to water for each transect and image, we could estimate median coastline position estimates for a given year (Figure 4.2, B) as well as rates of change between years (Figure 4.2, E). Two metrics were considered here, firstly an endpoint rate methodology was applied to compute the rate of change from coastline positions at the beginning and end of the timeseries. Secondly, annual changes were computed from median coastline positions between each year.

Simultaneously, the median coastline positions were used to compute the orientation and curvature of the associated coastline segment. To do this, the coordinates of neighbouring pixels that make up the surrounding coastline were extracted. A Canny edge detection algorithm (Liu and Jezek, 2004), available in GEE, was applied to the annual median composite land masks. We used annual median binary land masks to select the longest features and avoid gaps that result from cloudmasking, as opposed to the individual for the coastline position estimates (Figure 4.2, B). This reduced the possibility of estimating incorrect curvature and coastline orientation values. After exporting the coordinates that correspond to the annual coastline pixels that are within a buffer of 250 m, we calculated their curvature and shore-normal orientation in R-studio (Figure 4.2, D), using R version 3.6.3 (R Core Team, 2020).

We computed the shore-normal orientation and curvature for each annual median coastline position (Figure 4.2, D) by ordering all coordinates with respect to the dominant orientation of

the concerning coastline section. Then we defined areas as convex or concave seaward, based on a positive or negative curvature (k), respectively, with k given by:

$$k = \frac{\frac{d^2y}{d^2y\text{-}dx^2}}{[1+\left(\frac{dy}{dx}\right)^2]^{3/2}} \qquad (4.1)$$

In equation (4.1), *x* and *y* are coordinates in m (UTM coordinate system). Smoothing is applied to avoid systematic errors related to the vectorization of the coastline feature and extract precise estimates of concavity from coarse resolution images (Cipolletti et al., 2012). By linearly smoothing each set of coastline points before calculating *k* is reduced *dy/dx* to zero (Lazarus and Murray, 2007). To do so, a kernel smoothing was applied that is available as standard in R-studio's *Smoothr* package with the function smooth function implemented (Strimas-Mackey, 2021). This removes small-scale (high frequency) variations related to the pixel size and reveals the larger scale curvature around the coastline position of interest (Lazarus and Murray, 2007).

4.3.4 Contribution of controlling factors to coastline change rates

To analyse the relationship between controlling factors, including frequency of mudbank occurrence (Section 4.3.2) and planform morphology (Section 4.3.3), and the rate of coastline change we applied single and stepwise multiple linear regression models (Figure 4.2, F). These models were optimized using a backward model selection procedure to ensure the depended variables followed

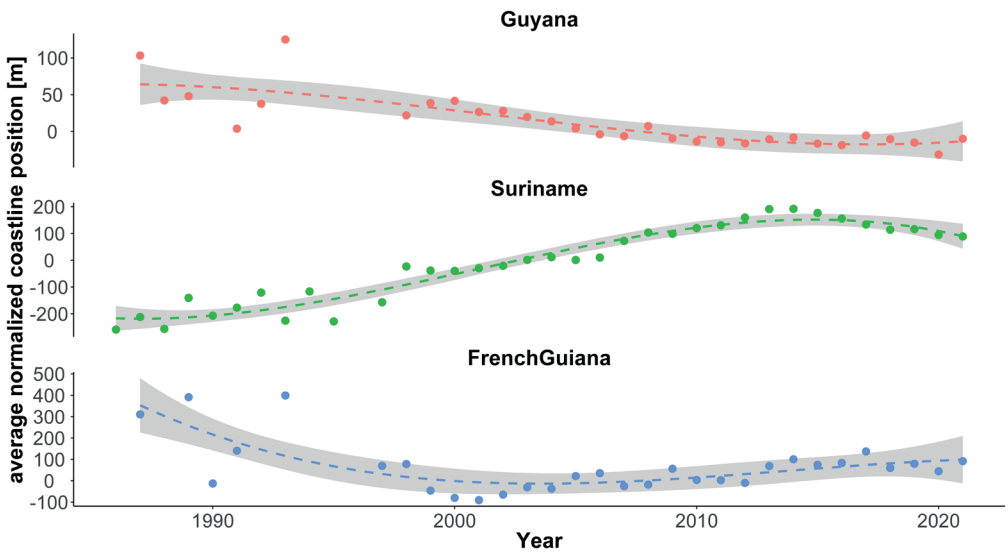

Figure 4.3: Temporal variability in country-averaged coastline changes (colored dots) for French Guiana, Suriname and Guyana between 1985 and 2021. The average coastline position (y-axes) contains all cross-shore distance estimates with respect to the coastline position at 1-1-2006, identified for each transect separately. Dashed lines indicate 3rd polynomial B-spline fit with the corresponding 95% confidence intervals indicated by the grey areas. Notice the difference in scale range on the y-axes.

approximate normal distributions. They were also checked for multicollinearity and showed relative homogeneous variances (Zuur et al., 2010). Regressions were conducted with raw, cantered and log-transformed variables, all showing similar correlation coefficients. We present scaled and cantered data to interpret the absolute contribution to the variance between different variables. The relative contribution to the total variation explained by the selected model was used as a measure of relative importance of each variable (R^2).

The significance of the variation in coastline changes and controlling factors was tested by using analysis of variance F-tests. Spatial autocorrelation was checked by performing Moran's I tests on the annual coastline position estimates. Significant spatial autocorrelation in the datasets ($p < 0.05$) was inherent to our dataset. All statistical analysis was conducted in R-studio, using R version 3.6.3 (R Core Team, 2020) using the library packages *relaimpo* (Grömping, 2006), *ape* (Paradis et al., 2004) and *broom* (Robinson, 2014).

4.4 Results

4.4.1 Coastal evolution

For Guianas' coastal zone, a total of 1,318 km coastline has been analysed at alongshore intervals of 1,000 m between 1985 and 2021 (Figure 4.1). On average the coastline accreted, yet more importantly, variability between and within countries exists (Figures 4.3 and 4.5). The observed difference in coastal changes can be grouped based on the administrative national boundaries (Figure 4.3). The coast of Suriname expanded between 1986 and 2021 by ~300 m, then stabilized and started to erode from 2013. French Guiana's coastlines showed overall accretion of ~200 m after 1998. Guyana experienced overall erosion between 1986 and 2021 of ~30 m, although changes

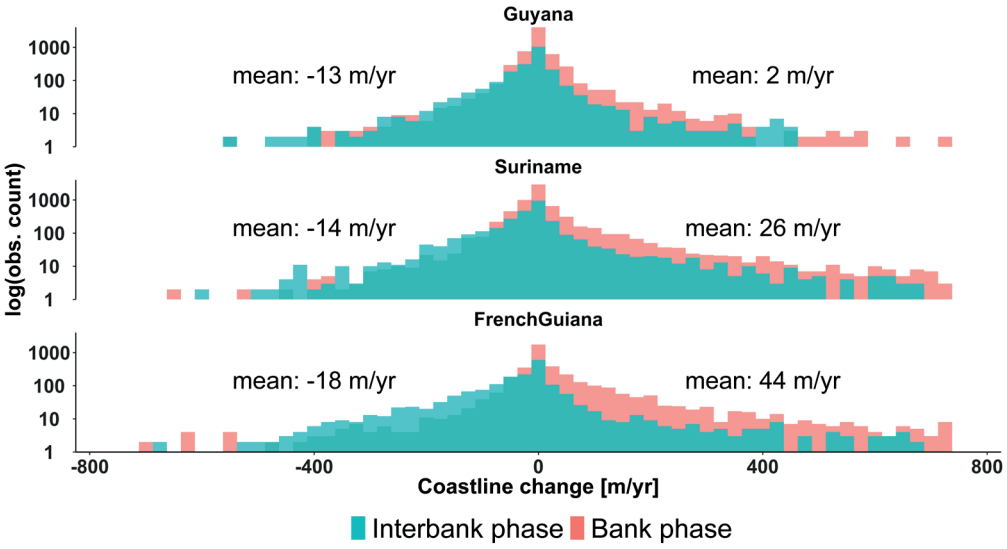

Figure 4.4: Annual coastline changes under influence of mudbank presence and absence. For each transect and year the cross-shore changes in coastline position are linked to the pressence and absence of mudbanks. Mean values are computed by averaging all annual changes for each country. For visualization purpose, the x-axis is limited between -800 and 800 meters and the y-axis log transformed.

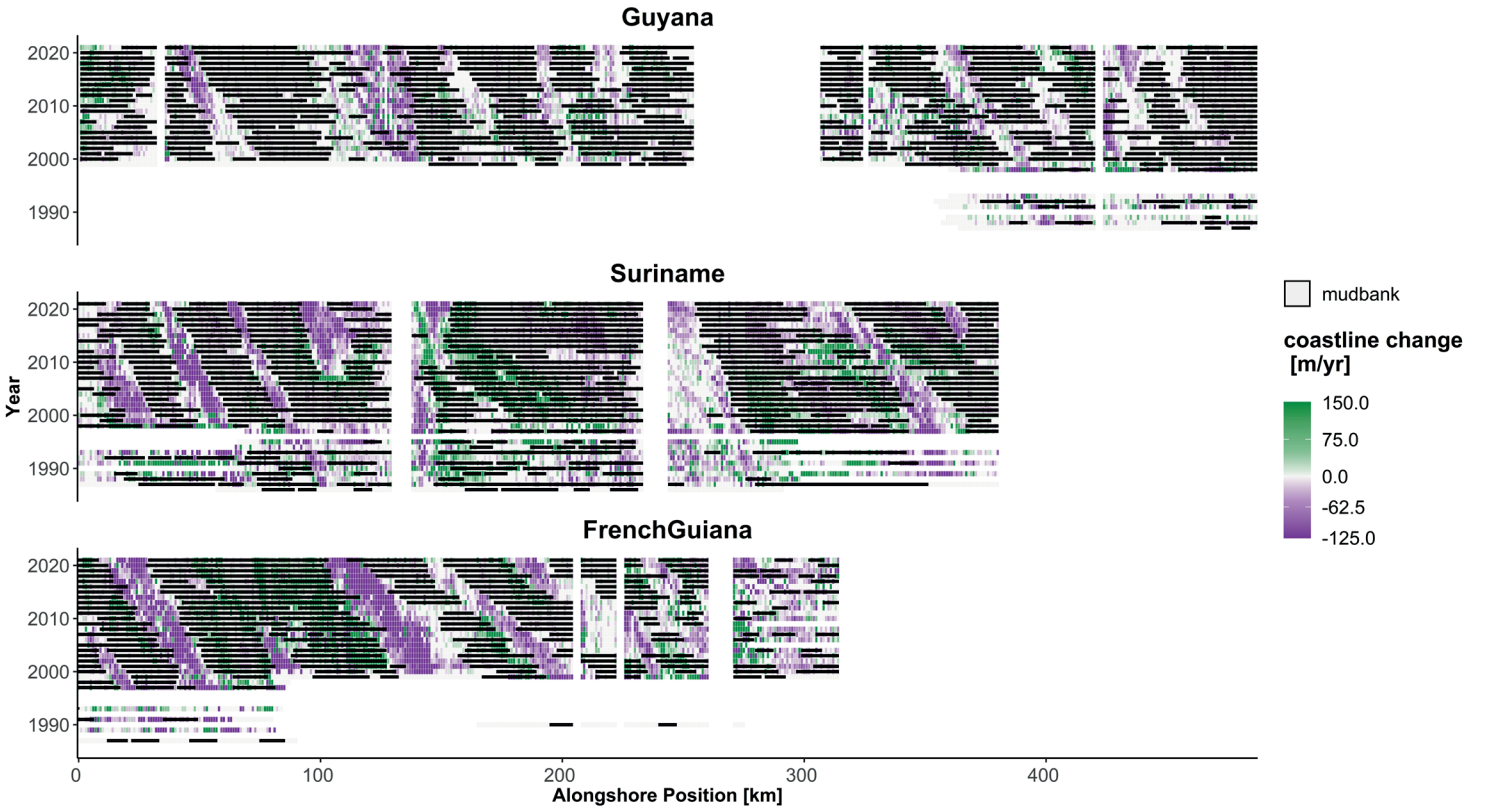

Figure 4.5: Spatiotemporal variation in coastline changes between 1985 and 2021 for French-Guiana, Suriname and Guyana. Colors indicate positive or negative annual coastline changes for each transects and the boxes correspond to the annual position estimates of mudbanks. Especially for Guyana and French Guiana many of the Landsat observations between 1985 and 1999 are missing from the T1 collections that ensures sufficient spatial accuracy for multitemporal change detection analysis. Also transects in (direct vicinity) river mouths are not included in this research and result in this figure in missing data.

are up to one order of magnitude smaller compared to Suriname and French Guiana (Figure 4.3). All countries show shorter periods (3-6 years) of expansion or enhanced coastal retreat, although the fluctuations are out of phase (Figure 4.3).

Spatial and temporal variability in coastline changes can, especially for French Guiana and Suriname, be related to alongshore migration of subtidal mudbanks (Figure 4.4). Overall, coastal sections are expanding when mudbanks are present and eroding when absent, although large local variability exists (Figure 4.5). Clear alternating and variable wide bands of both erosion and progradation are progressing from east to west. This coastal behaviour is supported by the observations in Figure 4.4, indicating that coastal progradation during mudbank phases can be considerably larger, with an average between 2 and 44 m/yr. During interbank phases, average coastline retreat is between 13 and 18 m/yr (Figure 4.4). This supports previous observations of expanding coastlines in French Guiana and Suriname on the medium (15-30 year) timescale (Froidefond et al., 1988).

Local-scale differences in coastline position changes (Figure 4.5) illustrate the spatiotemporal variability that can be found along Guianas' coastline. Nearby transects can show contrasting behaviour or a transect can undergo rapid shift from accreting to eroding and vice versa. Annual coastline changes go up to, and sometimes surpass 200 m/yr for some transects (Figure 4.5), with Suriname and French Guiana in particular showing larger spatial variability in coastline changes (Figure 4.4). For Guyana, such large coastline changes, either expanding or retreating, are less common as indicated by the lower average rates of retrogradation and progradation.

In addition to differences in coastline position, the shore-normal coastline orientations are considerably different (Appendix, Figure-C 2, Panel B). For Guyana, the average orientation is 43° (north-east), 12° (north) for Suriname and 33° (north to north-east) for French Guiana (Figure 4.1

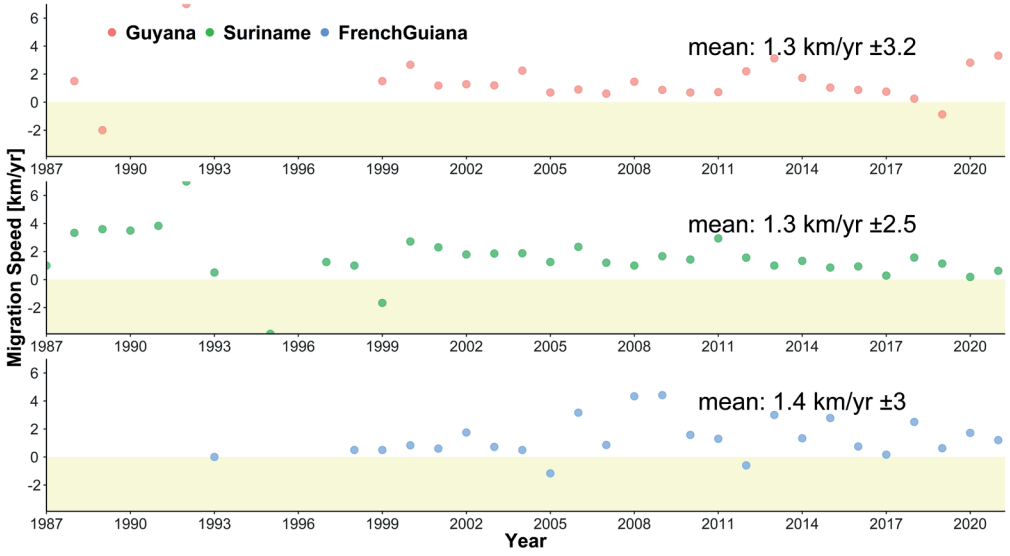

Figure 4.6: Temporal variation in average mudbank migration speed between 1985 and 2021 for French Guiana, Suriname and Guyana. Before 1998, insufficient Landsat observations prohibit accurate estimates of mudbank migration rates, averages are therefore based on the values after 1998.

and Panel B in Appendix C, Figure-C 2). The distributions have a standard deviation of 25°, 26° and 28° for Guyana, Suriname and French Guiana, respectively, indicating small correspondence between the distributions (Appendix C, Figure-C 2, Panel A). In general, temporal variation in coastline orientation is less than 20 degrees, except for locations where complex patterns of progradation or erosion causes the coastline orientation to change (Appendix C, Figure-C 2, Panel C).

4.4.2 Mudbank morphometrics

From Figures 4.4 and 4.5, we can reaffirm that mudbank phases can be associated with coastline expansion, and interbank phases can be associated with erosion (Section 4.4.1). On average, 30 mudbanks, each stretching 5-20 km of coastline and up to 8.1 km into the sea (Appendix, Figure-C 1), migrate along Guianas' coastline with average speeds ranging from two km per year in eastern direction and to six km per year in western direction (Figure 4.6). Spatial variability in mudbank morphology is especially obvious for alongshore mudbank length, with clearly on average shorter lengths (<10 km versus 15-20 km), yet more mudbanks (12), fronting the coast of Guyana, compared to Suriname (8) and French Guiana (10). As a result, mudbanks in Guyana (Appendix, Figure-C 3) are smaller in area (10-350 km^2) compared to mudbanks in French Guiana and Suriname (10-500 km^2).

Individual mudbanks fluctuate in their migration speed between -2 and 7.5 km/yr. Despite the challenges in deriving migration speeds, especially from 1998 onwards, migration tends to fluctuate around 1.05, 1.19 and 1.24 km/yr for Guyana, Suriname and French Guiana, respectively (Figure

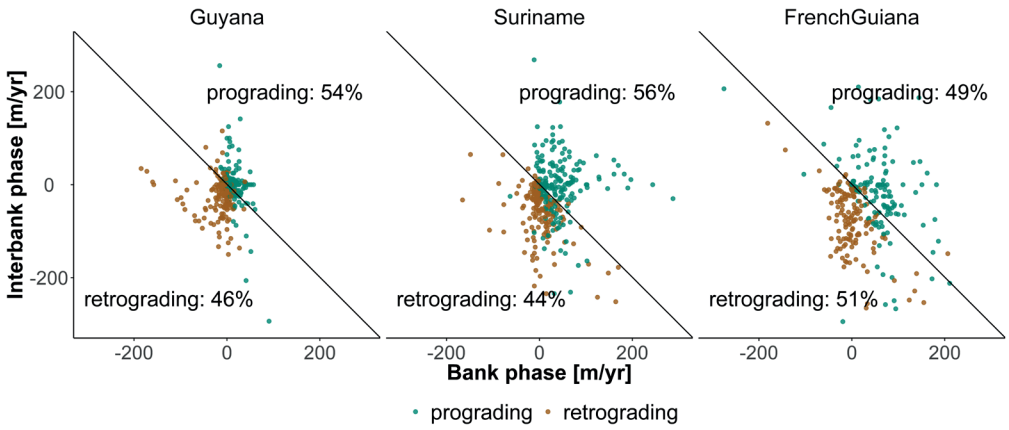

Figure 4.7: Coastline position changes for individual transects in Guyana, Suriname and French Guiana between 1985 and 2021. X-axis positions are based on the coastline changes under influence of mudbanks while the y-axis values represent the coastline changes when mudbanks are absent. Observations above the diagonal line indicate where the changes under influence of mudbanks are larger than when absent. Net annual change (prograding or retrograding) is indicated by the colored symbols and is computed by comparing the annual rate of change between the first and last coastline position. Green points below the diagonal line thus imply the erosion during interbank phases to surpass progradation during bank phases. The percentages tell how many transects showed progradation and retrogradation between 1985 and 2021.

Table 4.1: Summary of the linear model of frequency of occurrence and net coastline change rate (n = 1089 transects). For each model a summary of the significance and explained variance (R^2) is given. The model has been repeated for subsets of the data: French Guiana (n=299), Suriname (n =363) and Guyana (n =427), corresponding to linear fits in Figure 4.9.

Model	Coefficient	SE	t-value	p-value	R^2
Net coastline change ~ frequency of occurence					
Intercept (full data set)	-48.2	3.4	-14.2	2e-16	
Frequency of occurence (1985-2021)	73.1	4.7	15.4	2e-16	0.18
Intercept (French Guiana)	-93.8	7.8	-12.1	2e-16	
Frequency of occurence (1985-2021)	51.8	11.8	12.9	2e-16	0.36
Intercept (Suriname)	-35.8	5.9	-6.1	3.4e-09	
Frequency of occurence (1985-2021)	63.3	8.2	7.7	1.4e-13	0.14
Intercept (Guyana)	-37.6	3.4	-11.0	2e-16	
Frequency of occurence (1985 - 2021)	48.1	4.5	10.6	2e-16	0.21

Table 4.2: Summary of the multiple linear models of net coastline change predicted by the frequency of mudbank occurrence, mean curvature, mean shore normal orientation and the alongshore distance for the entire Guianas coastline (n = 1089).

Model	Coefficient	SE	t-value	p-value	R^2
Net coastline change					
Intercept	8.5	9.7	0.9	0.4	
Frequency Of Occurrence (1985-2021)	82.7	4.7	17.6	2e-16	0.2
Mean Curvature	1453.2	1476.1	-1.0	0.3	0.00
Mean Shore normal	-0.3	0.0	-8.1	2.2e-15	0.03
Alongshore distance (log(km))	-4.2	0.8	-5.6	2.9e-08	0.01
					0.25* **

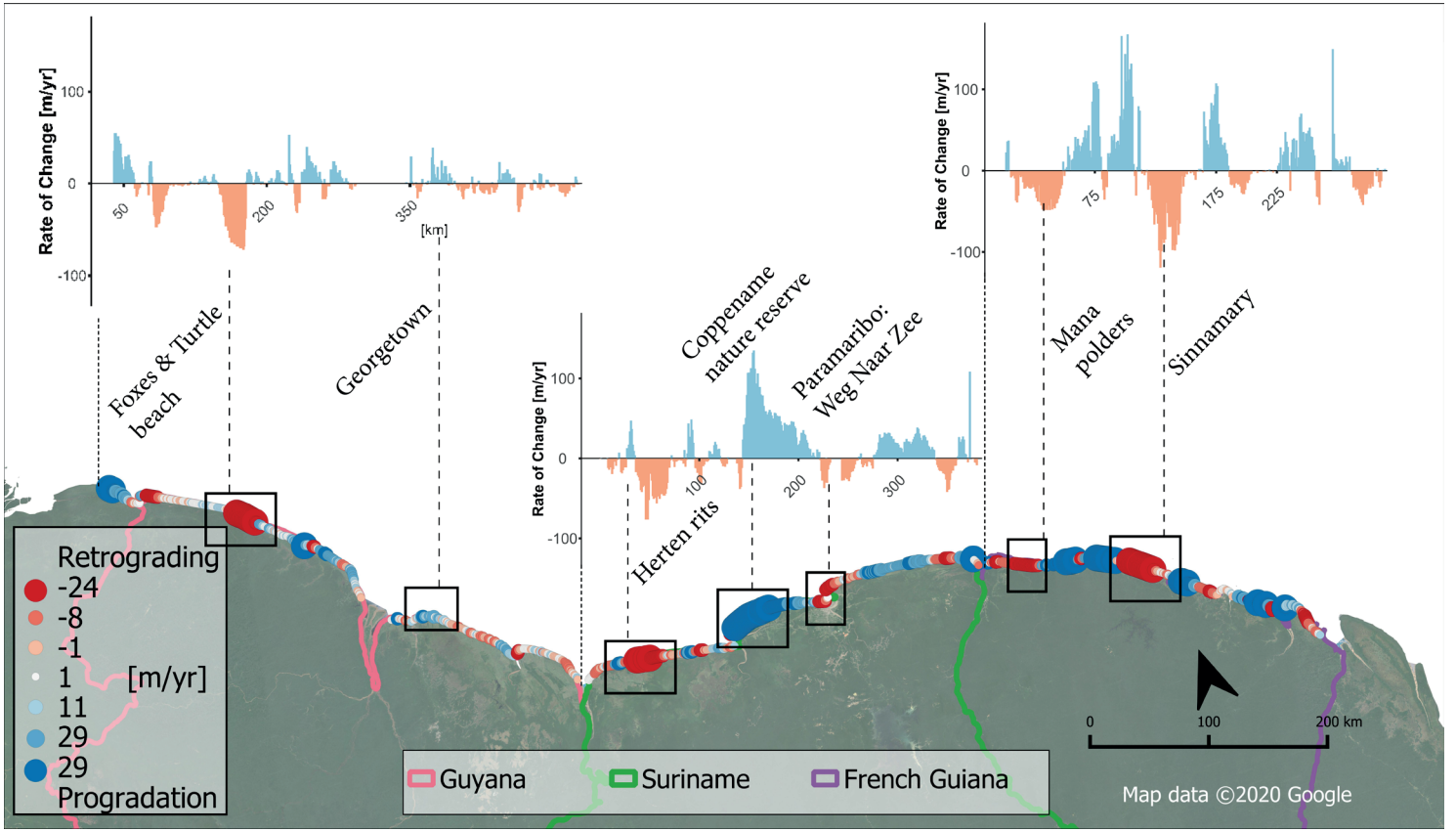

Figure 4.8: Coastline rates of change along the Guianas coastline. Clustered groups of transect show similarity in behavior, especially for the observed larger magnitudes of progradation (blue) and retrogradation (red).

4.6). The relative larger spread (up to 3.3 km/yr) in observed migration speeds suggest that observed country averages are not significantly different between 1985 and 2021.

4.4.3 Net coastline changes

Of the coastlines in Suriname and Guyana, 56% and 54% can be considered accreting based on the net rate of change between 1985 and 2021, whereas for French Guiana this is 49% (Figure 4.7). By adding annual position changes under mudbank presence and comparing that with those changes during interbank years for each transect (Section 4.3.3), we can determine the influence of mudbanks on net coastline changes (Figure 4.7). It is interesting to note that coastal sections with erosion during interbank phases surpassing the accretion during bank phases (Figure 4.7; below the diagonal line) are spatially clustered (Figure 4.8). These coastal sections, stretching alongshore between 10 and 30 km, surpass the average length of a mudbank. Also, exceptional accretion rates are found in clustered groups, especially in Suriname and French Guiana (Figure 4.8).

In general, when a stretch of coastline is fronted by a mudbank, more than 60% of the cases, coastline end-point change rates will be positive and ensure overall coastal progradation (Figure 4.9; Panel A and B). Differences in net coastline changes (Figure 4.8) can partially be explained by the frequency of mudbank occurrence (R^2 = ~0.18, p < 0.05; Table 1). Mean frequency of mudbank occurrence is highest for Guyana and lowest for French Guiana (Figure 4.9, Panel A). However, for French Guiana the net coastline changes cover a wider range (Figure 4.4) and are significantly stronger positively related to mudbank frequency of occurrence (R^2 = 0.356, p < 0.05) compared to Suriname (R^2 = 0.138, p < 0.05) and Guyana (R^2 = 0.207, p < 0.05; Table 1).

In addition, relative to other control factors, including mean coastline curvature, mean shore normal orientation and the alongshore coastline distance, the frequency of mudbank occurrence explains the greatest variation in observed coastline changes (R^2 = 0.197, p < 0.005; Table 2). Mean shore normal orientation and alongshore distance were negatively correlated and explained small proportions of variability in multi-decadal coastline change rates (R^2 = 0.03 for shore normal orientation and R^2 = 0.01 for alongshore position, p < 0.05).

4.5 Discussion

4.5.1 Coastline variability in the Guianas

Our observations (Figures 4.3 and 4.8) reaffirm that spatial and temporal variability in coastline changes are among the largest globally (Luijendijk et al., 2018). It has been suggested previously that spatial variability for such large coastline changes can be linked to the type of coastal landform, including erosive resistant features such as rock outcrops in French Guiana, sandy cheniers (Anthony et al., 2019) or the coastal protection measures, predominantly implemented in Guyana and Suriname (Nijbroek, 2014). On the other hand, the more erosion-prone strips of coastline, such as mangroves during interbank phases, have the potential to rapidly retreat (Trebossen et al., 2005). Previous case studies on the lack of resistance to erosion and reduced sediment storage capacity, for example due to the conversion of mangrove forest in aquaculture and agriculture in the Mana Polder, French Guiana (Brunier et al., 2019), can now be extended to all retrograding hotspots along the coast (Figure 4.8). Clear examples include Foxes and Turtle Beach in Guyana, Hertenrits and Weg naar Zee in Suriname and Sinnamary Delta in French Guiana (Figure 4.8).

The differences in coastline position changes (Figures 4.3 and 4.5) are larger compared to their difference in coastline morphology would suggest, especially for Guyana and French Guiana. The small difference in shore-normal orientation (Appendix, Figure-C 2) for French Guiana and

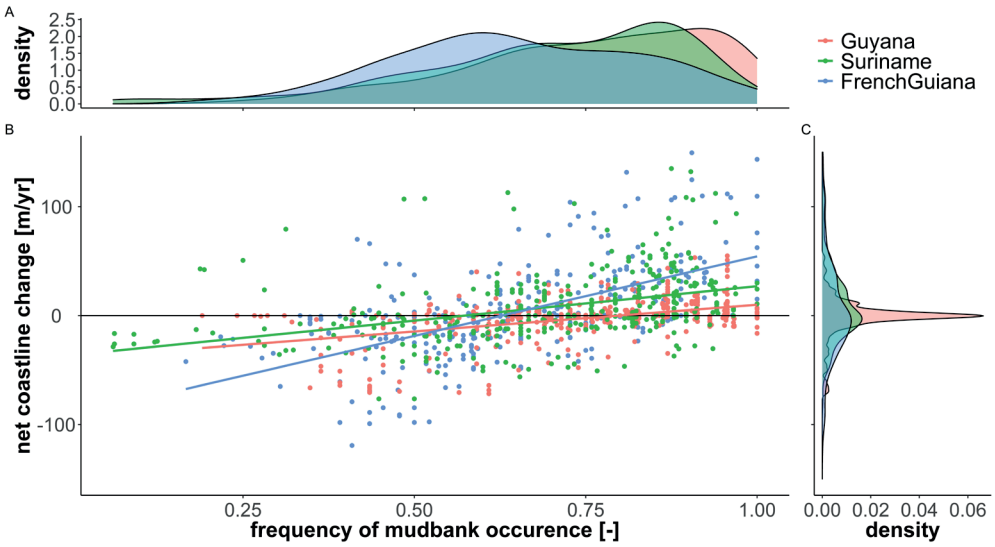

Figure 4.9: Frequency of mudbank occurrence and net coastline changes for all alongshore coastline positions in French Guiana, Suriname and Guyana. Panel A and C show the distribution of frequency of mudbank occurrence and net coastline changes for each country. Panel B shows relation between frequency of mudbank occurrence and net coastline change rates, where overall coastlines show progradation when the occurrence is higher and thus mudbank phases are longer or occur more frequent.

Guyana (33° and 43°, respectively), and the resemblance in their offshore wave climate (Allison et al., 2000) hint at other processes influencing the observed significant difference in coastline change trends (Figure 4.3). Guyana has experienced a slightly decreasing trend in average coastline position since ~2000 while French Guiana has had an increasing trend. These differences in coastline changes are therefore not solely dependent on shore-normal orientation and coastline planform morphology, normally associated with lower incoming wave angles (Gratiot et al., 2007). This is possibly because such responses in coastline morphology are obscured by undulations with a larger scale and magnitude effect, such as the migration of mudbanks in the Guianas (Figure 4.4). Or it could be due to the erosion resistance, associated with different coastal land cover classes such as agriculture or coastal protection measures (McLoughlin et al., 2015).

Long-term trends in coastline changes have previously been linked to large-scale changes in atmospheric and hydrodynamic forcing mechanisms (Gratiot et al., 2007). Processes that have been suggested include the north-eastern trade winds (Augustinus, 2004), the NAO (Walcker et al., 2015) and 18.6-year nodal cycle (Gratiot et al., 2008). Walcker et al., (2015) found a stronger correlation between variation in mangrove extent between 1950 and 2010 for French Guiana and increased swell wave activity that is thought to be associated with remote forcing related to NAO. Although Walcker et al. (2015) looked at changes in mangrove surface area, Gratiot et al. (2008) also found coastal progradation between 1998 and 2006 but linked that to the 18.6-year nodal cycle. Our results for French Guiana, although uncertain prior to 1999 due to a limited number of observations, are in line with these findings indicating accretion since 1990 (Fromard et al., 2004). And, we can now extend the progradation phase in French Guiana to 2021 (Figure 4.3). This progradation trend seems to contrast with the retrograding trend of coastline position changes for

Guyana and partially for Suriname since 2015 (Figure 4.3). Additionally, increased coastal erosion was expected for Suriname from the 1990's onward (Augustinus, 2004). This also contrasts with our observations of discontinuous progradation between 1985 and 2021 (Figure 4.3), and can be partially explained by variable coastline response to the presence or absence of mudbanks along the coast (de Vries et al., 2022; Chapter 3).

4.5.2 Mudbanks Morphometrics

We demonstrated here the first detailed study of semi-automatic detection of mudbank footprints along Guianas' coastline from remote sensing images, showcasing the spatiotemporal variability in their morphometrics (Appendix, Figure-C 1). The estimates of mud abundance indicated the presence of up to 30 mudbanks, each stretching between 12 and 21 km alongshore. Their subtidal parts, as can be detected from remote sensing images, extended up to eight km perpendicular to the shore. Mudbanks are separated by 10-15 km wide interbank phases, characterized by relatively lower mud fractions. Variability between the individual mudbank footprints is reflected in the morphometric estimates such as length and the migration rates (Figure 4.6). Overall, mudbanks in Suriname are longer than those in French Guiana and especially Guyana, resulting in larger areas of mudbank footprints (Appendix, Figure-C 3). Additionally, different spatial patterns, including breaking, merging, growing, and shrinking of mudbanks can be observed (Appendix, Figure-C 1). The similarity in footprint area with previous estimates of mudflat area (Froidefond et al., 1988) and lower computed alongshore mudbank lengths (Augustinus, 2004) suggest that our mudbank footprints are conservative estimates and most likely exclude the active migration zone of subtidal mudbanks (Zorrilla et al., 2018).

The consistent identification of mudbank footprints did allow us to semi-automatically estimate the alongshore migration speed for all mudbanks along Guianas' coastline (Figure 4.6). From our results we can see that deriving migration speeds from changes in the mudbanks leading edge position (Gardel and Gratiot, 2005) might not reflect the migration rate alone, as deformation of the footprint also can significantly influence the movement of its infliction point (Froidefond et al., 1988). It is the external factors, like wave-mud interactions that cause resuspension of fluid mud and the incoming wave angle under influence of the trade winds. These are known to enhance variability in footprints on daily to weekly timescales and thus migration rates on seasonal to multi-decadal timescales (Anthony et al., 2013a; Augustinus, 2004; Gardel and Gratiot, 2005). Despite the difficulty of computing the migration speed for mudbanks from constantly changing footprints, estimated migration rates up to six km/yr (Figure 4.6) align with previous studies focusing on one (Gratiot et al., 2007; Péron et al., 2013) or a selection of mudbanks (Zorrilla et al., 2018), often within a limited timeframe (Gensac et al., 2016) or low (multiple years to decades) temporal resolution (Augustinus, 2004). There appears to be a difference in average migration speeds between mudbanks in French Guiana (1.24 km/yr) compared to smaller banks in Guyana (1.05 km/yr) and bigger ones in Suriname (1.19 km/yr), This suggests there is link between migration speed, mudbank dimensions and geographical location of the mudbank (Appendix, Figure-C 3).

4.5.3 Mudbanks controlling coastline changes

Both the migration speed and footprint (Section 4.5.2) of mudbanks control the duration of mudbank presence in front of any coastline stretch, and thus the continued wave damping potential and sediment supply that facilitates continued coastal progradation. Because the opposite is also true for interbank phases, with prolonged exposure to wave forcing and lack of sediment supply, mudbank morphometrics are a dominant control to the underlying mechanisms for coastline

changes. We therefore introduced the frequency of mudbank occurrence to incorporate both the migration rate and changes in mudbank shape for determining the influence of mudbanks, and for the first time their morphometrics, on long-term coastline change rates of the Guianas at 1,000-m resolution (Figure 4.8). Significant spatiotemporal differences in rates of coastline change (Section 4.4.1 and Figure 4.3) can be attributed to the migration of subtidal mudbanks, with accretion up to 44 m/yr when present and 10 m/yr of erosion when absent (Figure 4). As a result, the alternating phases leave a strong imprint on the coastline changes, as already demonstrated from mapped coastlines as early as the 18th century (Plaziat and Augustinus, 2004). Guyana showed less recognizable alternating phases (Figure 4.5) of coastline retreat and expansion compared to French Guiana and Suriname, which can potentially be associated with the irregular behaviour of mudbank migration along its coast or reduced volume of the mudbank (Augustinus, 2004).

The observations of coastline changes, under the influence of migrating mudbanks, suggest overall progradation in French Guiana, Suriname and Guyana for 49%, 56% and 54% of the coastlines, respectively, between 1985 and 2021 (Figure 4.7). Yet, stretches of coastlines with more erosion during interbank phases than progradation, or no progradation at all, during bank phases can be observed (Figure 4.8). This indicates potential state transitions due to complex interactions that result in often episodic, rather than gradual, coastline changes (Augustinus, 2004). Unbalanced phases of erosion and progradation indicate system disturbances and potential irreversible (land cover) transitions (Phillips, 2018). Additionally, this instability can be amplified by the variable response of mudbanks on different stretches of coastline they pass during migration, as not every mudbank has the same effect on each stretch of coastline it passes (Figure 4.4).

When a coastline is fronted by a mudbank, net progradation occurred between 1985 and 2021 at least 50% of the time, although differences in the minimum duration exist between countries (Figure 4.9). Frequencies of mudbank occurrence explain the relatively large proportion in the observed variance of coastline changes ($R^2 = 0.356$, $p < 0.05$) especially in French Guiana compared to Suriname ($R^2 = 0.138$, $p < 0.05$) and Guyana ($R^2 = 0.207$, $p < 0.05$; Table 4.1). The relatively low explained variance suggests that factors not included here, such as coastline type, land cover changes and wave climate, should be included in order to improve the prediction model. Additionally, coastal zones in Suriname and French Guiana seem to have a quicker response to the passing of a mudbank as indicated by the change from net retrograding to progradation at lower frequencies of mudbank occurrence (Figure 4.9).

Due to a nearly symmetric offshore wave climate and the differences in shore-normal coastline orientations (Appendix, Figure-C 2), the wave climate in Suriname can be characterized by high incoming wave angles. For both Guyana and French Guiana, it can be characterized by lower incoming waves. We show that the coastline orientation ($R^2 = 0.03$, $p < 0.05$), in combination with other internal control factors coastline curvature ($R^2 = 0.00$, $p > 0.05$) and alongshore distance ($R^2 = 0.01$, $p < 0.05$), hardly influence the long-term rate of coastline changes (Table 4.2). Additionally, temporal trends in coastline changes are different between countries, while large-scale climate patterns in atmospheric variability (e.g. NAO) and offshore wave climate are thought to be similar (Allison et al., 1995; Anthony et al., 2010). The persistence of significant variability in coastline trends between countries (Figure 4.3, and Section 4.5.1) indicates that large-scale external controlling factors are most likely only part of the explanation for the variability in observed coastline changes between 1985 and 2021. This re-emphasizes that the duration of wave damping by mudbanks, here expressed as frequency of mudbank occurrence, significantly influences the long-term fate of coastlines ($R^2 = 0.2$, $p < 0.05$; Table 4.2).

The significant contribution of mudbank occurrence to coastline changes (Figure 4.9) suggests that future research should focus, more than already being done, on the factors that influence the spatial footprints of subtidal mudbanks. Observed local differences in progradation (or sometimes lack thereof) in response to mudbank presence (Figure 4.7) indicates that not all mudbanks result in the same response at each location they pass. Potential suggestions for these observed patterns include the accommodation space for sediment storage and consequential mangrove colonization, the effect of wind-generated waves, and hydrodynamic forcing on the mudbank footprint (Anthony et al., 2010).

Our results can assist in directing intervention measures that aim to prevent exposure of communities to coastal flooding resulting from erosion. This provides coastal managers and decision makers with easily accessible information regarding past coastline changes along the entire coastline of the Guianas. As shown, mere alternating phases of retreat and expansion under the influence of migrating mudbanks are not guaranteed (Figure 4.4). The lack of progradation during mudbank phases might be potentially harmful in areas where mangroves are already infringing on urban expansion or agricultural activities. Also, the increased attention on enhancing coastal mangrove development for coastal protection and carbon sequestration (Alongi, 2012) requires knowledge of the location of mudbanks, their migration rates and the anticipated natural coastline response (Sanderman et al., 2018).

4.5.4 Methodology: drawbacks and modifications

In this chapter, we applied an UDT that consistently applies an Otsu thresholding algorithm to identify coastlines positions and ultimately the planform morphology (de Vries et al., 2021; Chapter 2). The UDT uses linear spectral unmixing to simultaneously derive comparable estimates of mud abundance to estimate the position, width, length and migration speed of subtidal mudbanks (de Vries et al., 2022; Chapter 3). The combination of well-established remote sensing methods can still occasionally return false positive detection of mudbanks or inadequate position estimates of coastlines positions, despite additional outlier detection and filtering. For example, mud bars, which are often rapidly colonized by juvenile mangroves (Balke et al., 2011), are a common feature resulting from mudbank migration and are sometimes falsely detected as rapid accretion. Although these mud bars are often the new coastline position in the long-term (Proisy et al., 2009), the instantaneous progradation rate then overestimates the true annual progradation. Similarly, coastline retreat is sometimes falsely detected when the true land-water boundary is obscured by clouds and inland waterbodies near the shore. Potentially correcting coastline positions for wave run up and tidal elevation could improve position estimates by an estimated 50%, assuming accurate bathymetry and wave breaking hindcasts are available for the area of interest (Castelle et al., 2022, 2021; Vos et al., 2020).

Estimates are needed for mudbank footprints to avoid unrealistic lengths and offshore extents of mudbanks and other inadequate representation of mudbanks. The parameterization of inputs is also required, including minimal length of mudbanks and the amount of mudbank indications per year (Section 4.3.1). This might be one explanation for the underestimation of mudbank width (Appendix, Figure-C 1), false positive and false negative detections of mudbank footprints (Figure 4.6). A multitemporal database with mudbank footprints estimates of sufficient spatial and temporal resolution to capture hourly to daily fluctuations in mudbank extent is required to truly determine the accuracy of our approach. Such a database would make it possible to quantify detection limit of mudbank footprints from remote sensing images in general, with respect to the high natural variability of mudbanks (Zorrilla et al., 2018).

Improvements to the morphometric estimates of mudbanks are especially necessary to constrain the naturally occurring variability in mudbank footprints. This information can be useful to guide future numerical modelling efforts on the mudbank footprints and their migration under influence of factors external to the system, such as wave regime, climate indices (e.g., NAO, ENSO and 18.6-year nodal cycle) and sea-level rise. Also factors internal to system, such as variation in sediment concentrations, alongshore currents and anthropogenic land cover changes, can only properly be addressed with sufficient coastline change observations going back at least two cycles of mudbank migration. This would require a time series for each controlling factor to match our continuously growing database of annual coastline changes and estimates of mudbank footprints and to indicate causalities between them.

4.6 Conclusions

Landsat observations, individually processed to avoid spatial and temporal averaging and thus masking of important spatiotemporal variability in the system, provide insight into the dominant influence of migrating mudbanks on coastline changes in the Guianas. Progradation during mudbank phases was considerably larger between 1985 and 2021, with an average between 2 and 44 m/yr, compared to interbank phases, when mudbanks are not damping waves. Here average coastline retreat is between 13 and 18 m/yr. Guyana had coastline changes (2 m/yr) up to an order of magnitude smaller compared to French Guiana and Suriname (26-45 m/yr). Local variability in coastline changes can for the first time be attributed to the spatial differences in mudbank morphometrics and their migration speeds, expressed here as a frequency of mudbank occurrence. Overall, mudbanks stretch between 10 and 20 km alongshore and migrate with average speeds of one to five km per year along Guianas' coastline between 1985 and 2021. Mudbanks in Guyana, however, are smaller and migrate more slowly compared to Suriname and French Guiana. This reaffirms that a part of the observed variability in coastline changes in the Guianas can be directly linked to alternating phases of erosion and progradation, and thus mudbank migration. But more specifically; the factors that control the position and shape of mudbanks, indirectly influence the number of years a coast is protected and facilitated to accrete.

By combining coastline changes and morphological descriptors with migration patterns of mudbanks along the Guianas' coastline, intriguing patterns of net coastline changes have become easily accessible for coastal managers. Hotspots of erosion, progradation or unusual response to the presence and absence of mudbanks can easily be identified based on the full available time series of Landsat observations. An estimated 52% of the entire coastline experienced net progradation between 1985 and 2021. The remainder of the coastline is retrograding because of one of the following reasons: 1) natural erosion during interbank phases is larger than progradation, 2) unusually large erosion indicates system change, either natural or by anthropogenic land cover changes, 3) coastal accretion during mudbank phases is insufficient to balance the natural erosion, and 4) potential outliers where often accretion is underestimated.

Data availability

Code to generate coastline position estimates together with the mud abundance estimates can be found in Google Earth Engine repository that includes an interactive viewer allowing readers to explore coastline changes for all processed transects in this manuscript:
https://code.earthengine.google.com/?accept_repo=users/jobdevries90/MangroMud

Additionally, all post-processing, to estimate the presence of mudbanks in combination with the figures can be accessed through GitHub's initial pre-release version (v0.2):
https://github.com/jobbo90/offshore_boundary/releases

Chapter 5 | Mangrove ecosystem response to a cyclic change regime controlled by migrating mudbanks in the Guianas

Abstract

Mangroves are among the most dynamic coastal ecosystems globally, where changes are a direct result from a range of controlling factors including climate change, (a)biotic stressors, natural disturbance events and anthropogenic landcover changes. All these changes influence the natural functioning, including structure, phenology and invaluable ecosystem services, of these forests differently. Consequently, a mosaic of interrupted and sometimes fragmented succession sequences of mangrove patches can reflect natural ecosystem functioning, drivers of change and the capability to withstand irreversible changes. In the coastal zone of the Guiana shield countries, alongshore mudbank migration causes a cyclic change regime with prolonged phases of coastline progradation and erosion. It remains unknown, however, how these natural dynamics influence the functional attributes, such as frequency and patch size of losses or gains in mangrove cover.

By applying a temporal segmentation algorithm on Landsat derived NDVI timeseries we show that net changes between 2000 and 2021 are -4,052, 702 and -5,769 ha in mangrove forest of Guyana, Suriname and French Guiana. Average patch sizes of these changes range from 1 to 2.2 ha but are significantly left skewed. This suggests that average net mangrove changes are also controlled by the frequency of occurrence and changes that occur near smaller and fragmented mangrove forest. At the landscape scale (i.e., 10km hexagons) hotspots of change, associated with mudbank migration, are spatially clustered; however, more and significantly larger changes occur in the coastal hinterland, 500 m away from the coastline. These observations suggests that the often-placed emphasis on the conceptual view of mangrove changes in this region, with losses when mudbanks are absent and mangrove colonization when present, deserves additional attention. Additionally, by analysing the temporal changes in the functional attributes of gained or lost patches of mangrove forest we aimed to contribute to the understanding of the ecological impacts of spatiotemporal variability in functional attributes of both gains and losses. Such information is crucial to highlight the impact of management strategies on the changes in mangrove forest induced by alongshore mudbank migration and thus their natural protection against waves, storms and sea level rise in the Guianas.

Elements from sections 5.3.1 and 5.3.2 are based on:
de Jong, S. M., Shen, Y., de Vries, J., Bijnaar, G., van Maanen, B., Augustinus, P., & Verweij, P. (2021). Mapping mangrove dynamics and colonization patterns at the Suriname coast using historic satellite data and the LandTrendr algorithm. *International Journal of Applied Earth Observation and Geoinformation*, 97, 102293.

Verhoeve, Steye; Vries, Job de; van Bijsterveldt, Celine; de Jong, Steven (2021): Monitoring mangrove erosion and settlement over space and time in Suriname (Weg naar Zee) & Indonesia (Demak Region). figshare. Thesis. https://doi.org/10.6084/m9.figshare.16602365.v1

5.1 Introduction

Mangrove forests are among the most dynamic coastal systems in the world and comprise of vegetation species that only occur along (sub)tropical coastal zones (Spalding, 2010). They can survive these saline coastal environments due to specific adaptations, such as aerial roots, pneumatophores and buoyant propagules. They provide invaluable ecosystem services such as coastline protection (Horstman et al., 2015), carbon sequestration (Alongi, 2012), resources for local communities (Walters et al., 2008) and nursery habitats for flora and fauna (Nagelkerken et al., 2008). Due to anthropogenic activities, such as aquaculture development and urbanization, mangrove forests have become fragmented and are decreasing in area globally (Bryan-Brown et al., 2020; Goldberg et al., 2020). Together with the natural changes, mangrove cover alterations create biological legacies, including the structure and phenology of plant populations and communities. The total effect of all changes in mangrove cover are thus important drivers for ecosystem functioning, recovery and therefore, coastal protection and livelihood of coastal inhabitants (Alongi, 2008; Johnstone et al., 2016; Kominoski et al., 2020).

Until the 2000s an estimated one-third of the world's mangroves were lost (Alongi, 2008, 2002). Regional differences, with for example major losses in South-East Asia (Gebhardt et al., 2012), are attributed to differences in conservation effort (Friess et al., 2019) and the variety of drivers that influence structure and functioning of mangroves. These drivers work on spatial scales that range from individual plants to patch to ecosystem and on time scales from seconds to tidal cycles and multiple decades. They also include environmental factors that influence the balance between vertical sediment accretion and sea level rise, like tidal inundation duration (hydroperiod), sediment supply, wind and wave energy (Crase et al., 2013; Osland et al., 2017; Rodriguez et al., 2016; Xie et al., 2022). Also, increased exposure to wave forcing can induce mangrove losses or reduce the sediment storage capacity and the potential elevated area that is suitable for mangrove colonization (Balke et al., 2013). All such control mechanisms influence the effectiveness of mangrove adaptations to survival and thus gains and losses in mangrove forest areas around the globe (Osland et al., 2018).

Differences in the resistance of mangrove trees to these controls depend on the type of species (Xie et al., 2020), tree properties such as age and size (Kumara et al., 2010), salinity tolerance and the sedimentation rate these trees can endure during colonization (Balke et al., 2011). Mangrove species have thus adapted to sustain different stressors or perturbations (Piégay et al., 2020a), resulting in relatively homogeneous vegetated patches of the same species and age that can be observed from model outputs (van Maanen et al., 2015; Xie et al., 2020), field data (Barbier et al., 2011; Ellison et al., 2000; Fagherazzi et al., 2017) and remote sensing observations (Bullock et al., 2017; Rogers et al., 2017). Additionally, these patches of mangrove, and associated invaluable ecosystem services, vary spatially and temporally in response to spatial gradients in (a)biotic factors (Barbier et al., 2011; Bullock et al., 2017; Fagherazzi et al., 2017) and continuous temporal changes in control factors. On the whole, this leads to a mosaic of interrupted, sometimes fragmented (Tran and Fischer, 2017), and arrested succession sequences (Alongi, 2008; Duke et al., 1998).

Regardless if changes in mangrove cover are instantaneous or gradual, long lasting impacts on the structure and demography of forests can occur (Jimenez et al., 1985). This suggests that gradual or small changes in control factors can already influence the development of mangroves (Krauss et al., 2008) and cause abrupt ecosystem shifts (Balke et al., 2015). This results in forest cover changes with specific properties that can be related to the overall ecosystem's functioning and the drivers of change in a given time and area (Koch et al., 2009). This implies that properties of lost and

gained mangrove patches can be indicative of successional dynamics (Turner, 2010) and thus the capability to withstand disturbances and perhaps even climate changes. The functional attributes of the gain and losses include patch-level characteristics, such as their spatial distribution, size, measure of fragmentation and connectivity (Tran and Fischer, 2017). Also functional attributes that capture cumulative effects of changes in given time and area, such as frequency of occurrence and return interval, are required (Lawley et al., 2016; Pimple et al., 2022; Uuemaa et al., 2013). For example, the size of disturbed patches can influence the accommodation space, and thus the type of mangrove species colonizing them (Woodroffe et al., 2016). Also, the connectivity between patches can influence propagule dispersal (van der Stocken et al., 2015) or the interaction between species (Herbeck et al., 2020). This focus on the spatial dimensions of gain and losses has been limited thus far for mangrove ecosystems around the world (Murillo-sandoval et al., 2022; Murillo-Sandoval et al., 2021). In spite that it is increasingly acknowledged that it allows coastal managers to assess the capacity of mangrove forest to remain their naturally functioning ecosystem services under a changing climate.

Spatiotemporal variability in functional mangrove loss and gain attributes over longer periods of time, referred to as change regimes (Piégay et al., 2020b; Turner, 2010; White, 1979), and the consequential mangrove development patterns (Lawley et al., 2016; Seidl et al., 2016), require observations spanning multiple decades. Remote sensing has been used to map ongoing changes, ecosystem distribution and species succession on broad ranges of spatial and temporal scales (Kuenzer et al., 2011). Yet, subtle differences in plant properties (e.g. species composition, biomass and leaf area index; Bollock et al., 2017) and waver level variations make the spectral analysis of mangrove properties difficult and with mixed success (Kuenzer et al., 2011). Only few studies have used all available observations in the time series, despite the clear advantage of using more images to, for example, reduce the signal to noise ratio and to discriminate mangrove and wetland vegetation (Toosi et al., 2022; Younes Cárdenas et al., 2017). Such time series analysis allows to consider the temporal trajectory of a pixel and its spectral response rather than the instantaneous pixel value alone. For example, the temporal segmentation algorithm LandTrendr (Kennedy et al., 2012) has been successfully applied to forest systems (Senf and Seidl, 2021a), urban area (Yan and Wang, 2021) and permafrost (Runge et al., 2022).The difficulty in separating mangroves from other vegetation types limited the algorithm's use to quantify mangrove gain and loss regimes (Murillo-sandoval et al., 2022).

The fast-changing mangrove coastline of the Guianas, situated between the mouth of the Amazon River in Brazil and the Orinoco Delta in Venezuela. This coastal ecosystem is influenced by alongshore migrating subtidal mudbanks (Fromard et al., 2004) that facilitate coastal progradation and thus mangrove growth when they move in front of a coastline stretch (Anthony et al., 2010; Augustinus et al., 1989; Toorman et al., 2018). After 10-15 years, when these 10-15 km long mudbanks have moved on again, mangrove coastlines are fully exposed to waves and erode up to, sometimes even surpassing, 200 m/yr (Allison et al., 1995; Chapter 4). A large body of research has focused on mapping these coastline changes, elucidating on driving forces like large-scale atmospheric processes (Gratiot et al., 2008; Walcker et al., 2015), climatic changes and wave damping (Best et al., 2022). Variability in mudbank migration rates and sediment exchange between mudbanks and the coastal zone result in unpredictable and inconsistent coastal development (Chapter 4). This makes it uncertain how mudbank migration influences mangrove forests change regime, succession and thus coastal safety on the long-term (Bhargava et al., 2021). Given the increasing interest in building-with-nature initiatives (van Bijsterveldt et al., 2020) and carbon sequestration in mangrove ecosystems (Ahmed and Glaser, 2016) it is fundamental to better

understand past losses and development of mangrove forest for managing these ecological systems today (Koch et al., 2009; van Zelst et al., 2021).

The aim of this chapter is to assess the mangrove change regimes in the Guianas between 2000 and 2021 to better understand ongoing gains and losses in mangrove forest cover and to what extent this can be explained by alongshore mudbank migration. More specifically our work focusses on the size, frequency and interval of mangrove forest gains and losses, while taking the natural variability related to mudbank migration into account. We base our work on the LandTrendr algorithm to detect changes in mangrove cover at 30-m resolution and how mudbank migration affects regeneration, development and succession of mangrove ecosystem in the Guianas.

5.2 Study area

The Guiana coastal zone constitutes of the coasts of French Guiana, Suriname and Guyana (Figure 5.1). The low-lying coast is characterized by a relatively undisturbed and pristine tropical mangrove forest. Mangroves occur naturally along the entire Guianas' coastline in a ~3 km wide coastal zone. Mangrove species dominating the Guiana coasts are *Avicennia germinans* and *Laguncularia racemosa* on the mudflats, while *Rhizophora racemosa* and *Rhizophora mangle* are common in the estuarine swamp areas and along riverbanks (Fromard et al., 2004; Proisy et al., 2016). Further inland, the

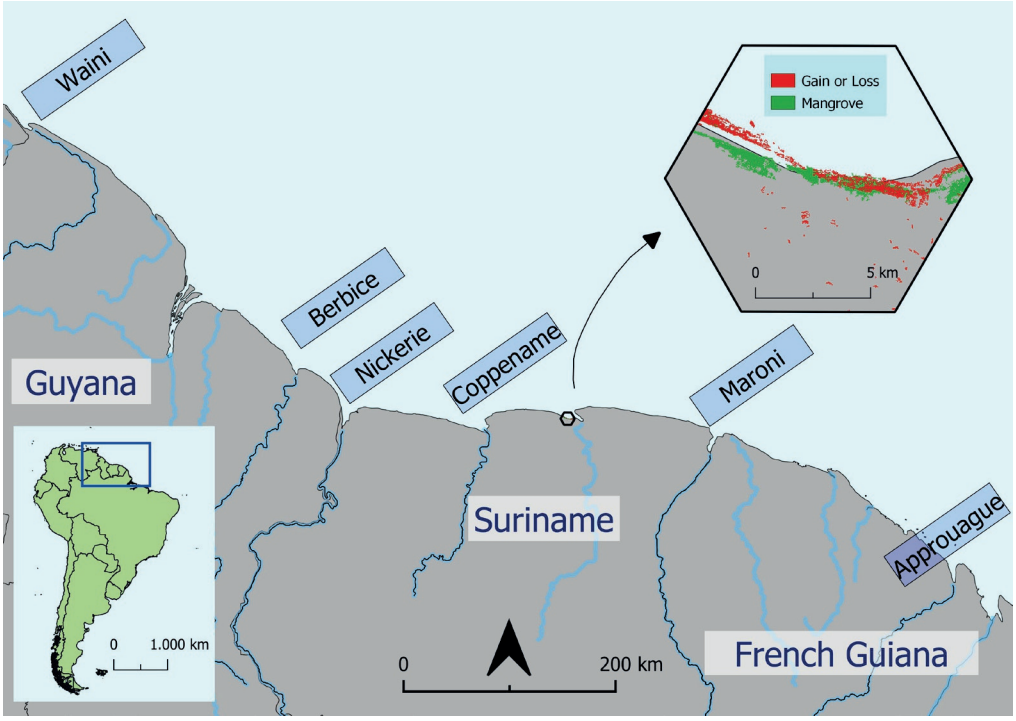

Figure 5.1: Guiana shield countries, including Guyana, Suriname and French Guiana and the major rivers in blue. The smaller inset shows a hexagon (10 x 10 km) example highlighting unchanged mangrove area (green) and either lost and/or gained area in red. The unchanged mangrove area (green) is derived from Giri et al., (2011) while the changed area is either gain or loss pixels, as explained in Section 5.3. The rivers mentioned in the manuscript are labelled and highlighted.

transition to freshwater facilitates more dominant cover of marshes and patches of swamp forests or mixed dryland forests (Teunissen, 1976). Upstream of the main river mouths (Figure 5.1) and tidal creeks, patches of mangrove cover can also be found.

The tropical climate of the Guianas is characterized by seasonal variations in trade winds (Augustinus, 2004). In the period February and March, (the short dry season), the north-east trade winds (3-9 m/s) are dominant. In the long dry period, August to October, lower velocity winds are coming from the north-east and are more variable with respect to direction and strength (Augustinus, 1980). Wind patterns along the Guiana Coastal zone are a direct consequence of changes in large-scale atmospheric forcing mechanisms, such as the movement of the ITCZ and the air circulation within the so-called Hadley or Walker cells. These control storms, fronts, precipitation and therefore the seasonality in the Guianas (Poveda et al., 2006). Total precipitation ranges from 2-3 m/yr, with the largest share falling in the wet seasons between December and July (Xie and Carton, 2004). Despite the high precipitation, the larger rivers along the Guiana coast, such as the Maroni, Nickerie and Berbice rivers (Figure 5.1) have relatively low discharges that range from 46 m^3/s to 2,104 m^3/s for the Maroni River (Gardel et al., 2022).

The morphological dynamics along the coast are influenced by mud that originates from the Amazon, which has an estimated average annual sediment yield of 1.2 × 100,000 (Anthony et al., 2010). These volumes of mud self-organize in banks and migrate from the Amazon to the Orinoco and cause erosion or accretion at the coast in cycles that last up to 35 years. Erosion and accretion rates can go up to, and even surpass 200 m/year (Allison et al., 1995; Chapters 3 and 4). These

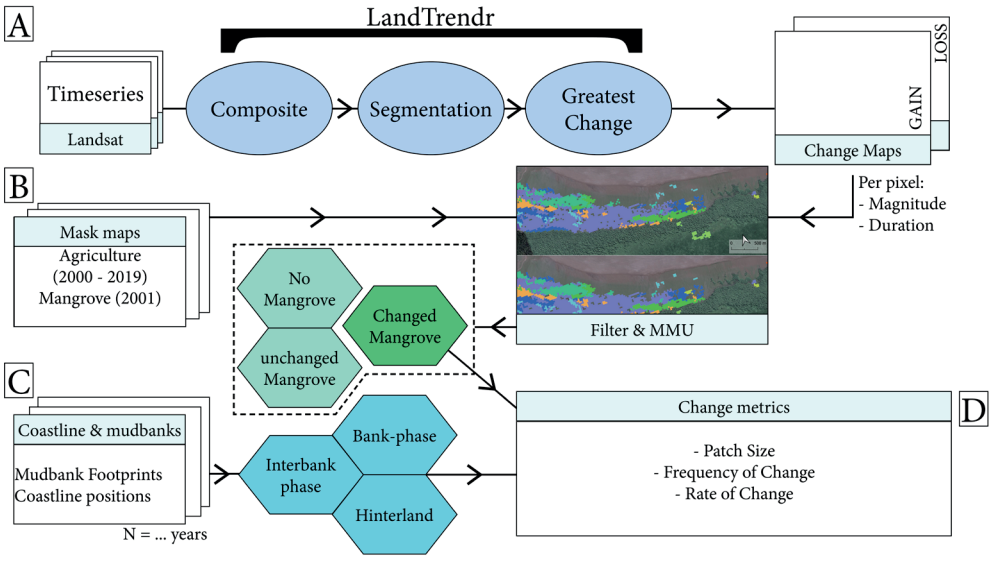

Figure 5.2: Applied workflow to derive change metrics from LandTrendr outputs. The general steps compromise of applying the LandTrendr Algorithm on annual Medoid composite images by applying temporal segmentation and selecting for each pixel the greatest change event (step A). After filtering, masking agricultural land and applying a minimum mapping unit the annual change maps patches are defined with their corresponding change metrics (step B). Finally, for each patch an estimate is made if it is near the coastline, considered as interbank or bank phase (step C).

banks migrate under the direct influence of tides and wave forcing, especially between December and April when offshore waves are up to two m high, with a period that ranges from 6-10 s (Wells and Coleman, 1981). The tide is semidiurnal and reaches 2.5 m during spring tide.

Prolonged phases of enhanced sediment supply and protection against incoming waves facilitates rapid mangrove growth, or loss when mudbanks continue to migrate along the coast and an interbank phase starts. With the passing of each cycle the coexisting vegetation with different ages and structures develops and/or erodes (Fromard et al., 2004). The (a)biotic conditions, including salinity, morphology, propagule dispersal potential, precipitation and sedimentation rates also exert a zonation of vegetation with their corresponding functional diversity. Most of these control mechanisms develop and change under natural circumstances, with the passing of tides, seasons, years or even multiple decades, causing natural variability with prolonged phases of erosion and colonization.

The cumulative exposure to sea-level rise, flooding and phases of erosion, associated with mudbank migration, has resulted in increasing risks to coastal flooding in the Guianas (Simpson et al., 2009). The risks are increasing at locations where mangroves have eroded and the overall efficiency of wave damping (e.g., mudbank/coastal protection) has reduced over the last decades. This is especially true in Guyana but also for stretches of coastline in Suriname (Berrenstein, 2010; Nijbroek, 2014) and French Guiana (Brunier et al., 2019). Human interventions, such as earth-walls, dikes, agricultural development and sand mining, have altered the natural capacity of coastline stretches to prograde during mudbank phases and to partially resist erosion during interbank phases (Anthony and Gratiot, 2012).

5.3 Methods and data

5.3.1 Temporal segmentation of Landsat observations

Cloud-based processing platforms like Google Earth Engine (GEE) provide a vast amount of publicly available geospatial datasets, including remote sensing observations like Landsat imagery (Gorelick et al., 2017). Simultaneously, GEE facilitates fast data access and parallel processing capabilities for regional to global analysis. Landsat is the longest running operational set of spaceborne platforms, collecting images with unprecedented spatiotemporal resolution, of the Earth surface. Annual Landsat image availability for Suriname is nowadays around five to ten images with a revisit time of 16 days. However, image quality and availability before 2000 is low and for the year 1995, not one image of the study area is available in the archive. Therefore, we focus on the period 2000 to 2021 while using all available Tier 1 surface reflectance observations.

To detect changes in mangrove coverage by their approximate rate and timing, the LandTrendr ('*Landsat-based detection of trends in disturbance and recovery*') algorithm (Kennedy et al., 2012) was applied to timeseries of satellite images (Figure 5.2, step A). LandTrendr is a spectral-temporal segmentation algorithm useful for change detection in a time series (also called temporal trajectories) of moderate-resolution satellite imagery on a pixel-by-pixel basis while reducing background noise (Kennedy et al., 2018). LandTrendr was originally developed for monitoring terrestrial forest disturbance and is especially suitable for detecting annual changes in vegetation cover (Hislop et al., 2020; Kennedy et al., 2012; Sengupta et al., 2019).

The multi-dimensional median (medoid) technique was used to produce the best available yearly pixel composite. As opposed to using individual images and thus maximal temporal resolution, compositing minimizes impact of missing data and noise in images by reducing a selection of observations to a single best (Roberts et al., 2017). The medoid method selects the pixel

value with the minimum sums-of-squared differences between the median values and observations across bands. This composite method is robust against extreme pixel values and preserves the relationships between bands, because the selected pixel value is one of the observations of that pixel's timeseries (Flood, 2013). This furthers reduces short-term (i.e. less than the compositing period) noise originating from changes in sun angle, phenology and atmosphere conditions (Kennedy et al., 2012, 2010). Additionally, by applying a cloud masking algorithm on the input images the effect of clouds on the annual medoid reflectance values was minimized.

With these annual best available pixel composites, LandTrendr uses a statistical fitting algorithm to segment spectral trajectories (Figure 5.2, step A). The algorithm can detect abrupt changes, gradual trends and time to recovery from continuous signals. To do so, the Normalized Difference Vegetation Index (NDVI) was used in the LandTrendr algorithm, scaled by a factor 1,000. NDVI values overall highlight contrasts between the green mangrove vegetation and grey-dark mudflats (Pastor-Guzman et al., 2018; Valderrama-Landeros et al., 2018). Spectral vegetation indices like NDVI are particularly insightful in this context as mangrove vegetation is evergreen, and erosion and colonization can thus be detected.

The NDVI rasters were used as input for the LandTrendr algorithm, which comprised of several steps (Kennedy et al., 2018), including the removal if of spikes in the signal, identification of potential breakpoints by regression, culling segmentation by removing too small and local segments, fitting of segments, streamlining of the segmentation by removing the weakest breakpoints, and the selection of the best segmentation model using fitting statistics (Figure 5.2, step A). Standard LandTrendr parameter settings were used and include a minimum change in NDVI (change in NDVI >300), NDVI value before change (-100 and 300 for gain and loss events, respectively) and a Minimum Mapping Unit of four pixels. The LandTrendr algorithm was thus finetuned for detecting complete removal of mangrove vegetation (e.g., stand-replacing) and the colonization of intertidal flats by mangroves at pixel level. Partial reduction in biomass or leaf area per pixel, for example because of diseases or partial removal of vegetation, were therefore not well represented

Table 5.1: Landscape metrics with their description, units if applicable and scale.

Metric	Description	Units	Scale
Number of Patches [n]	Number of patches considered as a gain or loss event.	[-]	Landscape / country
Patch size	Average surface area of a group of connected pixels with the same year of detected change.	[ha]	Patch / Landscape / country
Frequency	Number of changed patches relative to the area of unchanged mangrove forest (i.e., stable mangrove between 2000 and 2021).	[n/ha]	Landscape / country
Interval of change	Time between two events which is approached by using the rotation period as proxy: average time needed to disturb the size of the focal area.	Years	Landscape / country

due to the implementation of a minimum NDVI change of 300. Competition between mangroves and other vegetation types, where mangroves were gradually replaced by other vegetation types, were also not distinguishable. The succession from young or juvenile mangroves, where colonization occurred before the start of time series, was also not explicitly represented.

The outcome of the algorithm contains various rasters with greatest gain and loss segments of NDVI, from which a set of metrics describing the magnitude, duration, rate, signal to noise ratio, value before and after following the moment of greatest change in the pixel's trajectory were derived (Figure 5.2, step A). From the pixels in these rasters, the loss and gain maps for the Guiana coastal zones were created, by applying a mask and spatial filtering steps (Figure 5.2, step B). This included removing false positive change events that were considered as agriculture in the year of mangrove loss or after a mangrove gain event. Cropland maps per four year epoch between 2000 and 2019, indicating the presence of annual and perennial herbaceous crops at 30 m resolution, were used to mask false positive detection of changes (Potapov et al., 2022). The cropland maps have an estimated overall accuracy of more than 99 % for each selected epoch. Additionally, all patches smaller than the minimum mapping unit for each year were assigned the year of the surrounding disturbed pixels, thus accounting for the uncertainties in correct identification of disturbance year. Next, holes within patches smaller than two pixels were filled with the year of the surrounding pixels (Senf and Seidl, 2021b). A change patch is thus defined as contiguous pixels that changed in the same year with a minimum mapping unit of four pixels.

5.3.2 Characterization loss and gain regimes

From the annual loss and gain maps (Section 5.3.1) several landscape metrics were computed with the *Landscapemetrics* package (Hesselbarth et al., 2019) in RStudio (RStudio, 2021) at the individual patch level, and aggregated to landscape and country levels (Johnstone et al., 2016; Turner, 2010). To this purpose, a grid of hexagons was used, intersecting the buffered (6 km wide) coastline of the Guianas, to represent the landscape level (Birch et al., 2007). Each hexagon has an area of 8,660 ha, with a total of 84, 70 and 76 hexagons across the land and intertidal area of Guyana, Suriname and French Guiana, respectively. From the derived greatest change pixels (Section 5.3.1), together with the global mangrove data set (Giri et al., 2011), each pixel was classified in either non-mangrove, unchanged mangrove or changed mangrove (Senf and Seidl, 2021b). Changed mangrove implies at least one gain or loss event during the timeseries (2000 till 2021) and unchanged mangrove overlaps with pixels that were indicated as mangrove in 2000 and did not change (Figure 5.1, step C).

For each hexagon, the number of changed patches per year were counted and divided by the total unchanged mangrove area to estimate frequency of occurrence for gain and loss events, expressing the disturbed patches per area of mangrove (Table 5.1). The size of the patches was computed for each patch separately, while frequency of occurrence was calculated at landscape level (Table 5.1). Rotation period was used here as a proxy for interval of change, because the relatively short time series available does not allow for estimating true intervals between changes. Rotation period is the average time needed to change an area of the size of the focal area (e.g., forest area of a hexagon or country), and is calculated by dividing the total unchanged mangrove area by the average annual mangrove area disturbed (Senf and Seidl, 2021a). For trend analysis and spatial comparison, patch level, landscape scale and country scale indicators (Table 5.1) were computed by taking the corresponding mean values. Temporal trends in the mean metrics were quantified using a non-parametric Theil-Sen estimator according to the workflow applied by Senf et al. (2021b).

Table 5.2: Functional attributes aggregated per country and shown for gain and loss patches. Where applicable positive trends or negative trends between 2000 and 2022 are indicated as + and -, respectively.

		Guyana	Suriname	French Guiana
total	Gain	12,369	18,641	10,639
[ha]	Loss	16,421	17,938	16,408
Patch size	Gain	1.1 (+)	1.9 (-)	1.5 (+)
[ha]	Loss	1.3 (+)	2.2 (-)	1.9 (+)
Patches	Gain	13.2 (+)	16.2 (-)	10.1 (-)
[n/yr.]	Loss	19.9 (-)	14.2 (-)	11.1 (-)
Frequency	Gain	1,003 (+)	7 (-)	731 (-)
[n/ha]	Loss	2,571 (-)	8 (-)	603 (-)
Interval	Gain	117	413	744
[Years]	Loss	100	339	728

Additionally, to quantify the effect of migrating mudbanks on the mangrove landscape, indications of annual coastline positions and mudbank footprints were used, computed in chapter 4, to indicate for each patch if they were in the coastal hinterland, interbank or bank zone. Here, the bank zone refers to all patches within 500 m of coastline that were fronted by a mudbank for a given year. Similarly, the interbank zone refers to patches within 500 m of a coastline not fronted by a mudbank. The remaining patches are in the coastal hinterland (i.e., assumed not to be directly influenced by coastal forcing mechanisms). The coastline position estimates were derived annually (see Chapters 3 and 4) with a spatial resolution of 1,000 m (interval between transect positions) buffered with 500 m around the coastline estimates.

5.4 Results

5.4.1 Mangrove loss and gain

Various parts of the coast experienced significant changes between 2000 and 2021 (Figure 5.3), amounting to net changes of -4,052, 702 and -5,769 ha of mangrove in Guyana, Suriname and French Guiana, respectively (Table 5.2). Overall gain and loss of mangrove occurred in areas with abundant mangrove forests (indicated by larger centroids in Figure 5.3), often concentrated in hotspots of erosion and/or mangrove colonization. Gain indicates new mangroves colonizing intertidal areas or, especially further inland, near lakes and wetlands. Losses results from mangrove cover changing to e.g., bare ground or water. Near Coppename (f), Hertenrits (d), Bigi Pan (c) and

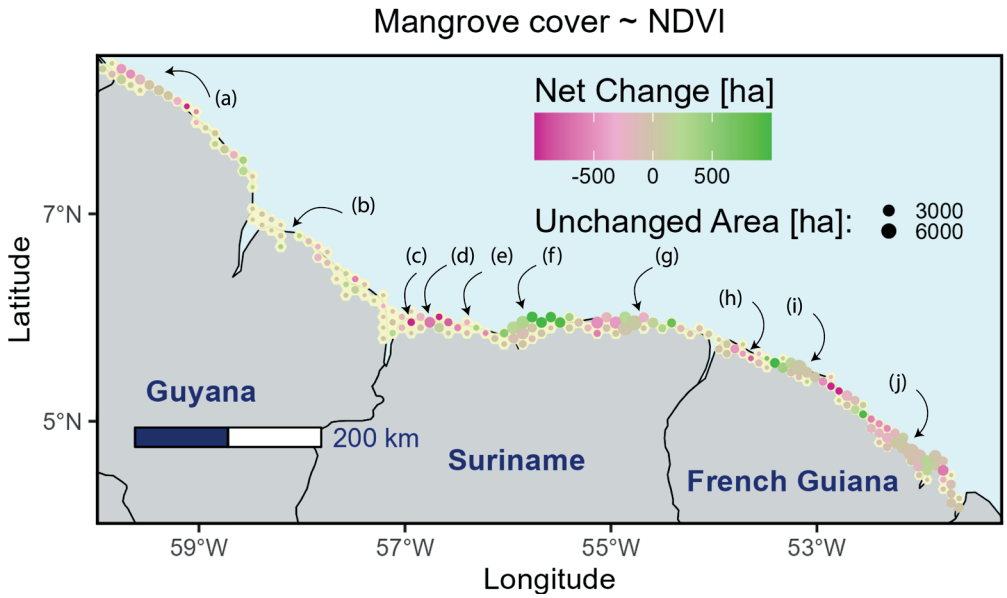

Figure 5.3: Mangrove gain and loss per landscape unit (hexagon) where green corresponds to increasing mangrove area and pink indicates decreasing mangrove area. The center point is scaled in size to the unchanged mangrove area inside each hexagon. Units are total hectare change between 2000 and 2021. Annotation letters correspond to locations referred to in the text: (a) Waini, (b) Georgetown, Bigi Pan (c), Hertenrits (d), Totness (e), Coppename (f), Wia-Wia (g), Mana (h), Iracoubo (i) and Approuague (j). Annotation letters correspond to locations referred to in the text: (a) Waini, (b) Georgetown, Bigi Pan (c), Hertenrits (d), Totness (e), Coppename (f), Wia-Wia (g), Mana (h), Iracoubo (i) and Approuague (j).

Wia-Wia nature reserves (g) in Suriname, substantial changes can be observed (Figure 5.3). Smaller areas of mangrove change, compared to abundant mangrove forest are mainly found near Iracoubo (i) and Approuague (j) in French Guiana (Figure 5.3). There are also areas that are associated with more changed surface area, while there are relatively smaller areas of unchanged mangrove forest, for example near Totness (e) in Suriname, but also Mana (h) in French Guiana and east of George Town (b) in Guyana (Figure 5.3).

Figures 5.4 and 5.5 show examples (A) of hotspots of mangrove gain and loss in Suriname, with the associated year of detection (B), magnitude of changes (C) and patch sizes (D). Figure 5.4 highlights a location east of Coppename in Suriname (see also Figure 5.1), with initial mangrove growth in 2001 in the east, while further west development starts to occur later. This east-to-west zonation is often associated with alongshore migration of mudbanks (Fromard et al., 2004). The increase in NDVI index (Figure 5.4, panel C) shows a heterogeneous and mixed pattern of changes at pixel level. Detected patches (Figure 5.4, panel D) for 2001, 2010 and 2020, with their associated sizes ranging from 0.1 to 431 ha, are indicative of regular zonation in bands parallel to the coastline (Fromard et al., 2004). Figure 5.5 highlights a large area of mangrove loss east of Hertenrits in Suriname (Figure 5.5, panel B). Again, the magnitude in index change is heterogeneous, reflecting mixed patches, although the magnitude of losses is larger (Figure 5.5, panel C) compared to the magnitude of gain in Figure 5.4, panel C. Alongshore oriented bands of gain and particularly losses are reflected in the patch layout (Figure 5.5, panel D).

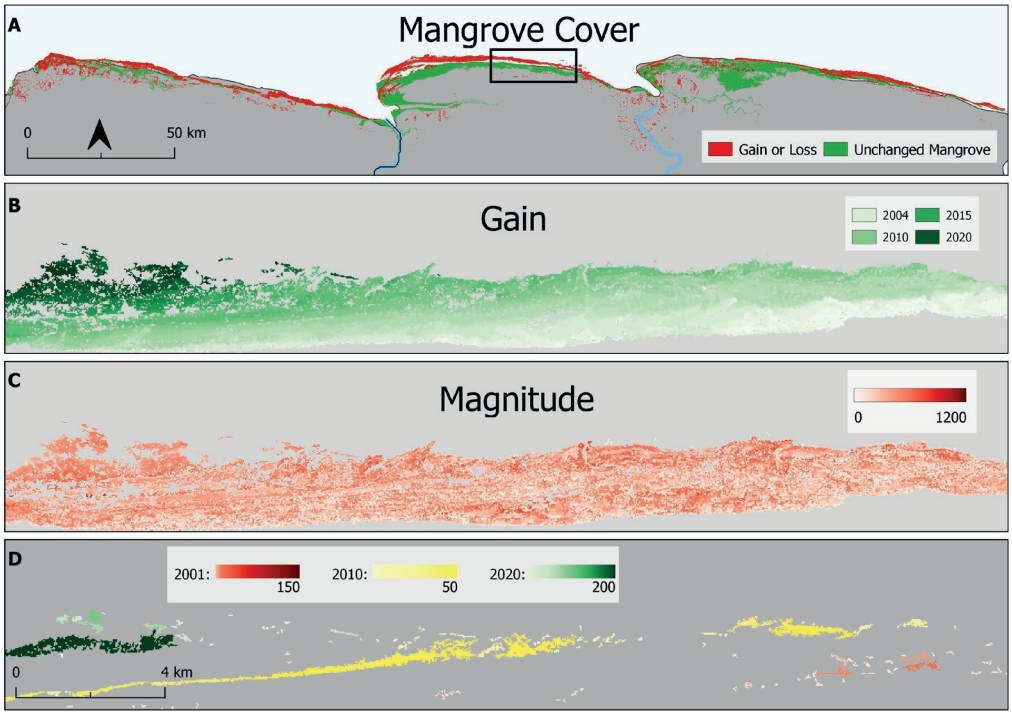

Figure 5.4: Detected mangrove gain along the coast of Suriname with respect to the total mangrove area (a). The square in (a) indicates the location shown in (b), (c) and (d). These insets show the detected year of gain (b), corresponding magnitude of change in NDVI index (c) and the derived patches in 2001, 2010 and 2020 (d) with the color's intensity corresponding to the patch size (in ha) and the upper limit given in the legend.

At the landscape scale on average 20, 14 and 11 loss and 13, 16 and 10 gain patches were detected per year from the LandTrendr outputs for Guyana, Suriname and French Guiana respectively (Table 5.2). The average patch size for forest disturbance ranged from 1.1 ha to 2.1 ha with overall the gain patches being larger compared to the patch size of lost mangrove forest (Appendix D, Figure-D 2). Loss patches in Guyana (~1.3 ha) were smaller compared to Suriname (~2.2 ha) and French Guiana (~1.9 ha). Average patch size for mangrove gain was 1.1, 1.9 and 1.5 ha respectively and thus smaller, yet comparable to the loss patches (Appendix D, Figure-D 1 and Table 5.2).

The average frequency of loss and gain, indicating the amount of changed patches per hectare of mangrove forest, varied between country (Table 5.2) but was significantly left skewed (Appendix D, Figure-D 3). Frequency of gain and loss in Guyana was the largest with on average 1,002.8 and 2,750.5 patches per hectare of mangrove per year. In both Suriname and French Guiana these differences between gain and loss were smaller with 7.0 and 8.1 for Suriname and 731.4 and 602.7 for French Guiana (Table 5.2). The interval of change, indicating the average time needed to change an area with the size of a hexagon, varied from 117 to 743.8 years for gain and 100.6 to 727 years for loss events. At country scale, the average interval of change was larger for gain events compared to the detected loss events (Appendix D, Figure-D3).

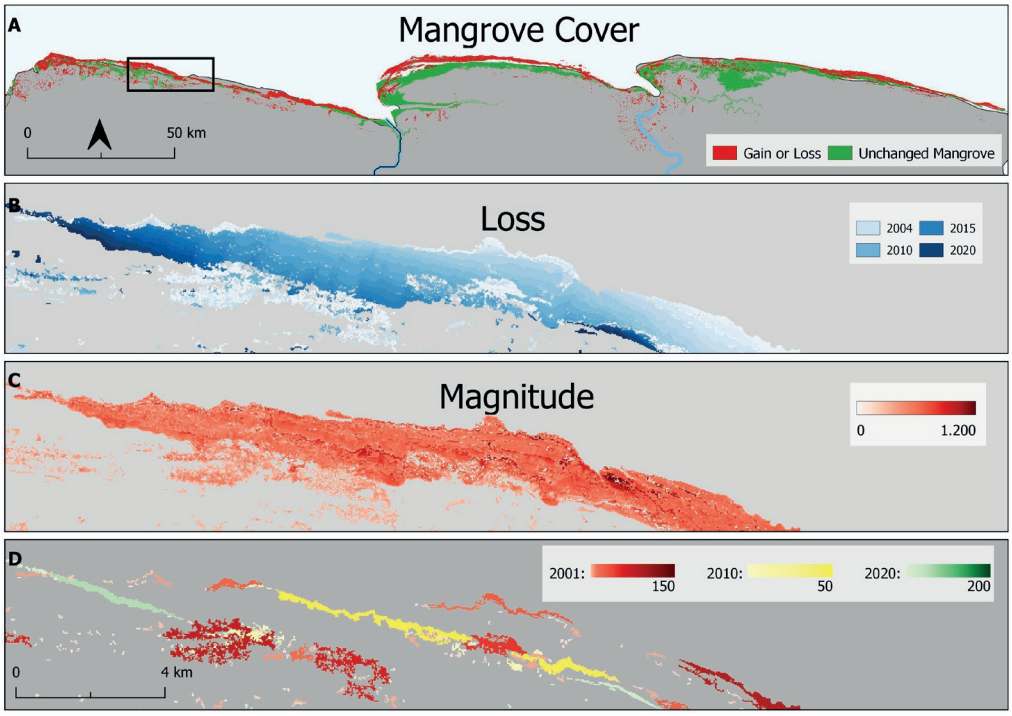

Figure 5.5: Detected mangrove loss along the coast of Suriname with respect to the total mangrove area (a). The square in (a) indicates the location shown in (b), (c) and (d). The insets show the detected year of loss (b), corresponding magnitude of change in NDVI index (c) and the derived patches in 2001, 2010 and 2020 (d) with the color's intensity corresponding to the patch size (in ha) and the upper limit given in the legend.

5.4.2 Variability in mangrove loss and gain

Between 2000 and 2021, variability in the size and frequency of mangrove losses was high and spatially clustered along the coastal zone of the Guianas (Figures 5.6 and 5.7). Patch sizes were larger in areas with abundant mangrove forest and that also experienced the largest total changes (Figure 5.3). Exceptions with relatively smaller patch size in areas with abundant mangroves were found (Figure 5.6) east of Coppename (f) in Suriname and in the east of French Guiana near Iracoubo (i) and Approuague (j). Above-average frequency of losses was found in areas with smaller unchanged mangrove forests, with the loss frequency being especially high east of Georgetown (b) in Guyana (Figure 5.7). These higher loss frequencies occurred in areas with relatively small unchanged mangrove areas (Figure 5.7).

The spatial distribution of mangrove gain (Figures 5.8 and 5.9) showed similar patterns and clustering compared to the loss patches. The largest patch sizes of mangrove gain (Figure 5.8) were found near Copename (f) in Suriname and the highest frequency of occurrence (Figure 5.9) east of Georgetown in Guyana (b). More specifically, most areas with relatively larger and/or more frequent changes (Figures 5.6 and 5.7) also showed the largest gain patches. This implies that the amount and frequency of losses and gains were likely to be in balance between 2000 and 2021, especially for areas with larger unchanged mangrove areas.

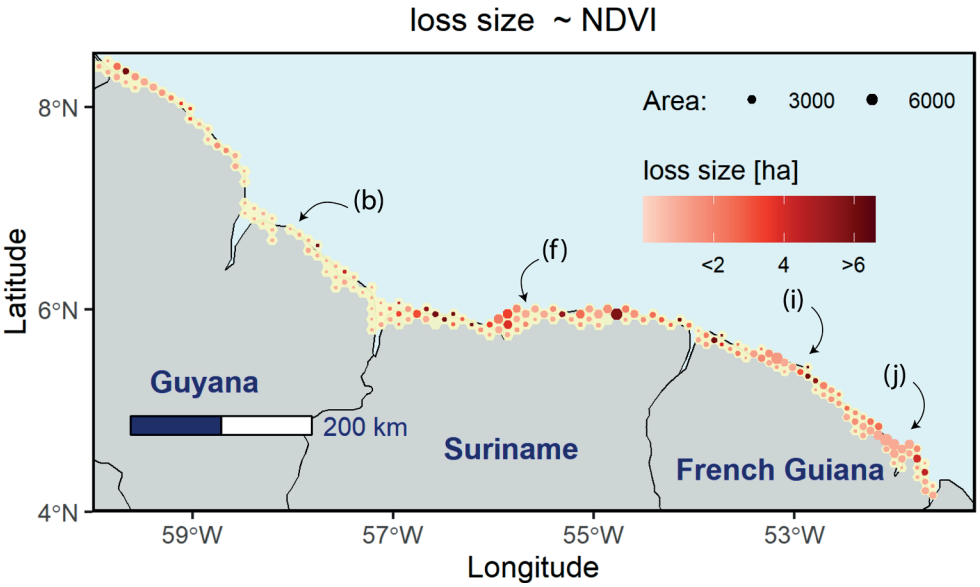

Figure 5.6: Average size of lost mangrove patches (ha) at landscape level (10 km hexagons) along the Guiana coastal zone. The colors correspond to the average size while the size of the of hexagon's centroids are scaled to the unchanged mangrove forest area

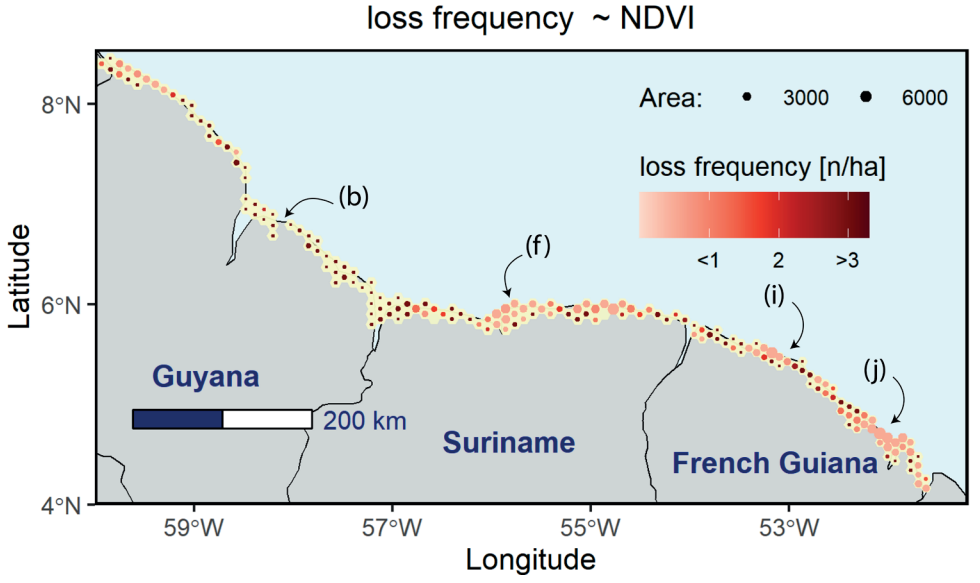

Figure 5.7: Average frequency of loss patches per area of mangrove forest along the Guiana coastal zone at landscape scale (10 km hexagons). The colours correspond to the average frequency of occurrence while the size of the of hexagon's centroids are scaled to the unchanged mangrove forest area.

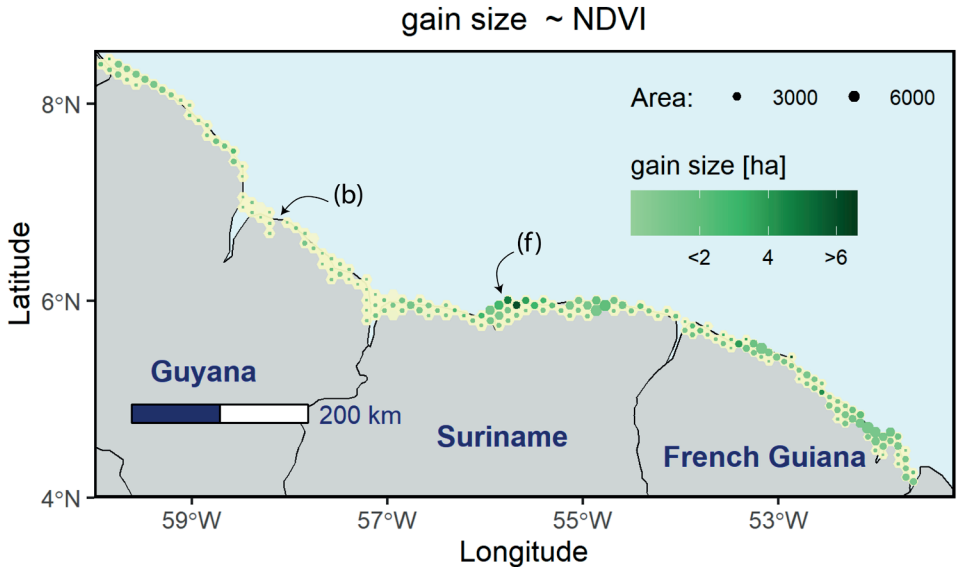

Figure 5.8: Average size of mangrove gain patches (ha) at landscape level (10 km hexagons) along the Guiana coastal zone (top). The colours correspond to the average patch size, while the size of the of hexagon's centroids are scaled to the unchanged mangrove forest area.

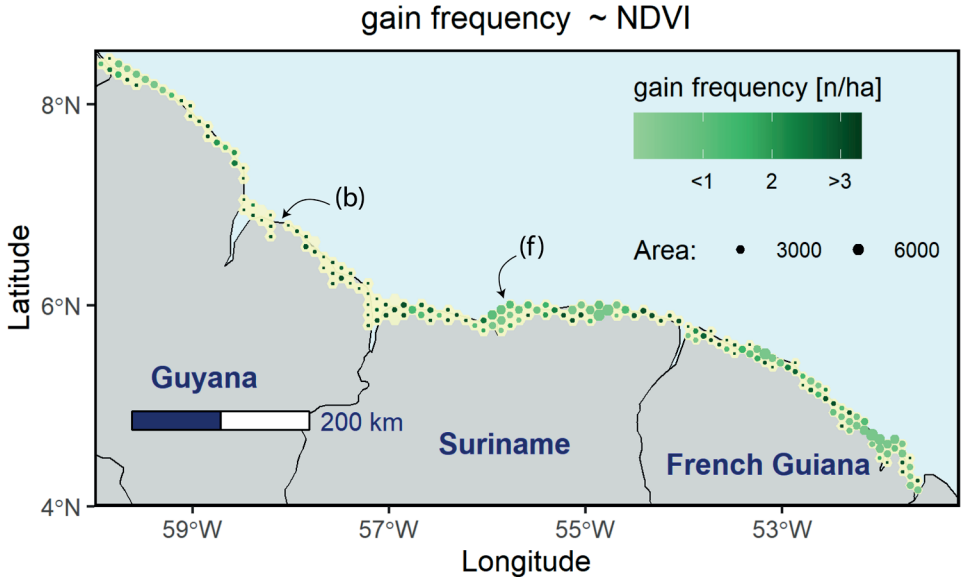

Figure 5.9: Average frequency of gain patches per area of mangrove forest along the Guiana coastal zone at landscape scale (10 km hexagons). The colours correspond to the average frequency of occurrence, while the size of the of hexagon's centroids is scaled to the unchanged mangrove forest area.

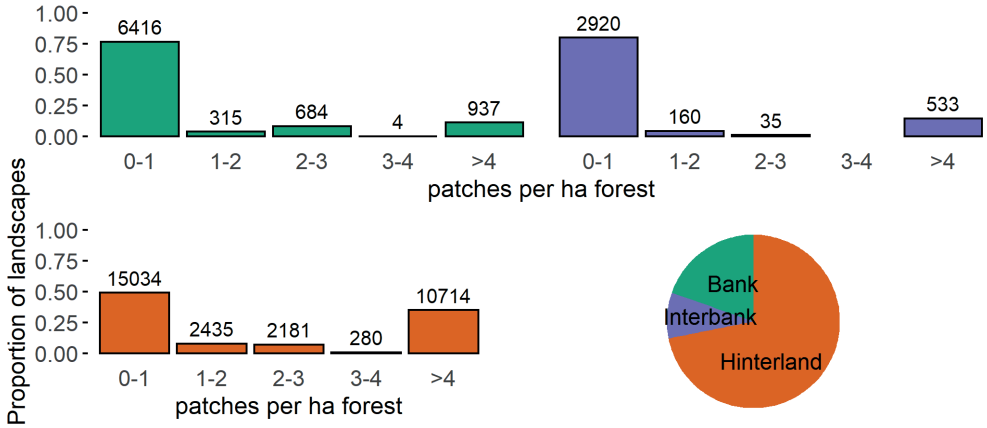

Figure 5.10: Relative frequency distribution of loss patches per ha of forest for interbank, bank zone and coastal hinterland along the Guiana coastline between 2000 and 2020. Relative values on the y-axis correspond to the losses in mangrove area for each coastal land class (coastal hinterland, bank and interbank) with respect to the total observed changes in the respective class. Coastal hinterland corresponds to mangrove changes further away (500m) from the coast.

5.4.3 Analysis of metrics

Patches of mangrove losses during interbank phases (n=6,149) were detected more frequently compared to losses during bank zones (n=5,672), although the difference was relatively small (Figure 5.10). The detected changes were most often 0-1 ha large and showed on average up to one disturbance event per year and hectare of mangrove forest. Losses in interbank zones were more frequently larger than one ha (39,8%) compared to bank zones (18.1%). Yet, such larger changes were even more frequent (53.3%) in the coastal hinterland (Figure 5.10). The majority of losses were detected in the coastal hinterland (n = 42,124, 78.1%).

A total of 42,634 gain patches were detected, although more frequently during bank phases (n = 8,346) compared to interbank phases (n = 3,650) (Figure 5.11). The majority (57.1 %) of all these patches were 0-1 ha large (Figure 5.11) and up to one gain event per ha of mangrove forest was detected (Appendix D, Figure-D 3). This makes the distributions highly skewed with ~75% of the gain being smaller than one ha in bank and interbank phases. The vast majority (~ 70%) of the detected gain was in the coastal hinterland (n = 30,638) (Figure 5.11). Here gain patches were in 34.8 % (n=10,714) of the total observed patches larger than four ha (Figure 5.11), which is more than during bank (11.2 %) or interbank phases (14.6 %).

5.4.4 Trends in disturbance and regeneration regimes

Functional attributes of loss and gain patches changed profoundly between 2000 and 2021, with trends also varying along the coast of the Guiana countries (Figures 5.12 and 5.13). The size of loss patches was increasing on average, while gain patches were becoming smaller (Figures 5.12 and 5.13, panel III and IV). In Suriname, however, the patch size of losses in mangrove cover decreased on average with ~0.7% per year and increased in French Guiana and Guyana with 1.4% and 0.9%, respectively (Table 5.2). The patch size of gain events increased by 0.2% and 1% in French Guiana and Guyana respectively, while in Suriname the average size decreased with 1.1% At various locations along the coast increasing patch sizes for losses and decreasing patch sizes for gain events

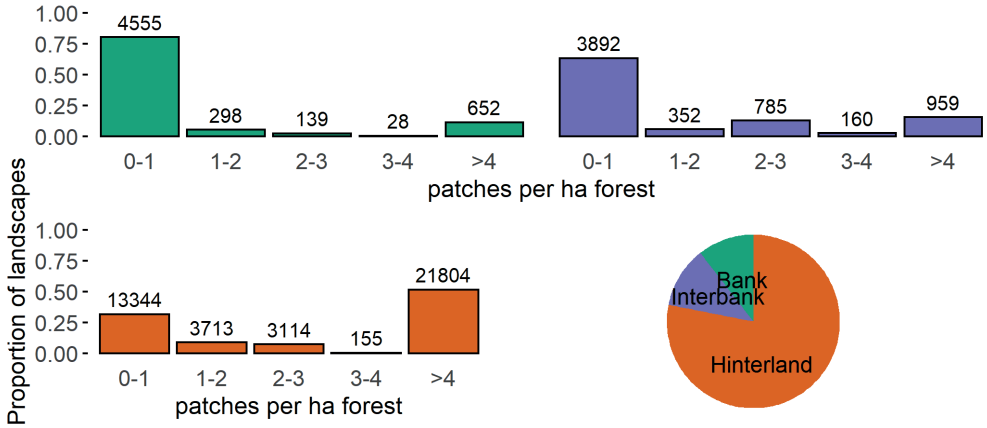

Figure 5.11: Relative frequency distribution of gain patches per ha of forest for interbank, bank zone and coastal hinterland along the Guiana coastline between 2000 and 2021. Relative values on the y-axis correspond to the gain in mangrove area for each coastal land class (coastal hinterland, bank zone and interbank) with respect to the total observed changes in the respective class. Coastal hinterland corresponds to mangrove changes further away (500m) from the coast

were observed. The most pronounced example was near the mouth of the Approuague River (j) in the east of French Guiana (Figures 5.12 and 5.13).

The frequency of change events was mostly stable between 2000 and 2021, although hot spots with significant increasing and decreasing trends were found along the Guiana coastal zone (Figures 5.12 and 5.13, IV). At such locations, a decreasing frequency of gain events (Figure 5.13) and simultaneously increasing frequency of disturbance (Figure 5.12) were found. Examples include the Mana Polder (h) in French Guiana, Nieuw Nickerie (c) in Suriname and the Waini River in Guyana (a). Especially in French Guiana and Suriname, both the gain and loss frequency have decreased (Table 5.2). On the other hand, in Guyana the frequency of gain events increased while the disturbance events decreased between 2000 and 2021 (Table 5.2). In locations along the coast where gain sizes were decreasing, they also occurred less frequently. This link in trends between size and frequency was also observed for loss events (Figure 5.12).

5.5 Discussion

5.5.1 Mangrove loss and gain related to mudbank migration

A total of -4,052, 702 and -5,769 ha of net mangrove change was detected between 2000 and 2021 with the LandTrendr algorithm in Guyana, Suriname and French Guiana, respectively (Figure 5.3). Also the spatiotemporal variability in functional attributes, such as average disturbance size (Table 5.2), with smaller (1.3 ha) patches in Guyana compared to Suriname (2.2 ha) and French Guiana (1.9 ha), re-emphasizes the difference in dynamics of mangrove ecosystems between these countries. This has previously been attributed to national intervention measures, including construction of coastal protection in Guyana since the 1950s, resulting in nation-wide mangrove degradation (Anthony and Gratiot, 2012; Nijbroek and Basu, 2012). As a result, the here detected gain patches in Guyana were small (1.1 ha), potentially indicating a limited natural capacity of mangrove forest to regenerate without sufficient mangrove forest to start with (Pimple et al., 2022).

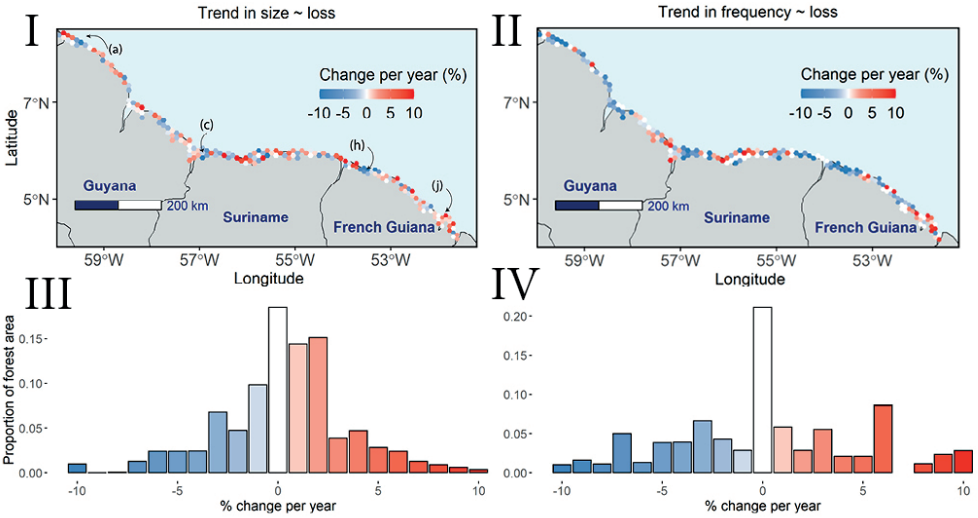

Figure 5.12: Trends patch size (Panel I) and frequency of occurence (Panel II) for loss events. Annotated locations (a-j) correspond to locations introduced in figure 5.3 and mentioned in the results section. Note the different y-axis ranges of the histograms (Panels III and IV).

Net changes in mangrove cover for the largest part of the Guyana coast (Figure 5.3), compared to Suriname and French Guiana, was in the same order of magnitude, with significantly larger frequency of occurrence in both loss and gain patches (Table 5.2).

Functional attributes of observed changes (Figures 5.6, 5.7, 5.8 and 5.9) showcase the variability in loss and gain patterns in mangrove forest and thus the variety of potential causes. Especially observed frequencies of occurrence were different between countries, with more frequent yet smaller changes in French Guiana and especially Guyana (Table 5.2). Also, for both gain and loss changes, small patches (< 1 ha) occurred more frequently, as indicated by the left skewed distributions in patch size (Figures 5.10 and 5.11). This aligns with previous observations of frequent small losses in mangrove cover in, for example, the Dominican Republic (Sherman et al., 2000). This highlights the importance of connectivity in mangrove forests at patch level for the development of mangrove forest at country scale.

At landscape level (i.e., hexagon), large and frequent changes between 2000 and 2021 were detected in areas that can be considered as pristine mangrove forest along the Guiana coastal zone (Figure 5.3). These results are indicative for spatiotemporal patterns of mangrove erosion and colonization with larger changes in forests with abundant mangroves (Figure 5.3). Especially in the coastal hinterland substantial proportions of losses (53%) and gains (34.8 %) were larger than four ha (Figures 5.10 and 5.11) and sometimes surpassing reported examples of 21-28 ha within a year in French Guiana (Proisy et al., 2009). This difference between zones suggests that processes, including proximity to water, other mangrove stands and human settlement (Otero et al., 2020), potentially control loss characteristics, such as size and frequency of occurrence. Together with subsequent success of gain at patch level, these local changes manifest at landscape level in the Guianas, illustrated by the detected gain and loss at patch level (Figures 5.4 and 5.5). Previously, different patterns of mangrove settlement and expansion, including arc-shaped, regular zonation and patch shaped development (Fromard et al., 2004), were found at various locations along the

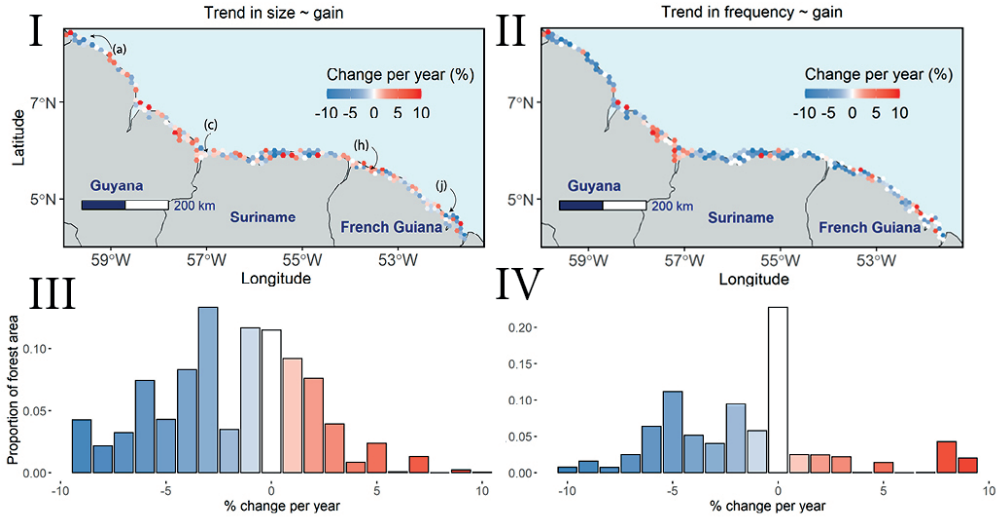

Figure 5.13: Trends in patch size (Panel I) and frequency of occurrence (Panel II) for gain events. Annotated locations (a-j) correspond to locations introduced in figure 5.3 and mentioned in the results section. Note the different y-axis ranges of the histograms (panels III and IV).

coast (de Jong et al., 2021). Figure 5.4 exemplifies arc-shaped expansion of mangroves in an east-west direction, while Figure 5.5 illustrates relative regular zonation retreat.

A comparison between the gain and loss frequency of occurrence is not a direct measure of mangrove recovery at patch scale (Otero et al., 2019). It does, however, indicate the occurrence of change events and thus the potential to analyse resilience of mangrove forest at landscape level. For instance, frequent gain and loss changes are spatially clustered (Figures 5.6, 5.7, 5.8 and 5.9). Such spatial clustering, with relative similar functional attributes of changes, indicates that the patches, and the extremes in frequency and especially size, are influenced by spatially variable processes that affect mangrove gain and loss. Specifically for the Guianas processes that have been suggested include mudbank migration, hydrodynamic forcing (Gratiot et al., 2008), salinity, freshwater supply from the hinterland (Toorman et al., 2018) and sediment accumulation (Proisy et al., 2009).

The migration of mudbanks is known to enhance coastline accretion when present and coastal erosion when absent (Anthony et al., 2013a; Chapter 4) and thus offers a partial explanation for observed clustering of net coastline changes between 2000 and 2021 (Figure 5.3). Gain (n = 8,346 patches) was more often detected than loss (n = 6,148) during mudbank phases (Figure 5.11). This highlights the potential for mangrove colonization due to the wave damping capacity and enhanced sediment supply induced by mudbanks(Anthony et al., 2013a). Loss patches were more frequently detected during interbank phases (n = 6,149) compared to bank phases (n = 5,672), especially for patch sizes larger than three ha (Figure 5.10). Despite the relatively small difference, this indicated that mangrove losses were also detected for stretches of coastline protected by mudbanks. For a part this might be explained in the false positive detection of mudbank footprints (Chapter 4) and the false positive detection of mangrove loss from changes in NDVI with the LandTrendr algorithm (Section 5.3.1). Despite removing croplands, difficulty in separating mangrove forest (changed and unchanged) from other vegetation and land cover types remained (Green et al., 1998). Nonetheless,

mangrove may be lost during mudbank phases, with potential drivers being conversions to agri- and aquaculture (Mukherjee et al., 2014).

The complex response of coastal zone changes to mudbank migration is often simplified by assuming its dominant control on mangrove ecosystem changes in the Guianas (Baltzer et al., 2004). We can now also see that major changes in mangrove cover happen further away (>500m) from the coastline in the coastal hinterland (Figures 5.10 and 5.11). Thus, highlighting the importance of considering the entire mangrove forest cover and the associated changes that were not directly related to mudbank migration. These changes in the coastal hinterland were also more frequently larger, compared to the changes in the interbank and bank zones. This is especially true for detected losses, which were predominantly larger than four ha (Figure 5.10). Such large changes can potentially be attributed to conversion of mangrove into wetland vegetation or other anthropogenic influences but should be considered with care. For example, the changes could be related to overestimation due to the relatively small coastal buffer of 500 m or to the false positive detection of mangrove changes from the NDVI trajectories (Section 5.3.1). It remains clear that despite the importance of mudbank migration for changes in mangrove cover, other drivers that influenced mangrove changes further away from the coastline should be studied more carefully.

5.5.2 Temporal trends

Gain and loss patterns changed profoundly between 2000 and 2021, although the trends in patch size and frequency of occurrence were different and varied spatially (Figures 5.12 and 5.13). Overall, the size of loss patches increased, while the frequency of occurrence of losses remained stable (Figure 5.12, panel IV). The increasing patch size of losses, especially in Guyana and French Guiana, may be related to changing interventions, such as increasing land cover conversion and the construction of protection measures, causing enhanced susceptibility to erosion. Frequency of gain events mostly decreased between 2000 and 2021 in Suriname and French Guiana (Figure 5.13, panel IV), whereas the patch sizes were predominantly increasing between 2000 and 2021. Near Coppename, the patch size decreased and thus influencing the average values of Suriname (Table 5.2). Such spatial variability in trends have been linked to anthropogenic and natural control factors, that are potentially responsible for the changing patterns in mangrove losses at global scales (Friess et al., 2019; Goldberg et al., 2020; Maina et al., 2021). Here we have shown variability in trends for the Guianas and thus additional attention is required to elucidate further on potential drivers, including atmospheric forcing and wave climate. Additionally, this highlights the importance of managing existing mangrove forest that are required for sufficiently large and frequent mangrove gains. This is especially important for the Guiana coastal zone, where sometimes natural mangrove growth, resulting from the migration of mudbanks, is too easily expected but controlled by a more complex combination of control factors.

For the largest part, the frequency of gain and especially losses remained relatively stable, suggesting that observed overall trends in total surface area between 2000 and 2021 were mainly driven by changing patch sizes rather than the frequency of occurrence. Although, the presented results now show where such generalization deserves additional explanations or research. For example, near Waini (a) in Guyana, Bigi Pan (c), Hertenrits (d) in Suriname and Mana (h) in French Guiana, where gain and losses are not balanced (Figure 5.3) or changing rapidly (Figures 5.12 and 5.13). This relationship implies that if frequency of occurrence and patch size are treated separately or not considered at all, management may develop inadequate restoration objectives in the Guianas (Anthony et al., 2021).

The observed increasing frequency of occurrence in gain and loss in the Berbice region, east of Georgetown (b) in Guyana (Figures 5.12 and 5.13), results from changes in coastal zone management (Anthony et al., 2021; Anthony and Gratiot, 2012). The implementation of hard structures as coastal defence resulted in major losses of mangroves forest before 2000, the start of the timeseries of Landsat observations included here. These changes are therefore not represented in the annual biggest change events we derived from the LandTrendr dataset. The trends here detected thus reflect frequent but small changes in relatively small natural mangrove areas (Figure 5.3), which can be related to the inability to sequester sufficient sediment for mangrove development in absence of mangrove trees (Proisy et al., 2021; Willemsen et al., 2016). This limited sediment capture has been attributed to the streaming of mudbanks (Anthony et al., 2013b; Winterwerp et al., 2020) and the lack of wave damping and therefore settling of sediment in mangrove forest.

The timeseries used here was relatively short to capture the full range of naturally occurring dynamics that have been shown to govern the multi-decadal mangrove development along the Guiana coastline (Gratiot et al., 2008; Walcker et al., 2015). The net mangrove changes (Figure 5.3) and the annual trends presented here should be handled with care until the timeseries of observations are sufficiently long. Areas identified as hotspots of net losses, together with changing trends in the functional attributes of these losses (patch size and frequency of occurrence), are as explained earlier likely to have compromised functionality inside remaining mangrove forest (Bryan-Brown et al., 2020). For example, increasing disturbed patch sizes, combined with more frequently occurring changes might indicate loss of resistance to wave forcing (Alongi, 2008; Horstman et al., 2015; Koch et al., 2009). Simultaneously, decreasing gain patch size and frequency of occurrence might indicate reduced potential for natural mangrove colonization (Balke et al., 2011). As we can see from our results (Figure 5.3) and previous observations in other parts of the world (van Bijsterveldt et al., 2022), it is exactly these remaining forests that facilitate the natural development of mangrove forest (Balke et al., 2011).

5.5.3 Mangrove surveying from satellite imagery

In the research presented here the remote sensing work on large-scale mapping of mangrove changes in the Guianas (Proisy et al., 2009) and the identification of functional attributes (Senf and Seidl, 2021a, 2021b) was extended. We explored the potential of LandTrendr to provide a baseline regarding temporal changes in mangrove cover at 30-m resolution. The integration of cloud computing in GEE, the public availability of sufficient Landsat data since 2000 and the automatic LandTrendr segmentation algorithm allowed for monitoring in remote areas along the Guianas' coastal zone. LandTrendr provided a robust and semi-automated approach that proved to be effective in detecting mangrove dynamics over larger spatial and temporal scales from NDVI timeseries. The resemblance in the order of magnitude changes with previous work (Augustinus, 1980; Gratiot et al., 2007; Walcker et al., 2015) on loss and gain of mangrove cover provides confidence in detected trends. The derived landscape metrics in gain and loss patterns, including patch size and frequency, also the provided opportunity to detect unwanted trends in landscape changes.

Nevertheless, methodological limitations to our approach remain and should therefore be considered when using the data or approach. For example, a distinction between different control factors, both natural and anthropogenic, was not made, so attributing the origin of mangrove cover changes at the patch level was not possible. Key steps that should be incorporated to facilitate such a distinction include: 1) reference data on the occurrence of different control factors, 2) further

improvements of differentiating between mangrove and non-mangrove vegetation cover through machine learning and image classification algorithms.

In the applied approach only the largest changes (gain and loss) were considered, resulting in the maximum of two recorded events in the timeseries per pixel. This limited the analyses of mangrove losses to stand replacing changes only, and thus do not include additionally important processes like degradation and competition between mangrove species. Together with the saturation of NDVI at higher forest covers, cross-sensor differences in reflectance and the difficulty in separating mangrove vegetation from other types of wetland vegetation, mangrove detection from multispectral data could be further improved (Younes Cárdenas et al., 2017). One way of doing so could be to use additional LandTrendr runs, including those with Tasselled Cap wetness, Normalized Burn Ration or specific indices such as the Modular Mangrove Recognition Index (Diniz et al., 2019), for random forest classification (Senf and Seidl, 2021a, 2021b). This facilitates the possibility to further improve mangrove detection and associated changes, including degradation and succession(Murillo-sandoval et al., 2022; Murillo-Sandoval et al., 2021).

Finally, remotely sensed images are inherently noisy, therefore potentially obscuring fine-scale and slow-rate changes. On top of the sensitivity of our approach to the LandTrendr input parameters, these considerations remain important but are intrinsic to the data and methodology. Despite these limitations and the simple fact that alternative data sources at the spatial and temporal scales considered here are non-existent in the region, the results presented here provide a first step to better understanding ongoing changes in mangrove cover in the Guiana coastal zone.

5.6 Conclusions

Here we provided a quantitative remote sensing approach to characterize gain and loss in mangrove forests along the Guiana coastal zone in relation to alongshore mudbank migration. By using the LandTrendr temporal segmentation algorithm and annual composites of NDVI-derived Landsat observations we were able to associate the largest index changes to patches of gain or loss of mangrove forest. A total of -4,052, 702 and -5,769 ha net mangrove changes were detected between 2000 and 2021 in Guyana, Suriname and French Guiana respectively. Variability at landscape scale clearly exists and we found that losses in mangrove cover were often associated with smaller and fragmented pristine mangrove forest. Additionally, the results highlight the variability the functional attributes, such as frequency and size at patch level, of the observed changes in mangrove cover. Change patches between are relatively small with averages between 1 and 2 ha, although patch sizes surpassing 400 ha are also detected. This indicates that the total surface area changes are predominantly explained by small, yet frequently occurring changes.

The variability in the temporal trends of the functional attributes, including patch size and frequency of occurrence, are indicative for the existence of different driving forces, including mudbank migration. While mudbank migration is known to cause this alongshore variability in gain and loss of mangrove forest, it is probably also the variability in coastal management between countries that explains observed spatial and temporal patterns. Especially implementation of coastal protection across the Guianas result in changes that can be characterized by smaller size, yet more frequently occurring in the coastal zone. Changes detected in the hinterland are more often larger, which can potentially be attributed to land cover conversions of mangrove into other types of vegetation or agriculture, or mangrove die-off.

Data availability

Code to generate coastline position estimates together with the mudbank estimates can be found in Google Earth Engine repository:
https://code.earthengine.google.com/?accept_repo=users/jobdevries90/MangroMud

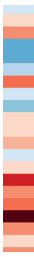

Chapter 6 | Synthesis

The main aim of the thesis was to increase the understanding of multi-decadal variability in local changes along the Suriname coastal zone induced by the migration of subtidal mudbanks along the entire Guianas' coastline and regional-scale differences in control factors. As I emphasize in this thesis, the observed cyclicity in the coastal landscape of all Guiana shield countries can be explained by the conceptual model of mudbank migration. However, spatiotemporal variable and non-linear changes in coastline positions, mudbank footprints and mangrove development found along the Guianas' coastal zone have remained largely unquantified. This makes it difficult to differentiate between the natural variability, anthropogenic induced changes and the effect of climate changes. This suggests that the oft-placed strong emphasis on the conceptual view of mangrove and coastline changes, with erosion and mangrove losses when mudbanks are absent and vice versa mangrove colonization and coastal progradation when present, deserves additional attention.

In this chapter the developed remote sensing approach to characterize mudbank boundaries in Suriname (Chapter 2) and mudbank footprints in the wider Guianas' coastal region (Chapters 3 and 4) are discussed first. This is followed by a discussion on the findings of the observed coastal zone changes, including coastline changes in response to the presence and absence of mudbank migration (Chapter 3), the contribution of mudbanks to observed coastline morphology, variability and complexity (Chapter 4) and the effect of mudbank migration on mangrove losses and gains (Chapter 5). Then, in the succeeding section, the main findings are discussed in the perspective of coastal safety, mangrove development and livelihood of local communities. The value of the developed approach for coastal managers is discussed and supplemented with recommendations, both on policy and directions for future research.

6.1 Main conclusions

In this thesis, mudbanks and associated coastal dynamics were studied using multi-decadal remote sensing observations. This has been achieved by focussing on the following research questions (RQs):

1. How can mudbanks and their fuzzy boundaries be detected in medium-resolution Landsat images given the heterogeneous and dynamic character of the Suriname coastal landscape?
2. What is the spatiotemporal variability in the position of the Suriname coastline imposed by alongshore migrating mudbanks, as mapped from Landsat images available between 1985 and 2020?
3. What is the spatiotemporal variability in coastlines changes along the entire Guianas' coast and to what extent are these differences due to variability in mudbank footprints or to external control factors?
4. What is the spatiotemporal variability in mangrove loss and recovery along the Guiana coast and to what extent can this variability be explained by alongshore mudbank migration?

6.1.1 Mudbank dynamics

Mudbank migration causes spatiotemporal variability in coastal zone dynamics, expressed by the variable response of coastline positions and mangrove forest to mudbank presence and absence. However, due to their spectral similarity with intertidal morphology, surface features and high concentrations of suspended sediment in the water column (Ryu et al., 2002), it remained challenging to semi-automatically untangle subtidal mudbanks from their surroundings. This semi-automatic identification of migrating mudbanks is a prerequisite to study the variability in mudbank footprint on seasonal to multi-decadal timescales, at appropriate spatial scales to investigate their link with local changes in mangrove cover and coastline positions.

In this thesis I showed that remote sensing-based estimates of mud abundance represent cross-shore (Chapter 2) gradients and alongshore variation (Chapter 3) in sediment concentrations present at the coast of Suriname. An unsupervised decision tree, based on multi-decadal timeseries of Landsat observations, was tested for a section of the Suriname coast in chapter 2 and extended for the entire Guianas' coast in chapters 3 and 4. The consistent and iterative sampling of potential end-member candidates, from initial estimates of water, intertidal and land surfaces, resulted in spatially explicit and spectrally coherent image endmembers. This allowed to directly link the associated spectral signatures of these morphological units to the circumstances during image acquisition and thus unmix signals into sub-pixel proportions of mud abundance. As a result, the natural variability of mudbank footprints and their fuzzy boundaries could be accounted for. Considering the large temporal variability in mudbank footprints (Chapter 2), this is crucial for the successful detection of their diffuse boundaries (RQ 1).

The detection of mudbank boundaries (Chapter 2) allowed for the first time to semi-automatically estimate mudbank presence and absence (Chapter 3), and to characterize their morphometrics, including migration speed, width and length (Chapter 4). Previously, mudbanks were demarcated manually or detected from satellite derived estimates of sediment concentration, making such efforts subjective, highly dependent on limited observations, fixed thresholds, and as such subjective and non-reproducible (Baghdadi and Oliveros, 2007; Froidefond et al., 2002; Péron et al., 2013). Here I processed individual Landsat observations and analysed abrupt changes in sediment abundance along cross shore orientated transects. With the observed absolute difference in mud abundance, I showed that fixed thresholds, to separate mudbanks from their surroundings, cannot be consistently applied for the entire Guianas. Additionally, per-image and thus dynamic thresholds must be applied between different acquisitions in time (Chapter 2). It was estimated that the final footprints presented in this thesis are most likely a conservative estimate of subtidal mudbank footprints, excluding their active migration zone (Zorrilla et al., 2018).

Migration speeds (on average 1-1.25 km / yr) differ between different stretches along the Guianas' coastal zone, with faster migrating, yet smaller mudbanks in Guyana compared to those in French Guiana and Suriname (Chapter 4). Additionally, large-scale external control factors that originate from atmospheric variability (e.g. NAO and ENSO) are known to enhance variability in footprints on daily to weekly timescales and thus migration rates on seasonal to multi-decadal timescales (Murty et al., 1984; Rodriguez and Mehta, 1998; Vantrepotte et al., 2013; Walcker et al., 2015). This can be expressed as the frequency of mudbank occurrence (Chapter 4), a comprehensive metric that incorporates migration rate, size, and morphometric dynamics of a mudbank to describe the time a coastline stretch is covered by a mudbank.

6.1.2 Coastal zone changes

Local to regional variability in coastline positions (Chapter 3), variable long-term coastline trajectories (Chapter 4) and patterns in mangrove gain and loss (Chapter 5) hint at scale dependencies that reflect a complex combination of natural and anthropogenic controlling factors. Examples include the 18.6 year nodal cycle (Gratiot et al., 2008), shifting of the NAO that affects the offshore wave climate (Walcker et al., 2015), trade winds associated with the movement of the ITCZ (Augustinus, 2004), slow onset processes such as sea level rise or anthropogenic induced land cover changes (e.g. Brunier et al., 2019). However, these studies did not separate the effect of mudbanks on coastline changes from these other controlling factors due to the inability to separate mudbank footprints from their surroundings (Section 6.1.1). As a result, local-scale variability in coastline response, due to the presence or absence of mudbanks, has remained unquantified, or lacked the temporal coverage and spatial resolution that is required to avoid masking trends. In chapters 3 and 4 spatiotemporal variability in coastline changes for Suriname and the wider Guianas are therefore analysed at local scales using timeseries of Landsat imagery. These were linked to changing mudbank footprints, derived from the methodology developed in chapter 2 and further extended in chapters 3 and 4.

The development of the above discussed image analysis methodology proved essential to separate coastlines changes associated with mudbank presence to the changes during interbank phases (Chapter 3) or those related to anthropogenic interference and other external control mechanisms (Chapter 4). As a result I was able to reaffirm the dominant effect of migrating mudbanks on coastline changes, yet extend previous monitored periods and trends (Augustinus, 2004; Gratiot et al., 2008; Walcker et al., 2015) till 2022 for the entire Guianas at annual intervals. Additionally, I clearly show that differences in coastline observations within Suriname (RQ2) and between countries (RQ3) exemplify that not every mudbank has the same effect on each stretch of coastline it is passing. This is partially explained by factors that influence position and shape of mudbanks, and thus the frequency of mudbank occurrence on decadal time scales (RQ3). Overall, progradation during mudbank phases was considerably larger (2-44 m/yr) and happened more frequently (52% of the coast) compared to interbank phases, when mudbanks are not damping waves and average coastline retreat is between 13 and 18 m/yr (RQ2). The difference in long term coastline changes between Guyana on the one hand and both French Guiana and Suriname on the other hand reflect anthropogenic influences. For example, as a result of constructing coastal protection in Guyana, coastline changes are an order magnitude smaller. However, also within Guyana clear variability exists, potentially induced by natural control factors like the presence of abundant mangrove cover to facilitate natural (re)colonization (Chapter 5).

The variable response of mudbank migration to (hydrodynamic) forcing mechanisms results in significant non-linearity and regional variability in the observed changes in the Guianas' coastal zone (Chapters 3 and 4). However, it remained uncertain how cyclic behaviour in coastline changes, related to mudbank migration, influences mangrove forests losses, recovery, succession and thus beneficial ecosystem services that are associated with their presence. By focussing on the spatial dimensions of mangrove losses and recovery patches, I was able to assess the persistence of mangrove forests (Chapter 5). This offers insights on how the mangrove forests are altered by migrating mudbanks and thus define the historical range in gain, losses and recovery patterns (RQ 4). A total of -4,052, 702 and -5,769 ha net mangrove changes were detected in Guyana, Suriname and French Guiana between 2000 and 2021, respectively. However, the response of mangrove forest to mudbank migration was remarkably variable in space and time (Chapter 5), especially variability in patch size, frequency of occurrence and change intervals of gains and losses. These landscape scale

changes, together with the observed disparity in temporal trends indicate that changing control mechanisms can potentially be responsible. For example, variation in coastal management between countries, and the coastal hinterland compared to the coastal zone, highlight the contribution of different types of land cover conversions to changes observed in mangrove forests.

6.2 Coastal safety and natural dynamics

The complexity of changes in coastal zones and the lack of data due to the inaccessibility of the coastal zone, both common for Suriname and the wider Guianas, pose a challenge for coastal management. Until now, changes along the coastal zone of the Guianas were often measured by visual inspection or field visits, with small-scale campaigns or at insufficient temporal resolution to capture the full range of variability. Such approaches are neither precise, nor repeatable, nor objective, nor geographically comprehensive. The differences in change rates are therefore difficult to quantify, making management implementation either unnecessarily early or too late. This is especially relevant for interventions that need to account for the arrival (or departure) of a mudbank and the likely response in mangrove cover and coastal change. The tools developed in this thesis can provide coastal managers at all levels with the information to see where relevant changes are occurring and might occur in the future. By providing near-continuous updates and a detailed view of the natural variability, the results presented in this thesis can assist in timely adaptation measures, even in remote and data poor regions.

6.2.1 Progress in mapping coastal zone changes

The workflows that are applied in this thesis are partially derived from open-source remote sensing products and allow for parameter adjustment in post-processing. More specifically this thesis highlights the use of our methodology to: 1) monitor spatiotemporal patterns of mudbank migration, 2) quantification of spatiotemporal variability in coastline changes, 3) decipher patterns in mangrove cover changes, 4) determining which parts of the coastal zone are more vulnerable to erosion or vice versa expected to accrete, 5) facilitate prioritizing efforts in mitigation against flooding, 6) quantify the natural range of changes and related frequency of coastline changes, and 7) elucidate on factors controlling the naturally occurring variability in coastline changes.

An established edge detection algorithm was applied to Landsat satellite images in combination with adaptive Otsu thresholding, to simultaneously separate land and vegetation from water. The capacity of this approach has been tested frequently (Bishop-taylor et al., 2019; Donchyts et al., 2016) and it was shown (Chapters 3 and 4) that by applying it to each individual image, uncorrected estimates of coastline positions can be identified and long-term trends evaluated. By comparing these estimates with visual interpretation of coastlines in high-resolution (50 cm) drone imagery I showed (Chapter 3) that also for the mud-dominated coast of the Guianas such a workflow can be invaluable for detecting coastline changes. This information aids in managing these complex coastal systems consisting of different land-water transitions, fuzzy boundaries and spanning different countries and ecosystems.

Additionally, by using individual images, rather than annually aggregated composite satellite observations, I was able to highlight the exceptional temporal variability in mudbank footprints. This re-emphasizes the dynamic nature of the sediment redistribution in front of the coast and thus the difficulty in defining mudbank migration rates between two static observations in time (Zorrilla et al., 2018). However, such observations need to be linked to tidal stages and wave energy fluxes. These influence the total suspended sediment concentrations and thus variability in footprints as are

visible in remote sensing images. Simultaneously, this gap in data availability on such an elementary and important process stresses the importance to continue in-situ observations for validation.

In chapter 3 I show that UAV images can be particularly valuable as ground truth or validation. Similarly, UAV data can be used for downscaling or validation and calibration of satellite data, like coastline position estimates (Chapter 3), mangrove properties, intertidal morphology or sedimentation rates (Kim et al., 2019; Zanutta et al., 2020). Additionally, the assimilation, validation, parameterization or calibration of process-based models and thus the potential to upscale to larger regions can be supported from these high-resolution observations. Future studies could expand on the integration of in-situ, remote sensing and UAV data. Due to the limited extent these UAVs can cover, a substantial effort of UAV acquisition is required, preferably at different locations to capture the natural variability of the coastline.

6.2.2 Contributions towards coastal safety

Coastal management is costly, making it important that investments are effective (Gijsman et al., 2021; Temmerman et al., 2013; van Zelst et al., 2021). Comprehensive understanding of natural mangrove forests, historic changes in coastline positions and potential future scenarios are therefore essential for coastal managers. Also adequate design of intervention measures, such as nature-based solutions, and their evaluation rely heavily on proper monitoring over sufficiently long period and large areas (Sutton-Grier et al., 2015). With the results in this thesis, I aimed to provide coastal managers in Suriname, and the wider Guianas, with much needed spatial information regarding coastline and mangrove position estimates and changes.

The methodology developed in this thesis (Chapters 2 and 3) provides continuous updates of annual coastline changes and estimates of mudbank footprints. The applied methods can help to efficiently determine natural dynamics at timescales from seasons to multiple decades and local, landscape to regional spatial scales. This facilitates monitoring management measurements over a range of scales that are often difficult to oversee without the continuous bird's-eye perspective that satellite images can provide. Simultaneously, it provides coastal managers the tools to move beyond reporting aggregated country level average change statistics or linear trends, as they might conceal complexity that is inherently associated with coastal zone changes in the Guianas. This may thus support informed decisions on intervention, conservation or regeneration and the identification where to do so to improve coastal safety and natural function of ecosystems (Barbier, 2016).

Besides the possibility to detect unexpected behaviour, variable coastline changes reflect the effects of natural and anthropogenic control factors on the coast of Suriname and the wider Guianas' coastal zone. However, predictions of coastline change should be conducted with extreme care as they might create a false sense of security on short to medium timescales. For example, the results in chapters 3 and 4 illustrate that not all changes can be attributed to mudbank migration alone. Specifically, not every mudbank triggers the same coastline response at each location it is passing. Also, the potential for erosion during an interbank phase can be significantly larger than accretion rates in the previous mudbank phase. These examples suggest that local coastal behaviour, not captured by linear rates of change, should be included in theoretical frameworks that thus far predominantly looked at large wave forcing and climate variability (Gratiot et al., 2008; Walcker et al., 2015). The information products generated in this thesis can provide a framework for such coastal development policy, aid in monitoring historic coastal behaviour and thus facilitate the analysis of intervention measures.

6.2.3 Nature based engineering

Ecosystem based coastal defence efforts aim at reducing flood risk by, for example, planting mangrove trees (Gijsman et al., 2021; Temmerman et al., 2013; van Zelst et al., 2021). This has the additional advantage of continuous carbon sequestration in the order of 1-2 Mg C ha/yr (Breithaupt et al., 2012; Sanderman et al., 2018). Also, landscape restoration is a nature-based intervention that has gained increasing attention in recent years, related to achieving SDG 14 and 15 (Life on Land; Life below Water). Together they show that it has become even more important to understand what monetizing the protection and carbon-storage function of mangrove ecosystems adds to the already increasing demands for space in coastal zones (Oppenheimer et al., 2019; Seddon et al., 2020). However, also the implementation, reliability and cost effectiveness of such nature-based solutions rely heavily on adequate monitoring, for example, to let coastal managers decide where and when specific coastal protection or nature conservation measures are required. Additionally, the focus of international nature conservation policies, which ultimately result in safer and habitable coastal zones should increasingly focus on the protection of existing natural (yet sometimes degraded) mangrove forest and wetlands present along the Guianas' coastline.

Currently, nature-based engineering efforts in the Guianas are scattered and often unregulated (Anthony and Gratiot, 2012). This can lead to (ownership) conflicts when 'new' land is created, or 'old' land regenerated. Additionally, natural cyclicity in phases of degradation and progradation of coastlines in the Guianas undermine the revenue model of coastal building with nature initiatives due to future phases of erosion. Specifically, the minimum required width of a mangrove fringe, to protect the hinterland from incoming waves, should be maintained in existing mangrove forest along the entire length of the Guianas' coastline, while taking potential future changes in mangrove cover into account. These examples stress the importance of successful prediction of mudbank migration, in combination with projected mangrove development estimates.

Mapping baseline conditions and monitoring changes are key to preserve natural mangrove coastlines, successful implementation of coastal management interventions or nature-based engineering projects. For that purpose, remote sensing observations at diverse levels of scale and frequency (satellite, airborne, UAVs) are indispensable, allowing low-cost monitoring over inaccessible areas and compare similar ecosystems that are often crossing administrative boundaries. Only by looking at all changes in similar coastal systems, including those in other countries, one can truly grasp future variability. Identification of the extent of mangrove cover and the coastline positions are examples in this thesis that allow constructing policy frameworks that are suitable for coastal managers.

6.3 Recommendations and future outlook

The research presented in this thesis provides a way forward to develop further insights in spatiotemporal changes in the coastal zones in Suriname and the wider region of the Guianas. I focussed specifically on detecting mudbanks and analysing their effect on the coastal system of the Guianas. Simultaneously, I explored the optimal use of the open-source Landsat archive to detect mudbanks and the changes they initiate. This gave insights into their characteristics, spatiotemporal distribution along the coast of the Guianas and variable response of coastline changes. Although these mudbanks play a dominant role in the observed coastline dynamics, they only explain part of the natural occurring variability in the system. To fully understand this variability and the full impact of climate change, it is therefore important to understand all factors, both internal and

external to the system. However, there are still missing links and scientific challenges that should be addressed to further enhance knowledge on the coastal dynamics in Suriname and the wider coastal region of the Guianas.

6.3.1 Internal controls

In chapter 4 I stress the high dependency of the entire Guianas' coastal zone on the spatiotemporal patterns of mud abundance and the migrating mudbanks. However, on scales smaller than a single mudbank, sediment dynamics are still uncertain, and there is relatively little known about the spatial variability of suspended sediment in the water column (Gratiot et al., 2007). With the rising and falling of the tides, enhanced wave activity and swell waves, the temporal variability in the footprint of a mudbank has been shown (Chapters 2 and 3) to vary significantly (Zorrilla et al., 2018). Yet, knowledge gaps remain with respect to the intrinsic properties of mudbanks, including depth profiles of sediment concentrations, height of fluid mud above the bed and variability in thickness of the bank. These knowledge gaps limit the possibility to improve the detection of mudbank footprints from remote sensing images and thus the possibility to explain spatial variability and improve estimates of migration rates. This leaves questions unanswered on our system understanding, for example related to wave damping potential of mudbanks.

Although the long-term trends in coastline response are shown here in this thesis to depend significantly on mudbank migration, variability in coastline changes along Guianas' coast can be attributed to controlling factors other than mudbank migration (Chapter 4). Therefore the established conceptual model of mudbank migration along Guianas' coastline (Chapter 1), that prescribes a cyclic instability of progradation and erosion related to bank and interbank phases (Allison et al., 1995; Anthony et al., 2010), requires refinement. Especially the lack of progradation during mudbank phases should be included in the conceptual model. This has previously been attributed to the streaming of a mudbank, where it is effectively disconnected from the shoreline and thus not exchanging any sediment (Rodriguez and Mehta, 1998). Together with inundation this can be considered as an important factor for sediment exchange and thus progradation and erosion (Crase et al., 2013). These controls contribute to successful colonization of mangroves on mudflats at specific locations along the coast.

Natural resistance to erosion during interbank phases has been attributed to the presence of cheniers (Anthony et al., 2019, 2013; Augustinus, 1989). These sandy or shelly ridges are made up of local (riverine) sand and accumulate due to winnowing or continuous alongshore transport of these coarser sediments (Anthony et al., 2019; Tas et al., 2020, 2022). Even though I did not explicitly map the position of cheniers in this thesis there are clear examples of their effect on long-term coastline trends in chapters 3 and 4. Future research can focus on demarcating these cheniers and link their properties, such as heigh, width and changing positions, to the here observed trends of coastline changes to quantify their contribution to coastal safety.

With the increased attention to building-with-nature and mangrove restoration it is valuable to determine relevant control factors for mangrove loss and especially gain. While planting mangroves indeed contributes to sustainable ecosystem restoration, it can be necessary to assess technical design conditions, wave breaking features and sediment storage capacity to stimulate development and growth in artificial mangrove forests. A valuable starting point could be answering questions on why mangroves are not colonizing a selected intertidal mudflat naturally. Potential internal controls, or the window of opportunity (Balke et al., 2011), that can be considered then include insufficient seed dispersal, inadequate elevation above sea level, intolerable saline conditions, insufficient hydrological connection with the hinterland and more morphological attributes such as coastline

morphology and bathymetry (Dahdouh-guebas et al., 2011; Krauss et al., 2008; van der Stocken et al., 2015). These factors are examples that are underlining the importance of increasing knowledge on how mangroves colonize, develop and ultimately retain sediment under a changing climate.

6.3.2 External controls

Variable hydrodynamic and atmospheric forcing mechanisms influence the wave climate (Geleynse et al., 2012; Lazarus and Murray, 2007; Murray and Ashton, 2013; Shaw et al., 2008). Additionally, the presence of mangrove forests protects the coast against flood risks due to their traits that ensure sediment accumulation, survival in saline environment and wave damping properties (Furukawa et al., 1997; Furukawa and Wolanski, 1996; Horstman et al., 2014). For the Guianas, this implies that the strength of these external controls provides invaluable information on coastline changes that can realistically be expected. It is therefore also crucial to understand the response in mudbank migration to the same changing conditions. In chapter 4, I studied the role of different factors on coastline changes for the entire coastal zone of the Guianas by applying a multivariate regression analysis. However, to be able to specify when, where and which external controls exert an influence on variability in coastline changes, yearly coastline position differences can be considered as opposed to long-term rates of change. Such an approach would require improvements on the accuracy and resolution of coastline position estimates and information on the strength of each external control factor, with sufficient spatiotemporal resolution and cover to capture the full range of variability in the system.

In addition to mudbank migration, the Amazon River also provides a more direct flux of sediment to Guianas' coastline through ocean currents (Allison et al., 2000; Wells and Coleman, 1981). This sediment flux is projected to increase due to deforestation in the decades to come (Anthony et al., 2021). However, most of the fine sediment in front of Guianas' coast is supplied to the system with a considerable time lag due to the relative slow migration of mudbanks. Recent and ongoing changes in the sediment budget of the Amazon River are therefore not expected to quickly influence the amount of sediment available in Guianas' coastal zone, as it takes an approximate 25-100 years for mudbanks to reach the east coast of French Guiana. Because the distribution in sediment delivered through mudbanks (slowly) and currents (relative quickly) remains uncertain, the direct consequences to sediment availability for coastal progradation remains unquantified. Modelling of the full range of hydrodynamic and sediment interactions, including streaming, wave damping, fine sediment transport and the formation of fluid mud, can provide a way forward to explain the contribution of such large-scale control factors (van Ledden et al., 2009; Winterwerp et al., 2007).

6.3.3 Further advancing coastal monitoring

Several promising research directions on monitoring in coastal zones arise from the findings in this thesis. The developed methodology to mapping coastline changes and spatiotemporal variability in subtidal bedforms is expected to be portable to other mud-dominated coasts. Due to the use of well-developed image information extraction methodologies, the avoidance of fixed thresholds and the use of image-based endmembers for linear spectral unmixing, classification of coastal landforms and detecting trends are possible in landscapes that show similar complexity. The developed methodology can be especially beneficial to other data poor regions, where in-situ observations with sufficient spatiotemporal coverage, regarding changes in coastal zones, are absent or scarce.

In regions where collecting field data will always remain a challenge, remote sensing observations and associated processing techniques can provide valuable information to downscale

global datasets or upscale distributed and scattered point observations. However, in-situ monitoring campaigns that span multiple years and follow sequences of erosion and progradation, linked with mudbank migration, have been very limited in the Guianas (SBB, 2019; Teunissen, 1976). This prohibits the validation and calibration of new mapping approaches. Also, the applied vegetation change methodology (Chapter 5) also lacks such a validation. Future field monitoring campaigns should focus on information regarding biomass, tree height, leaf area index and (above and below ground) carbon storage. When such an intensive campaign is repeated or initiated, upscaling to larger areas, by for example using GEDI spaceborne LiDAR observations, can contribute to understanding of, for example, carbon storage, zonation in mangrove forest or variability in mudbank footprints (Dubayah et al., 2020; Hancock et al., 2019).

Recent advances in cloud computing, in combination with the increasing availability of open-source remote sensing observations, provide opportunities to collect high-resolution land cover changes in dynamic coastal environments. The here developed monitoring workflow fits this trend where timely and processed spatial data are essential (Matthews, 2011). Yet, consistent methodologies and applicable data products are required as the identification of mangroves, coastlines, mudbanks and the fuzzy boundaries between them relies on the consistent use of available spectral information. Artificial intelligence and machine learning algorithms, including neural networks and random forest classifiers are examples of developments that allow to extract meaningful information from large spatial datasets. Additional data, acquired at multiple spatial scales, can then be combined to truly explain the dynamics of mud in the water column and thus the processes behind mudbank migration. This makes the skills in processing such quantities of data, in combination with comprehensive understanding of the natural system, invaluable for coastal monitoring and remote sensing in general.

Unravelling historic variability lies at the base of understanding potential future coastal evolution under a changing climate. To understand coastal changes and possible implications for its inhabitants it is key to first quantify baselines and natural variability. Only then process based models and climate projections provide a larger understanding of the environment and means to estimate expected changes in the coming decades.

Appendix

A. Supplements to Chapter 2

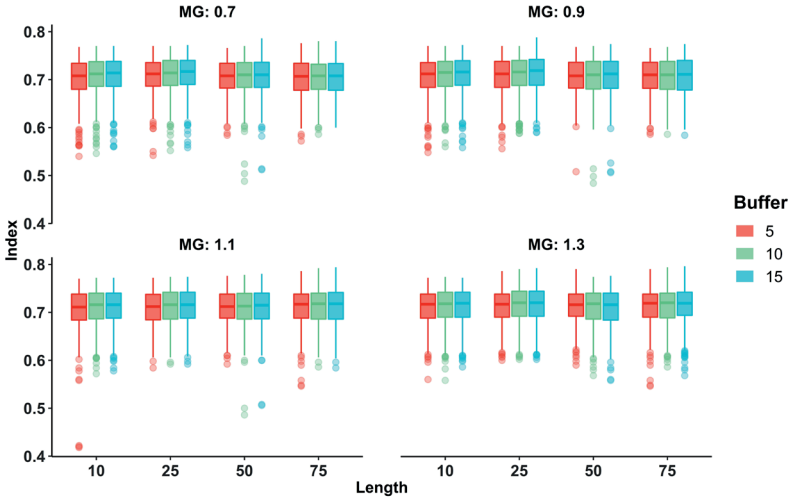

Figure A.1: NDVI peak variation between 2008 and 2010 (n = 68) for different parameter combinations. This peak value is used to select potential end-membercandidates from the derived canny edge neighborhood zones. By including a 5% buffer on both sides of this peak value, potential end member candidates for vegetation were selected in the same neighbourhood zone. Parameter sets include different buffer values (5, 10 and 15 pixels), minimum edge length thresholds (10, 25, 50 and 75 pixels), MG values (0.7, 0.9, 1.1 and 1.3) and the GPF at its default of 0.7.

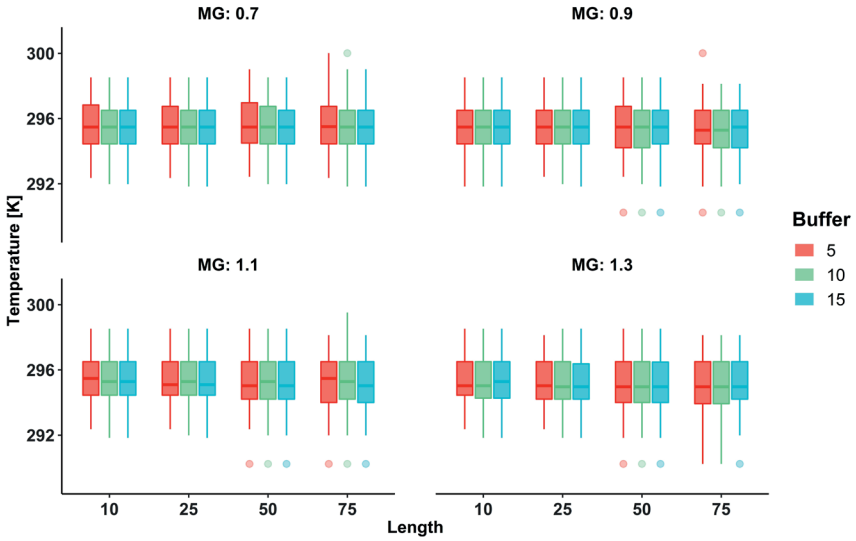

Figure A.2: Temperature threshold variation (n = 68) for images acquired between 2008 and 2010 for different parameter sets. This threshold value was used to make an initial estimate of the intertidal area for the entire coastal area in the concerning Landsat image. Parameter sets include different buffer values (5, 10 and 15 pixels), minimum edge length thresholds (10, 25, 50 and 75 pixels), MG values (0.7, 0.9, 1.1 and 1.3) and the GPF at its default of 0.7.

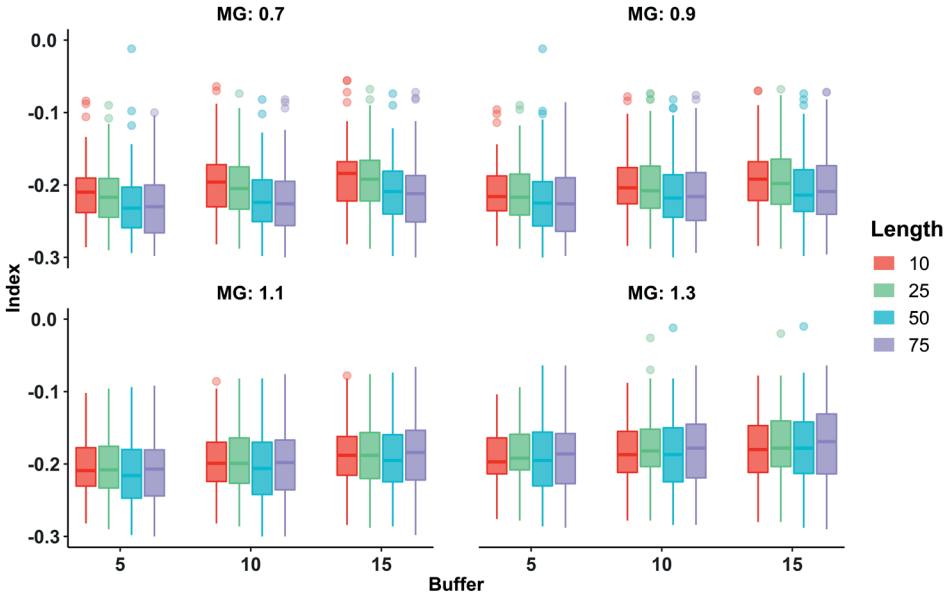

Figure A.3: Variation in the NDWI threshold (n = 68) used to separate land and water for different parameter sets: variation of the buffer size (5, 10 and 15 pixels), different minimum edge length values (10, 25, 50 and 75 pixels), MG values (0.7, 0.9, 1.1 and 1.3.) and the GPF at its default of 0.7. Difference with Figure 2.8 is that the x-axis contains the buffer values to clearly show the effect of varying minimal length values on the thresholds.

Table A.1: For the two example images five scenarios with different input parameters result in a different threshold, and thus a unique land mask, indicated by the absolute and relative amount of land pixels. Pure vegetation, pure water and pure mud indicate the number of pixels used to derive the mean end-member signatures. SNR is the sum of the standard deviation in reflectance for each band divided by the mean value, added up together for the 3 end member classes. The RMSE is the mean pixel error from the LSU (e_i in equation 2.2) analysis.

Date	Scenario				T	Pixels Land	%	Pure Vegetation	Pure Water	Pure mud	SNR	RMSE
	MG	GPF	Buffer	Length				[Number of pixels]				
12-9-2009	0.9	0.7	10	25	-0.186	20,363,626	100	8,252	88,266	16,456	8.04	0.009
	0.9	0.7	5	75	-0.198	20,358,385	99.97	4,425	88,266	5,182	7.87	0.009
	1.3	0.3	10	25	-0.184	20,364,540	100	7,817	88,266	11,015	8.39	0.009
	1.3	1.0	10	25	-0.174	20,368,298	100.02	10,159	88,266	1,308	9.32	0.010
	0.9	0.7	15	10	-0.186	20,363,626	100	8,252	88,266	16,456	8.04	0.009
15-11-2009	0.9	0.7	10	25	-0.246	20,050,838	100	12,381	233,724	5,417	8.13	0.016
	0.9	0.7	5	75	-0.254	20,045,963	99.98	2,419	233,724	2,563	8.50	0.016
	1.3	0.3	10	25	-0.242	20,053,377	100.01	7,414	233,724	5,631	8.30	0.016
	1.3	1.0	10	25	-0.202	20,070,963	100.1	3,043	233,724	1,057	7.87	0.015
	0.9	0.7	15	10	-0.242	20,053,377	100.01	21,262	233,724	,8314	7.80	0.015

B. Supplements to Chapter 3

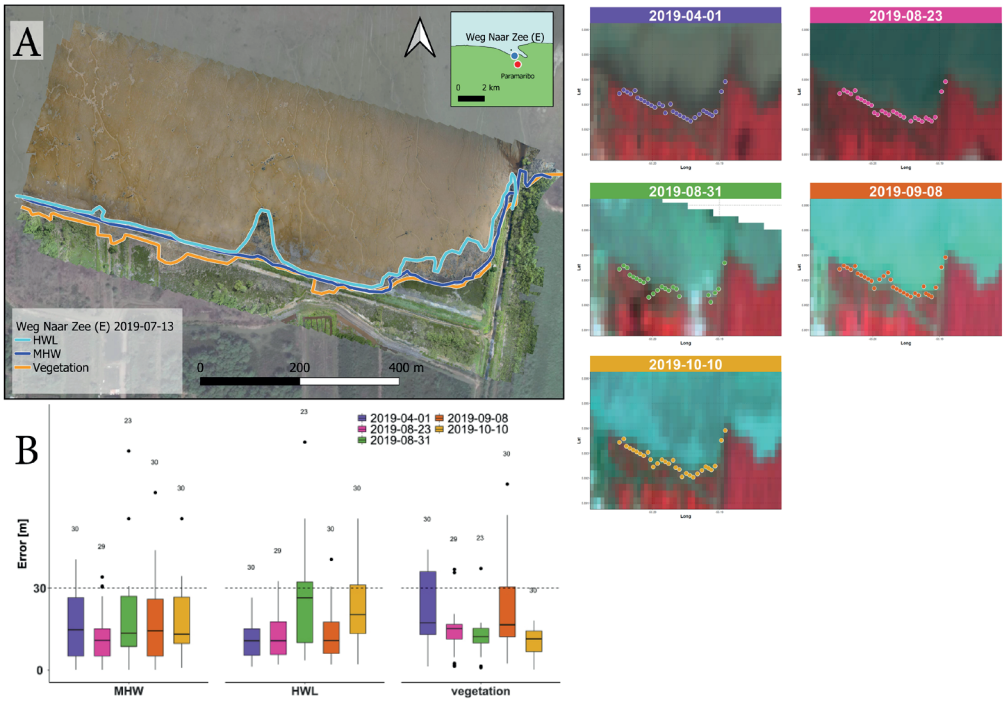

Figure B.1: Validation results of the Landsat images acquired within 100 days of collecting the high-resolution UAV images near Weg naar Zee East (2019-07-13). Only Landsat images are shown on the right that are not obstructed from sight by clouds or missing data. Panel A shows the digitized shorelines in the UAV image that are used for validation. The panels on the right show the different Landsat images that were used together with the automatically derived shoreline positions. The colored boxplots in Panel B summarize the difference for each of these Landsat derived shoreline positions compared to the different digitized shoreline positions visible in panel A (MHW, HWL and vegetation interface). The Landsat 7 image acquired at 2019-08-31 is an example that illustrates missing data related SLC-off striping

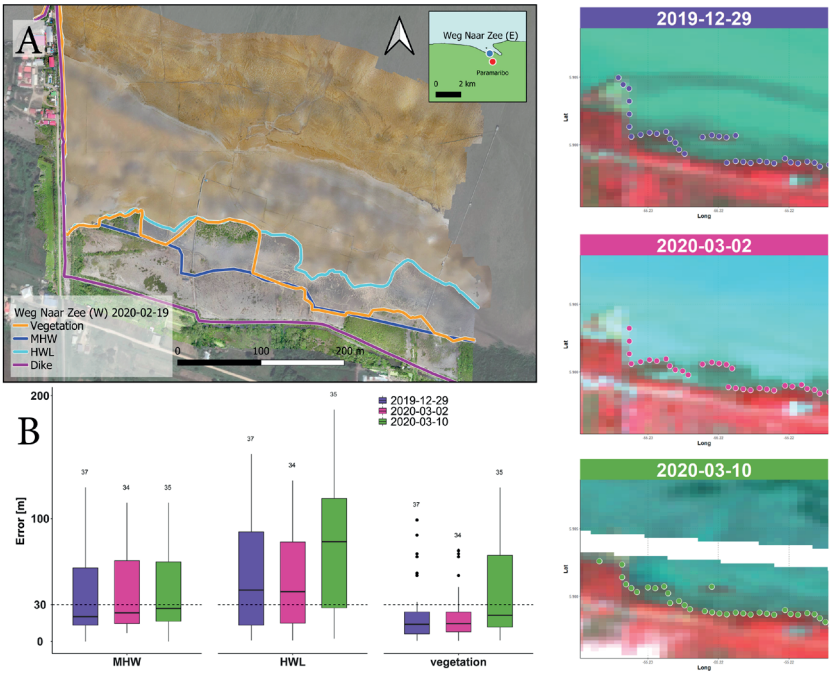

Figure B.2: Same as Figure B1 but now for Weg Naar Zee-West in 2020.

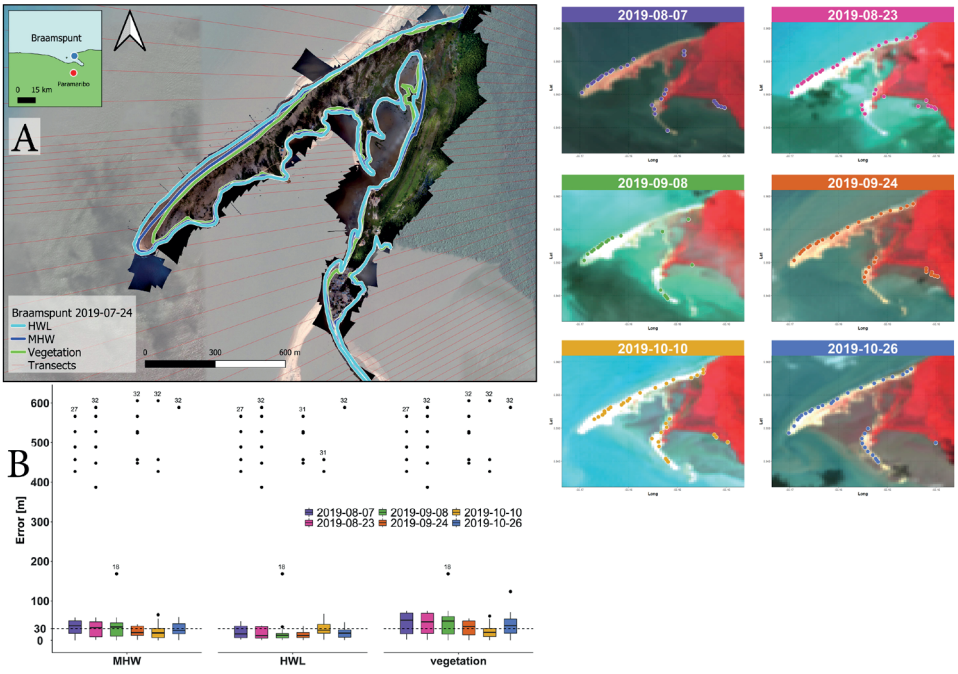

Figure B.3: Same as Figure B1 but now for Braamspunt in 2019.

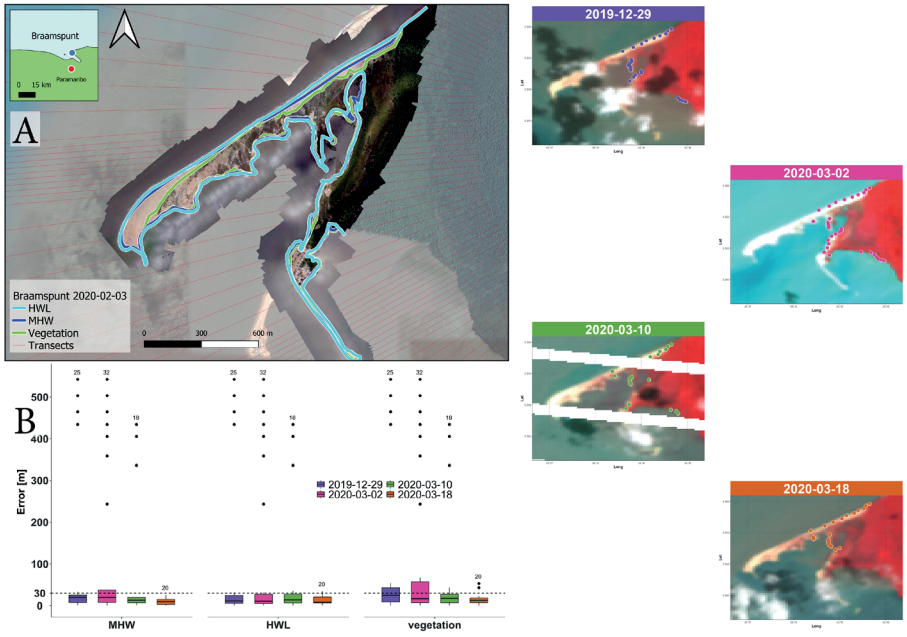

Figure B.4: Same as Figure B1 but now for Braamspunt in 2020.

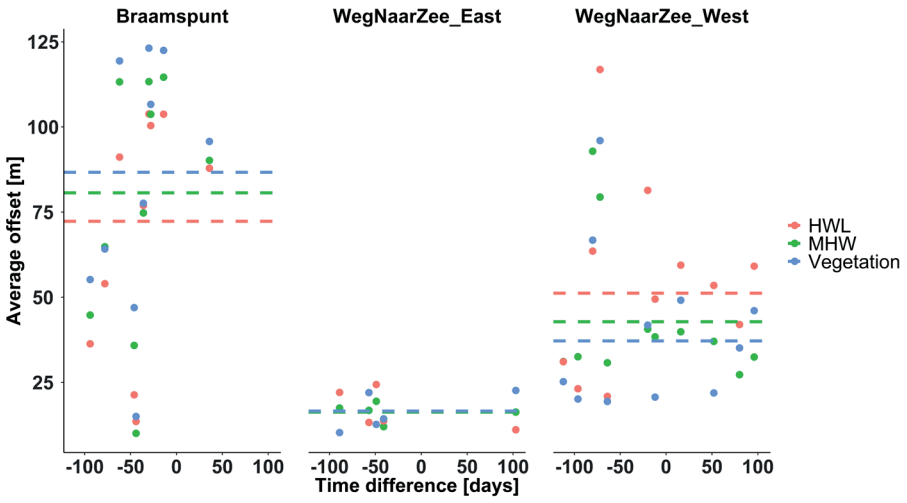

Figure B.5: Average offset between Landsat position estimates and the different coastline proxies from UAV orthophotos. The average offset on the y-axis is linked to the acquisition date of the corresponding Landsat image, defined as the number of days it differs with the acquisition of the UAV image (x-axis). The dots represent mean offsets, computed for each Landsat observation compared to the selected coastline proxy in each UAV image. The dashed lines correspond to the overall mean offset of all position estimates from the used Landsat observations, separated for the different coastline proxies used in this analysis.

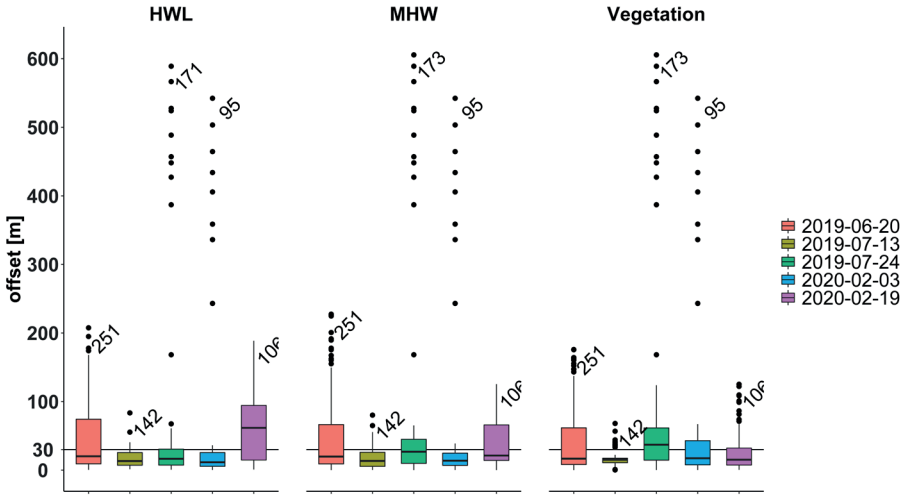

Figure B.6: Variability accuracy for the different coastline proxies defined in the selected UAV orthophotos. Each boxplots contains all Landsat position estimates that are compared to the coastline proxies as defined in the different UAV images. The acquisition over Braamspunt (2019-07-24 and 2020-02-03) contain relative more and larger outliers compared to the acquisition over Weg Naar Zee. Especially the acquisition at Weg naar Zee west (2019-06-20 and 2020-02-19) has a relatively large offset between the coastline position estimates and the different coastline indicators. Thiscan be related to the more complex and heterogeneous coastal morphology.

C. Supplements to Chapter 4

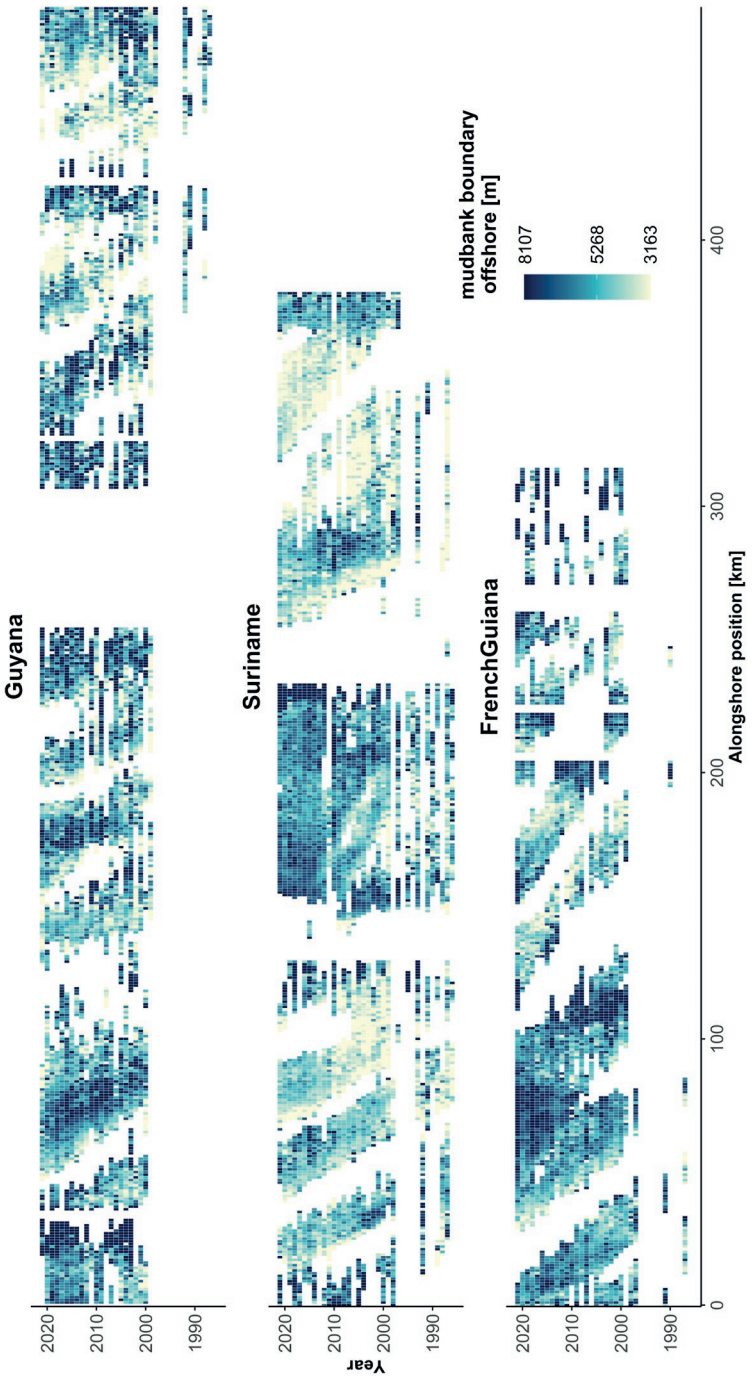

Figure C.1: Spatial and temporal variability in mudbank morphometrics between 1985 and 2021 for French Guiana, Suriname and Guyana. Colors indicate the distance to the offshore mudbank boundary for the individual transects that are linked to the presence of a mudbank. Along the x-axis the alongshore distance is shown from west to east, where each country is shown separately. Alongshore connected pixels represent the length of a mudbank. Observations near river-mouths are excluded from these analysis. Landsat observations, before 1999 are often missing.

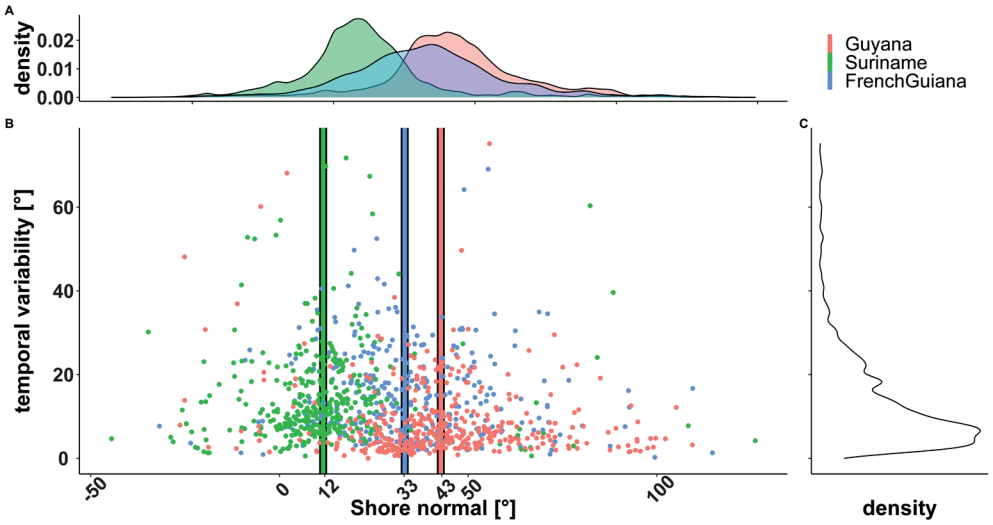

Figure C.2: The spatial variability in mean shore-normal orientation compared to the temporal variation indicated by the standard deviation for each transect (y-axis). The top panel shows the distribution of shore-normal orientation for each country and the side panel the density distribution of standard deviation values found for each separate transect. Higher standard deviations suggest larger spread of shore-normal orientation and thus more temporal variation and occasional outliers in the dataset.

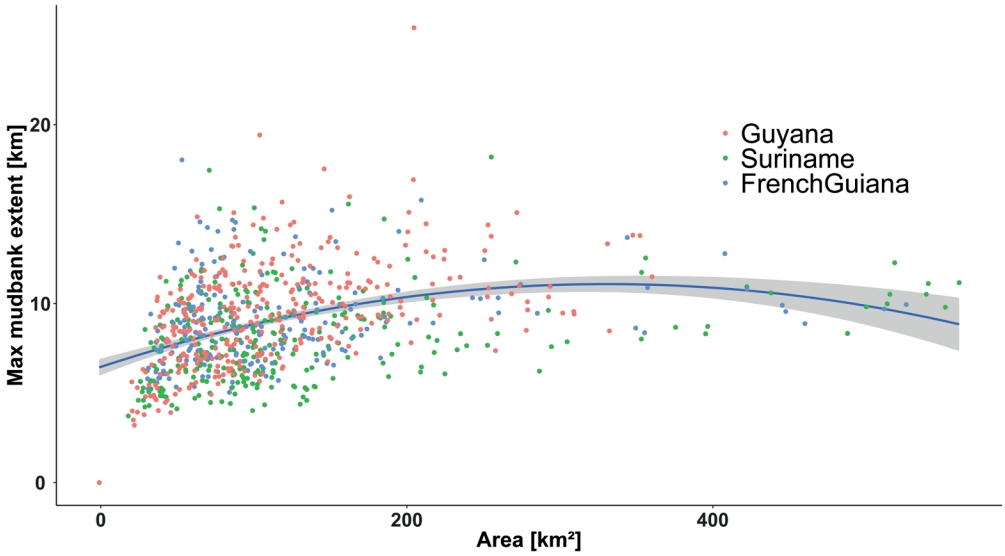

Figure C.3: Range of observed mudbank extents (y-axis) in relation to their total area (x-axis) in French Guiana, Suriname and Guyana (colored dots).

D. Supplements to Chapter 5

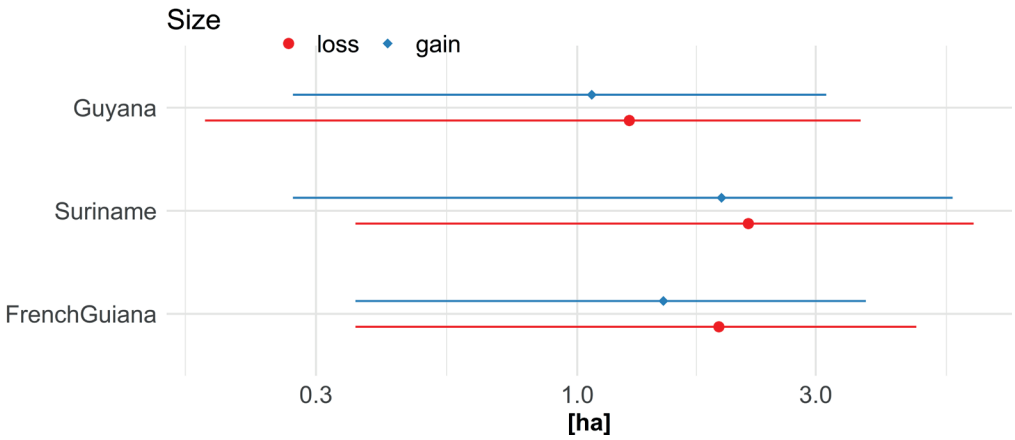

Figure D.1: Mean annual patch size for losses (dot) and gains (diamond) changes. The line indicates the (log-scaled) variability observed along the coastline of individual countries.

Figure D.2: Average frequency of occurrence for losses (dot) and gains (diamond) changes. The line indicates the (log-scaled) variability observed along the coastline of individual countries.

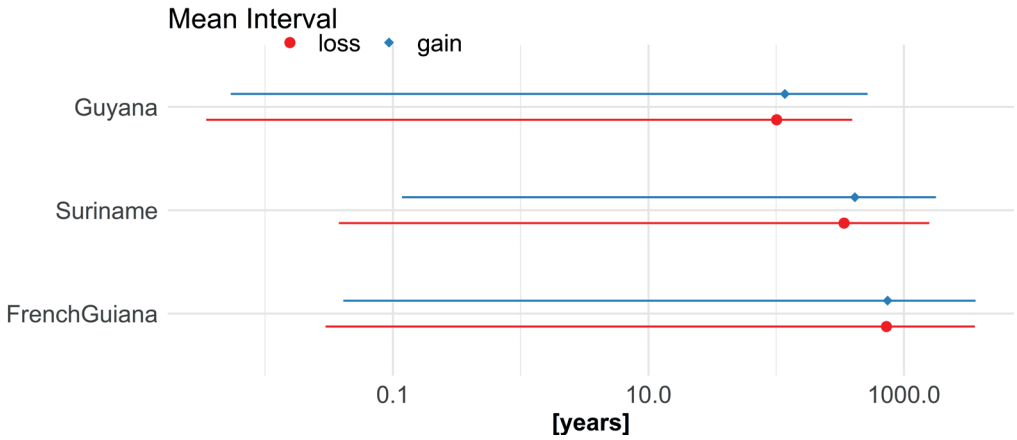

Figure D.3: Average interval of change for losses (dot) and gains (diamond) changes. The line indicates the (log-scaled) variability observed along the coastline of individual countries.

Bibliography

Ahmed, N., & Glaser, M. (2016). Coastal aquaculture, mangrove deforestation and blue carbon emissions: Is REDD+ a solution? *Marine Policy*, 66, 58–66. https://doi.org/10.1016/j.marpol.2016.01.011

Albeke, S. E., Nibbelink, N. P., Mu, L., & Ellsworth, D. J. (2010). Measuring boundary convexity at multiple spatial scales using a linear "moving window" analysis: An application to coastal river otter habitat selection. *Landscape Ecology,* 25(10), 1575–1587. https://doi.org/10.1007/s10980-010-9528-4

Alcântara, E., Barbosa, C., Stech, J., Novo, E., & Shimabukuro, Y. (2009). Improving the spectral unmixing algorithm to map water turbidity distributions. *Environmental Modelling and Software*, 24(9), 1051–1061. https://doi.org/10.1016/j.envsoft.2009.02.013

Allison, M. A., & Lee, M. T. (2004). Sediment exchange between Amazon mudbanks and shore-fringing mangroves in French Guiana. *Marine Geology*, 208(2–4), 169–190. https://doi.org/10.1016/j.margeo.2004.04.026

Allison, M. A., Lee, M. T., Ogston, A. S., & Aller, R. C. (2000). Origin of Amazon mudbanks along the northeastern coast of South America. *Marine Geology*, 163(1–4), 241–256. https://doi.org/10.1016/S0025-3227(99)00120-6

Allison, M. A., Nittrouer, C. A., & Faria, L. E. C. (1995). Rates and mechanisms of shoreface progradation and retreat downdrift of the Amazon river mouth. *Marine Geology*, 125(3–4), 373–392. https://doi.org/10.1016/0025-3227(95)00020-Y

Allison, M. A., Nittrouer, C. A., & Kineke, G. C. C. (1995). Seasonal sediment storage on mudflats adjacent to the Amazon River. *Marine Geology*, 125(3–4), 303–328. https://doi.org/10.1016/0025-3227(95)00017-S

Almonacid-caballer, J., Sánchez-garcía, E., Pardo-pascual, J. E., Balaguer-beser, A. A., & Palomar-vázquez, J. (2016). Evaluation of annual mean shoreline position deduced from Landsat imagery as a mid-term coastal evolution indicator. *Marine Geology*, 372, 79–88. https://doi.org/10.1016/j.margeo.2015.12.015

Alongi, D. M. (2002). Present state and future of the world's mangrove forests. *Environmental Conservation*, 29(3), 331–349. https://doi.org/10.1017/S0376892902000231

Alongi, D. M. (2008). Mangrove forests: resilience, protection from tsunamis, and responses to global climate change. *Estuarine, Coastal and Shelf Science*, 76(1), 1–13. https://doi.org/10.1016/j.ecss.2007.08.024

Alongi, D. M. (2012). Carbon sequestration in mangrove forests. *Carbon Management*, 3(3), 313–322. https://doi.org/10.4155/cmt.12.20

Amatali, M. A. (1993). Climate and surface water hydrology. In *The freshwater ecosystems of Suriname* (Vol. 2). Springer.

Anthony, E. J., & Aagaard, T. (2020). The lower shoreface: Morphodynamics and sediment connectivity with the upper shoreface and beach. *Earth-Science Reviews*, 210(August), 103334. https://doi.org/10.1016/j.earscirev.2020.103334

Anthony, E. J., Brondizio, E. S., Gardel, A., & Besset, M. (2021). Sustainable management, conservation, and restoration of the Amazon river delta and Amazon - influenced Guianas coast: a review. *Water,* 13(1371). https://doi.org/https://doi.org/10.3390/w13101371

Anthony, E. J., Brunier, G., Gardel, A., Hiwat, M., Cooper, A., & Fitzgerald, D. (2019). Chenier morphodynamics on the Amazon-influenced coast of Suriname, South America: Implications for beach ecosystem services. *Frontiers in Earth Science*, 7(March), 1–20. https://doi.org/10.3389/feart.2019.00035

Anthony, E. J., & Dolique, F. (2004). The influence of Amazon-derived mud banks on the morphology of sandy headland-bound beaches in Cayenne, French Guiana: A short- to long-term perspective. *Marine Geology*, 208(2–4), 249–264. https://doi.org/10.1016/j.margeo.2004.04.011

Anthony, E. J., Dolique, F., Gardel, A., Gratiot, N., Proisy, C., & Polidori, L. (2008). Nearshore intertidal topography and topographic-forcing mechanisms of an Amazon-derived mud bank in French Guiana. *Continental Shelf Research*, 28(6), 813–822. https://doi.org/10.1016/j.csr.2008.01.003

Anthony, E. J., Gardel, A., Dolique, F., & Guiral, D. (2002). Short-term changes in the plan shape of a sandy beach in response to sheltering by a nearshore mud bank, Cayenne, French Guiana. *Earth Surface Processes and Landforms*, 27(8), 857–866. https://doi.org/10.1002/esp.357

Anthony, E. J., Gardel, A., & Gratiot, N. (2013). Fluvial sediment supply, mud banks, cheniers and the morphodynamics of the coast of South America between the Amazon and Orinoco river mouths. *Geological Society, London*, Special Publications, 388(1), 533–560. https://doi.org/10.1144/sp388.8

Anthony, E. J., Gardel, A., Gratiot, N., Proisy, C., Allison, M. A., Dolique, F., & Fromard, F. (2010). The Amazon-influenced muddy coast of South America: A review of mud-bank-shoreline interactions. *Earth-Science Reviews*, 103(3–4), 99–121. https://doi.org/10.1016/j.earscirev.2010.09.008

Anthony, E. J., Gardel, A., Proisy, C., Fromard, F., Gensac, E., Peron, C., Walcker, R., & Lesourd, S. (2013). The role of fluvial sediment supply and river-mouth hydrology in the dynamics of the muddy, Amazon-dominated Amapá-Guianas coast, South America: A three-point research agenda. *Journal of South American Earth Sciences*, 44, 18–24. https://doi.org/10.1016/j.jsames.2012.06.005

Anthony, E. J., & Gratiot, N. (2012). *Coastal Engineering* and large-scale mangrove destruction in Guyana, South America: Averting an environmental catastrophe in the making. *Ecological Engineering*, 47, 268–273. https://doi.org/10.1016/j.ecoleng.2012.07.005

Ashton, A. D., Brad Murray, A., & Arnault, O. (2001). Formation of coastline features by large-scale instabilities induced by high-angle waves. *Nature*, 414(November), 1–6.

Ashton, A. D., & Murray, A. B. (2006). High-angle wave instability and emergent shoreline shapes: 2. Wave climate analysis and comparisons to nature. *Journal of Geophysical Research: Earth Surface*, 111(4), 1–17. https://doi.org/10.1029/2005JF000423

Asokan, A., & Anitha, J. (2020). Adaptive Cuckoo Search based optimal bilateral filtering for denoising of satellite images. *ISA Transaction*s, 100, 308–321. https://doi.org/10.1016/j.isatra.2019.11.008

Augustinus, P. G. E. F. (1978). The changing shoreline of Suriname (South America). University Utrecht.

Augustinus, P. G. E. F. (1980). Actual development of the chenier coast of Suriname (South America). *Sedimentary Geology*, 26(1–3), 91–113. https://doi.org/10.1016/0037-0738(80)90007-X

Augustinus, P. G. E. F. (1989). Cheniers and chenier plains: A general introduction. *Marine Geology*, 90(4), 219–229. https://doi.org/10.1016/0025-3227(89)90126-6

Augustinus, P. G. E. F. (2004). The influence of the trade winds on the coastal development of the Guianas at various scale levels: A synthesis. *Marine Geology*, 208(2–4), 145–151. https://doi.org/10.1016/j.margeo.2004.04.007

Augustinus, P. G. E. F., Hazelhoff, L., & Kroon, A. (1989). The chenier coast of Suriname: Modern and geological development. *Marine Geology*, 90(4), 269–281. https://doi.org/10.1016/0025-3227(89)90129-1

Baghdadi, N., Gratiot, N., Lefebvre, J.-P., Oliveros, C., & Bourguignon, A. (2004). Coastline and mudbank monitoring in French Guiana: Contributions of radar and optical satellite imagery. *Canadian Journal of Remote Sensing,* 30(2), 109–122. https://doi.org/10.5589/m03-059

Baghdadi, N., & Oliveros, C. (2007). Potential of ASAR/Envisat data for mud bank monitoring in French Guiana compared to ASTER imagery. *Journal of Coastal Research*, 236, 1509–1517. https://doi.org/10.2112/05-0477.1

Balke, T., Bouma, T. J., Horstman, E. M., Webb, E. L., Erftemeijer, P. L. A., & Herman, P. M. J. (2011). Windows of opportunity: Thresholds to mangrove seedling establishment on tidal flats. *Marine Ecology Progress Series*, 440, 1–9. https://doi.org/10.3354/meps09364

Balke, T., Swales, A., Lovelock, C. E., Herman, P. M. J., & Bouma, T. J. (2015). Limits to seaward expansion of mangroves: Translating physical disturbance mechanisms into seedling survival gradients. *Journal of Experimental Marine Biology and Ecology,* 467, 16–25. https://doi.org/10.1016/j.jembe.2015.02.015

Balke, T., Webb, E. L., van den Elzen, E., Galli, D., Herman, P. M. J., & Bouma, T. J. (2013). Seedling establishment in a dynamic sedimentary environment: A conceptual framework using mangroves. *Journal of Applied Ecology,* 50(3), 740–747. https://doi.org/10.1111/1365-2664.12067

Baltzer, F., Allison, M. A., & Fromard, F. (2004). Material exchange between the continental shelf and mangrove-fringed coasts with special reference to the Amazon-Guianas coast. *Marine Geology*, 208(2–4), 115–126. https://doi.org/10.1016/j.margeo.2004.04.024

Barbier, E. B. (2015). Climate change impacts on rural poverty in low-elevation coastal zones. *Estuarine, Coastal and Shelf Science*, 165, A1–A13. https://doi.org/10.1016/j.ecss.2015.05.035

Barbier, E. B. (2016). The protective service of mangrove ecosystems: A review of valuation methods. *Marine Pollution Bulletin*, 109(2), 676–681. https://doi.org/10.1016/j.marpolbul.2016.01.033

Barbier, E. B., Hacker, S. D., Kennedy, C., Koch, E. W., Stier, a. C., & Silliman, B. R. (2011). The value of estuarine and coastal ecosystem services. *Ecological Monographs*, 81(2), 169–193. https://doi.org/10.1890/10-1510.1

Barbier, E. B., Koch, E. W., Silliman, B. R., Hacker, S. D., Wolanski, E., Primavera, J., Granek, E. F., Polasky, S., Aswani, S., Cramer, L. A., Stoms, D. M., Kennedy, C. J., Bael, D., Kappel, C. V, Perillo, G. M. E., & Reed, D. J. (2008). Coastal Ecosystem – Based Management with Nonlinear Ecological Functions and Values. *Science*, 319(5861), 321–324.

Berrenstein, H. J. (2010). Coastal changes along the Suriname coast with emphasis on the changing coastline of Coronie from 1914 to 2007 and its influence on Avicennia germinans L. (Avicenniaceae). *Academic Journal of Suriname*, 1, 86–95.

Best, Ü. S. N., van der Wegen, M., Dijkstra, J., Reyns, J., van Prooijen, B. C., & Roelvink, D. (2022). Wave attenuation potential, sediment properties and mangrove growth dynamics data over Guyana's intertidal mudflats: Assessing the potential of mangrove restoration works. *Earth System Science Data Discussions*, 14, 1–24.

Bhargava, R., Sarkar, D., & Friess, D. A. (2021). A cloud computing-based approach to mapping mangrove erosion and progradation: Case studies from the Sundarbans and French Guiana. *Estuarine, Coastal and Shelf Science*, 248(December 2019), 106798. https://doi.org/10.1016/j.ecss.2020.106798

Birch, C. P. D., Oom, S. P., & Beecham, J. A. (2007). Rectangular and hexagonal grids used for observation, experiment and simulation in ecology. *Ecological Modelling*, 206(3–4), 347–359. https://doi.org/10.1016/j.ecolmodel.2007.03.041

Bishop-taylor, R., Sagar, S., Lymburner, L., Alam, I., & Sixsmith, J. (2019). Sub-pixel waterline extraction: Characterising accuracy and sensitivity to indices and spectra. *Remote Sensing,* 11(24), 2984. https://doi.org/10.3390/rs11242984

Bitencourt, V. J. B., Dillenburg, S. R., Manzolli, R. P., & Barboza, E. G. (2020). Control factors in the evolution of Holocene coastal barriers in Southern Brazil. *Geomorphology,* 360, 107180. https://doi.org/10.1016/j.geomorph.2020.107180

Boak, E. H., & Turner, I. L. (2005). Shoreline definition and detection: A review. *Journal of Coastal Research*, 21(4), 688–703. https://doi.org/10.2112/03-0071.1

Bolam, S. G., & Rees, H. L. (2003). Minimizing impacts of maintenance dredged material disposal in the coastal environment: A habitat approach. *Environmental Management,* 32(2), 171–188. https://doi.org/10.1007/s00267-003-2998-2

Brad Murray, A., & Ashton, A. D. (2013). Self-organization of large-scale coastline shapes. *Philos. Transcation R. Soc. A,* 371(2004).

Breithaupt, J. L., Smoak, J. M., Smith, T. J., Sanders, C. J., & Hoare, A. (2012). Organic carbon burial rates in mangrove sediments: Strengthening the global budget. *Global Biogeochemical Cycles*, 26(3), 1–11. https://doi.org/10.1029/2012GB004375

Brown, S., Nicholls, R. J., Hanson, S., Brundrit, G., Dearing, J. A., Dickson, M. E., Gallop, S. L., Gao, S., Haigh, I. D., Hinkel, J., Jiménez, J. A., Klein, R. J. T., Kron, W., Lázár, A. N., Neves, C. F., Newton, A., Pattiaratachi, C., Payo, A., Pye, K., … Woodroffe, C. D. (2014). Shifting perspectives on coastal impacts and adaptation. *Nature Climate Change*, 4(9), 752–755. https://doi.org/10.1038/nclimate2344

Brunier, G., Anthony, E. J., Gratiot, N., & Gardel, A. (2019). Exceptional rates and mechanisms of muddy shoreline retreat following mangrove removal. *Earth Surface Processes and Landforms*, 44(8), 1559–1571. https://doi.org/10.1002/esp.4593

Brunier, G., Fleury, J., Anthony, E. J., Gardel, A., & Dussouillez, P. (2016). Close-range airborne structure-from-motion photogrammetry for high-resolution beach morphometric surveys: Examples from an embayed rotating beach. *Geomorphology,* 261. https://doi.org/10.1016/j.geomorph.2016.02.025

Bryan-Brown, D. N., Connolly, R. M., Richards, D. R., Adame, F., Friess, D. A., & Brown, C. J. (2020). Global trends in mangrove forest fragmentation. *Scientific Reports*, 10(1), 1–8. https://doi.org/10.1038/s41598-020-63880-1

Bryan, K. R., Nardin, W., Mullarney, J. C., & Fagherazzi, S. (2017). The role of cross-shore tidal dynamics in controlling intertidal sediment exchange in mangroves in Cù Lao Dung, Vietnam. *Continental Shelf Research*, 147, 128–143. https://doi.org/10.1016/j.csr.2017.06.014

Bullock, E. L., Fagherazzi, S., Nardin, W., Vo-Luong, P., Nguyen, P., & Woodcock, C. E. (2017). Temporal patterns in species zonation in a mangrove forest in the Mekong Delta, Vietnam, using a time series of Landsat imagery. *Continental Shelf Research*, 147(September 2016), 144–154. https://doi.org/10.1016/j.csr.2017.07.007

Cahoon, D. R., Hensel, P. F., Spencer, T., Reed, D. J., Mckee, K. L., & Saintilan, N. (2006). Coastal wetland vulnerability to relative sea-level rise: Wetland elevation trends and process controls. In *Wetlands and natural resource management* (Vol. 190, pp. 271–292). Springer. https://doi.org/10.1007/978-3-540-33187-2_12

Cai, W., McPhaden, M. J., Grimm, A. M., Rodrigues, R. R., Taschetto, A. S., Garreaud, R. D., Dewitte, B., Poveda, G., Ham, Y. G., Santoso, A., Ng, B., Anderson, W., Wang, G., Geng, T., Jo, H. S., Marengo, J. A., Alves, L. M., Osman, M., Li, S., … Vera, C. (2020). Climate impacts of the El Niño–Southern Oscillation on South America. *Nature Reviews Earth and Environment*, 1(4), 215–231. https://doi.org/10.1038/s43017-020-0040-3

Carbonneau, P. E., & Dietrich, J. T. (2017). Cost-effective non-metric photogrammetry from consumer-grade sUAS: implications for direct georeferencing of structure from motion photogrammetry. *Earth Surface Processes and Landforms*, 42(3), 473–486. https://doi.org/10.1002/esp.4012

Castelle, B., Masselink, G., Scott, T., Stokes, C., Konstantinou, A., Marieu, V., & Bujan, S. (2021). Satellite-derived shoreline detection at a high-energy meso-macrotidal beach. *Geomorphology,* 383, 107707. https://doi.org/10.1016/j.geomorph.2021.107707

Castelle, B., Ritz, A., Marieu, V., Lerma, A. N., & Vandenhove, M. (2022). Primary drivers of multidecadal spatial and temporal patterns of shoreline change derived from optical satellite imagery. *Geomorphology,* 413(July), 108360. https://doi.org/10.1016/j.geomorph.2022.108360

Cazenave, A., Meyssignac, B., Ablain, M., Balmaseda, M., Bamber, J., Barletta, V., Beckley, B., Benveniste, J., Berthier, E., Blazquez, A., Boyer, T., Caceres, D., Chambers, D., Champollion, N., Chao, B., Chen, J., Cheng, L., Church, J. A., Chuter, S., … Wouters, B. (2018). Global sea-level budget 1993-present. *Earth System Science Data,* 10(3), 1551–1590. https://doi.org/10.5194/essd-10-1551-2018

Chevalier, C., Baklouti, M., & Ramamonjiarisoa, A. (2004). Modeling the Influence of Wind and Rivers on Current, Salinity and Temperature over the French Guiana Continental Shelf during the Rainy Season. *Journal of Coastal Research*, 204, 1183–1197.

Chevalier, C., Froidefond, J. M. M., Devenon, J.-L., Le Chevalier, C., Froidefond, J. M. M., Devenon, J.-L., Chevalier, C., Froidefond, J. M. M., & Devenon, J.-L. (2008). Numerical analysis of the combined action of littoral current, tide and waves on the suspended mud transport and on turbid plumes around French Guiana mudbanks. *Continental Shelf Research*, 28, 545–560. https://doi.org/10.1016/j.csr.2007.09.011

Church, J. A., White, N. J., Coleman, R., Lambeck, K., & Mitrovica, J. X. (2004). Estimates of the regional distribution of sea level rise over the 1950-2000 period. *Journal of Climate*, 17(13), 2609–2625. https://doi.org/10.1175/1520-0442(2004)017<2609:EOTRDO>2.0.CO;2

Cipolletti, M. P., Delrieux, C. A., Perillo, G. M. E., & Cintia Piccolo, M. (2012). Superresolution border segmentation and measurement in remote sensing images. *Computers and Geosciences*, 40, 87–96. https://doi.org/10.1016/j.cageo.2011.07.015

Cohen, J. E., & Small, C. (1998). Hypsographic demography: The distribution of human population by altitude. *Proceedings of the National Academy of Sciences of the United States of America,* 95(24), 14009–14014. https://doi.org/10.1073/pnas.95.24.14009

Cohen, J. E., Small, C., Mellinger, A., Gallup, J., & Sachs, J. (1997). Estimates of coastal populations. *Science*, 278(5341), 1209–1213.

Cowell, P. J., Stive, M. J. F., Niedoroda, A. W., De Vriend, H. J., Swift, D. J. P., Kaminsky, G. M., & Capobianco, M. (2003). The coastal-tract (part 1): A conceptual approach to aggregated modeling of low-order coastal change. *Journal of Coastal Research*, 19(4), 812–827.

Crase, B., Liedloff, A., Vesk, P. A., Burgman, M. A., & Wintle, B. A. (2013). Hydroperiod is the main driver of the spatial pattern of dominance in mangrove communities. *Global Ecology and Biogeography*, 22(7), 806–817. https://doi.org/10.1111/geb.12063

Dachs, J., & Méjanelle, L. (2010). Organic pollutants in coastal waters, sediments, and biota: A relevant driver for ecosystems during the anthropocene? *Estuaries and Coasts*, 33(1), 1–14. https://doi.org/10.1007/s12237-009-9255-8

Dahdouh-guebas, F., Koedam, N., Satyanarayana, B., & Cannicci, S. (2011). Human hydrographical changes interact with propagule predation behaviour in Sri Lankan mangrove forests. *Journal of Experimental Marine Biology and Ecology,* 399(2), 188–200. https://doi.org/10.1016/j.jembe.2010.11.012

de Jong, S. M., Shen, Y., de Vries, J., Bijnaar, G., van Maanen, B., Augustinus, P. G. E. F., Verweij, P., Jong, S. M. De, Shen, Y., Vries, J. De, Bijnaar, G., Maanen, B. Van, Augustinus, P. G. E. F., & Verweij, P. (2021). Mapping mangrove dynamics and colonization patterns at the Suriname coast using historic satellite data and the LandTrendr algorithm. *International Journal of Applied Earth Observation and Geoinformation*, 97(November 2020), 102293. https://doi.org/10.1016/j.jag.2020.102293

Diniz, C., Cortinhas, L., Nerino, G., Rodrigues, J., Sadeck, L., Adami, M., & Souza-Filho, P. W. M. (2019). Brazilian mangrove status: Three decades of satellite data analysis. *Remote Sensing,* 11(7). https://doi.org/10.3390/rs11070808

Dolan, R., Fenster, M. S., & Holme, S. J. (1991). Temporal analysis of shoreline recession and accretion. *Journal of Coastal Research*, 7(3), 723–744.

Donchyts, G., Baart, F., Winsemius, H. C., Gorelick, N., Kwadijk, J., van de Giesen, N., Giesen, N. Van De, & van de Giesen, N. (2016). Earth's surface water change over the past 30 years. *Nature Climate Change*, 6(9), 810–813. https://doi.org/10.1038/nclimate3111

Donchyts, G., Schellekens, J., Winsemius, H. C., & Eisemann, E. (2016). A 30 m resolution surface water mask including estimation of positional and thematic differences using Landsat 8 , SRTM and OpenStreetMap: A case study in the Murray-Darling Basin, Australia. *Remote Sensing,* 8(5). https://doi.org/10.3390/rs8050386

Douglas, B. C., & Peltier, W. R. (2002). The puzzle of global sea-level rise. *Physics Today,* 55(3), 35–40. https://doi.org/10.1063/1.1472392

Dubayah, R., Blair, J. B., Goetz, S., Fatoyinbo, L., Hansen, M., Healey, S., Hofton, M., Hurtt, G., Kellner, J., Luthcke, S., Armston, J., Tang, H., Duncanson, L., Hancock, S., Jantz, P., Marselis, S., Patterson, P. L., Qi, W., & Silva, C. (2020). The global ecosystem dynamics investigation: High-resolution laser ranging of the Earth's forests and topography. Science of *Remote Sensing,* 1(January), 100002. https://doi.org/10.1016/j.srs.2020.100002

Duke, N. C., Ball, M. C., & Ellison, J. C. (1998). Factors influencing biodiversity and distributional gradients in mangroves. *Global Ecology and Biogeography* Letters, 7(1), 27–47. https://doi.org/10.2307/2997695

Duke, N. C., Meynecke, J. O., Dittmann, S., Ellison, A. M., Anger, K., Berger, U., Cannicci, S., Diele, K., Ewel, K. C., Field, C. D., N. Koedam, S. Y., Lee, C. M., Nordhaus, I., & Dahdouh-Guebas, F. (2007). A World without mangroves? *Science*, 317(5834), 47–55.

Eisma, D., Augustinus, P. G. E. F., Alexander, C., & D. Eisma; P.G.E.F. Augustinus; C. Alexander. (1991). Recent and subrecent changes in the dispersal of Amazon mud. *Netherlands Journal of Sea Research*, 28(3), 181–192.

Eisma, D., & Marel, H. W. van der M. (1971). Marine muds along the Guyana coast and their origin from the Amazon basin. Contribtions Mineral and Petrol, 31, 321–334.

Ellison, A. M., Mukherjee, B. B., & Karim, A. (2000). Testing patterns of zonation in mangroves: Scale dependence and environmental correlates in the Sundarbans of Bangladesh. *Journal of Ecology,* 88(5), 813–824. https://doi.org/10.1046/j.1365-2745.2000.00500.x

Ellison, J. C. (2008). Long-term retrospection on mangrove development using sediment cores and pollen analysis: A review. *Aquatic Botany*, 89(2), 93–104. https://doi.org/10.1016/j.aquabot.2008.02.007

Ellison, J. C. (2015). Vulnerability assessment of mangroves to climate change and sea-level rise impacts. Wetlands *Ecology and Management*, 23(2), 115–137. https://doi.org/10.1007/s11273-014-9397-8

Ericson, J. P., Vörösmarty, C. J., Dingman, S. L., Ward, L. G., & Meybeck, M. (2006). Effective sea-level rise and deltas: Causes of change and human dimension implications. *Global and Planetary Change*, 50(1–2), 63–82. https://doi.org/10.1016/j.gloplacha.2005.07.004

Fabre, A., Fromard, F., & Trichon, V. (1999). Fractionation of phosphate in sediments of four representative mangrove stages (French Guiana). *Hydrobiologia*, 392, 13–19. https://link-springer-com.proxy.library.uu.nl/content/pdf/10.1023%2FA%3A1003553307731.pdf

Fagherazzi, S., Bryan, K. R., & Nardin, W. (2017). Buried alive or washed away. Oceanography, 30(3), 48–59. https://doi.org/10.5670/oceanog.2017.313

Ferguson, G., & Gleeson, T. (2012). Vulnerability of coastal aquifers to groundwater use and climate change. *Nature Climate Change*, 2(5), 342–345. https://doi.org/10.1038/nclimate1413

Flood, N. (2013). Seasonal composite landsat TM/ETM+ Images using the medoid (a multi-dimensional median). *Remote Sensing,* 5(12), 6481–6500. https://doi.org/10.3390/rs5126481

Friedl, M., & Sulla-Menashe, D. (2015). MCD12Q1 MODIS/Terra+Aqua Land Cover Type Yearly L3 Global 500m SIN Grid V006. *NASA EOSDIS Land Processes DAAC.* https://doi.org/https://doi.org/10.5067/MODIS/MCD12Q1.006

Friess, D. A., Krauss, K. W., Horstman, E. M., Balke, T., Bouma, T. J., Galli, D., & Webb, E. L. (2012). Are all intertidal wetlands naturally created equal? Bottlenecks, thresholds and knowledge gaps to mangrove and saltmarsh ecosystems. *Biological Reviews*, 87(2), 346–366. https://doi.org/10.1111/j.1469-185X.2011.00198.x

Friess, D. A., Rogers, K., Lovelock, C. E., Krauss, K. W., Hamilton, S. E., Lee, S. Y., Lucas, R., Primavera, J., Rajkaran, A., & Shi, S. (2019). The state of the world's mangrove forests: Past, present, and future. *Annual Review of Environment and Resources,* 44, 89–115. https://doi.org/10.1146/annurev-environ-101718-033302

Froidefond, J. M., Gardel, L., Guiral, D., Parra, M., & Ternon, J.-F. J. f. J.-F. (2002). Spectral remote sensing reflectances of coastal waters in French Guiana under the Amazon influence. *Remote Sensing of Environment*, 80(2), 225–232. www.elsevier.com/locate/rse

Froidefond, J. M., Lahet, F., Hu, C., Doxaran, D., Guiral, D., Prost, M. . T., & Ternon, J.-F. F. (2004). Mudflats and mud suspension observed from satellite data in French Guiana. *Marine Geology*, 208(2–4), 153–168. https://doi.org/10.1016/j.margeo.2004.04.025

Froidefond, J. M., Pujos, M., & Andre, X. (1988). Migration of mud banks and changing coastline in French Guiana. *Marine Geology*, 84(1–2), 19–30. https://doi.org/10.1016/0025-3227(88)90122-3

Fromard, F., Puig, H., Mougin, E., Marty, G., Betoulle, J. L., & Cadamuro, L. (1998). Structure, above-ground biomass and dynamics of mangrove ecosystems: New data from French Guiana. *Oecologia*, 115(1–2), 39–53. https://doi.org/10.1007/s004420050489

Fromard, F., Vega, C., & Proisy, C. (2004). Half a century of dynamic coastal change affecting mangrove shorelines of French Guiana. A case study based on remote sensing data analyses and field surveys. *Marine Geology*, 208(2–4), 265–280. https://doi.org/10.1016/j.margeo.2004.04.018

Furukawa, K., & Wolanski, E. (1996). Sedimentation in mangrove forests. In *Mangroves and Salt Marshes* (Vol. 1, Issue 1, pp. 3–10). https://doi.org/10.1023/A:1025973426404

Furukawa, K., Wolanski, E., & Mueller, H. (1997). Currents and sediment transport in mangrove forests. *Estuarine, Coastal and Shelf Science*, 44(3), 301–310. https://doi.org/10.1006/ecss.1996.0120

Gardel, A., Anthony, E. J., Santos, V. F., Huybrechts, N., Lesourd, S., Sottolichio, A., & Maury, T. (2022). A remote sensing - based classification approach for river mouths of the Amazon - influenced Guianas coast. *Regional Environmental Change*, 22(65), 1–12. https://doi.org/10.1007/s10113-022-01913-3

Gardel, A., Gensac, E., Anthony, E. J., Lesourd, S., Loisel, H., & Marin, D. (2011). Wave-formed mud bars: Their morphodynamics and role in opportunistic mangrove colonization. *Journal of Coastal Research*, 64, 384–387.

Gardel, A., & Gratiot, N. (2005). A satellite image–based method for estimating rates of mud bank migration, French Guiana, South America. *Journal of Coastal Research*, 214, 720–728. https://doi.org/10.2112/03-0100.1

Gardel, A., & Gratiot, N. (2006). Monitoring of coastal dynamics in French Guiana from 16 years of SPOT satellite images. *Journal of Coastal Research*, 3(39), 1502–1505.

Gardel, A., Proisy, C., Lesourd, S., Philippe, S., Caillaud, J., Gontharet, S., Brutier, L., Lesourdf, S., Philippef, S., Gontharetf, S., Anthony, E. J., Proisy, Lesourd, S., Philippe, S., Caillaud, J., Gontharet, S., Anthony, E. J., & Brutier, L. (2009). A better understanding of mud cracking processes gained from in situ measurements on an intertidal mudflat in French Guiana. *Journal of Coastal Research*, 2009(56), 424–428.

Gebhardt, S., Nguyen, L. D., & Kuenzer, C. (2012). Mangrove ecosystems in the Mekong Delta – Overcoming uncertainties in inventory mapping using satellite remote sensing data. *The Mekong Delta System: Interdisciplinary Analyses of a River Delta* 315–330. https://doi.org/10.1007/978-94-007-3962-8_12

Geleynse, N., Voller, V. R., Paola, C., & Ganti, V. (2012). Characterization of river delta shorelines. *Geophysical Research Letters*, 39(17), 2–7. https://doi.org/10.1029/2012GL052845

Gensac, E., Lesourd, S., Gardel, A., Anthony, E. J., Proisy, C., & Loisel, H. (2011). Short-term prediction of the evolution of mangrove surface areas: The example of the mud banks of Kourou and Sinnamary, French Guiana. *Journal of Coastal Research*, 64, 388–392.

Gensac, E., Martinez, J.-M. M., Vantrepotte, V., & Anthony, E. J. (2016). Seasonal and inter-annual dynamics of suspended sediment at the mouth of the Amazon river: The role of continental and oceanic forcing, and implications for coastal geomorphology and mud bank formation. *Continental Shelf Research*, 118, 49–62. https://doi.org/10.1016/j.csr.2016.02.009

Gersie, K., Augustinus, P. G. E. F., Balen, R. T. Van, & Mountain, W. (2018). Marine and anthropogenic controls on the estuary of the Suriname River over the past 50 years. 2016, 419–428. https://doi.org/10.1017/njg.2016.18

Gijsman, R., Horstman, E. M., van der Wal, D., Friess, D. A., Swales, A., & Wijnberg, K. M. (2021). Nature-based engineering: A review on reducing coastal flood risk with mangroves. *Frontiers in Marine Science*, 8(July). https://doi.org/10.3389/fmars.2021.702412

Gilman, E. L., Ellison, J., Duke, N. C., & Field, C. (2008). Threats to mangroves from climate change and adaptation options: A review. *Aquatic Botany*, 89(2), 237–250. https://doi.org/10.1016/j.aquabot.2007.12.009

Giri, C., Ochieng, E., Tieszen, L. L., Zhu, Z., Singh, A., Loveland, T., Masek, J., & Duke, N. C. (2011). Status and distribution of mangrove forests of the world using earth observation satellite data. *Global Ecology and Biogeography*, 20(1), 154–159. https://doi.org/10.1111/j.1466-8238.2010.00584.x

Goldberg, L., Lagomasino, D., Thomas, N., & Fatoyinbo, T. (2020). Global declines in human-driven mangrove loss. *Global Change Biology*, March, 1–12. https://doi.org/10.1111/gcb.15275

Gorelick, N., Hancher, M., Dixon, M., Ilyushchenko, S., Thau, D., & Moore, R. (2017). Google Earth Engine: Planetary-scale geospatial analysis for everyone. *Remote Sensing of Environment*, 202, 18–27. https://doi.org/10.1016/j.rse.2017.06.031

Gratiot, N., & Anthony, E. J. (2016). Role of flocculation and settling processes in development of the mangrove-colonized, Amazon-influenced mud-bank coast of South America. *Marine Geology*, 373, 1–10. https://doi.org/10.1016/j.margeo.2015.12.013

Gratiot, N., Anthony, E. J., Gardel, A., Gaucherel, C., Proisy, C., & Wells, J. T. (2008). Significant contribution of the 18.6 year tidal cycle to regional coastal changes. *Nature Geoscience*, 1(3), 1–8. https://doi.org/10.1038/ngeo127

Gratiot, N., Gardel, A., & Anthony, E. J. (2007). Trade-wind waves and mud dynamics on the French Guiana coast, South America: Input from ERA-40 wave data and field investigations. *Marine Geology*, 236(1–2), 15–26. https://doi.org/10.1016/j.margeo.2006.09.013

Green, E. P., Clark, C. D., Mumby, P. J., Edwards, A. J., & Ellis, A. C. (1998). Remote sensing techniques for mangrove mapping. *International Journal of Remote Sensing,* 19(5), 935–956. https://doi.org/10.1080/014311698215801

Green, M. O., & Coco, G. (2014). Review of wave driven sediment resuspension and transport in estuaries. *Reviews of Geophysics,* 52(1), 77–117. https://doi.org/10.1002/2013RG000437.Received

Grömping, U. (2006). Relative importance for linear regression in R: The package relaimpo. *Journal of Statistical Software*, 17(1), 1–27. https://doi.org/10.18637/jss.v017.i01

Guzman, A., Castano-Isaza, J., Ferguson, S., Bovolo, I., Lawless, M., Eliot, M., Dale, A., & Sabatini, J. (2017). Coastal Resilience Assessment. http://documents.worldbank.org/curated/en/684611538551863364/pdf/Suriname-Coastal-Resilience-Assessment-Feb-9-Low-Res.pdf

Hancock, S., Armston, J., Hofton, M., Sun, X., Tang, H., Duncanson, L. I., Kellner, J. R., & Dubayah, R. (2019). The GEDI simulator: A large-footprint waveform lidar simulator for calibration and validation of spaceborne missions. *Earth and Space Science*, 6(2), 294–310. https://doi.org/10.1029/2018EA000506

Herbeck, L. S., Krumme, U., Andersen, T. J., & Jennerjahn, T. C. (2020). Decadal trends in mangrove and pond aquaculture cover on Hainan (China) since 1966: Mangrove loss, fragmentation and associated biogeochemical changes. *Estuarine, Coastal and Shelf Science*, 233(December 2019). https://doi.org/10.1016/j.ecss.2019.106531

Hermosilla, T., Wulder, M. A., White, J. C., Coops, N. C., & Hobart, G. W. (2015). Regional detection, characterization, and attribution of annual forest change from 1984 to 2012 using Landsat-derived time-series metrics. *Remote Sensing of Environment*, 170, 121–132. https://doi.org/10.1016/j.rse.2015.09.004

Hesselbarth, M. H. K., Sciaini, M., With, K. A., Wiegand, K., & Nowosad, J. (2019). landscapemetrics: An open-source R tool to calculate landscape metrics. *Ecography*, 42(10), 1648–1657. https://doi.org/10.1111/ecog.04617

Heumann, B. W. (2011). Satellite remote sensing of mangrove forests: Recent advances and future opportunities. *Progress in Physical Geography*, 35(1), 87–108. https://doi.org/10.1177/0309133310385371

Hislop, S., Haywood, A., Jones, S., Soto-berelov, M., Skidmore, A., & Nguyen, T. H. (2020). A satellite data driven approach to monitoring and reporting fire disturbance and recovery across boreal and temperate forests. *Int J Appl Earth Obs Geoinformation*, 87(October 2019), 102034. https://doi.org/10.1016/j.jag.2019.102034

Horstman, E. M., Dohmen-Janssen, C. M., Bouma, T. J., & Hulscher, S. J. M. H. M. H. (2015). Tidal-scale flow routing and sedimentation in mangrove forests: Combining field data and numerical modelling. *Geomorphology,* 228, 244–262. https://doi.org/10.1016/j.geomorph.2014.08.011

Horstman, E. M., Dohmen-Janssen, C. M., Narra, P. M. F., van den Berg, N. J. F., Siemerink, M., & Hulscher, S. J. M. H. (2014). Wave attenuation in mangroves: A quantitative approach to field observations. *Coastal Engineering*, 94, 47–62. https://doi.org/10.1016/j.coastaleng.2014.08.005

Housman, I. W., Chastain, R. A., & Finco, M. V. (2018). An evaluation of forest health insect and disease survey data and satellite-based remote sensing forest change detection methods: Case studies in the United States. *Remote Sensing,* 10(8). https://doi.org/10.3390/rs10081184

Hu, Z., van der Wal, D., Cai, H., van Belzen, J., Bouma, T. J., Wal, D. Van Der, Cai, H., Belzen, J. Van, Bouma, T. J., van der Wal, D., Cai, H., van Belzen, J., Bouma, T. J., Wal, D. Van Der, Cai, H., Belzen, J. Van, Bouma, T. J., van der Wal, D., Cai, H., … Bouma, T. J. (2018). Dynamic equilibrium behaviour observed on two contrasting tidal flats from daily monitoring of bed-level changes. *Geomorphology,* 311, 114–126. https://doi.org/10.1016/j.geomorph.2018.03.025

Jimenez, J. A. ., Lugo, A. E. ., & Cintron, G. (1985). Tree mortality in mangrove forests. Biotropica, 17(3), 177–185.

Johnstone, J. F., Allen, C. D., Franklin, J. F., Frelich, L. E., Harvey, B. J., Higuera, P. E., Mack, M. C., Meentemeyer, R. K., Metz, M. R., Perry, G. L. W., Schoennagel, T., & Turner, M. G. (2016). Changing disturbance regimes, ecological memory, and forest resilience. *Frontiers in Ecology and the Environment*, 14(7), 369–378. https://doi.org/10.1002/fee.1311

Jones, E. R., Bierkens, M. F. P., Wanders, N., Sutanudjaja, E. H., van Beek, L. P. H., & van Vliet, M. T. H. (2022). Current wastewater treatment targets are insufficient to protect surface water quality. *Communications Earth and Environment*, 3(1), 1–8. https://doi.org/10.1038/s43247-022-00554-y

Jones, E. R., Van Vliet, M. T. H., Qadir, M., & Bierkens, M. F. P. (2021). Country-level and gridded estimates of wastewater production, collection, treatment and reuse. *Earth System Science Data,* 13(2), 237–254. https://doi.org/10.5194/essd-13-237-2021

Kennedy, R. E., Yang, Z., Cohen, W. B., Pfaff, E., Braaten, J., & Nelson, P. (2012). Spatial and temporal patterns of forest disturbance and regrowth within the area of the Northwest Forest Plan. *Remote Sensing of Environment*, 122, 117–133. https://doi.org/10.1016/j.rse.2011.09.024

Kennedy, R. E., Yang, Z., Cohen, W. B., Yang, Z., & Kennedy, R. E. (2010). Detecting trends in forest disturbance and recovery using yearly Landsat time series: 1. LandTrendr - Temporal segmentation algorithms. *Remote Sensing of Environment*, 114(12), 2897–2910. https://doi.org/10.1016/j.rse.2010.07.008

Kennedy, R. E., Yang, Z., Gorelick, N., Braaten, J., Cavalcante, L., Cohen, W. B., & Healey, S. (2018). Implementation of the LandTrendr algorithm on Google Earth Engine. *Remote Sensing,* 10(5), 1–10. https://doi.org/10.3390/rs10050691

Kim, K.-L., Kim, B.-J., Lee, Y.-K., & Ryu, J.-H. (2019). Generation of a large-scale surface sediment classification map using unmanned aerial vehicle (UAV) data: A case study at the Hwang-do tidal flat, Korea. *Remote Sensing,* 11(3), 229. https://doi.org/10.3390/rs11030229

Kirby, R. (2000). Practical implications of tidal flat shape. *Continental Shelf Research*, 20(10–11), 1061–1077. https://doi.org/10.1016/S0278-4343(00)00012-1

Kirwan, M. L., & Megonigal, J. P. (2013a). Human impacts and sea-level rise. *Nature*, 504(53), 3–10. https://doi.org/10.1038/nature12856

Kirwan, M. L., & Megonigal, J. P. (2013b). Tidal wetland stability in the face of human impacts and sea-level rise. *Nature*, 504(7478), 53–60. https://doi.org/10.1038/nature12856

Klemas, V. (2013). Remote sensing of emergent and submerged wetlands: An overview. *International Journal of Remote Sensing,* 34(18), 6286–6320. https://doi.org/10.1080/01431161.2013.800656

Koch, E. W., Barbier, E. B., Silliman, B. R., Reed, D. J., Perillo, G. M. E., Hacker, S. D., Granek, E. F., Primavera, J. H., Muthiga, N., Polasky, S., Halpern, B. S., Kennedy, C. J., Kappel, C. V., & Wolanski, E. (2009). Non-linearity in ecosystem services: Temporal and spatial variability in coastal protection. *Frontiers in Ecology and the Environment*, 7(1), 29–37. https://doi.org/10.1890/080126

Kombiadou, K., Costas, S., Carrasco, A. R., Plomaritis, T. A., Ferreira, Ó., & Matias, A. (2019). Bridging the gap between resilience and geomorphology of complex coastal systems. *Earth-Science Reviews*, 198(March), 102934. https://doi.org/10.1016/j.earscirev.2019.102934

Kominoski, J. S., Gaiser, E. E., Castañeda-Moya, E., Davis, S. E., Dessu, S. B., Julian, P., Lee, D. Y., Marazzi, L., Rivera-Monroy, V. H., Sola, A., Stingl, U., Stumpf, S., Surratt, D., Travieso, R., & Troxler, T. G. (2020).

Disturbance legacies increase and synchronize nutrient concentrations and bacterial productivity in coastal ecosystems. *Ecology,* 101(5), 1–13. https://doi.org/10.1002/ecy.2988

Koohafkan, M. C., & Gibson, S. (2018). Geomorphic trajectory and landform analysis using graph theory: A panel data approach to quantitative geomorphology. *Progress in Physical Geography*, 42(6), 679–696. https://doi.org/10.1177/0309133318783143

Krauss, K. W., Lovelock, C. E., McKee, K. L., López-Hoffman, L., Ewe, S. M. L., & Sousa, W. P. (2008). Environmental drivers in mangrove establishment and early development: A review. *Aquatic Botany*, 89(2), 105–127. https://doi.org/10.1016/j.aquabot.2007.12.014

Krauss, K. W., Mckee, K. L., Lovelock, C. E., Cahoon, D. R., Saintilan, N., Reef, R., & Chen, L. (2014). How mangrove forests adjust to rising sea level. New Phytologist, 202(1), 19–34. https://doi.org/10.1111/nph.12605

Kuenzer, C., Bluemel, A., Gebhardt, S., Quoc, T. V., & Dech, S. (2011). Remote sensing of mangrove ecosystems: A review. In *Remote Sensing* (Vol. 3, Issue 5). https://doi.org/10.3390/rs3050878

Kuenzer, C., Heimhuber, V., Huth, J., & Dech, S. (2019). Remote sensing for the quantification of land surface dynamics in large river delta regions-a review. *Remote Sensing,* 11(17). https://doi.org/10.3390/rs11171985

Kumara, M. P., Jayatissa, L. P., Krauss, K. W., Phillips, D. H., & Huxham, M. (2010). High mangrove density enhances surface accretion, surface elevation change, and tree survival in coastal areas susceptible to sea-level rise. *Oecologia*, 164(2), 545–553. https://doi.org/10.1007/s00442-010-1705-2

Kummu, M., De Moel, H., Salvucci, G., Viviroli, D., Ward, P. J., & Varis, O. (2016). Over the hills and further away from coast: Global geospatial patterns of human and environment over the 20th-21st centuries. *Environmental Research Letters*, 11(3). https://doi.org/10.1088/1748-9326/11/3/034010

Kushnir, Y., Robinson, W. A., Chang, P., & Robertson, A. W. (2006). The physical basis for predicting Atlantic sector seasonal-to-interannual climate variability. *Journal of Climate*, 19(23), 5949–5970. https://doi.org/10.1175/JCLI3943.1

Labat, D., Espinoza, J. C., Ronchail, J., Cochonneau, G., de Oliveira, E., Doudou, J. C., & Guyot, J. L. (2012). Fluctuations in the monthly discharge of Guyana Shield rivers, related to Pacific and Atlantic climate variability. *Hydrological Sciences Journal*, 57(6), 1081–1091. https://doi.org/10.1080/02626667.2012.695074

Laengner, M. L., Siteur, K., & van der Wal, D. (2019). Trends in the seaward extent of saltmarshes across Europe from long-term satellite data. *Remote Sensing,* 11(14), 1–25. https://doi.org/10.3390/rs11141653

Lakhan, V. C., & Pepper, D. A. (1997). Relationship between concavity and convexity of a coast and erosion and accretion patterns. *Journal of Coastal Research*, 13104109(13), 226–232. http://www.jstor.org/stable/4298609%5Cnhttp://www.jstor.org/stable/4298609?seq=1&cid=pdf-reference#references_tab_contents%5Cnhttp://about.jstor.org/terms

Lauzon, R., Murray, A. B., Cheng, S., Liu, J., Ells, K. D., & Lazarus, E. D. (2019). Correlation between shoreline change and planform curvature on wave-dominated, sandy coasts. *Journal of Geophysical Research: Earth Surface*, 124(12), 3090–3106. https://doi.org/10.1029/2019JF005043

Lawley, V., Lewis, M., Clarke, K., & Ostendorf, B. (2016). Site-based and remote sensing methods for monitoring indicators of vegetation condition: An Australian review. *Ecological Indicators,* 60, 1273–1283. https://doi.org/10.1016/j.ecolind.2015.03.021

Lazarus, E. D., & Murray, A. B. (2007). Process signatures in regional patterns of shorelin change on annual to decadal time scales. *Geophysical Research Letters*, 34(19), 1–5. https://doi.org/10.1029/2007GL031047

Lefebvre, J.-P. P., Dolique, F., & Gratiot, N. (2004). Geomorphic evolution of a coastal mudflat under oceanic influences: An example from the dynamic shoreline of French Guiana. *Marine Geology*, 208(2–4), 191–205. https://doi.org/10.1016/j.margeo.2004.04.008

Li, W., & Gong, P. (2016). Continuous monitoring of coastline dynamics in western Florida with a 30-year time series of Landsat imagery. *Remote Sensing of Environment*, 179, 196–209. https://doi.org/10.1016/j.rse.2016.03.031

Lindeman, J. C. (1953). The vegetation of the Coastal Region of Suriname . Results of the scientific expedition to Suriname 1948 — 49. Botanical Series, 1.

Liu, H., & Jezek, K. C. (2004). Automated extraction of coastline from satellite imagery by integrating Canny edge detection and locally adaptive thresholding methods. *International Journal of Remote Sensing,* 25(5), 937–958. https://doi.org/10.1080/0143116031000139890

Losada, I. J., Reguero, B. G., Méndez, F. J., Castanedo, S., Abascal, A. J., & Mínguez, R. (2013). Long-term changes in sea-level components in Latin America and the Caribbean. *Global and Planetary Change*, 104, 34–50. https://doi.org/10.1016/j.gloplacha.2013.02.006

Lotze, H. K., Lenihan, H. S., Bourque, B. J., Bradbury, R. H., Cooke, R. G., Kay, M. C., Kidwell, S. M., Kirby, M. X., Peterson, C. H., Jackson, J. B. C., & Bay, M. (2006). Depletion, degradation, and recovery potential of estuaries and coastal seas. *Science*, 312(June), 1806–1809.

Lu, S., Wu, B., Yan, N., & Wang, H. (2011). Water body mapping method with HJ-1A/B satellite imagery. *International Journal of Applied Earth Observation and Geoinformation*, 13(3), 428–434. https://doi.org/10.1016/j.jag.2010.09.006

Luijendijk, A. P., Hagenaars, G., Ranasinghe, R., Baart, F., Donchyts, G., & Aarninkhof, S. (2018). The state of the world's beaches. *Scientific Reports*, 8(1), 6641. https://doi.org/10.1038/s41598-018-24630-6

Macreadie, P. I., Anton, A., Raven, J. A., Beaumont, N., Connolly, R. M., Friess, D. A., Kelleway, J. J., Kennedy, H., Kuwae, T., Lavery, P. S., Lovelock, C. E., Smale, D. A., Apostolaki, E. T., Atwood, T. B., Baldock, J., Bianchi, T. S., Chmura, G. L., Eyre, B. D., Fourqurean, J. W., … Duarte, C. M. (2019). The future of Blue Carbon science. *Nature Communications*, 10(1), 1–13. https://doi.org/10.1038/s41467-019-11693-w

Maina, J. M., Bosire, J. O., Kairo, J. G., Bandeira, S. O., Mangora, M. M., Macamo, C., Ralison, H., & Majambo, G. (2021). Identifying global and local drivers of change in mangrove cover and the implications for management. *Global Ecology and Biogeography*, 30(10), 2057–2069. https://doi.org/10.1111/geb.13368

Mancini, F., Dubbini, M., Gattelli, M., Stecchi, F., Fabbri, S., & Gabbianelli, G. (2013). Using unmanned aerial vehicles (UAV) for high-resolution reconstruction of topography: The structure from motion approach on coastal environments. *Remote Sensing,* 5(12), 6880–6898. https://doi.org/10.3390/rs5126880

Marchand, C., Baltzer, F., Lallier-Vergès, E., & Albéric, P. (2004). Pore-water chemistry in mangrove sediments: Relationship with species composition and developmental stages (French Guiana). *Marine Geology*, 208(2–4), 361–381. https://doi.org/10.1016/j.margeo.2004.04.015

Masselink, G., & Lazarus, E. D. (2019). Defining coastal resilience. *Water,* 11(12), 1–21. https://doi.org/10.3390/w11122587

Matthews, M. W. (2011). A current review of empirical procedures of remote sensing in Inland and near-coastal transitional waters. *International Journal of Remote Sensing,* 32(21), 6855–6899. https://doi.org/10.1080/01431161.2010.512947

McFeeters, S. K. (1996). The use of the Normalized Difference Water Index (NDWI) in the delineation of open water features. *International Journal of Remote Sensing,* 7(17), 1425–1432. https://doi.org/10.1080/01431169608948714

McKee, K. L. (1995). Seedling recruitment patterns in a Belizean mangrove forest: Effects of establishment. *Oecologia*, 101(4), 448–460.

McKee, K. L., Rogers, K., & Saintilan, N. (2012). Response of Salt Marsh and Mangrove Wetlands to Changes in Atmospheric CO2, Climate, and Sea Level. In *Global Change and the Function and Distribution of Wetlands*. https://doi.org/10.1007/978-94-007-4494-3

McLoughlin, S. M., Wiberg, P. L., Safak, I., & McGlathery, K. J. (2015). Rates and forcing of marsh edge erosion in a shallow coastal bay. *Estuaries and Coasts*, 38(2), 620–638. https://doi.org/10.1007/s12237-014-9841-2

Meijer, L. J. J., van Emmerik, T., van der Ent, R., Schmidt, C., & Lebreton, L. (2021). More than 1000 rivers account for 80% of global riverine plastic emissions into the ocean. *Science Advances*, 7(18), 1–14. https://doi.org/10.1126/sciadv.aaz5803

Melet, A., Meyssignac, B., Almar, R., & Le Cozannet, G. (2018). Under-estimated wave contribution to coastal sea-level rise. *Nature Climate Change*, 8(3), 234–239. https://doi.org/10.1038/s41558-018-0088-y

Millard, S. P. (2014). EnvStats, an R Package for Environmental Statistics. In *Encyclopedia of Environmetrics*. Springer. https://doi.org/10.1002/9780470057339.vae043.pub2

Milne, G. A., Long, A. J., & Bassett, S. E. (2005). Modelling Holocene relative sea-level observations from the Caribbean and South America. Quaternary Science Reviews, 24(10–11), 1183–1202. https://doi.org/10.1016/j.quascirev.2004.10.005

Moffett, K. B., Nardin, W., Silvestri, S., Wang, C., & Temmerman, S. (2015). Multiple stable states and catastrophic shifts in coastal wetlands: Progress, challenges, and opportunities in validating theory using remote sensing and other methods. *Remote Sensing,* 7(8), 10184–10226. https://doi.org/10.3390/rs70810184

Mondal, P., Trzaska, S., De Sherbinin, A., & Sherbinin, A. De. (2018). Landsat-derived estimates of mangrove extents in the Sierra Leone coastal landscape complex during 1990-2016. Sensors, 18(1). https://doi.org/10.3390/s18010012

Moore, L. J., Ruggiero, P., & List, J. H. (2006). Comparing mean high water and high water line shorelines: Should proxy-datum offsets be incorporated into shoreline change analysis? *Journal of Coastal Research*, 22(4), 894–905. https://doi.org/10.2112/04-0401.1

Mukherjee, N., Sutherland, W. J., Khan, M. N. I., Berger, U., Schmitz, N., Dahdouh-Guebas, F., & Koedam, N. (2014). Using expert knowledge and modeling to define mangrove composition, functioning, and threats and estimate time frame for recovery. *Ecology and Evolution*, 4(11), 2247–2262. https://doi.org/10.1002/ece3.1085

Murillo-sandoval, P. J., Fatoyinbo, L., & Simard, M. (2022). Mangroves cover change trajectories 1984-2020 : The gradual decrease of mangroves in Colombia. *Frontiers in Marine Science*, 9(July), 1–14. https://doi.org/10.3389/fmars.2022.892946

Murillo-Sandoval, P. J., Gjerdseth, E., Correa-Ayram, C., Wrathall, D., Van Den Hoek, J., Dávalos, L. M., & Kennedy, R. E. (2021). No peace for the forest: Rapid, widespread land changes in the Andes-Amazon region following the Colombian civil war. *Global Environmental Change*, 69(May). https://doi.org/10.1016/j.gloenvcha.2021.102283

Murray, N. J., Phinn, S. R., Clemens, R. S., Roelfsema, C. M., & Fuller, R. A. (2012). Continental scale mapping of tidal flats across east Asia using the landsat archive. *Remote Sensing,* 4(11), 3417–3426. https://doi.org/10.3390/rs4113417

Murray, N. J., Phinn, S. R., Dewitt, M., Ferrari, R., Johnston, R., Lyons, M. B., Clinton, N., Thau, D., & Fuller, R. A. (2019). The global distribution and trajectory of tidal flats. *Nature*, 565(7738), 222–225. https://doi.org/10.1038/s41586-018-0805-8

Murty, A. V. S., Rao, D. S., Regunathan, A., & Gopinathan, C. P. (1984). Hypotheses on mud banks. CMFRI Bulletin, 31, 8–17.

Nagelkerken, I., Blaber, S. J. M., Bouillon, S., Green, P., Haywood, M., Kirton, L. G., Meynecke, J. O., Pawlik, J., Penrose, H. M., Sasekumar, A., & Somerfield, P. J. (2008). The habitat function of mangroves for terrestrial and marine fauna: A review. *Aquatic Botany*, 89(2), 155–185. https://doi.org/10.1016/j.aquabot.2007.12.007

Neumann, B., Vafeidis, A. T., Zimmermann, J., & Nicholls, R. J. (2015). Future coastal population growth and exposure to sea-level rise and coastal flooding - A global assessment. *PLoS ONE,* 10(3). https://doi.org/10.1371/journal.pone.0118571

Nicholls, R. J. (2011). Planning for the impacts of sea level rise. *Oceanography*, 24(2), 144–157. https://doi.org/10.5670/oceanog.2011.34

Nicholls, R. J., Lincke, D., Hinkel, J., Brown, S., Vafeidis, A. T., Meyssignac, B., Hanson, S. E., Merkens, J. L., & Fang, J. (2021). Author Correction: A global analysis of subsidence, relative sea-level change and coastal flood exposure. *Nature Climate Change*, 11(7), 634. https://doi.org/10.1038/s41558-021-01064-z

Nicholls, R. J., Wong, P. P., Burket, V. R., Codignotto, J., Hay, J. E., McLean, R. F., Ragoonaden, S., & Woodroffe, C. D. (2007). Coastal systems and low-lying areas. In *Coastal Systems and low-lying areas*.

Nijbroek, R. (2012). Mangroves, mudbanks and seawalls: Political ecology of adaptation to sea level rise in Suriname. http://scholarcommons.usf.edu/etd/4184

Nijbroek, R. (2014). Mangroves, mudbanks and seawalls: Whose environmental knowledge counts when adapting to sea level rise in Suriname? *Journal of Political Ecology,* 21, 533–550. https://doi.org/10.1016/0037

Nittrouer, C. A., Demaster, D. J., Kuehl, S. A., Jr, A. G. F., Sternberg, R. W., Faria, L. E. C., Silveira, O. M., Allison, M. A., Kineke, G. C., Ogston, A. S., Filho, P. W. M. S., & Asp, N. E. (2021). Amazon sediment transport and accumulation along the continuum of mixed fluvial and marine processes. *Annual Review of Marine Science*, 13, 1–36.

Odermatt, D., Gitelson, A., Ernesto, V., Schaepman, M. E., Brando, V. E., Schaepman, M. E., Ernesto, V., & Schaepman, M. E. (2012). Review of constituent retrieval in optically deep and complex waters from satellite imagery. *Remote Sensing of Environment*, 118, 116–126. https://doi.org/10.1016/j.rse.2011.11.013

Oppenheimer, M., Glavovic, B., Hinkel, J., van de Wal, R., Magnan, A. K., Abd-Elgawad, A., & Sebesvari, Z. (2019). Sea level rise and implications for low-lying islands, coasts and communities. In IPCC Special Report on the Ocean and Cryosphere in a Changing Climate (Issue September). https://doi.org/10.1017/9781009157964.006

Orseau, S., Zorrilla, N. A., Huybrechts, N., Lesourd, S., Gardel, A., Huybrechts, N., Lesourd, S., & Gardel, A. (2020). Decadal-scale morphological evolution of a muddy open coast. *Marine Geology*, 420(November 2019), 106048. https://doi.org/10.1016/j.margeo.2019.106048

Ortega, G., Arias, P. A., Villegas, J. C., Marquet, P. A., & Nobre, P. (2021). Present-day and future climate over central and South America according to CMIP5/CMIP6 models. *International Journal of Climatology*, 41(15), 6713–6735. https://doi.org/10.1002/joc.7221

Osland, M. J., Feher, L. C., Griffith, K. T., Cavanaugh, K. C., Enwright, N. M., Day, R. H., Stagg, C. L., Krauss, K. W., Rebecca, J., Howard, R. J., Grace, J. B., & Rogers, K. (2017). Climatic controls on the global distribution, abundance, and species richness of mangrove forests. *Ecological Monographs*, 87(2), 341–359.

Osland, M. J., Feher, L. C., Griffith, K. T., Cavanaugh, K. C., Enwright, N. M., Day, R. H., Stagg, C. L., Krauss, K. W., Rebecca, J., Howard, R. J., Grace, J. B., Rogers, K., Osland, M. J., Feher, L. C., Griffith, K. T., Cavanaugh, K. C., Enwright, N. M., Day, R. H., Stagg, C. L., … Rogers, K. (2017). Climatic controls on the global distribution , abundance , and species richness of mangrove forests. *Ecological Monographs*, 87(2), 341–359.

Osland, M. J., Feher, L. C., López-Portillo, J., Day, R. H., Suman, D. O., Guzmán Menéndez, J. M., & Rivera-Monroy, V. H. (2018). Mangrove forests in a rapidly changing world: Global change impacts and conservation opportunities along the Gulf of Mexico coast. *Estuarine, Coastal and Shelf Science*, 214(March), 120–140. https://doi.org/10.1016/j.ecss.2018.09.006

Otero, V., Lucas, R., Van De Kerchove, R., Satyanarayana, B., Mohd-Lokman, H., Dahdouh-Guebas, F., Kerchove, R. Van De, Satyanarayana, B., Mohd-Lokman, H., Dahdouh-Guebas, F., Van De Kerchove, R., Satyanarayana, B., Mohd-Lokman, H., & Dahdouh-Guebas, F. (2020). Spatial analysis of early mangrove regeneration in the Matang Mangrove Forest Reserve , Peninsular Malaysia , using geomatics. *Forest Ecology and Management*, 472(August 2019), 118213. https://doi.org/10.1016/j.foreco.2020.118213

Otero, V., Van De Kerchove, R., Satyanarayana, B., Mohd-Lokman, H., Lucas, R. M., & Dahdouh-Guebas, F. (2019). An Analysis of the early regeneration of mangrove forests using Landsat time series in the Matang Mangrove Forest Reserve, Peninsular Malaysia. *Remote Sensing,* 11(7), 774. https://doi.org/10.3390/rs11070774

Paradis, E., Claude, J., & Strimmer, K. (2004). APE: Analyses of phylogenetics and evolution in R language. *Bioinformatics*, 20(2), 289–290. https://doi.org/10.1093/bioinformatics/btg412

Pardo-Pascual, J. E., Almonacid-Caballer, J., Ruiz, L. A., & Palomar-Vázquez, J. (2012). Automatic extraction of shorelines from Landsat TM and ETM+ multi-temporal images with subpixel precision. *Remote Sensing of Environment*, 123, 1–11. https://doi.org/10.1016/j.rse.2012.02.024

Pardo-Pascual, J. E., Sánchez-García, E., Almonacid-Caballer, J., Palomar-Vázquez, J. M., de los Santos, E. P., Fernández-Sarría, A., Balaguer-Beser, Á., & Elena, S. (2018). Assessing the accuracy of automatically extracted shorelines on microtidal beaches from landsat 7, landsat 8 and sentinel-2 imagery. *Remote Sensing,* 10(2), 1–20. https://doi.org/10.3390/rs10020326

Passeri, D. L., Hagen, S. C., Medeiros, S. C., Bilskie, M. V, Alizad, K., & Wang, D. (2015). The dynamic effects of sea level rise on low-gradient coastal landscapes : A review. *Earth ' s Future*. https://doi.org/10.1002/2015EF000298. Received

Pastor-Guzman, J., Dash, J., & Atkinson, P. M. (2018). Remote sensing of mangrove forest phenology and its environmental drivers. *Remote Sensing of Environment*, 205(November 2017), 71–84. https://doi.org/10.1016/j.rse.2017.11.009

Pendleton, L., Donato, D. C., Murray, B. C., Crooks, S., Jenkins, W. A., Sifleet, S., Craft, C., Fourqurean, J. W., Kauffman, J. B., Marbà, N., Megonigal, P., Pidgeon, E., Herr, D., Gordon, D., & Baldera, A. (2012). Estimating global "Blue Carbon" emissions from conversion and degradation of vegetated coastal ecosystems. *PLoS ONE*, 7(9). https://doi.org/10.1371/journal.pone.0043542

Péron, C., Chatelet, A., Gensac, E., & Gardel, A. (2013). Mud bank migration from remote sensing and bathymetric data : The example of the Kourou River Estuary, French Guina, South America. *Journal of Coastal Research*, 65(65), 558–563. https://doi.org/10.2112/SI65-095.1

Phillips, J. D. (2018). Coastal wetlands, sea level, and the dimensions of geomorphic resilience. *Geomorphology,* 305, 173–184. https://doi.org/10.1016/j.geomorph.2017.03.022

Piégay, H., Chabot, A., & Lay, Y. Le. (2020). Some comments about resilience: From cyclicity to trajectory, a shift in living and nonliving system theory. *Geomorphology,* 367, 106527. https://doi.org/10.1016/j.geomorph.2018.09.018

Pimple, U., Leadprathom, K., Simonetti, D., Sitthi, A., Peters, R., Pungkul, S., Pravinvongvuthi, T., Dessard, H., Berger, U., Siri-on, K., Kemacheevakul, P., & Gond, V. (2022). Assessing mangrove species diversity, zonation and functional indicators in response to natural, regenerated, and rehabilitated succession. *Journal of Environmental Management,* 318(November 2021). https://doi.org/10.1016/j.jenvman.2022.115507

Plaziat, J. C., & Augustinus, P. G. E. F. (2004). Evolution of progradation/erosion along the French Guiana mangrove coast: A comparison of mapped shorelines since the 18th century with Holocene data. *Marine Geology*, 208(2–4), 127–143. https://doi.org/10.1016/j.margeo.2004.04.006

Potapov, P., Turubanova, S., Hansen, M. C., Tyukavina, A., Zalles, V., Khan, A., Song, X. P., Pickens, A., Shen, Q., & Cortez, J. (2022). Global maps of cropland extent and change show accelerated cropland expansion in the twenty-first century. *Nature Food*, 3(1), 19–28. https://doi.org/10.1038/s43016-021-00429-z

Poveda, G., Waylen, P. R., & Pulwarty, R. S. (2006). Annual and inter-annual variability of the present climate in northern South America and southern Mesoamerica. *Palaeogeography, Palaeoclimatology, Palaeo Ecology,* 234(1), 3–27. https://doi.org/10.1016/j.palaeo.2005.10.031

Proisy, C., Degenne, P., Anthony, E. J., Berger, U., Blanchard, E., Fromard, F., Gardel, A., Olagoke, A., Santos, V., Walcker, R., & Lo Seen, D. (2016). A multiscale simulation approach for linking mangrove dynamics to coastal processes using remote sensing observations. *Journal of Coastal Research*, 75(sp1), 810–814. https://doi.org/10.2112/si75-163.1

Proisy, C., Gratiot, N., Anthony, E. J., Gardel, A., Fromard, F., & Heuret, P. (2009). Mud bank colonization by opportunistic mangroves: A case study from French Guiana using lidar data. *Continental Shelf Research*, 29(3), 632–641. https://doi.org/10.1016/j.csr.2008.09.017

Proisy, C., Walcker, R., Blanchard, E., Gardel, A., & Anthony, E. J. (2021). Mangroves: a natural early-warning system of erosion on open muddy coasts in French Guiana. *Dynamic Sedimentary Environments of Mangrove Coasts*, 47–66. https://doi.org/10.1016/b978-0-12-816437-2.00011-2

Pujos, M., & Froidefond, J. M. (1995). Water masses and suspended matter circulation on the French Guiana continental shelf. *Continental Shelf Research*, 15(9), 1157–1171. https://ac.els-cdn.com/027843439400062R/1-s2.0-027843439400062R-main.pdf?_tid=63d7621f-47da-4c83-91a9-6778169be732&acdnat=1522325421_e54f20bdff410656c53104a405f55a01

Rine, J. M., & Ginsburg, R. N. (1985). Depositional facies of a mud shoreface in Suriname, South America - A mud analogue to sandy shallow-marine deposits. *Journal of Sedimentary Petrology,* 55(5), 633–652.

Roberts, D., Mueller, N., & Mcintyre, A. (2017). High-Dimensional pixel composites from earth observation time series. IEEE Transactions on Geoscience and *Remote Sensing,* 55(11), 6254–6264.

Robinson, D. (2014). broom: An R Package for Converting Statistical Analysis Objects Into Tidy Data Frames. ArXiv Preprint *ArXiv*, 1412.3565, 1–24. http://arxiv.org/abs/1412.3565

Rodriguez, H. N., & Mehta, A. J. (1998). Considerations on wave-induced fluid mud streaming at open coasts. *Sedimentary Processes in the Interidal Zone*, 139, 177–186.

Rodriguez, W., Feller, I. C., & Cavanaugh, K. C. (2016). Spatio-temporal changes of a mangrove–saltmarsh ecotone in the northeastern coast of Florida, USA. *Global Ecology and Conservation*, 7. https://doi.org/10.1016/j.gecco.2016.07.005

Rogers, K., Lymburner, L., Salum, R., Brooke, B. P., & Woodroffe, C. D. (2017). Mapping of mangrove extent and zonation using high and low tide composites of Landsat data. *Hydrobiologia*, 803(1), 49–68. https://doi.org/10.1007/s10750-017-3257-5

Rosner, B. (1983). Percentage points for a generalized ESD many-outlier procedure. *Technometrics*, 25(2), 165–172. https://doi.org/10.1080/00401706.1983.10487848

RStudio. (2022). RStudio: Integrated development environment for R (Version '0.548'). In *The Journal of Wildlife Management* (Vol. 75, Issue 8). http://doi.wiley.com/10.1002/jwmg.232

Ruessink, B. G., & Terwindt, J. H. J. (2000). The behaviour of nearshore bars on the time scale of years: A conceptual model. *Marine Geology*, 163, 289–302.

Runge, A., Nitze, I., & Grosse, G. (2022). Remote sensing annual dynamics of rapid permafrost thaw disturbances with LandTrendr. *Remote Sensing of Environment*, 268(October 2021), 112752. https://doi.org/10.1016/j.rse.2021.112752

Ruwaimana, M., Satyanarayana, B., Otero, V., Muslim, A. M., Muhammad Syafiq, A., Ibrahim, S., Raymaekers, D., Koedam, N., & Dahdouh-Guebas, F. (2018). The advantages of using drones over space-borne imagery in the mapping of mangrove forests. *PLoS ONE*, 13(7). https://doi.org/10.1371/journal.pone.0200288

Ryu, J.-H., Won, J. S., & Min, K. D. (2002). Waterline extraction from Landsat TM data in a tidal flat a case study in Gomso Bay, Korea. *Remote Sensing of Environment*, 83(3), 442–456. https://doi.org/10.1016/S0034-4257(02)00059-7

Sagar, S., Phillips, C., Bala, B., Roberts, D., & Lymburner, L. (2018). Generating continental scale pixel-based surface reflectance composites in coastal regions with the use of a multi-resolution tidal model. *Remote Sensing,* 10(3). https://doi.org/10.3390/rs10030480

Sagar, S., Roberts, D., Bala, B., & Lymburner, L. (2017). Extracting the intertidal extent and topography of the Australian coastline from a 28 year time series of Landsat observations. *Remote Sensing of Environment*, 195, 153–169. https://doi.org/10.1016/j.rse.2017.04.009

Saintilan, N., Khan, N. S., Ashe, E., Kelleway, J. J., Rogers, K., Woodroffe, C. D., & Horton, B. P. (2020). Thresholds of mangrove survival under rapid sea level rise. *Science*, 368(6495), 1118–1121. https://doi.org/10.1126/science.aba2656

Samiksha, S. V, Vethamony, P., Rogers, W. E., Pednekar, P. S., Babu, M. T., & Dineshkumar, P. K. (2017). Wave energy dissipation due to mudbanks formed off southwest coast of India. *Estuarine, Coastal and Shelf Science*, 196, 387–398. https://doi.org/10.1016/j.ecss.2017.07.018

Sanderman, J., Tomislav, H., Greg, F., Kylen, S., Maria Fernanda, A., Lisa, B., Jacob, J. B., Paul, C., Miguel, C.-J., Daniel, D., Clare, D., Ebrahem, M. E., Philine zu, E., Carolyn, J. E. L., Peter, I. M., Leah, G., Selena, G., Sunny, L. J., Trevor, G. J., … Landis, E. (2018). A global map of mangrove forest soil carbon at 30 m spatial resolution. *Environmental Research Letters*, 13(5), 55002. https://doi.org/10.1088/1748-9326/aabe1c

SBB. (2019). GCCA+ Suriname adaptation project: Setting up a mangrove biodiversity monitoring system. https://sbbsur.com/wp-content/uploads/2020/03/final-technician-report-mangrove-project-november-2019.pdf

Seddon, N., Chausson, A., Berry, P., Girardin, C. A. J., Smith, A., & Turner, B. (2020). Understanding the value and limits of nature-based solutions to climate change and other global challenges. *Philosophical Transactions of the Royal Society B: Biological Sciences,* 375(1794). https://doi.org/10.1098/rstb.2019.0120

Seidl, R., Spies, T. A., Peterson, D. L., Stephens, S. L., & Hicke, J. A. (2016). Searching for resilience: Addressing the impacts of changing disturbance regimes on forest ecosystem services. *Journal of Applied Ecology,* 53(1), 120–129. https://doi.org/10.1111/1365-2664.12511

Senf, C., & Seidl, R. (2021a). Mapping the forest disturbance regimes of Europe. *Nature Sustainability*, 4(1), 63–70. https://doi.org/10.1038/s41893-020-00609-y

Senf, C., & Seidl, R. (2021b). Post- disturbance canopy recovery and the resilience of Europe's forests. *Global Ecology and Biogeography*, August, 1–12. https://doi.org/10.1111/geb.13406

Sengupta, D., Chen, R., & Meadows, M. E. (2018). Building beyond land: An overview of coastal land reclamation in 16 global megacities. *Applied Geography*, 90(December 2017), 229–238. https://doi.org/10.1016/j.apgeog.2017.12.015

Sengupta, D., Chen, R., Meadows, M. E., Choi, Y. R., Banerjee, A., & Zilong, X. (2019). Mapping trajectories of coastal land reclamation in nine deltaic megacities using google earth engine. *Remote Sensing,* 11(22), 1–13. https://doi.org/10.3390/rs11222621

Servain, J., Caniaux, G., Kouadio, Y. K., McPhaden, M. J., & Araujo, M. (2014). Recent climatic trends in the tropical Atlantic. *Climate Dynamics*, 43(11), 3071–3089. https://doi.org/10.1007/s00382-014-2168-7

Shanmugam, P., Ahn, Y. H., & Sanjeevi, S. (2006). A comparison of the classification of wetland characteristics by linear spectral mixture modelling and traditional hard classifiers on multispectral remotely sensed imagery in southern India. *Ecological Modelling*, 194(4), 379–394. https://doi.org/10.1016/j.ecolmodel.2005.10.033

Shaw, J. B., Wolinsky, M. A., Paola, C., & Voller, V. R. (2008). An image-based method for shoreline mapping on complex coasts. *Geophysical Research Letters*, 35(12), 1–5. https://doi.org/10.1029/2008GL033963

Sherman, R. E., Fahey, T. J., & Battles, J. J. (2000). Small-scale disturbance and regeneration dynamics in a neotropical mangrove forest. *Journal of Ecology,* 88(1), 165–178. https://doi.org/10.1046/j.1365-2745.2000.00439.x

Shi, C., & Wang, L. (2014). Incorporating spatial information in spectral unmixing: A review. *Remote Sensing of Environment*, 149, 70–87. https://doi.org/10.1016/j.rse.2014.03.034

Simpson, M., Scott, D., New, M., Sim, R., Smith, D., Harrison, M., Eakin, C. M., Warrick, R., Strong, A. E., Kouwenhoven, P., Harrison, S., Wilson, M., Nelson, G. C., Donner, S., Kay, R., Geldhill, D. K., Liu, G., Morgan, J. A., Kleypas, J. A., … Stager, H. (2009). An overview of modelling climate change: impacts in the caribbean region with contribution from the Pacific Islands. *Climate Change*, 16. https://doi.org/10.1126/science.1202087

Smith, M. W., Carrivick, J. L., & Quincey, D. J. (2015). Structure from motion photogrammetry in physical geography. *Progress in Physical Geography*, 40(2), 247–275. https://doi.org/10.1177/0309133315615805

Somers, B., Asner, G. P., Tits, L., & Coppin, P. (2011). Endmember variability in spectral mixture analysis: A review. *Remote Sensing of Environment*, 115(7), 1603–1616. https://doi.org/10.1016/j.rse.2011.03.003

Sørensen, T. H., Bartholdy, J., Christiansen, C., & Pedersen, J. B. T. T. (2006). Intertidal surface type mapping in the Danish Wadden Sea. *Marine Geology*, 235(1-4 SPEC. ISS.), 87–99. https://doi.org/10.1016/j.margeo.2006.10.007

Spalding, M. (2010). World Atlas of Mangroves. Routledge. https://doi.org/https://doi.org/10.4324/9781849776608

Stive, M. J. F., Aarninkhof, S. G. J., Hamm, L., Hanson, H., Larson, M., Wijnberg, K. M., Nicholls, R. J., & Capobianco, M. (2002). Variability of shore and shoreline evolution. *Coastal Engineering*, 47(2), 211–235. https://doi.org/10.1016/S0378-3839(02)00126-6

Strimas-Mackey, M. (2021). Package ' smoothr ' (0.2.0; p. 16). https://orcid.org/0000-0001-8929-7776

Sutton-Grier, A. E., Wowk, K., & Bamford, H. (2015). Future of our coasts: The potential for natural and hybrid infrastructure to enhance the resilience of our coastal communities, economies and ecosystems. *Environmental Science and Policy,* 51, 137–148. https://doi.org/10.1016/j.envsci.2015.04.006

Syvitski, J. P. M., Kettner, A. J., Overeem, I., Hutton, E. W. H., Hannon, M. T., Brakenridge, G. R., Day, J., Vörösmarty, C., Saito, Y., Giosan, L., & Nicholls, R. J. (2009). Sinking deltas due to human activities. *Nature Geoscience*, 2(10), 681–686. https://doi.org/10.1038/ngeo629

Tas, S. A. J., Maren, D. S. van, & Reniers, A. J. H. M. (2020). Observations of Cross-Shore Chenier Dynamics in Demak, Indonesia. *Journal of Marine Science and Engineering*, 8(12), 972. https://doi.org/10.3390/jmse8120972

Tas, S. A. J., Maren, D. S. Van, & Reniers, A. J. H. M. (2022). Chenier formation through wave winnowing and tides. J*ournal of Geophysical Research : Earth Surface*, 127. https://doi.org/10.1029/2022JF006792

Taylor, K. H., & Purkis, S. J. (2012). Evidence for the southward migration of mud banks in Florida Bay. *Marine Geology*, 311–314, 52–56. https://doi.org/10.1016/j.margeo.2012.04.007

Team, R. core. (2021). R: A language and environment for statistical computing. R Foundation for Statistical Computing, Vienna, Austria. https://www.r-project.org/

Temmerman, S., Meire, P., Bouma, T. J., Herman, P. M. J., Ysebaert, T., & De Vriend, H. J. (2013). Ecosystem-based coastal defence in the face of global change. *Nature*, 504(7478), 79–83. https://doi.org/10.1038/nature12859

Teunissen, P. A. (1976). Notes on the vegetation of Suriname. Acta Amazonica, 6(2), 117–150.

Tomasi, C., & Manduchi, R. (1998). aBilateral filtering for gray and color images. In Proceedings of the IEEE International Conference on Computer Vision (pp. 839–846). https://doi.org/10.1109/iccv.1998.710815

Toorman, E. A., Anthony, E. J., Augustinus, P. G. E. F., Gardel, A., Gratiot, N., Homenauth, O., Huybrechts, N., & Monbaliu, J. (2018). Interaction of mangroves, coastal hydrodynamics, and morphodynamics along the coastal fringes of the Guianas. *Coastal Research Library*, 25, 429–473.

Toosi, N. B., Soffianian, A. R., Fakheran, S., & Waser, L. T. (2022). Mapping disturbance in mangrove ecosystems: Incorporating landscape metrics and PCA-based spatial analysis. *Ecological Indicators*, 136, 108718. https://doi.org/10.1016/j.ecolind.2022.108718

Tran, L. X., & Fischer, A. (2017). Spatiotemporal changes and fragmentation of mangroves and its effects on fish diversity in Ca Mau Province (Vietnam). *Journal of Coastal Conservation*, 21(3), 355–368. https://doi.org/10.1007/s11852-017-0513-9

Trebossen, H., Deffontaines, B., Classeau, N., Kouame, J., & Rudant, J.-P. (2005). Monitoring coastal evolution and associated littoral hazards of French Guiana shoreline with radar images. C. R. Geoscience, 337(13), 1140–1153. https://doi.org/10.1016/j.crte.2005.05.013

Tucker, C. J. (1979). Red and photographic infrared linear combinations for monitoring vegetation. *Remote Sensing of Environment*, 2(8), 127–150.

Turner, M. G. (2010). Disturbance and landscape dynamics in a changing world. *Ecology,* 91(February), 2833–2849. https://doi.org/https://doi.org/10.1890/10-0097.1

United Nations. (2015). Transforming our world: the 2030 Agenda for Sustainable Development. In UN General Assembly. https://doi.org/10.1201/b20466-7

Uuemaa, E., Mander, Ü., & Marja, R. (2013). Trends in the use of landscape spatial metrics as landscape indicators: A review. *Ecological Indicators*, 28, 100–106. https://doi.org/10.1016/j.ecolind.2012.07.018

Valderrama-Landeros, L., Flores-de-Santiago, F., Kovacs, J. M., & Flores-Verdugo, F. (2018). An assessment of commonly employed satellite-based remote sensors for mapping mangrove species in Mexico using an NDVI-based classification scheme. *Environmental Monitoring and Assessment*. https://doi.org/10.1007/s10661-017-6399-z

van Bijsterveldt, C. E. J., Debrot, A. O., Bouma, T. J., Maulana, M. B., Pribadi, R., Schop, J., Tonneijck, F. H., & van Wesenbeeck, B. K. (2022). To plant or not to plant: When can planting facilitate mangrove restoration? *Frontiers in Environmental Science*, 9(February), 1–18. https://doi.org/10.3389/fenvs.2021.690011

van Bijsterveldt, C. E. J., van Wesenbeeck, B. K., van der Wal, D., Afiati, N., Pribadi, R., Brown, B., & Bouma, T. J. (2020). How to restore mangroves for greenbelt creation along eroding coasts with abandoned aquaculture ponds. *Estuarine, Coastal and Shelf Science*, 235(December 2019), 106576. https://doi.org/10.1016/j.ecss.2019.106576

Van Der Stocken, T., Vanschoenwinkel, B., De Ryck, D. J. R., Bouma, T. J., Dahdouh-Guebas, F., & Koedam, N. (2015). Interaction between water and wind as a driver of passive dispersal in mangroves. *PLoS ONE*, 10(3), 1–17. https://doi.org/10.1371/journal.pone.0121593

van Ledden, M., Vaughn, G., Lansen, J., Wiersma, F., & Amsterdam, M. (2009). Extreme wave event along the Guyana coastline in October 2005. *Continental Shelf Research*, 29(1), 352–361. https://doi.org/10.1016/j.csr.2008.03.010

van Maanen, B., Nicholls, R. J., French, J. R., Barkwith, A., Bonaldo, D., Burningham, H., Brad Murray, A., Payo, A., Sutherland, J., Thornhill, G., Townend, I. H., van der Wegen, M., Walkden, M. J. A. A., Murray, A. B., Payo, A., Sutherland, J., Thornhill, G., Townend, I. H., van der Wegen, M., … Walkden, M. J. A. A. (2015). Simulating mesoscale coastal evolution for decadal coastal management: A new framework integrating multiple, complementary modelling approaches. *Geomorphology,* 256, 68–80. https://doi.org/10.1016/j.geomorph.2015.10.026

van Zelst, V. T. M., Dijkstra, J. T., van Wesenbeeck, B. K., Eilander, D., Morris, E. P., Winsemius, H. C., Ward, P. J., & de Vries, M. B. (2021). Cutting the costs of coastal protection by integrating vegetation in flood defences. *Nature Communications*, 12(1), 1–11. https://doi.org/10.1038/s41467-021-26887-4

Vantrepotte, V., Gensac, E., Loisel, H., Gardel, A., Dessailly, D., & Mériaux, X. (2013). Satellite assessment of the coupling between in water suspended particulate matter and mud banks dynamics over the French Guiana coastal domain. *Journal of South American Earth Sciences*, 44, 25–34. https://doi.org/10.1016/j.jsames.2012.11.008

Vantrepotte, V., Loisel, H., Meriaux, X., Neukermans, G., Dessailly, D., Jamet, C., Gensac, E., & Gardel, A. (2011). Seasonal and inter-annual (2002-2010) variability of the suspended particulate matter as retrieved from satellite ocean color sensor over the French Guiana coastal waters. *Journal of Coastal Research*, 64, 1750–1754. https://doi.org/0749-0208

Viles, H. A., & Goudie, A. S. (2003). Interannual, decadal and multidecadal scale climatic variability and geomorphology. *Earth-Science Reviews*, 61(1–2), 105–131. https://doi.org/10.1016/S0012-8252(02)00113-7

Vos, K., Harley, M. D., Splinter, K. D., Simmons, J. A., & Turner, I. L. (2019). Sub-annual to multi-decadal shoreline variability from publicly available satellite imagery. *Coastal Engineering*, 150(February), 160–174. https://doi.org/10.1016/j.coastaleng.2019.04.004

Vos, K., Harley, M. D., Splinter, K. D., Walker, A., & Turner, I. L. (2020). Beach slopes from satellite-derived shorelines. *Geophysical Research Letters*, 47(14). https://doi.org/10.1029/2020GL088365

Vos, K., Harley, M. D., Turner, I. L., & Splinter, K. D. (2023). Pacific shoreline erosion and accretion patterns controlled by El Niño / Southern Oscillation. *Nature Geoscience*, 16(February), 140–146. https://doi.org/10.1038/s41561-022-01117-8

Vuik, V., Borsje, B. W., Willemsen, P. W. J. M., & Jonkman, S. N. (2019). Salt marshes for flood risk reduction: Quantifying long-term effectiveness and life-cycle costs. *Ocean and Coastal Management*, 171(February), 96–110. https://doi.org/10.1016/j.ocecoaman.2019.01.010

Walcker, R., Anthony, E. J., Cassou, C., Aller, R. C., Gardel, A., Proisy, C., Martinez, J. M., & Fromard, F. (2015). Fluctuations in the extent of mangroves driven by multi-decadal changes in North Atlantic waves. *Journal of Biogeography*, 42(11), 2209–2219. https://doi.org/10.1111/jbi.12580

Walters, B. B., Rönnbäck, P., Kovacs, J. M., Crona, B., Hussain, S. A., Badola, R., Primavera, J. H., Barbier, E. B., & Dahdouh-Guebas, F. (2008). Ethnobiology, socio-economics and management of mangrove forests: A review. *Aquatic Botany*, 89(2), 220–236. https://doi.org/10.1016/j.aquabot.2008.02.009

Warrick, J. A., Vos, K., East, A. E., & Vitousek, S. (2022). Fire (plus) flood (equals) beach: coastal response to an exceptional river sediment discharge event. *Scientific Reports*, 12(1). https://doi.org/10.1038/s41598-022-07209-0

Wells, J. T., & Coleman, J. M. (1981a). Physical processes and fine-grained sediment dynamics, coast of Surinam, South America. SEPM *Journal of Sedimentary Research*, Vol. 51(4), 1053–1068. https://doi.org/10.1306/212F7E1E-2B24-11D7-8648000102C1865D

Wells, J. T., & Coleman, J. M. (1981b). Periodic Mudflat Progradation, Northeastern Coast of Sout-America: A Hypothesis. *Journal of Sedimentary Petrology*, 51(4), 1069–1075. https://doi.org/10.2110/jsr.51.1069

Westoby, M. J., Brasington, J., Glasser, N. F., Hambrey, M. J., & Reynolds, J. M. (2012). "Structure-from-Motion" photogrammetry: A low-cost, effective tool for geoscience applications. *Geomorphology,* 179, 300–314. https://doi.org/10.1016/j.geomorph.2012.08.021

White, J. C., Wulder, M. A., Hobart, G. W., Luther, J. E., Hermosilla, T., Griffiths, P., Coops, N. C., Hall, R. J., & Hostert, P. (2014). Pixel-Based Image Compositing for Large-Area Dense Time Series Applications and Science. *Canadian Journal of Remote Sensing,* 8992(40), 192–212. https://doi.org/10.1080/07038992.2014.945827

White, P. S. (1979). Pattern, process, and natural disturbance in vegetation. *The Botanical Review*, 45(3), 229–299. https://doi.org/10.1007/BF02860857

Willems, T., De Backer, A., Wan Tong You, K., Vincx, M., & Hostens, K. (2015). Spatio-temporal distribution patterns of the epibenthic community in the coastal waters of Suriname. *Continental Shelf Research*, 108, 25–40. https://doi.org/10.1016/j.csr.2015.08.006

Willemsen, P. W. J. M. J. M., Horstman, E. M., Borsje, B. W., Friess, D. A., & Dohmen-janssen, C. M. (2016). Sensitivity of the sediment trapping capacity of an estuarine mangrove forest. *Geomorphology,* 273, 189–201. https://doi.org/10.1016/j.geomorph.2016.07.038

Winterwerp, J. C., Albers, T., Anthony, E. J., Friess, D. A., Gijón, A., Moseley, K., Muhari, A., Naipal, S., Noordermeer, J., Oost, A., Saengsupavanich, C., Tas, S. A. J., Tonneijck, F. H., Wilms, T., Bijsterveldt, C. Van, Eijk, P. Van, Lavieren, E. Van, & Wesenbeeck, B. K. Van. (2020). Managing erosion of mangrove-mud coasts with permeable dams – lessons learned. *Ecological Engineering*, 158(September), 106078. https://doi.org/10.1016/j.ecoleng.2020.106078

Winterwerp, J. C., Graaff, R. F. d. De, Groeneweg, J., & Luijendijk, A. P. (2007). Modelling of wave damping at Guyana mud coast. *Coastal Engineering*, 54(3), 249–261. https://doi.org/10.1016/j.coastaleng.2006.08.012

WMO. (2019). The Global Climate in 2011 - 2015. Centre for Research on the Epidemiology of Disasters National Institute for Space Research, 32. https://library.wmo.int/doc_num.php?explnum_id=9936

Wong, T. E. (1992). Quaternary stratigraphy of Suriname. Évolution Des Littoraux de Guyane et de La Zone Caraïbe Méridionale Pendant Le Quaternaire, 559–578.

Wong, T. E., de Kramer, R., de Boer, P. L., Langereis, C., & Sew-A-Tjon, J. (2009). The influence of sea-level changes on tropical coastal lowlands; the Pleistocene Coropina Formation, Suriname. *Sedimentary Geology*, 216(3–4), 125–137. https://doi.org/10.1016/j.sedgeo.2009.02.003

Woodroffe, C. D., & Grime, D. (1999). Storm impact and evolution of a mangrove-fringed chenier plain, Shoal Bay, Darwin, Australia. *Marine Geology*, 159(1–4), 303–321. https://doi.org/10.1016/S0025-3227(99)00006-7

Woodroffe, C. D., Rogers, K., McKee, K. L., Lovelock, C. E., Mendelssohn, I. A., & Saintilan, N. (2016). Mangrove sedimentation and response to relative sea-level rise. *Annual Review of Marine Science*, 8(1), 243–266. https://doi.org/10.1146/annurev-marine-122414-034025

Wright, L. D., & Nittrouer, C. A. (1995). Dispersal of river sediments in coastal seas: Six contrasting cases. *Estuaries*, 18(3), 494–508. https://doi.org/10.1007/BF02690131

Wulder, M. A., White, J. C., Loveland, T. R., Woodcock, C. E., Belward, A. S., Cohen, W. B., Fosnight, E. A., Shaw, J., Masek, J. G., & Roy, D. P. (2016). The global Landsat archive: Status, consolidation, and direction. *Remote Sensing of Environment*, 185, 271–283. https://doi.org/10.1016/j.rse.2015.11.032

Xie, D., Schwarz, C., Brückner, M. Z. M. M., Kleinhans, M. G., Urrego, D. H., Zhou, Z., Maanen, B. Van, & van Maanen, B. (2020). Mangrove diversity loss under sea-level rise triggered by bio-morphodynamic feedbacks and anthropogenic pressures. *Environmental Research Letters*, 15(11). https://doi.org/10.1088/1748-9326/abc122

Xie, D., Schwarz, C., Kleinhans, M. G., Zhou, Z., & van Maanen, B. (2022). Implications of coastal conditions and sea-level rise on mangrove vulnerability: A bio-morphodynamic modeling study. *Journal of Geophysical Research: Earth Surface*, 127(3), 1–28. https://doi.org/10.1029/2021JF006301

Xie, S. P., & Carton, J. A. (2004). Tropical atlantic variability: Patterns, mechanisms, and impacts. *Geophysical Monograph Series*, 147, 121–142. https://doi.org/10.1029/147GM07

Xu, N. (2018). Detecting coastline change with all available landsat data over 1986-2015: A case study for the state of Texas, USA. *Atmosphere*, 9(3). https://doi.org/10.3390/atmos9030107

Yan, X., & Wang, J. (2021). Dynamic monitoring of urban built-up object expansion trajectories in Karachi, Pakistan with time series images and the LandTrendr algorithm. *Scientific Reports*, 11(1), 1–15. https://doi.org/10.1038/s41598-021-02565-9

Younes Cárdenas, N., Joyce, K. E., & Maier, S. W. (2017). Monitoring mangrove forests: Are we taking full advantage of technology? *International Journal of Applied Earth Observation and Geoinformation*, 63(April), 1–14. https://doi.org/10.1016/j.jag.2017.07.004

Zanutta, A., Lambertini, A., & Vittuari, L. (2020). UAV photogrammetry and ground surveys as a mapping tool for quickly monitoring shoreline and beach changes. *Journal of Marine Science and Engineering*, 8(1), 52. https://doi.org/10.3390/jmse8010052

Zhang, Y., Woodcock, C. E., Arévalo, P., Olofsson, P., Tang, X., Stanimirova, R., Bullock, E., Tarrio, K. R., Zhu, Z., & Friedl, M. A. (2022). A global analysis of the spatial and temporal variability of usable landsat observations at the pixel scale. Frontiers in *Remote Sensing,* 3(June), 1–14. https://doi.org/10.3389/frsen.2022.894618

Zhu, Z., & Woodcock, C. E. (2014). Automated cloud, cloud shadow, and snow detection in multitemporal Landsat data: An algorithm designed specifically for monitoring land cover change. *Remote Sensing of Environment*, 152, 217–234. https://doi.org/10.1016/j.rse.2014.06.012

Zorrilla, N. A., Vantrepotte, V., Gensac, E., Huybrechts, N., & Gardel, A. (2018). The advantages of Landsat 8-OLI-derived suspended particulate matter maps for monitoring the subtidal extension of Amazonian coastal mud banks (French Guiana). *Remote Sensing,* 10(11), 1–17. https://doi.org/10.3390/rs10111733

Zuur, A. F., Ieno, E. N., & Elphick, C. S. (2010). A protocol for data exploration to avoid common statistical problems. *Methods in Ecology and Evolution*, 1(1), 3–14. https://doi.org/10.1111/j.2041-210x.2009.00001.x

Dankwoord

Aan het begin van mijn weg naar volwassenheid wilde ik, waarschijnlijk net als de meeste van mijn leeftijdgenoten, brandweerman of politieagent worden. Ik denk dat ik de mensheid een dienst heb bewezen dat niet door te zetten maar een hele, hele, hele lange zoektocht te beginnen naar wat het dan wel moest zijn. Ergens tijdens de legendarische lessen aardrijkskunde van **Mr. Meijers** kwam ik er achter dat het iets met topografie, atlassen, geografie en reizen moest worden. Hoewel het daarmee nog geen uitgemaakte zaak was dat ik fysische geografie zou gaan studeren, laat staan dat ik wist wat het betekende, werd er daar een eerste zaadje geplant. Eerst ging ik VWO doen en op wereldreis naar Australië zodat ik nog geen keuze hoefde te maken, bleef ik ietsjepietsje langer weg om nog steeds geen keuze te maken en bleef ik daar bijna permanent zodat ik überhaupt niet meer hoefde te kiezen. Gelukkig was er daarna een tijd dat het me eigenlijk niet zoveel uitmaakte wat ik ging doen. "Als het maar geen PhD is" riep ik tot aan het afronden van mij master in Utrecht. Tijdens deze zoektocht waren er velen die mij, bedoeld en onbedoeld, op het rechte pad hielden en een zetje in de juiste richting gaven. Ik ben iedereen daarvoor ontzettend dankbaar, maar er zijn een aantal mensen die ik vooral wil benoemen.

Steven, zonder jou zou ik niet de onderzoeker zijn geworden die dit proefschrift had kunnen maken. Ik ben je dankbaar voor jouw vertrouwen vanaf het moment dat ik mijn MSc thesis ging doen bij jou. Boven alles liet je me zien waar vasthoudendheid en heel veel enthousiasme me konden brengen. **Gerben**, bedankt dat je met zo veel gevoel de wetenschappelijke lat hoog hebt gehouden én tegelijkertijd mij het vertrouwen gaf dat ik daar kon komen. Hoe jij er soms schijnbaar moeiteloos in slaagt tot de essentie van een probleem of boodschap te komen zal ik altijd met me meedragen. **Barend**, bedankt dat je altijd scherp bleef op de inhoud maar tegelijkertijd zó positief over de mogelijkheden. Als ik ook maar een vleugje van jouw wetenschappelijke creativiteit heb opgepikt de afgelopen jaren dan zit ik gebakken. Ik waardeer het ontzettend dat je, ondanks de fysieke afstand, zo trouw bleef aan het project en aan mij. **Pita**, bedankt dat je altijd scherp was op de boodschap van mijn oeverloze gebrabbel en mijn teksten. Je liet me vooral zien hoe een goedgeschreven verhaal een betere boodschap overbrengt maar vooral dat een belangrijke boodschap een goedgeschreven verhaal verdiend.

Ik had Suriname niet leren kennen, en dus geen proefschrift kunnen maken, zonder de hulp van velen. Want dat is óók Suriname, behulpzaamheid. **Ginny** bedankt voor je gastvrijheid en geduld om deze *Bakra* wegwijs te maken in Suriname. **Pieter**, je liet me inzien wat het echt betekent *to be standing on the shoulders of giants*. Bedankt dat ik mocht voortborduren op jouw levenswerk. Tevens ben je de hoofdpersoon in mijn favoriete anekdote over bevlogen fysisch geografen. Ik zal namelijk nooit vergeten hoe jij over strand van Braamspunt liep en van elke schelp de Latijnse naam wist op te lepelen. En Braamspunt was toen nog een groot strand. **Michael Hiwatt**, bedankt voor je gastvrijheid, behulpzaamheid en bevlogenheid. Je bent voor mij de meest iconische en bevlogen ambassadeur van Suriname. Dear **Edward Anthony**, **Tanguy Maury** and **Antoine Gardel** thank you giving me a taste for doing fieldwork in the Guianas, it has been a joy!

Dear colleagues at DFG, thank you for the most educative years of my life. Thank you for taking me to the high mountains of Asia, coldest planets, muddiest deltas, the most majestic rivers

and all the beautiful fieldwork locations in the world. We have the best jobs in the world. To all the fellow PhD's at the department: thank you for sharing the wonderous roads of a PhD student. Especially a huge thanks to Jana, Jorn and Tatjana for sharing the office for so long. Thank you **Matthieu**, **Logambal** and **Jorge** for setting up the Remote Sensing group together. Thanks for all the "kings" in the coffee corner. **Bas** (yeah yeah, you are the true one), **Ed**, **Daniël, Teun** and **Tim** thanks for sharing the burdens of a PhD life over even worse cups of coffee. I definitely would have finished my PhD one year ago if it wasn't for all the coffee we had. **Teun**, bedankt dat je mijn paranimf wil zijn, je hulp de afgelopen jaren en vooral je gekke ideeën. Ik hoop dat het je ooit alsnog lukt alle dijken in de wereld te karteren, want als iemand het kan ben jij het wel.

Elizabeth, **Tjalling** en **Wiebe**, bedankt dat ik mocht ruiken aan het geven van onderwijs en dat de deur altijd open stond voor vragen over alles wat met drones, satellieten en meer van dat soort gadgets te maken had. **Youchen**, **Steye**, **Lars** en **Celine** het was een plezier om met jullie samen te werken, bedankt voor jullie inzichten en bijdrage aan het MangroMud project. **Niels**, **Tessa**, **Eirini**, **Maud**, **Tirza** en **Nienke**, bedankt dat ik met jullie mee mocht denken over jullie MSc onderzoeken. Ik heb ontzettend veel geleerd van jullie werk en kan alleen maar hopen dat ik iets heb kunnen bijdragen aan dat van jullie.

Dr. Steffan Strohmeier, you possess a rare combination of scientific realism and enthusiasm for scientific challenges that sparked an interest with me. Thank you for being the first to show me the fun in science, accidently setting me on the path towards an scientific career and making my time at ICARDA in Jordan so memorable.

Dan zijn er nog alle familie en vrienden die onvermoeibaar bleven vragen wat ik nu eigenlijk deed voor mijn werk. Jullie interesse in wat ik de afgelopen jaar heb gedaan heeft mij altijd trots gemaakt.

Jaap, **Marloes**, **Nina** en **Joop** bedankt dat jullie me door dik en dun hebben gesteund. Vooral dik. Ik vind het echt vet dat we zo'n omvangrijke vriendschap hebben opgezet. Vol met forse overdrijvingen en bol van de dramatiek.

Jelle en **Milou**, bedankt voor alle gezelligheid, spelletjes en de warme vriendschap. En koffie, natuurlijk ook bedankt voor alle koffie. **Jelle**, jij bezit en ongekende vermogen om te relativeren en, indien nodig, elk probleem plat te slaan tot een heerlijke flauwe grap, hoewel je timing af en toe nog beroerder is dan die van mij. Ik ben vooral heel blij dat we meer interesses delen dan die voor pixels.

Lieve **Ron** en **Jessica**, *plukkie al*? Ik heb het tot op de bodem uitgezocht: Down-Under was *bekant* alles *superdik* en helemaal *gouwd*. Gelukkig hebben we hier in Nederland, en dan vooral het Westland natuurlijk, veel méér om van te genieten. Fijn dat we elkaar hebben, om af en toe te *komen tuinen* voor een *bakkie* en nostalgisch te dromen over Australië. Ik ben *zo groos als een ouwe aap* op jullie.

Jasper, **Arjan**, **Matthijs**, **Maarten**, **Annemieke**, **Kylie** en **Floris**, ergens in de afgelopen jaren delen we een hele berg herinneringen. Of het nu kerstbomen verzamelen is in Joure, Oktoberfest vieren of Uilenstede (504) onveilig maken was, ik kijk er met plezier op terug. Ik zal altijd me best doen, en waarschijnlijk te kort schieten, om deze herinneringen nog te gaan overtreffen met jullie. **Aniek** bedankt voor het meelezen van stukjes van mijn proefschrift en het meeleven tijdens het promovoren. Glitters of niet, het is altijd feest met jou en **Justin**! Bedankt dat jullie ons een beetje jong houden!

Er is natuurlijk *thuis* en *thuis-thuis*. **Rein**, **Jantje**, **Jorrit**, **Barbara**, **Froukje** en **Joost** bedankt dat jullie *thuis-thuis* zo als *thuis* hebben laten voelen. Ik hoop dat het me lukt de lokroep van Zeewolde

nog heel lang te weerstaan, maar het is altijd fijn jullie daar te treffen. Of ergens anders in Europa, want *thuis-thuis* is dan misschien ook alleen maar daar waar jullie allemaal zijn.

Lieve **Sanne**, **Tim**, **Sem**, **Dex**, **Timo**, **Marlous**, **Berend** en **Loes**. Bedankt voor de basis en een plek om lief, leed maar vooral mijlpalen met elkaar te delen en te vieren. Niks is mooier dan zien hoe we allemaal onze eigen weg in zijn geslagen de afgelopen jaren, zonder elkaar uit oog te verliezen. Dat er altijd iemand is om je aan te moedigen, te voorzien van (misplaatst) advies (sorry!) of samen een nieuwe uitdaging mee aan te gaan. Wat er ook op ieders eigen pad komt, het geeft mij vertrouwen te weten dat die van jullie niet ver bij de mijne vandaan lopen.

Lieve **Marit**, de afgelopen 10 jaar waren een feest dat ik met niemand anders had willen vieren. Er zijn zoveel dingen die ik prachtig vindt aan jou, maar nu wil ik vooral zeggen dat ik me gelukkig prijs dat jij me elke dag laat zien hoe het óók kan. Hoe je ook uitdagingen aan kan gaan, de balans kan zoeken, kan groeien en heel zeker kan weten wat je er van vindt. Lieve **Marit** je weet me elke keer weer te verassen en alleen daarom al wil ik altijd jouw grootste fan zijn.

En zoals het hoort bij de erkenning van een gedegen wetenschappelijk product worden de mensen die het meeste werk verzetten als eerst bedankt, maar degene met de grootste bijdrage als laatst. Lieve **Pap** en **Mam**, moge het duidelijk zijn dat ik vandaag niet hand gestaan zonder jullie. Er is natuurlijk nog zoveel meer wat ik niet zonder jullie had gekund, maar boven alles wil ik jullie bedanken voor de liefde en het vertrouwen. Want wat ik ook probeerde, deed of juist heb nagelaten, jullie waren er altijd om me aan te moedigen. Dát gevoel van vertrouwen, wat mij heeft gebracht waar ik vandaag sta, wens ik iedereen toe.

About the author

Job de Vries was born on 28 January 1990 in Amsterdam. After graduating from het Rietveld Lyceum in Doetinchem in 2009 and travelling Australia and New-Zealand, he started his bachelor *Earth and Economics* in 2011 at the Vrij Universiteit in Amsterdam. During his master *Physical Geography - Earth Observation and Natural Hazards* at Utrecht University, he developed a strong interest in subjects that combine spatial analysis with land surface processes in complex ecosystems. For his master thesis he worked at reconstructing landslide stability through UAV remote sensing and hydrological field observations. During his internship at ICARDA in Amman he applied remote sensing observations to characterize water harvesting techniques in semi-arid agricultural areas of Jordan.

After graduating in 2017 he continued working as a project employee at NEO, a remote sensing company in Amersfoort. In October 2017 he started as a junior researcher at Utrecht University on a pilot project. During which he explored the possibility of object based image classification techniques for the purpose of ecosystem monitoring on the tidal flats in the Wadden sea. In March 2018 he started as a PhD candidate in the MangroMud project at the department of Physical Geography at Utrecht University. He presented his research on different national and international conferences including EGU 2019 in Vienna, AGU 2021 and Geo4Good 2019 in California. He was also involved in setting up and organizing bi-weekly remote sensing meetings for the department and wider remote sensing community at Utrecht University. During his PhD he was involved in teaching remote sensing courses and supervision of master thesis work.

List of publications

de Vries, J., van Maanen, B., Ruessink, G., Verweij, P. A., & de Jong, S. M. (2023). **The effect of mudbank morphometrics and coastal morphology on multidecadal coastline changes in the Guianas.** In preperation preparation for publication.

de Vries, J., van Maanen, B., Ruessink, G., Verweij, P. A., & de Jong, S. M. (2022). **Multi-decadal coastline dynamics in Suriname controlled by migrating subtidal mudbanks**. *Earth Surface Processes and Landforms, 47 (10)*. https://doi.org/10.1002/esp.5390.

Fu, S., de Jong. S. M., Hou, x., de Vries, J., Deijns, A., de Haas, T. (2022). A novel landslide dating framework using a combination of microwave and optical Sentinel 1 and 2 imagery. In preparation for publication.

Zhou, S., Huang, M., de Vries, J., Haurier, Y., (2022). Aridity and soil fertility, not species richness, interact to affect temporal stability along a large natural gradient in northern China. Submitted to *Annals of Botany.*

van Kuik, N., de Vries, J., Schwarz, C., & Ruessink, G. (2022). Surface-area development of foredune trough blowouts and associated parabolic dunes quantified from time series of satellite imagery. *Aeolian Research*, 57,. https://doi.org/10.1016/j.aeolia.2022.100812.

de Vries, J., van Maanen, B., Ruessink, G., Verweij, P. A., & de Jong, S. M. (2021). **Unmixing water and mud: Characterizing diffuse boundaries of subtidal mud banks from individual satellite observation**s. *International Journal of Applied Earth Observation and Geoinformation, 95,* 102252. https://doi.org/10.1016/j.jag.2020.102252

de Jong, S. M., Shen, Y., de Vries, J., Bijnaar, G., van Maanen, B., Augustinus, P., & Verweij, P. (2021). **Mapping mangrove dynamics and colonization patterns at the Suriname coast using historic satellite data and the LandTrendr algorithm**. *International Journal of Applied Earth Observation and Geoinformation, 97, 102293.*

Extra

Van Schie, S. (2020). Mangrove verdrinkt bij snelle zeespiegelstijging. Available at https://bionieuws.nl/article/588865/mangrove_verdrinkt_bij_snelle_zeespiegelstijging

Vermeer, N., de Vries, J., Nijland, W., 2021. Kustlijn dynamiek Suriname in kaart gebracht. Geografie.

Utrecht University
Faculty of Geosciences
Department of Physical Geography

ISSN 2211-4335